

Charles University

Faculty of Science

Ph.D. study programme: Inorganic Chemistry



Mgr. Tereza Krchová

Responsive Contrast Agents for Magnetic Resonance Imaging (MRI)

Responzivní kontrastní látky pro tomografii magnetické rezonance (MRI)

Ph.D. Thesis

Supervisor: doc. RNDr. Jan Kotek, Ph.D.

Prague 2017

Declaration

Hereby I declare that this Thesis is my original work and that I have properly cited all the information resources. This work has not been submitted either for any other or for the same academic degree.

In Prague, February 27th 2017

Tereza Krchová

TABLE OF CONTENTS

1	ABSTRACT	5
2	ABSTRAKT	6
3	PREFACE.....	7
4	INTRODUCTION TO MRI	9
4.1	<i>T</i> ₁ AND <i>T</i> ₂ CONTRAST AGENTS	10
4.2	CEST CONTRAST AGENTS	12
4.2.1	History	12
4.2.2	Principle	13
4.2.3	PARACEST CAs	15
4.2.4	Advantages of PARACEST CAs	18
4.3	PH IMAGING	19
4.3.1	Gd(III)-based CAs	20
4.3.2	PARACEST CAs	22
4.3.3	Agents for Magnetic Resonance Spectroscopy (MRS)	23
5	AIMS OF THE THESIS	26
6	RESULTS AND DISCUSSION	28
6.1	LANTHANIDE(III) COMPLEXES OF AMINOETHYL-DO3A	28
6.1.1	Synthesis and structure	28
6.1.2	PARACEST experiments	32
6.1.3	Conclusions	35

6.2	LANTHANIDE(III) COMPLEXES OF DIAMINE-DO3A	36
6.2.1	Synthesis and structure	36
6.2.2	PARACEST experiments	40
6.2.3	Conclusions	45
6.3	LANTHANIDE(III) COMPLEXES OF PHOSPHO-AMINO-DO3A	47
6.3.1	Synthesis.....	47
6.3.2	Thermodynamic behaviour of H ₅ do3aNP and its Eu(III) complex	48
6.3.3	Solution structure of the Eu(III)-H ₅ do3aNP complex	50
6.3.4	pH mapping using ³¹ P MRS	55
6.3.5	PARACEST experiments	56
6.3.6	Conclusions	60
7	CONCLUSIONS	61
8	LIST OF ABBREVIATIONS	64
9	DECLARATION OF CONTRIBUTION	66
10	ACKNOWLEDGEMENTS.....	67
11	REFERENCES	68
12	LIST OF APPENDICES	75

1 ABSTRACT

This work is focused on the synthesis of a family of new macrocyclic ligands with exchangeable protons on coordinating groups that could potentially serve (after complexation with suitable paramagnetic lanthanide(III) ions) as responsive contrast agents (CAs) for magnetic resonance imaging (MRI). It is expected that measurement of extracellular pH should bring information for tumorous disease diagnoses and/or for suggesting the most efficient treatment. Therefore, our attention was focused on pH-dependent CAs based on a PARAMagnetic Chemical Exchange Saturation Transfer (PARACEST) mechanism capable of reporting pH changes in tissue.

The PARACEST-related properties of a series of Ln(III) complexes with the CEST effect caused by amino groups coordinated to the central Ln(III) metal ions were investigated. Such a kind of PARACEST CA is new and has had no precedent in the literature. It was shown that these Ln(III) complexes produce a pH-sensitive PARACEST effect in the pH region relevant for living systems. The study brings proof-of-principle for utilization of complexes with a linear diamine pendant arm, *i.e.* complexes with two exchanging proton pools, for ratiometric pH determination by MRI independently on the probe concentration. In addition, to ensure a higher kinetic inertness of the complexes and PARACEST properties suitable for potential pH-sensitive CAs, a novel macrocyclic ligand containing aminophosphonate-coordinating pendant arm was prepared. It was found that its Ln(III) complexes could be used as concentration-independent ratiometric probes for pH determination using PARACEST measurements and also ^{31}P Magnetic Resonance Spectroscopy (MRS) techniques. Thus, these complexes extend the family of pH-sensitive probes for possible utilization *in vivo*.

2 ABSTRAKT

Tato práce je zaměřena na syntézu nových makrocyclických ligandů s vyměnitelnými protony na koordinujících se skupinách a na přípravu komplexů těchto ligandů s vhodnými paramagnetickými ionty trojmocných lanthanoidů. Takové komplexy by mohly sloužit jako tzv. responzivní kontrastní látky pro tomografii magnetické rezonance (MRI) vhodné ke sledování změn okolních podmínek. V rámci této dizertační práce byly studovány kontrastní látky citlivé na změnu pH, které využívají přenosu saturace (PARAMagnetic Chemical Exchange Saturation Transfer; PARACEST) a mohly by tak sloužit ke sledování změn pH v tkáních. Informace o těchto změnách jsou důležité například pro diagnostiku nádorových onemocnění a/nebo pro volbu vhodného způsobu léčby.

Byla připravena série komplexů makrocyclických ligandů s ionty trojmocných lanthanoidů s vyměnitelnými protony aminoskupin, které jsou koordinované k centrálnímu iontu kovu. U těchto komplexů byly podrobně studovány vlastnosti PARACEST. Kontrastní látky založené na výměně protonů z koordinovaných aminoskupin dosud nebyly v literatuře popsány. Bylo zjištěno, že tyto komplexy vykazují efekt PARACEST závislý na pH, a to při takových hodnotách pH, které odpovídají fyziologickým podmínkám. Tato studie ukázala, že komplexy s pendantním ramenem v podobě lineárního diaminu poskytují ve spektru CEST dva různé signály. Intenzity těchto signálů je možné porovnávat a vytvořit tak metodu umožňující určení hodnoty pH pomocí MRI nezávisle na koncentraci dané kontrastní látky. Aby byla zajištěna kinetická inertnost komplexů, byl navržen a připraven také nový makrocyclický ligand s aminofosfonátovým pendantním ramenem. Bylo zjištěno, že komplexy tohoto ligandu vykazují vlastnosti PARACEST důležité pro potenciální senzory pH a mohly by tak být použity jako kontrastní látky ke sledování změn pH. Stejně látky lze také použít k určení pH pomocí techniky ^{31}P MRS (Magnetic Resonance Spectroscopy). Komplexy připravených ligandů tedy mají velký potenciál pro další aplikace a rozšiřují tak možnosti využití kontrastních látek ke sledování pH za podmínek *in vivo*.

3 PREFACE

In 1945, Edward M. Purcell, Henry C. Torrey and Robert Pound observed the first radio-frequency signals generated by the hydrogen nuclei in paraffin wax. Independently a few months later, Felix Bloch, William W. Hansen and Martin E. Packard performed a different experiment in which they detected the signal of the hydrogen nuclei of water. In the years since then, *i.e.* after this “birth” of the field known today as nuclear magnetic resonance (NMR), this modality has become an important physical tool for investigating chemical compounds.¹

Over the next 30 years, the method was gradually developed and new ways of its utilization were discovered. In 1966, Richard Ernst explored application of a new Fourier transform technique to magnetic resonance spectroscopy. The method consisted of the application of a sequence of short radiofrequency (RF) pulses to the sample, record the response (FID; Free Induction Decay) of the system in a digital form on a computer, and Fourier transformation of the time-dependent signal. He demonstrated that it can enhance the signal-to-noise ratio of NMR spectra and that the NMR spectrum measured by this technique (compared to that recorded with the usual spectral sweep method) can be obtained in a much shorter time.^{2,3}

Over the next few years, scientists realized the potential of NMR for visualization of pathological changes in living subjects. In 1971, Raymond Damadian observed that NMR relaxation times of normal healthy tissues and those of tumours are different and he suggested that these differences could be used for the detection of cancer.⁴ He also designed a concept of 3D NMR apparatus for scanning a whole body which was patented in 1974 with a title “Apparatus and Method for Detecting Cancer in Tissue”.⁵ Between 1973 and 1975, several articles were published by Paul C. Lauterbur and Peter Mansfield (without knowledge of each other’s work) describing a way to spatially localize NMR signal using magnetic field gradients. Lauterbur measured the first images of two 1 mm capillaries filled with water in 1973 and called his imaging method *zeugmatography* (Greek word *zeugma* means *joining, connection*; this technique used a static magnetic field and spatially defined

radiofrequency field gradients).^{6,7} This term was later replaced by the term Nuclear Magnetic Resonance Imaging (Nuclear MRI) and then MRI.^{*8} Two years later, in 1975, application of Fourier transformation to reconstruct 2D images was described by Richard Ernst and this technique is the basis of today's MRI. All of the discoveries mentioned above laid the foundation for Magnetic Resonance Imaging and opened the door to novel opportunities in medicine.⁹

*In 1983, the editorials of the *American Journal of Roentgenology* suggested that the word "nuclear" should be eliminated to reduce patient anxiety; therefore, the method was renamed MRI.

4 INTRODUCTION TO MRI

Nowadays, MRI is one of the most valuable diagnostic methods used in clinical practice and biomedical research. This imaging modality uniquely offers convenient non-invasive application, spatial resolution and tomographic capability, and often represents the only reliable method for detection of cranial abnormalities or cerebral lesions. The principles of MRI predominantly rely on monitoring of different distributions and properties of water molecules in tissues and on a variation in its proton longitudinal (T_1)[†] and transversal (T_2)[‡] relaxation times (except for some less common MRI techniques utilizing other isotopes, *e.g.* ^{19}F and ^{31}P).^{10,11} Therefore, several types of MRI images can be generated that represent local differences in a water concentration (proton density weighted images) and relaxation times (T_1 - and T_2 -weighted images) in different tissues, healthy or pathological (**Figure 1**).

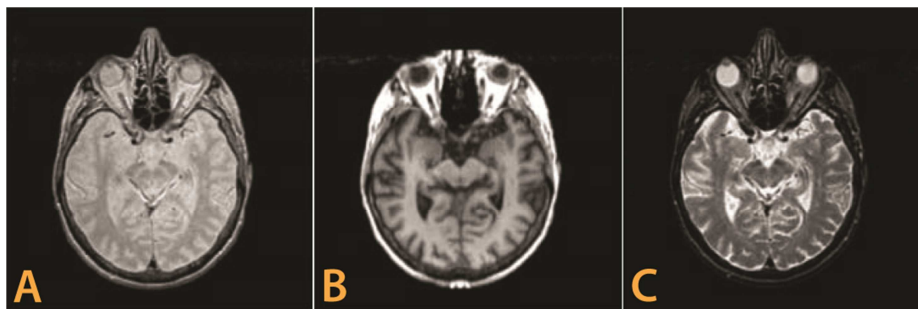


Figure 1: A: Proton density, B: T_1 - and C: T_2 -weighted MR images of a human brain. Adapted from [12].

As the human body is mostly composed of water ($\sim 70\%$), almost any tissue type generates a ^1H NMR signal and, therefore, relevant diagnostic information from MR images can be obtained even with a natural contrast. However, for further extension of the level of image contrast and resolution of anatomical features (*e.g.* to differentiate between cancerous and healthy tissue), exogenous MRI

[†] The longitudinal relaxation time T_1 characterizes the time at which the z -component of the nuclear spin magnetization vector (M_z) recovers towards its thermodynamic equilibrium (z -axis is parallel with B_0).

[‡] The transversal relaxation time T_2 characterizes the time at which the xy -component of the nuclear spin magnetization (M_{xy}) recovers towards its thermodynamic equilibrium.

contrast agents (CAs) were developed very soon after foundation of the method.¹³ Using CAs greatly enhances, for example, the possibility to depict disruption of the blood-brain barrier and the morphological details of lesions.¹⁴ With MR CAs, it also becomes possible to improve MRI sensitivity to detect and assess ischemically injured myocardium¹⁵ or, for example, to monitor vascular flow of the large arteries and veins using MR angiography.¹⁶ CAs also enable specific cell labelling and subsequent monitoring of the labelled cells *in vivo*.¹² Thus, the application of CAs has become an indispensable tool of modern medicine.

4.1 T_1 AND T_2 CONTRAST AGENTS

The most widely used CAs are those that enhance MR contrast by reducing the T_1 and/or T_2 relaxation times of the surrounding nuclei (*i.e.* bulk water protons) and provide an increase/decrease in the ^1H MR signal intensity of the affected tissue using a suitable measuring pulse sequence. Those that predominantly reduce T_1 are called “positive CAs” and, in T_1 -weighted images, their application results in increases in signal intensity. Those that affect T_2 are known as “negative CAs” and, in T_2 -weighted images, they provide reductions of signal intensity.¹⁷ The efficiency of the CAs is commonly expressed in terms of relaxivity r_i (where $i = 1, 2$ correspond to the particular relaxation processes; longitudinal or transversal) which is defined as the longitudinal or transversal relaxation rate $R_i (= 1/T_i)$ of water protons observed for millimolar solution of the CAs.¹⁰

From the chemical point of view, T_1 -CAs are complexes of appropriate organic ligands with highly paramagnetic metal ions, such as Mn(II), Fe(III) or Gd(III). These ions have a symmetric electronic state (d^5 , f^7) and, thus, a relatively long electronic relaxation time which is needed for efficient relaxation of neighbouring molecules. In these complexes, the presence of a water molecule coordinated to the central metal ion is needed because this water molecule exchanges with the surrounding water molecules and transfer the paramagnetic information to the bulk water. Therefore, efficiency of the T_1 -CAs depends on the number of inner-sphere water molecules (hydration number q). It also depends on the distance between the metal ion and the protons of the coordinated water molecule and on numerous physico-chemical parameters including residence time of the coordinated water molecules (τ_M), rotational correlation time of the complex (τ_R), and interaction of the complex

with water molecules in the second and outer spheres (hydration number q_{ss} and mean residence time τ_{Mss}).¹⁰ Currently, the mostly used T_1 -CAs are complexes that consist of a multidentate ligand and Gd(III) ion. However, free Gd(III) is significantly toxic. The ionic radius of this ion is close to that of Ca(II) and, therefore, this element is a blocker of many types of voltage-gated calcium channels.¹⁸ Thus, the ligands have to exhibit complexation selectivity for Gd(III) over endogenous metal ions such as Zn(II), Mg(II) or Ca(II) and the complexes must be thermodynamically stable. Another important toxicological feature is the rate of decomplexation and transmetalation in comparison with the rate of excretion of the complex from the body.^{10,19}

The most commonly used commercial T_1 -CAs utilize two types of octadentate polyamino-polycarboxylic ligands which employ nitrogen and oxygen donor atoms to coordinate the Gd(III) ion. The first type of ligands includes acyclic diethylenetriamine derivatives with several chelating pendant arms. The second type are tetraazamacrocyclic cyclen derivatives (cyclen = 1,4,7,10-tetraazacyclododecane). Selected Gd(III) complexes used in clinical practice are shown in **Figure 2**.¹⁰

On the other hand, T_2 -CAs are mostly superparamagnetic nanocrystalline iron oxides (maghemite γ -Fe₂O₃ or magnetite Fe₃O₄), for example coated by dextrans or siloxanes. The coated nanoparticles of several substituted ferrites (MnFe₂O₄, CoFe₂O₄, NiFe₂O₄ *etc.*), bivalent metal-doped lanthanide manganites with the perovskite structure (Ln_{1-x}M_xMnO₃) or lanthanide(III) oxides, such as Dy₂O₃, have also been investigated as potential T_2 -CAs.^{20,21,22} Nanoparticles of iron oxides are divided into three categories according to their hydrodynamic size, as follows: a) USPIO (Ultra-Small Super Paramagnetic Iron Oxides; <50 nm); b) SPIO (Super Paramagnetic Iron Oxides; hydrodynamic diameter from 50 nm to several microns); and c) MPIO (Micron-Sized Iron Oxide Particles) and their biological distribution and blood half-life is directly dependent on their size.¹²

Nanoparticles of iron oxides have a very large magnetic moment and create a strong magnetic field inhomogeneity around them and, thus, they considerably reduce the T_2 relaxation time of the water protons in their vicinity.^{12,20,23} The commercial T_2 -CAs based on iron oxide nanoparticles used in clinical practice are specifically SPIO and USPIO particles. Some SPIO nanoparticles are in clinical trials or already approved for the detection of liver metastases. A typical clinical application of USPIOs is lymph-node imaging.^{12,23,24}

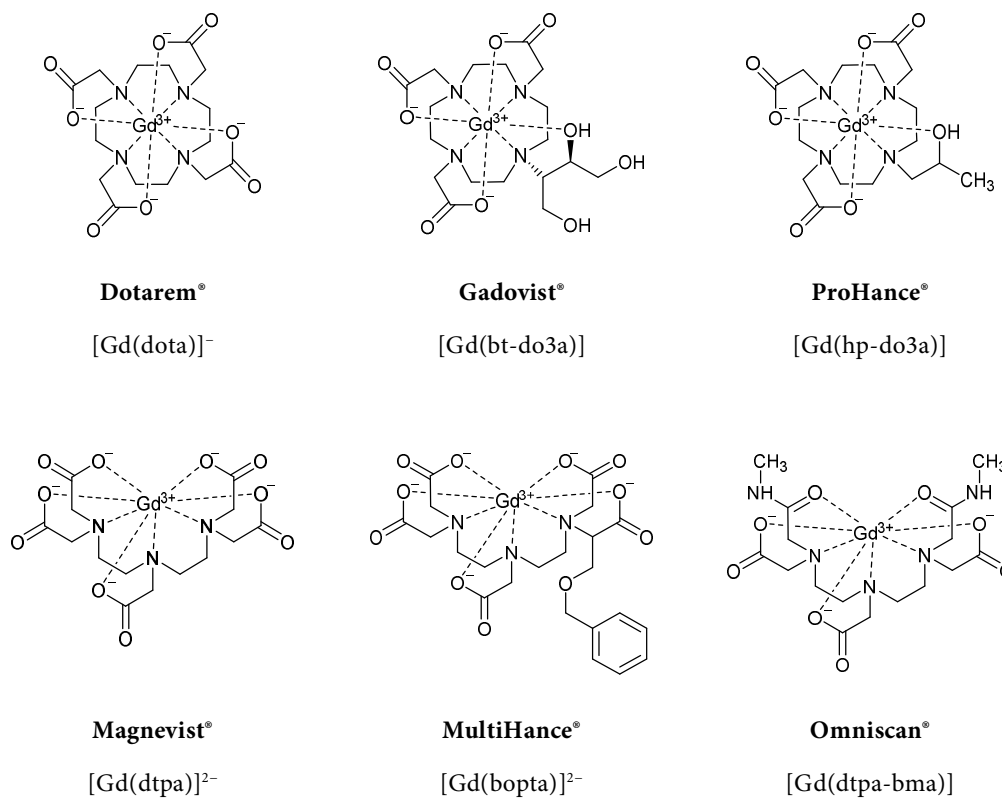


Figure 2: Selected clinically used Gd(III)-based MRI CAs. Coordinated water molecules ($q = 1$ in all cases) are omitted for clarity.

4.2 CEST CONTRAST AGENTS

4.2.1 History

Recently, a new class of MR CAs that operate through a completely different mechanism called Chemical Exchange Saturation Transfer (CEST) was introduced. The effect of chemical exchange process on NMR spectra was reported in 1951 and, in the years since then, it has been intensively investigated.²⁵ In 1957, Harden M. McConnell and Don D. Thompson used modified Bloch equations to describe a new transient nuclear magnetic resonance effect arising from the rapid transfer of non-equilibrium nuclear spin magnetization from one magnetic environment to another. They applied this method to study proton transfers between ammonium ions in acidified solution of ammonium

nitrate.²⁶ However, the first chemical exchange saturation transfer experiments were performed in 1963 by Sture Forsén and Ragnar A. Hoffman when they studied proton transfer rates between salicylaldehyde and water.²⁷ In 1989, Robert S. Balaban and Steven D. Wolff calculated the pseudo-first-order rate constant for the transfer of magnetization between water and exchangeable protons of some macromolecules in kidneys and skeletal muscle and introduced an alternative way to produce MR images using presaturation pulses.²⁸ They also studied proton exchange between ammonium chloride and water; they found that only the water resonance could be detected in the ¹H NMR spectrum while the ammonium proton signal was invisible. However, when they applied a RF presaturation pulse at the ammonium proton resonance frequency, they detected a decrease in the water signal intensity and they called this new MRI contrast mechanism chemical exchange saturation transfer (CEST).^{29,30} This approach has garnered significant attention as the same group has demonstrated that low-molecular-weight compounds containing OH and NH groups able to exchange protons with the bulk water may also be used to alter tissue contrast *via* saturation transfer. This new class of agents was named CEST CAs.^{31,32}

4.2.2 Principle

The mechanism of CEST imaging is based on chemical exchange of bulk water protons with labile (exchangeable) protons of some specific functional group (such as hydroxyl, amide, amine, thiol) or, in the case of paramagnetic metal complexes, with protons of a coordinated water molecule which resonate at a frequency different from that of the bulk water protons. At equilibrium, the number of spins aligned with the magnetic field slightly exceeds the number aligned against it (**Figure 3**). When a selective RF presaturation pulse is applied at the resonance frequency of the exchanging site, the Boltzmann distribution of nuclear spins is temporarily altered and the number of spins aligned against the field is increased. When the number of spins aligned with (N_α) and against (N_β) the field is equal ($N_\alpha = N_\beta$), the system is said to be saturated and no signal is observed in the NMR spectrum (**Figure 3**).^{27, 33} In the case that the exchange rate constant (k_{ex}) between exchanging site (H) and bulk water protons (H₂O) is not greater than the difference in Larmor frequency ($\Delta\omega$) between these two

chemical environments ($k_{ex} \leq \Delta\omega$), and the longitudinal relaxation rates (R_1) of two pools, H and H₂O, are lower compared to the rate of the exchange between these two pools, the saturation is transferred to the surrounding bulk water molecules (H₂O). It results in a decrease in the water signal intensity and, thus, in darkening of the corresponding area in the MR image (**Figure 3**).³³

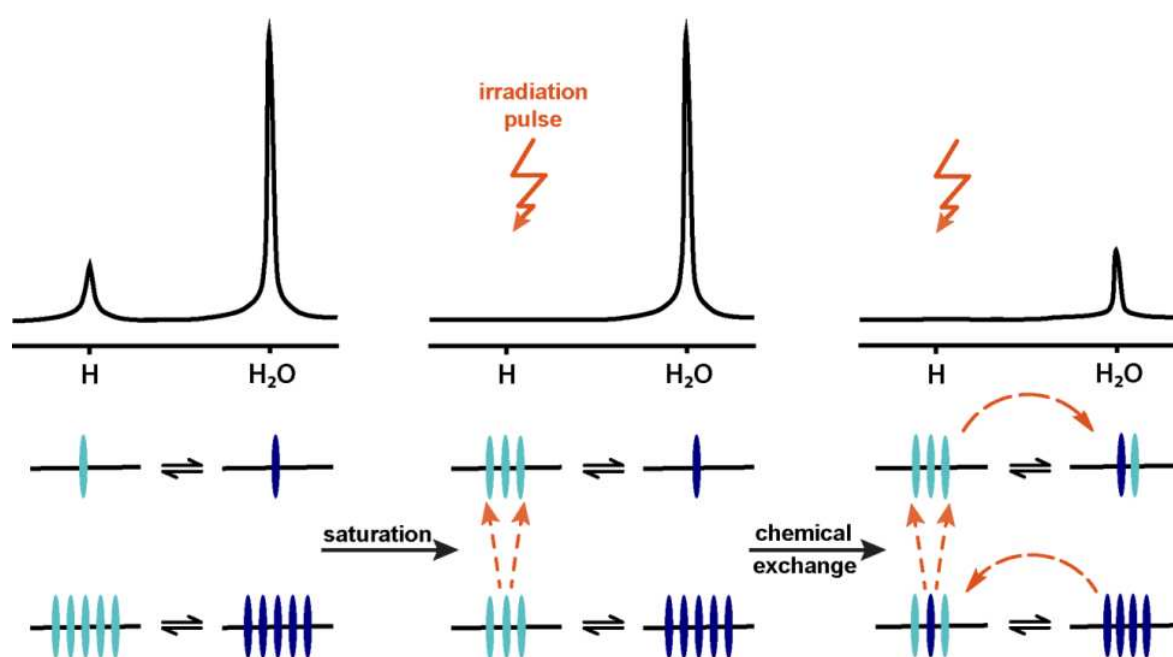


Figure 3: Schematic representation of spins distribution and simulated NMR spectra of two chemically distinct pools of nuclei (exchangeable and bulk water protons).

Results of CEST experiments are usually presented as so-called CEST spectra (or Z-spectra), *i.e.* as a dependence of the normalized bulk water signal intensity (magnetization; M_z/M_0) as a function of presaturation frequency. M_z corresponds to the water signal when a presaturation pulse is applied and M_0 represents magnetization of the water signal without RF saturation. The bulk water signal is commonly referenced as 0 ppm (**Figure 4**). Sometimes it is difficult to quantify the CEST effect due to close proximity of the CEST signals of exchangeable protons with the regions affected by direct water

presaturation. The magnitude of the CEST effect can therefore be better described in terms of a magnetization transfer ratio (MTR) parameter,³⁴ defined as (Equation 1)

$$\text{MTR} = M_{\Delta\omega}/M_0 - M_{-\Delta\omega}/M_0 \quad (1)$$

where $M_{\pm\Delta\omega}$ is the magnetization (*i.e.* intensity) of the water signal with the use of a presaturation frequency $\pm\Delta\omega$ away from the bulk water signal (Figure 4D).

4.2.3 PARACEST CAs

The first molecules used to demonstrate the CEST effect were diamagnetic endogenous compounds and, therefore, they had chemical shifts of labile protons not much different from that of bulk water. Recently, this modality has been extended to exogenous paramagnetic complexes to produce an MR contrast called PARAMagnetic CEST (PARACEST) effect. Paramagnetic agents enlarge the frequency range for exchanging sites by a few orders of magnitude (up to several hundred ppm). Therefore, these agents allow easy saturation of one of the exchangeable pools without partial saturation of the bulk water pool, *i.e.* reduce non-specific proton irradiation.^{33, 35} Moreover, paramagnetic complexes can provide additional saturation transfer between the bulk water and the water molecule coordinated to the central metal ion.¹³

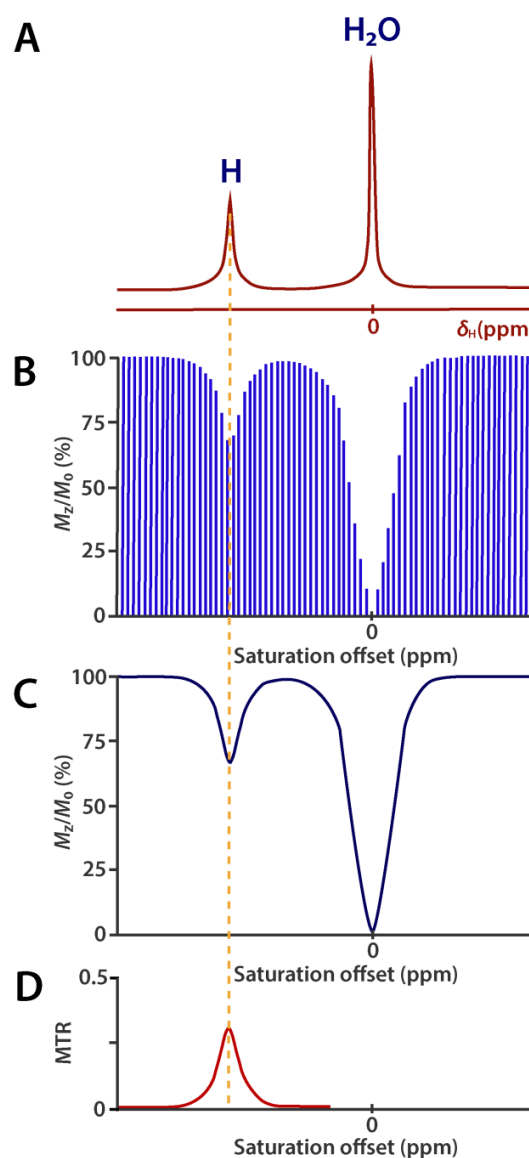


Figure 4: Schematic representation of **A:** ^1H NMR spectrum, **B:** bulk water signal intensity (magnetization; M_z/M_0) at different presaturation frequencies, **C:** corresponding Z- (or CEST) spectrum and **D:** MTR spectrum.

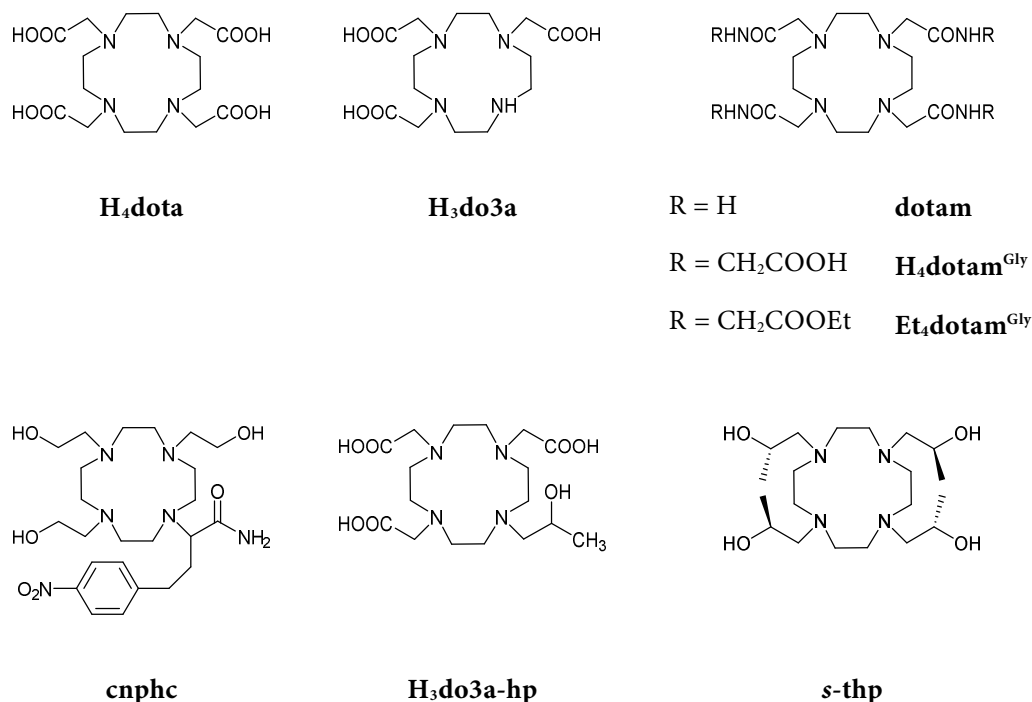


Figure 5: Macrocyclic ligands discussed in the text.

Most often, PARACEST CAs are complexes of macrocyclic (DOTA- or DO3A-like) ligands with lanthanide(III) ions ($\text{Ln} \neq \text{Gd}, \text{La}, \text{Lu}$). In 1998, S. Aime *et al.* reported the possibility to detect a ^1H NMR signal of bound water of $[\text{Eu}(\text{dotam})(\text{H}_2\text{O})]^{3+}$ complex (**Figure 5**) at low temperature in acetonitrile- d_3 .³⁶ Several years later, A. D. Sherry and co-workers were the first who demonstrated utilization of the lanthanide(III) complexes of the DOTA tetraamide derivative ($\text{Et}_4\text{dotam}^{\text{Gly}}$; **Figure 5**) for CEST imaging. These complexes exhibit unusually slow bound-water exchange (*i.e.* long residence time τ_{M}) in aq. solution (3–380 μs , depending on the Ln^{3+}). They found, from a series of lanthanide(III) complexes with different ligands, that the complex $[\text{Eu}(\text{Et}_4\text{dotam}^{\text{Gly}})(\text{H}_2\text{O})]^{3+}$ (which has a bound-water signal near $\delta_{\text{H}} = 50$ ppm with an exchange lifetime $\tau_{\text{M}} = 382$ μs)³¹ appears to be the most favourable PARACEST agent showing the largest CEST effect.^{37,38} Later on, S. Aime *et al.* investigated CEST properties of another series of Ln(III) complexes ($\text{Ln} = \text{Eu}, \text{Dy}, \text{Ho}, \text{Er}, \text{Tm}$ and Yb) with $\text{H}_4\text{dotam}^{\text{Gly}}$ (**Figure 5**). These complexes possess two pools of exchangeable protons. The first one is represented by the protons of a coordinated water molecule and the second one belongs to the amide protons. The

amide groups (or, in general, other suitable functional groups) are an alternative source of highly shifted exchangeable protons and might offer an advantage in increasing the number of labile protons (for example, there are four exchanging amide protons in these complexes compared to only two protons of coordinated water molecule). Consequently, the CEST effect of these CAs could be more intensive and, thus, their administered dose could be lower. Moreover, the exchange rate of the amide protons is base-catalysed and it was shown that the CEST effect of $[\text{Yb}(\text{dotam}^{\text{Gly}})]^-$ is strongly pH-dependent and this complex could be efficient pH-responsive probe in the physiological pH range.³⁹ Interesting behaviour was also found in the case of $[\text{Yb}(\text{dotam})]^{3+}$ complex with two magnetically non-equivalent amide protons on each amide group which appear as two broad CEST peaks at -14.5 and -17.7 ppm. Chemical exchange of these protons lays, depending on the pH (from 6.5 to 7.8), in the 440–5000 μs range.⁴⁰

More recently, M. Woods *et al.* identified another potential exchangeable group in Ln(III) complexes when they introduced hydroxyethyl pendant arms.⁴¹ Such a type of ligands has been widely employed for chelation of the Ln(III) ions and, thus, it is known that the hydroxyl groups of these ligands at neutral pH retain their protons upon coordination to a metal ion.⁴² This group then provides another type of chemical exchange site for the CEST activation.^{33,41,43} It was shown that the proton exchange rate of $[\text{Eu}(s\text{-thp})(\text{H}_2\text{O})]^{3+}$ complex^{§,44} (**Figure 5**) in aqueous solution is so fast that no appreciable CEST effect can be observed.⁴¹ On the other hand, Eu(III) complex of *cnphc* (**Figure 5**) possesses three CEST signals from the pendant nonequivalent hydroxyethyl groups, one CEST signal of coordinated water molecule and another one corresponding to exchange of the amide proton. However, this complex showed the CEST effect of the coordinated alcohol groups in acetonitrile as a solvent but not in pure water.⁴¹ Later on, Ce(III) complex of the *s-thp* was introduced as the first PARACEST agent that exhibits a CEST spectrum of alcohol group in aqueous solution at $\text{pH} = 7.0$.⁴⁵ Unfortunately, the CEST signals of these complexes are not highly shifted away from bulk water and the most efficient CEST probe, $[\text{Yb}(s\text{-thp})]^{3+}$, produces CEST effect only at acidic pH. Recently, it has been reported that Yb(III) analogue of the clinically used $[\text{Gd}(\text{do3a-hp})(\text{H}_2\text{O})]$ complex (ProHance®;

[§] *s-thp* = the stereoisomer of *thp* with all hydroxypropyl groups with the *S*-configuration.

Figure 2; ligand structure is shown in **Figure 5**) has CEST signals of the coordinated alcohol groups more shifted away from that of bulk water peak in the physiologically relevant pH range (two isomers; ~70 and ~100 ppm at pH = 7.3).⁴⁶

It has been demonstrated that administration of Ln(III)-based CAs to patients with severe renal insufficiency can result in a serious disease called nephrogenic systemic fibrosis (NSF).⁴⁷ NSF is a fibrosis of skin and internal organs related to exposure to the free Ln(III) ions which are released from the MRI CAs due to their prolonged stay in a blood pool of patients with impaired kidney function. Therefore, complexes that employ some endogenous transition metal ions with suitable magnetic properties, such as Fe(II), are another promising class of PARACEST agents and could be an alternative to lanthanide(III) CAs for patients with renal failure and predisposition to NSF. These are mainly complexes with derivatives of cyclen (1,4,7,10-tetraazacyclododecane), TACN (1,4,7-triazacyclononane) or 1,4,10-trioxa-7,13-diazacyclopentadecane having 2-hydroxypropyl or acetamide pendant arms, or with pendants containing derivatives of benzimidazole or pyridine.⁴⁸ The coordination chemistry of transition metal ions is different from that of the Ln(III) ions and, thus, this leads to new challenges in design of PARACEST CAs. Besides complexes of endogenous Fe(II), the PARACEST properties of Ni(II) and Co(II) complexes were also studied.⁴⁹ However, potential *in vivo* applications of these compounds require (as well as in the case of Ln(III) complexes) a high kinetic inertness of the metal complexes towards dissociation/transligation/transmetalation.

4.2.4 Advantages of PARACEST CAs

One of the major advantages of PARACEST CAs is the possibility to turn the image contrast produced by these agents “on” and “off” by application of a frequency-selective RF presaturation pulse and, thus, to modulate the water signal intensity at will. This feature makes it possible to get a response after the saturation of different CEST sites in the same experiment, *i.e.* to detect different exchanging sites of one agent or to detect several agents with different CEST signals in the same sample. This fact makes it possible to visualize and monitor labelled cell cultures after cell transplantation in one MR experiment or to detect different CEST signals for ratiometric purposes.

Moreover, MRI contrast produced by these agents is extremely sensitive to proton exchange rates (k_{ex}) and, therefore, to a number of external factors. This feature makes them attractive for measuring various physiological parameters, such as temperature, pH, metabolite or metal ion concentration. In addition, it is possible to use PARACEST CAs for quantitative concentration-independent measurements using ratiometric methods. Therefore, these agents extend the imaging capabilities of MRI and they could be used as biologically responsive sensors.¹³

4.3 pH IMAGING

In living systems, variations of physicochemical parameters (as concentration of ions and metabolites in tissues or in cellular microenvironment) can provide important information about the status of healthy or diseased tissues, organs and tumours.¹⁷ Therefore, nowadays, MRI CAs (usually called “responsive” or “smart”) with the ability to detect these parameters are of the great interest of researchers.^{12,16}

It is known that an extracellular tumour microenvironment is often slightly acidic (pH is about 0.5–0.6 units lower than that of healthy tissue).¹² It is caused by reduced buffering capacity, poor perfusion, and accumulation of lactic acid from increased anaerobic glycolysis.⁵⁰ Therefore, it is expected that measurement of extracellular pH *in vivo* using non-invasive techniques should provide important information for early detection of disease or some metabolic disorders. Moreover, it was demonstrated that some hypoxic tumour cells are resistant to radiation and to many anticancer drugs (a lower tumour pH can provide resistance to chemotherapeutics that are weak bases and/or enhance the efficacy of chemotherapeutics that are weak acids).^{51,52} Therefore, ability to detect extracellular pH could also be useful for suggesting the most efficient treatment or for monitoring the effects of pH-altering therapies.^{16,53} For the reasons mentioned above, it is unsurprising that this Thesis is focused on such responsive CAs that are pH-sensitive.

4.3.1 Gd(III)-based CAs

Several MRI approaches have already been devised to map pH. Some of them exploit endogenous MR resonances while others require the administration of exogenous CAs. Previous works have suggested relaxation-based MRI CAs, mainly Gd(III) complexes, with the longitudinal relaxivity (r_1) dependent on pH.⁵⁴ Some of them were based on a variation in the hydration state of the complex (*i.e.* on the number of inner-sphere water molecules q). Interesting results have been obtained, for example, with a series of Ln(III) macrocyclic complexes based on DO3A with variation of the p -substituent in the β -arylsulfonamide group in the pendant arm ($H_3do3a-sa-R$; **Figure 6**). It was shown that (de)protonation of this group and, thus, a change in the coordination ability of the β -arylsulfonamide pendant arm, is associated with changes in the number of coordinated water molecules ($q = 2$ at low pH to 0 at high pH values). It results in significant changes in relaxivity r_1 .⁵⁵

Similar features were found in the case of Gd(III) complexes based on DO3A with 2-aminoethyl ($H_3do3a-ae$; the results were published during work on this project)⁵⁶ or methylene- p -nitrophenol⁵⁷ pendant arms ($H_3do3a-mnp$; **Figure 6**). Strong and reversible pH-dependent relaxivity changes related to (de)protonation of the 2-aminoethyl/phenolic group were observed. Other interesting results have been obtained by J. Hall *et al.*,⁵⁸ who studied the Gd(III) complex with terpyridine-containing macrocycle, which demonstrated a significant decrease of relaxivity with increasing pH. The authors attributed it to a decrease in q from 3 to 0. These changes were ascribed to formation of the hydroxido species and hydroxido-bridged dimer with a negligible exchange rate of the coordinated OH^- ions.⁵⁸ However, an important limitation of the MRI methods for determination of pH using relaxation-based CAs is fact that the relaxation enhancement of these complexes is also dependent on their concentration. Therefore, it becomes difficult to distinguish whether the observed changes in MRI images are caused by changes in pH or changes in concentration of the probe and it, of course, requires separate measurement of agent concentration to obtain quantitative results. Thus, novel methods based on ratiometric approaches are investigated in order to remove dependence of the measurement on the local concentration of the CAs.^{17,19,59}

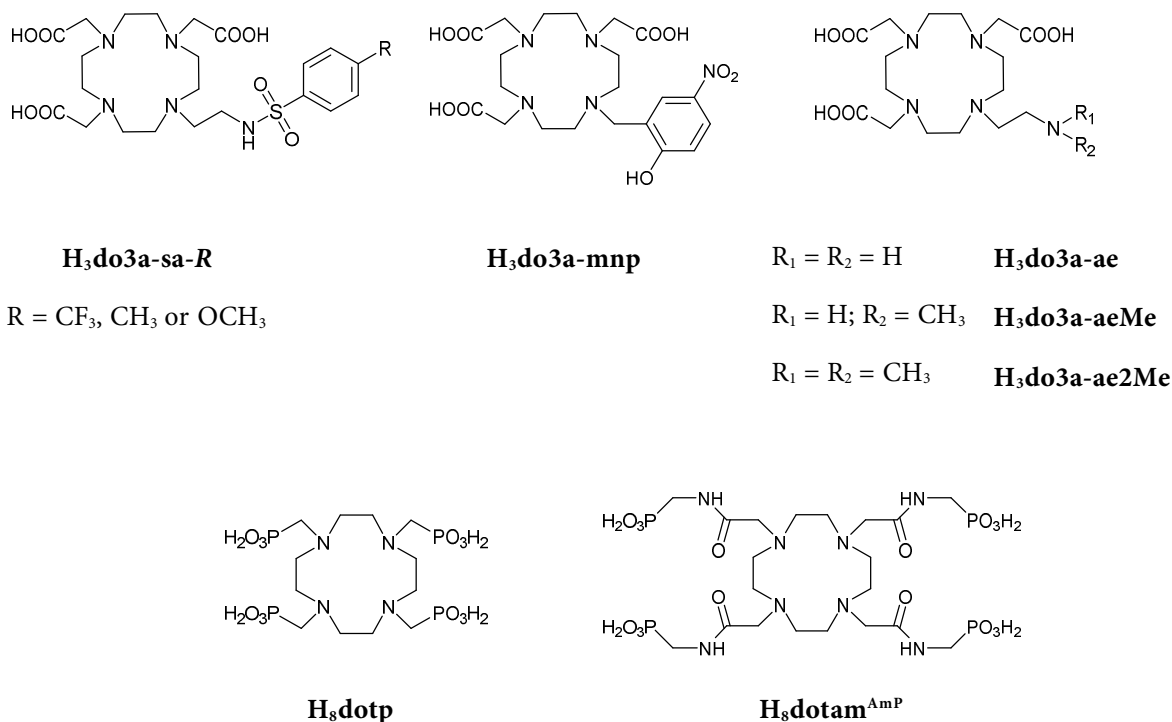


Figure 6: Macrocyclic ligands discussed in the text.

The first concentration-independent method was proposed in 2003 by A. D. Sherry, R. J. Gillies and co-workers.^{54b} They developed a relaxivity-based dual-contrast-agent strategy using two different Gd(III) complexes to obtain a pH map of mice kidneys and rat glioma. This method consists of consecutive injection of two compounds, pH-insensitive [Gd(dotp)]⁵⁻ and pH-sensitive [Gd(dotam^{Amp})]⁵⁻ complexes (**Figure 6**) containing four ionisable phosphonate groups. These complexes have similar tissue pharmacokinetics and biodistribution. Hence, the pH-insensitive CA can be used to predict concentration of the pH-sensitive one: knowledge of this local concentration allows access to a relaxivity-based image that directly reports on the pH-differences.^{20,54b,60} An alternative approach, introduced by E. Terreno and co-workers, deals with measurement of the ratio of transversal and longitudinal relaxation rates of water protons (R_2/R_1) after the injecting of a single paramagnetic Gd(III) complex of DOTA-functionalized polypeptide (poly-L-ornithine). Depending on the protonation state, this complex changes its τ_M or rotational mobility; it therefore allows an assessment which is independent of contrast agent concentration.⁶¹

4.3.2 PARACEST CAs

Another concentration-independent approach for detection of pH is based on (PARA)CEST agents having two independent and selectively detectable CEST signals. They can originate from two different exchangeable proton pools of the same molecule or from two conformations of the same complex generating CEST signals at different chemical shifts.¹⁶

As mentioned above, in 2002 S. Aime *et al.* explored the PARACEST properties of a series of Ln(III) complexes with the macrocyclic ligand H₄dotam^{Gly} (**Figure 5**). They proposed a ratiometric method utilizing a bound water exchange site from one PARACEST agent and an amide proton exchange site from another [mixture of Eu(III) and Yb(III) complexes was tested]. This ratiometry is possible because the exchange rate of amide protons of the [Yb(dotam^{Gly})]⁻ complex is base-catalysed and responsive to pH changes, and the CEST effect arising from the bound water of the [Eu(dotam^{Gly})(H₂O)]⁻ is pH-independent in the physiological pH range (*i.e.* pH = 6–8).^{**39} Later on, an improvement of this procedure was demonstrated when it was shown that the paramagnetic H₄dotam^{Gly} complexes of “lighter” Ln(III) ions (Pr, Nd and Eu) behave as pH-responsive “single-molecule” CEST agents. These agents have two CEST-active exchanging pools (protons of the coordinated water molecule and amide protons) with different pH dependencies of their CEST effects. Thus, the CEST signals can be analysed on a ratiometric basis allowing the pH readout.⁶²

Results of the experiments with Yb(III) complex of H₃do3a-hp (**Figure 5**), which is analogue of clinically used MRI CA, [Gd(do3a-hp)(H₂O)] complex (ProHance[®]), seem very promising.⁴⁶ This PARACEST probe is responsive to pH and also to temperature irrespective of the complex concentration. In this case, the proton exchanging pools are represented by the hydroxyl protons of two diastereoisomers (SA, Square Antiprism and TSA, Twisted Square Antiprism) of the same complex (well resolved PARACEST peaks at 71 and 99 ppm; pH = 5, 20 °C) and can be used to devise a

** The [Eu(dotam^{Gly})(H₂O)]⁻ complex also possesses one pool of the exchangeable protons of the amide groups in the ¹H NMR spectra. However, the first attempts to detect the CEST effect arising from the irradiation of the amide protons were unsuccessful because of the small chemical shift difference (~4 ppm) between the bulk water and amide-protons signals.

ratiometric concentration-independent procedure for pH mapping.⁴⁶ This probe has already been tested as a pH probe in mice murine melanoma.⁵³

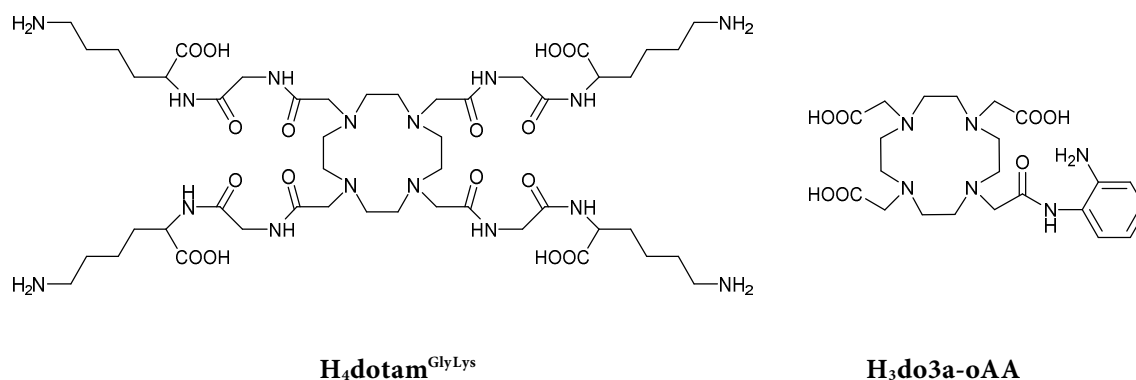


Figure 7: Ligands discussed in the text.

A novel method for *in vivo* extracellular pH measurement using amide protons of Tm(III) complex of H₄dotam^{GlyLys} (**Figure 7**) was also presented. This approach uniquely determines pH from the linewidth of the CEST signals in MTR spectrum.⁶³ The CEST signal of amide proton at -10 ppm (in combination with the CEST signal of amine protons at +10 ppm) of Yb(III) complex with H₃do3a-oAA (**Figure 7**) was also used to accurately measure pH with a single CA using ratiometry and some preclinical *in vivo* experiments with tumour tissues were presented.⁶⁴

4.3.3 Agents for Magnetic Resonance Spectroscopy (MRS)

MRS (Magnetic Resonance Spectroscopy) is an alternative approach for concentration-independent *in vivo* pH-determination exploiting endogenous and exogenous MR resonances. In general, such a method is a clinical imaging tool for detection of tissue metabolites *in vivo* to provide information about neurological, psychiatric and metabolic diseases.⁶⁵ In addition, spectral information of a metabolite/compound with a particular chemical shift can be encoded into the image and a map of its spatial distribution can be reconstructed by a method called Magnetic Resonance Spectroscopic Imaging (MRSI). MRS approaches for pH mapping are generally based on a difference in chemical

shifts between pH-dependent and pH-independent resonances and, over the years, several techniques and agents have been tested for this purpose.

It was shown that intracellular inorganic phosphate concentrations (P_i) are 2–3 mM, compared to ca. 1.0 mM for extracellular environment.⁵⁰ Therefore, the majority of P_i resonance is intracellular. As the resonance frequency of P_i is pH dependent in the physiological pH range (appropriate pK_a is ~7.2), intracellular pH (pH_i) may be estimated by measuring the ^{31}P NMR chemical shifts of this anion and some pH-independent compound as a reference compound (phosphocreatine or α -phosphorus atom of ATP).⁶⁶ On the other hand, extracellular pH (pH_e) of tumours in animal models has been monitored by administration of some nontoxic and membrane impermeant exogenous agents such as 3-aminopropylphosphonic acid (3-APP; **Figure 8**) with a chemical shift dependence of ~1 ppm per pH unit [$\delta_p = 24.32 \pm 0.01$ and $\delta_p = 21.10 \pm 0.01$ ppm for zwitterionic $\text{NH}_3^+(\text{CH}_2)_3\text{PO}_3\text{H}^-$ and deprotonated $\text{NH}_3^+(\text{CH}_2)_3\text{PO}_3^{2-}$ form, respectively; $pK_a = 6.9$].^{12,50,67}

Probes with the pH-sensitive ^{19}F signals having an advantage in total lack of endogenous ^{19}F resonances in normal tissues have also been developed. Fluorinated derivatives of vitamin B6, 6-FPOL and 6-FPAM, *i.e.* 6-fluoropyridoxol ($pK_a = 7.05$)⁶⁸ and 6-fluoropyridoxamine ($pK_a = 8.2$)⁶⁸, respectively (**Figure 8**), allow the measurement of both intra- and extracellular pH in rat tumours.⁶⁹

It was also shown that tissue pH can also be detected *in vivo* using probes with pH-sensitive ^1H nucleus.¹² For example, the imidazole ring has $pK_a = 6.49$ (*i.e.* close to physiological pH) and its three aromatic proton NMR resonances have chemical shifts far away from the water signal. Therefore, the imidazole ring-containing molecules are suitable candidates for this purpose. An exogenously administered 2-(imidazol-1-yl)-3-ethoxycarbonyl-propanoic acid (IEPA; **Figure 8**) has been utilized in non-invasive determination of pH_e of breast cancer or brain tumours *in vivo* using ^1H MRS.⁷⁰ This compound is nontoxic with pH-dependent chemical shift of the C-2 hydrogen atom resonance in the 7–9 ppm range.^{12,50}

However, the disadvantage of using diamagnetic compounds as pH probes for MRS is the fact that their signals can be overlapped with existing *in vivo* resonances. That is why macrocyclic complexes of paramagnetic Ln(III) ions have also been tested. The Yb(III) complex of H_8dotp has been introduced as a prototype of pH indicators because stepwise protonation of the complex is

accompanied by variations in the proton chemical shifts (6 signals in ^1H NMR spectrum). This enables creation of a calibration curve for determination of pH.⁷¹ Recently, it has been demonstrated that pH and temperature can be simultaneously measured using a three-dimensional chemical shift imaging (CSI) method called Biosensor Imaging of Redundant Deviation in Shift (BIRDS) that combines a high spatial resolution MRI with a high molecular specificity MRS. It was shown that Tm(III) complex of H_8dotp (**Figure 6**) infused through the blood stream can be used for pH and temperature determination of rat brain *in vivo*.⁷² Chemical shifts of nonexchangeable protons of this complex are shifted due to their close proximity to the metal ion. Protonation of the phosphonate groups of the pendant arms affects the molecular structure of the complex and, therefore, the chemical shifts of the proton signals are shifted in response to pH changes. Moreover, the proton chemical shifts also have temperature sensitivity and, therefore, it is possible to use 3D calibrations (chemical shift vs. pH vs. temperature) of different protons signals for pH and temperature determination. Complexes of Tm(III) and Yb(III) ions with phosphonate-carboxamide ligand $\text{H}_8\text{dotam}^{\text{AmP}}$ (**Figure 6**) also exhibit suitable pH sensitivity for BIRDS detection using chemical shift difference between two proton resonances. In addition, these agents are also CEST-active and, thus, the CEST effect observed together with BIRDS opens the way towards high-resolution and quantitative pH imaging.⁷³

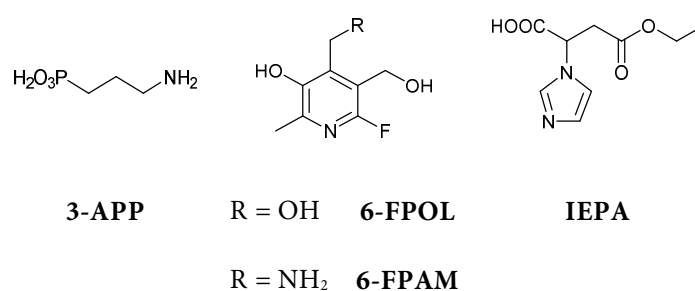


Figure 8: Compounds discussed in the text.

A large number of different approaches and probes for potential utilization in pH mapping has been reported in the literature and it is unsurprising that a current challenge is translation of the promising *in vitro* results into *in vivo* applications.

5 AIMS OF THE THESIS

The presented Thesis arose as a continuation of my previous research which has been started during my master's studies. In that work, I investigated PARACEST-related properties of a series of lanthanide(III) complexes with the CEST effect caused by amino groups coordinated to the central Ln(III) metal ions. Such a kind of PARACEST CA had not been reported in the literature. These macrocyclic ligands ($H_3do3a\text{-ae}$, $H_3do3a\text{-aeMe}$ and $H_3do3a\text{-ae2Me}$; **Figure 9**), as well as their Ln(III) complexes, were prepared and the PARACEST properties were studied by NMR spectroscopy and by MRI techniques. The first objective of this Thesis was to expand the previous work, optimize and improve synthesis of the ligands, and to study the PARACEST effect of their Ln(III) complexes in more details.

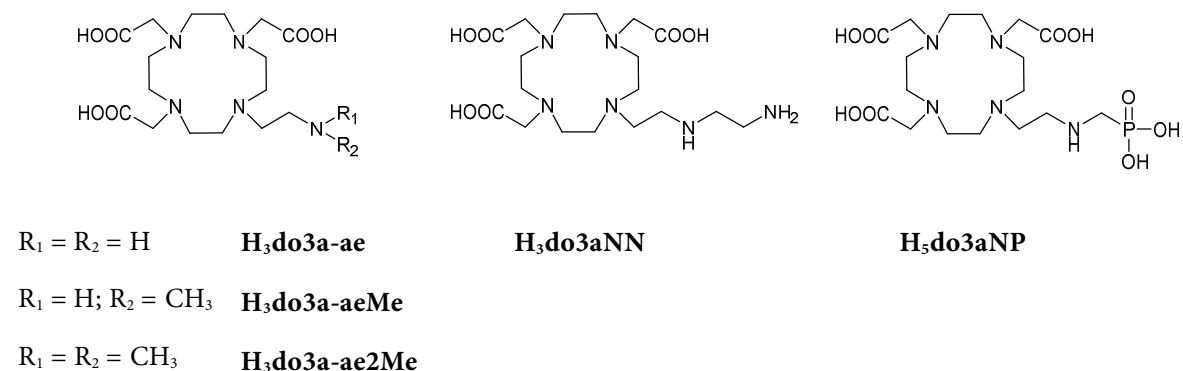


Figure 9: Structural formulas of the ligands studied in the Thesis.

It is expected that mapping tumour pH *in vivo* should provide important information concerning the aggressiveness of tumours and, thus, pH-responsive CAs are nowadays intensively investigated. They could serve as valuable markers of disease progression or indicators for the choice of the best treatment. In this respect, the second aim of this work was to synthesize a new macrocyclic ligand $H_3do3aNN$ (**Figure 9**) containing a semilabile coordinating pendant arm with two (primary and

secondary) amino groups as two potentially independent proton exchanging pools, to investigate the PARACEST properties of its Ln(III) complexes, and to develop a concentration-independent ratiometric approach for pH determination using MRI.

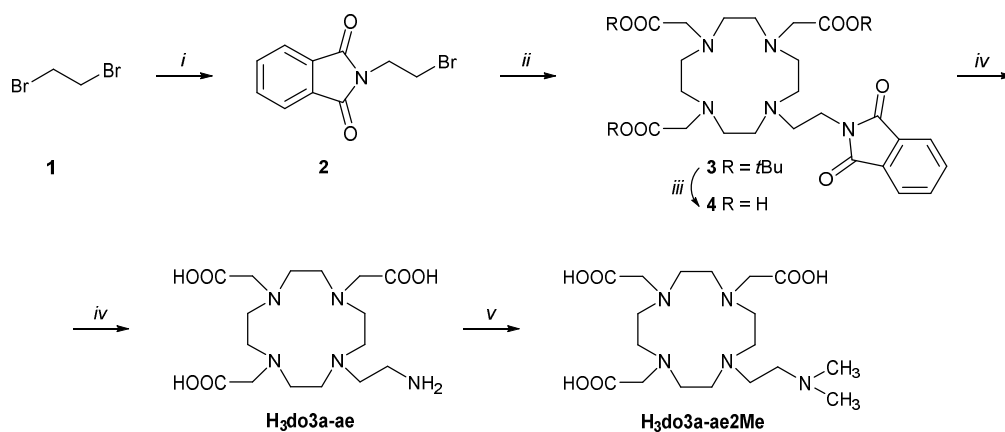
Based on the promising results of the previous study, we also defined the third goal of this project. To explore what progress could be made in the PARACEST properties of the complexes with aminophosphonate-coordinating pendant arm, a new macrocyclic ligand H₅do3aNP was designed (**Figure 9**). The Ln(III) complexes of this ligand were expected to be more kinetically inert and an existence of different isomers in solution was supposed. Isomers could provide different CEST signals to set up a ratiometric calibration that will report on the pH values, irrespective of the concentration of the CA. In addition, the presence of phosphorous atom could potentially be employed in ³¹P NMR-based applications (*e.g.* ³¹P MRS/MRSI) for determination of pH.

6 RESULTS AND DISCUSSION

6.1 LANTHANIDE(III) COMPLEXES OF AMINOETHYL-DO3A

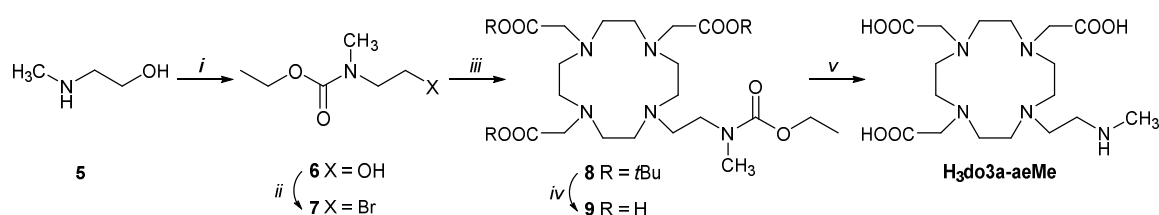
6.1.1 Synthesis and structure

Before I decided to design and synthesize Ln(III) complexes of analogues of DOTA, several PARACEST CAs were already known (see Introduction). However, the research area of the macrocyclic complexes with the CEST caused by amino groups was quite unexplored and, therefore, there was a good motivation to start with this topic. To ensure complex stability, the ligands studied in this work are based on a macrocyclic skeleton. They are derivatives of DOTA formally obtained by replacing one carboxylic arm with 2-aminoethyl pendants containing primary ($H_3do3a\text{-ae}$; referred as H_3L^1 in the paper),⁷⁴ partially methylated secondary ($H_3do3a\text{-aeMe}$; H_3L^2), and dimethylated tertiary ($H_3do3a\text{-ae2Me}$; H_3L^3) amino groups, see **Figure 9**.



Scheme 1: Synthesis of H₃do3a-ae and H₃do3a-ae2Me: (i) phthalimide, DMF, K₂CO₃, TBAB, 40 °C, 18 h; (ii) *t*Bu₃do3a-HBr, MeCN, K₂CO₃, 60 °C, 24 h; (iii) CF₃COOH/CHCl₃ (1:1), reflux, 24 h; (iv) 80% aq. NH₂NH₂·H₂O 90 °C, 18 h; (v) (CH₂O)_n, 10% aq. HCOOH, reflux, 24 h.

The ligands, as well as their Eu(III) and Yb(III) complexes, were prepared and characterized. To obtain ligand H₃do3a-ae, *N*-(2-bromoethyl)-phthalimide **2** was used as an alkylation agent reacting with *t*Bu₃do3a-HBr. After sequential deprotection by trifluoroacetic acid and hydrazine, and chromatography on an anion exchanger, the target ligand H₃do3a-ae was isolated as a zwitterion in 59% overall yield (based on *t*Bu₃do3a-HBr). Ligand H₃do3a-ae2Me with dimethylated tertiary amino group was prepared in a high yield by a simple direct methylation of H₃do3a-ae with a formaldehyde-formic acid mixture (**Scheme 1**).



Scheme 2: Synthesis of H₃do3a-aeMe: (i) CH₃CH₂OC(O)Cl, dioxan/H₂O (1:1), RT, 2 h; (ii) CBr₄, PPh₃, THF, RT, 1 h; (iii) *t*Bu₃do3a-HBr, K₂CO₃, MeCN, 60 °C, 24 h; (iv) CF₃COOH/CHCl₃ (1:1), reflux, 24 h; (v) 10% aq. NaOH, 90 °C, 24 h.

Compared to the synthesis presented in my Diploma Thesis,⁷⁵ the ligand H₃do3a-aeMe was prepared in a different way, providing a much higher yield. The 2-[*N*-(ethyloxycarbonyl)-*N*-methylamino]bromoethane **7** was synthesized by CBr₄/PPh₃ bromination of ethyl-carbamate-protected 2-(methylamino)ethanol **6**^{††} and used as the alkylation agent. By reaction with *t*Bu₃do3a-HBr, consecutive deprotection using trifluoroacetic acid and aq. NaOH, and chromatography on ion exchange resins column, the ligand was isolated in 30% overall yield (based on *t*Bu₃do3a-HBr). The structure of all three studied ligands was verified by single-crystal X-ray diffraction analysis.

Important information about potential MRI CAs can be obtained by investigation of the isomerism of macrocyclic complexes in solution (individual isomers of Gd(III) complexes can have, *e.g.* very different water exchange rates of directly coordinated water molecules, which is one of the most

^{††} In my Diploma Thesis, *N*-benzyloxycarbonyl-protected 2-(methylamino)ethanol was used for the synthesis of alkylation agent. Unfortunately, reaction of this alkylation agent with *t*Bu₃do3a-HBr provided *N*-benzylated *t*Bu₃do3a as a byproduct and, therefore, the yield of the reaction was low.

important parameters for T_1 -CAs). It is well known that Ln(III) complexes of DOTA-like ligands are usually nonacoordinated (eight donor atoms from the ligand and one site is occupied by a water molecule) and occur in solution as a mixture of isomers. The conformation of ethylene groups of the macrocycle causes one type of isomerism (δ/λ), and the orientation of the pendant arms causes the second one (Δ/Λ). A combination of these isomerisms leads to four isomers (two diastereomeric pairs of enantiomers): $\Delta\lambda\lambda\lambda/\Lambda\delta\delta\delta$ (SA; Square Antiprism) with the “oxygen” O_4 plane rotated by $\sim 40^\circ$ (ideal angle 45°) with respect to the “nitrogen” plane N_4 , and $\Lambda\lambda\lambda\lambda/\Delta\delta\delta\delta$ (TSA; Twisted Square Antiprism) where the O_4 and N_4 planes are mutually rotated by $\sim 24^\circ$ (ideal angle 22.5° , see **Figure 10**).^{10,76,77} In the case of octacoordinated species (*i.e.* without a coordinated water molecule; it was observed for small ions), these isomers are usually denoted as SA' and TSA'.

The isomer ratio in solution can be determined from the ^1H NMR spectra where the “axial” protons (**Figure 10**) of the macrocyclic chelate are the most “shifted” ones. These are closest to the Ln(III) ion and to the principal magnetic axis of the complex. The isomerism of the Eu(III) and Yb(III) complexes with $\text{H}_3\text{do3a-ae}$ was studied by variable-temperature ^1H NMR. Unfortunately, the ^1H NMR spectra of the Eu(III) complex at 25°C in slightly alkaline region (pD = 9.0; **Figure 11A**) were not

resolved enough to observe the signals of “axial” protons properly. Moreover, chemical shifts of these signals were just between the regions typical for SA(′) and TSA(′) species and, at low as well as at high

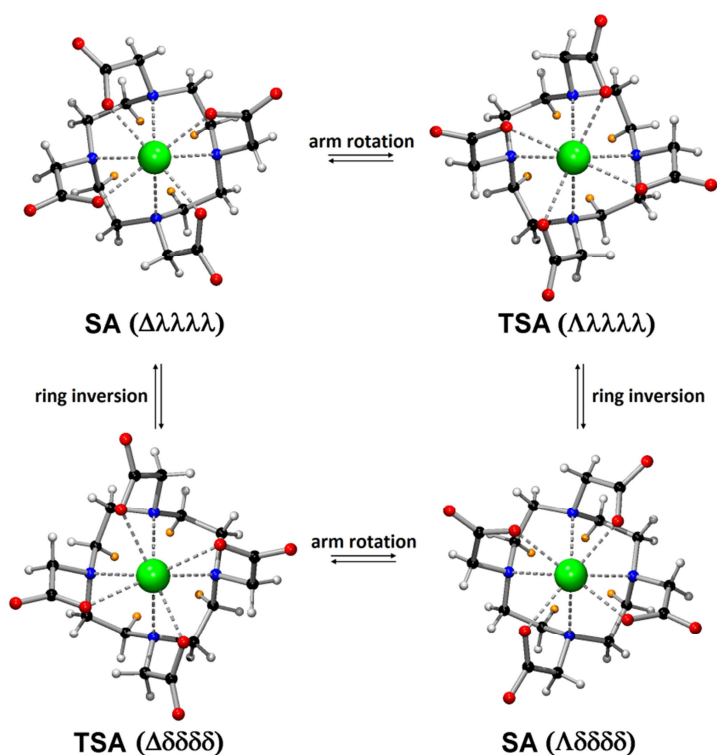


Figure 10: Illustration of possible isomers for Ln(III) complexes with DOTA-like ligands highlighting the “axial” protons (orange).

temperatures, the signals disappeared from the NMR spectra. It points to the fact that two relatively independent fluxional processes occurred, affecting the position of “axial” hydrogen atoms with respect to the Ln(III) ion and influencing its chemical shifts in the ^1H NMR. Due to these facts, we could only speculate that a mixture of SA/TSA isomers was present in solution at 25 °C.

Similarly, in the case of the Yb(III) complex (pD = 8.5, 25 °C), the signals of “axial” macrocycle protons were broad and their chemical shifts did not allow clear determination of the isomerism (Figure 11B). Heating up to 90 °C and cooling down to 0 °C led to a visual disappearance of the signals of “axial” protons. Therefore, one can assume the presence of SA(’)/TSA(’) exchange process. This hypothesis is supported by the solid-state structure of the Yb(III) complex. It was found

that no water molecule is directly bound to the metal centre in the [Yb(do3a-ae)] complex and disorder between the SA’ and TSA’ isomers was observed and successfully modelled (Figure 12).

Later on, the structural and dynamic properties of the Eu(III) complexes of H₃do3a-ae in more alkaline solution (pH = 10.0, *i.e.* pD = 10.4) were investigated by L. Tei *et al.* by using ^1H NMR spectroscopy ($B_0 = 500$ MHz) at low temperatures (270, 280 and 290 K). The predominance of one isomer (TSA) in solution at pD = 10.4 was observed in the ^1H NMR spectra of the [Eu(do3a-ae)(H₂O)] complex measured at low temperatures.^{56b} It points to the fact that the complex at higher pH (pD = 10.4) has more rigid structure, whereas the same complex at pD = 9.0 is characterized by a fast fluxional motion even at low temperature and, therefore, it is not possible to follow the isomerism more clearly.

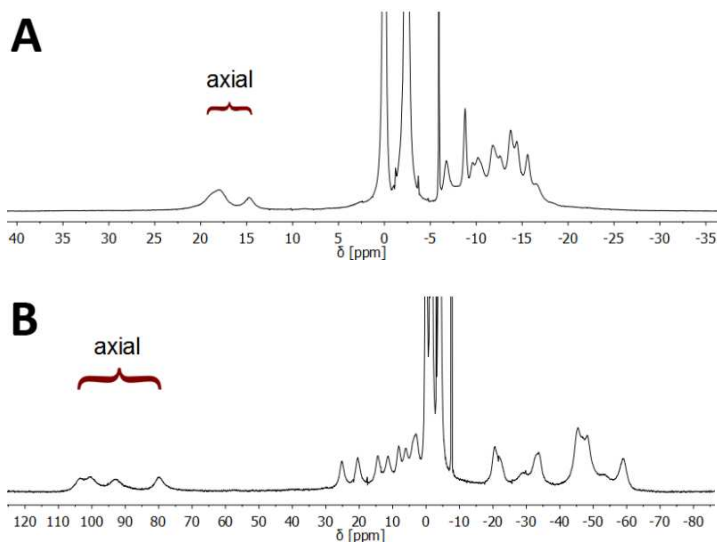


Figure 11: ^1H NMR spectra of the **A:** [Eu(do3a-ae)(H₂O)] complex in D₂O at pD = 9.0 (100 mM, $B_0 = 7.05$ T, 25 °C) and **B:** [Yb(do3a-ae)] complex in D₂O at pD = 8.5 (100 mM, $B_0 = 7.05$ T, 25 °C). Chemical shift of HDO in the sample solution was referenced to 0 ppm.

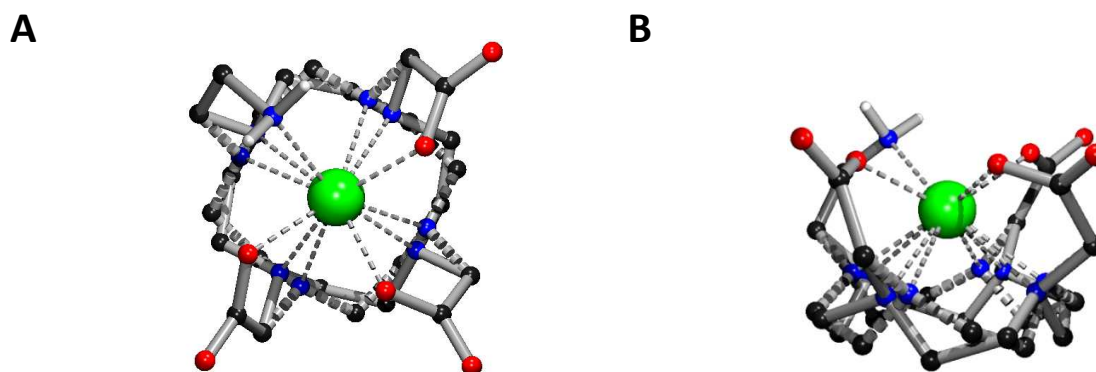


Figure 12: Disorder of the [Yb(do3a-ae)] molecule found in the solid-state structure of [Yb(do3a-ae)]·5H₂O. The figure shows an overlay of both disordered complex species; the more abundant (85%) TSA' isomer is represented using solid bonds and the less abundant (15%) SA' isomer using dashed bonds. **A:** Top view. **B:** Side view. Carbon-bound hydrogen atoms are omitted for clarity reasons. Colour code: Yb – green; N – blue; O – red; C – black; H – grey.

6.1.2 PARACEST experiments

Saturation transfer experiments investigated by NMR spectroscopy with aq. solutions of the H₃do3a-ae complexes revealed two broad signals in the Z-spectra. These signals have equal intensities with maxima at +19.5 ppm and +34 ppm (pH = 7.67, 25 °C) for the Eu(III) and +42 ppm and +89 ppm (pH = 7.4, 25 °C) for the Yb(III) complex (**Figure 13**) and are assigned to hydrogen atoms of the amino group. These two protons become magnetically non-equivalent after group coordination and, therefore, both can be distinguished in the Z-spectra. Surprising behaviour of the CEST peaks was observed while changing the solution pH. It is known that the CEST effect caused by a coordinated water molecule,⁷⁸ or by exchangeable protons of amide^{40,78,79} or hydroxy^{45,80} groups, drops with increasing pH due to faster base-catalysed prototropic exchange of the corresponding protons. In the case of Eu(III) and Yb(III) complexes of H₃do3a-ae, the CEST effect starts to be observable at pH ~ 6, reaches its maximum at pH ~ 8 and remains unchanged with further pH increase. Such behaviour has not yet been reported in the literature. Due to low “acidity” of the protons of the amino group (compared to that of the carboxylic amides), the base-catalysed proton exchange does not decrease the CEST effect in alkaline solutions. It was shown that pH dependence of the saturation transfer efficiency

parallels with abundance of the species with the coordinated amino group. The CEST signals disappear at lower pH values if the amino group is protonated and, thus, uncoordinated from the metal centre which corresponds to data obtained from potentiometry (pK_a of the protonated pendant amino group was determined to be 6.06 and 5.83 for the La^{3+} and Gd^{3+} complexes, respectively; see **Table 2** in Chapter 6.3.2).

In conclusion, the mechanism of the CEST effect is very probably based on coordination/decoordination of the pendant amino group. If the pendant arm is coordinated, no proton exchange occurs. In the moment of the pendant decoordination, the exchange between protons of the free amino group and those of bulk water proceeds very fast and the CEST effect is detectable.

PARACEST properties of the complexes with mono- and dimethylated ligands were also studied. Two close CEST signals (but with unequal

intensities) at +43 and +49.5 ppm were detected in the Z-spectra of the aq. $[\text{Eu}(\text{do3a-aeMe})(\text{H}_2\text{O})]$. One can conclude that two different species with the methyl substituent of the aminomethyl group in equatorial/axial (and hydrogen atom in reverse) positions are present in the solution. In the Z-spectra

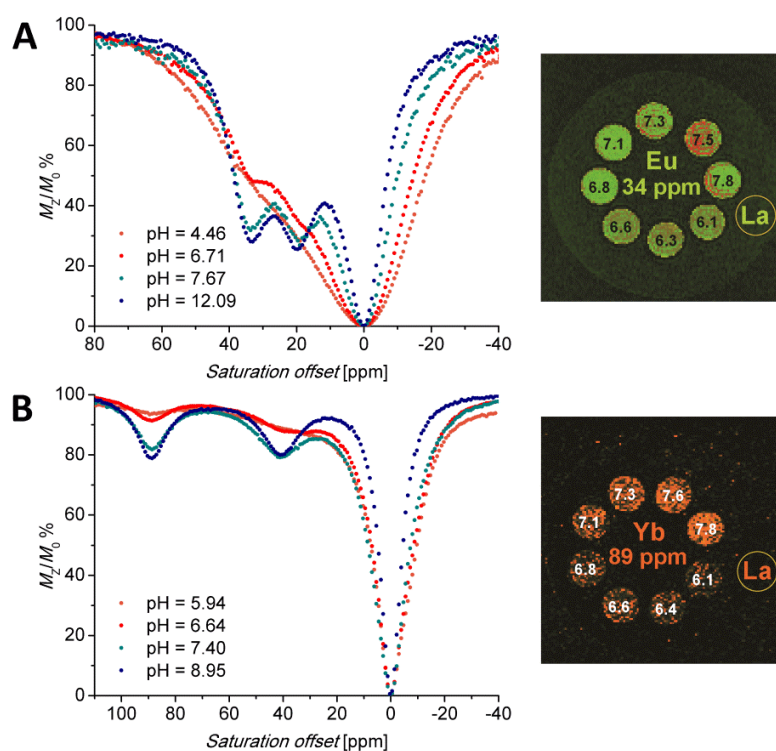


Figure 13: Z-spectra of a **A:** 80 mM; **B:** 100 mM aq. solution ($\text{H}_2\text{O}-\text{D}_2\text{O}$ 1:10) of **A:** Eu(III) and **B:** Yb(III) complex of $\text{H}_3\text{do3a-ae}$ [$B_0 = 7.05$ T, $B_1 = 21.7$ μT (920 Hz), RF presaturation pulse applied for 2 s] at 25 °C and MRI-CEST images of related phantoms of 80 mM aq. solution of these complexes and diamagnetic La(III) standard in false colours. $B_0 = 4.7$ T, $B_1 = 20$ μT , RF presaturation pulse applied for 2 s at **A:** 34 ppm; **B:** 89 ppm, TR = 5 s, TE = 8.9 ms, scan time 8 min at 20 °C.

of the complex with the smaller Yb(III) ion, only one CEST signal was observed, probably due to the preference of only one of these possibilities (**Figure 14**).

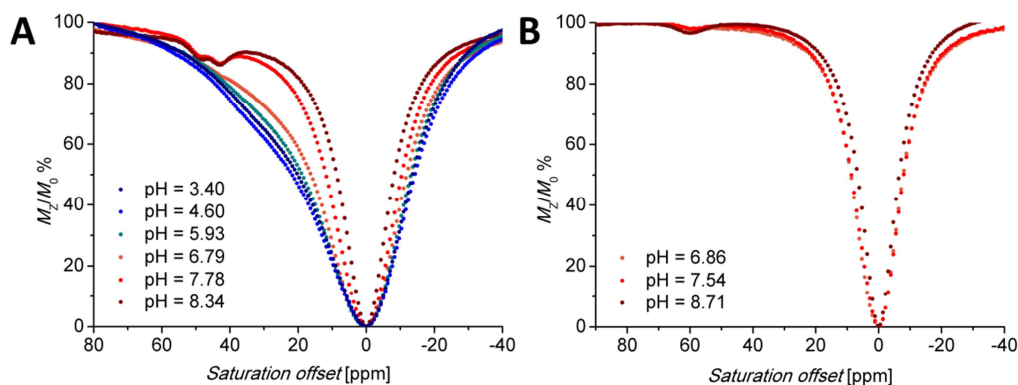


Figure 14: Z-spectra of a 25 mM aq. solution ($\text{H}_2\text{O}-\text{D}_2\text{O}$ 1:10) of **A:** Eu(III) and **B:** Yb(III) complex of $\text{H}_3\text{do3a-aeMe}$ [$B_0 = 7.05$ T, $B_1 = 21.7$ μT (920 Hz), RF presaturation pulse applied for 2 s].

Surprisingly, the Yb(III)- $\text{H}_3\text{do3a-ae2Me}$ complex is also CEST-active exhibiting the CEST signal (**Figure 15A**) with small intensity at +26 ppm in a narrow pH range (6–8.5) where the protonation/deprotonation of the $-\text{NMe}_2$ group is supposed.⁵⁶ Therefore, the saturation transfer to bulk water is very probably caused by the protons of the uncoordinated and protonated dimethylamino group which is still located close to the paramagnetic centre. This explanation is also supported by the fact that this CEST effect (due to an acceleration of the proton exchange process) disappears at relatively low temperature (~ 65 °C; **Figure 15B**), whereas the CEST signals of the complexes with $\text{H}_3\text{do3a-ae}$ are still visible even at 95 °C. In the case of the Eu(III)- $\text{H}_3\text{do3a-ae2Me}$ complex only some asymmetric broadening of the water signal was observed in the Z-spectra probably due to a lower magnetic moment of the Eu(III) ion [in comparison with the Yb(III) one], and due to a small influence of the chemical shift through the space.

The applicability of the Eu(III) and Yb(III) complexes of $\text{H}_3\text{do3a-ae}$ as CAs was tested by MRI scanner. MRI images were measured with phantoms consisting of a series of vials containing aqueous solutions of these complexes with different pH values or concentrations. The final CEST images were obtained by taking the difference of water signal intensity when the CEST signal frequency and symmetrical negative frequency were applied, and these were finally false colour coded (**Figure 13**).

The CEST effect was clearly detected and the results show that the complexes can be employed as PARACEST probes in the physiological pH range.

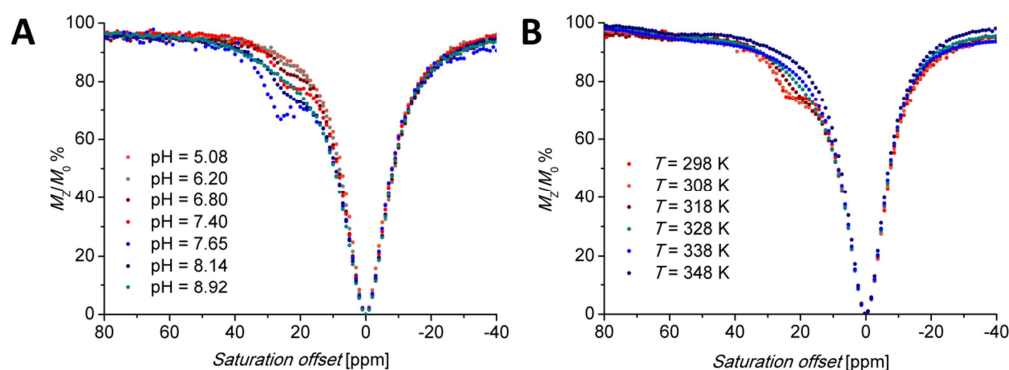


Figure 15: Z-spectra of a 50 mM aq. solution ($\text{H}_2\text{O}-\text{D}_2\text{O}$ 1:10) of Yb(III) complex of $\text{H}_3\text{do3a-ae2Me}$ [$B_0 = 7.05$ T, $B_1 = 21.7$ μT (920 Hz), RF presaturation pulse applied for 2 s] at **A:** 25 °C; **B:** at pH = 7.72.

6.1.3 Conclusions

In a summary, three macrocyclic ligands with pendant arms containing primary, secondary and tertiary amino groups were prepared, as well as their Eu(III) and Yb(III) complexes. The PARACEST properties were investigated by NMR spectroscopy and by MRI techniques; it was shown that coordination/decoordination of the amino group mediates saturation transfer to the bulk water in the pH range relevant for biological systems. A new mechanism for the PARACEST effect was suggested. This mechanism is based on a slow coordination and decoordination of the pendant amino group coupled with a fast proton exchange between the amino group and the bulk water while the pendant arm is uncoordinated. Therefore, these agents represent an innovative class of MR imaging probes which could be used as pH-sensitive probes for *in vivo* CEST MRI pH measurements. All details on this topic and full relevant experimental data are presented in more details in the paper⁷⁴ reprinted in Appendix 1.

6.2 LANTHANIDE(III) COMPLEXES OF DIAMINE-DO3A

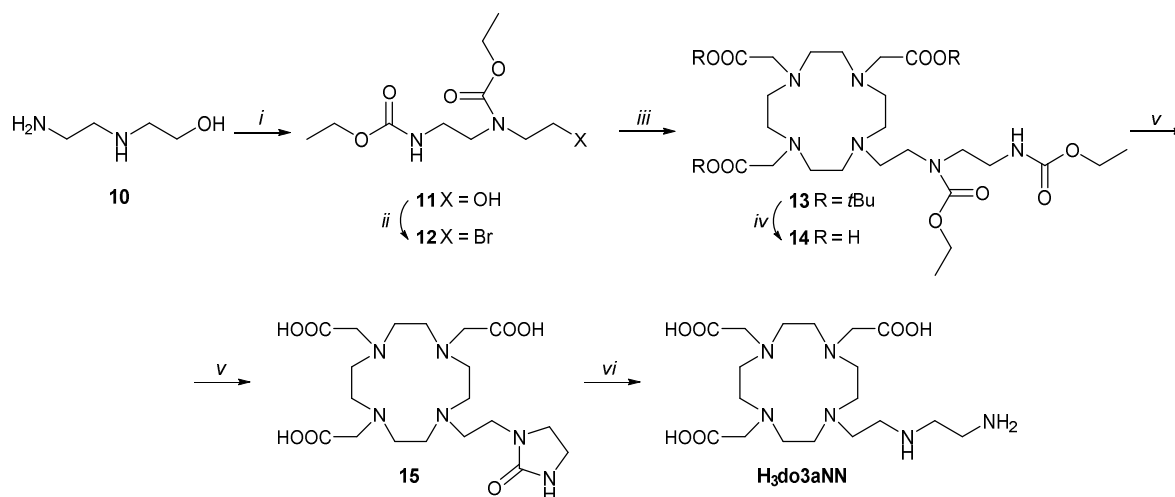
The successful testing of the Ln(III) complexes with amino groups such as pH-dependent PARACEST agents was a decisive impulse to search for other promising structures. As mentioned above (see Introduction), the PARACEST effect is sensitive to a number of external factors, also to the concentration of CA. Therefore, the exact determination of the pH value requires a separate measurement of the agent concentration to obtain quantitative results. Hence, ratiometric methods are explored to make the assessments independent from the local concentration. One of the possible approaches is to use a single CEST agent having different pools of exchangeable protons with different pH behaviour.^{46,62} Based on the results of the previous study, a new macrocyclic ligand H₃do3aNN (see **Figure 9**) was designed and synthesized. Choosing this molecule was motivated by the presence of a semilabile coordinating pendant arm with primary and secondary amino groups as two potentially independent proton exchanging pools. The PARACEST properties of its Ln(III) complexes were investigated to develop a concentration-independent ratiometric approach for pH mapping using MRI.

6.2.1 Synthesis and structure

The reaction of *t*Bu₃do3a·HBr with brominated ethyl-carbamate-protected *N*-(2-aminoethyl)ethanolamine **12** as the alkylation agent, consecutive deprotection in a CF₃COOH:CHCl₃ 1:1 mixture and hydrolysis in 10% aq. NaOH led to the forming of the urea derivative **15** (42% overall yield based on *t*Bu₃do3a·HBr; see **Scheme 3**). Structure of this surprising intermediate was confirmed by a single-crystal X-ray diffraction study. The target ligand H₃do3aNN was then prepared by hydrolysis of this intermediate with aq. HCl. The required ligand can also be prepared by acid hydrolysis of mother liquors after crystallization of the urea-intermediate **15** and consecutive chromatography on a column of strong (Dowex 50) and weak (Amberlite CG50) cation exchange resins.

The solution structure of the Eu(III) and Yb(III) complexes were investigated by ¹H NMR spectroscopy. In comparison with the spectra of the complexes with the previously discussed ligands, ¹H NMR spectra of the Ln(III)-H₃do3aNN complexes were much clearer. In both cases, only one set of

signals was detected. It points to the exclusive formation of only one diastereomer in solution. The chemical shifts of “axial” protons are in the region typical for TSA isomers [Eu(III): 9–13 ppm, Yb(III): 45–62 ppm; with respect to the signal of bulk water referenced to 0 ppm; **Figure 16**] and, therefore, the presence of this isomer in solution is assumed.



Scheme 3: Synthesis of H₃do3aNN. (i) CH₃CH₂OC(O)Cl, dioxane:H₂O (1:1), RT, 2 h; (ii) CBr₄, PPh₃, THF, RT, 1 h; (iii) *t*Bu₃do3a·HBr, K₂CO₃, MeCN, 60 °C, 24 h; (iv) CF₃COOH:CHCl₃ (1:1), reflux 18 h; (v) 10 % aq. NaOH, 90 °C, 24 h; (vi) aq. HCl (1:1), 95 °C, 7 d.

In the ¹H NMR spectra of the prepared complexes in H₂O, it is possible to identify signals of their exchangeable NH protons. In the case of Eu(III) complex, one narrow signal at +22.2 ppm and two symmetrical broad signals at +43.3 and +46.5 ppm (pH =11.7; **Figure 16A**) are detectable and disappear when measuring the ¹H NMR spectra in D₂O (pD =10.7; **Figure 16B**). The narrow signal at +22.2 ppm is shifted similarly as one of the protons of coordinated NH₂ group of the [Eu(do3a-ae)(H₂O)] complex (+19.5 ppm). Therefore, the resonance at +22.2 ppm was attributed to the proton of coordinated secondary amino group which adopts an analogous position as the primary amino group in the Eu(III) complex of H₃do3a-ae (nitrogen atom forms O₃N-plane with the pendant donor oxygen atoms). Coalescence of two symmetrical broad signals at higher chemical shifts was observed at higher temperature (45 °C). Hence, they can be assigned to the magnetically nonequivalent protons of coordinated primary amino group.

Surprisingly, in the ^1H NMR spectra of the $[\text{Eu}(\text{do3aNN})]$ complex in H_2O , a small signal at +35 ppm was found (pH = 11.7; **Figure 16A**) and it disappeared when the spectrum was measured in D_2O (pD = 10.7; **Figure 16B**). At the same chemical shift, a minor CEST signal of exchangeable protons was detected in the Z-spectra, accompanied by two CEST peaks lying at +10 and +15 ppm (see PARACEST experiments below). These peaks were attributed to exchangeable protons of another TSA isomer originating from the opposite chirality of the coordinated nitrogen atom of the secondary amino group. Therefore, simple molecular modelling was performed (see the results in **Figure 17**). It was shown that the apical coordination of the primary amino group is possible only in the $\Delta\delta\delta\delta\delta\text{-S}/\Lambda\lambda\lambda\lambda\lambda\text{-R}$ enantiomeric pair and, thus, this isomer is suggested to be the major one. In the case of $\Delta\delta\delta\delta\delta\text{-R}/\Lambda\lambda\lambda\lambda\lambda\text{-S}$ species (minor isomer), the position of primary amino group is not suitable for apical coordination. Therefore, the CEST signals of the primary amine in the Z-spectrum are significantly closer to the free water signal.

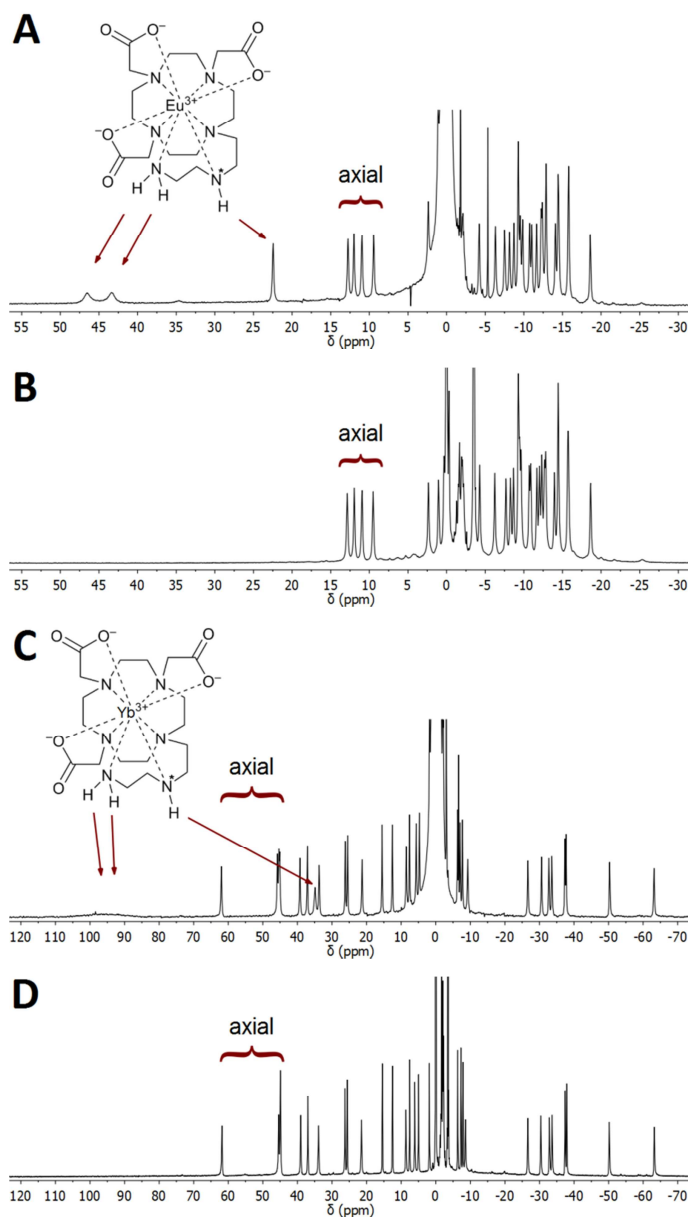


Figure 16: ^1H NMR spectra of the **A, B:** Eu(III); **C, D:** Yb(III) complex of $\text{H}_3\text{do3aNN}$ ($B_0 = 7.05$ T, 25°C) in **A:** H_2O , pH = 11.7, 90 mM; **B:** D_2O , pD = 10.73, 90 mM; **C:** H_2O , pH = 11.41, 90 mM; **D:** D_2O , pD = 11.34, 40 mM. Chemical shift of $\text{H}_2\text{O}/\text{HDO}$ in the sample solution was referenced to 0 ppm.

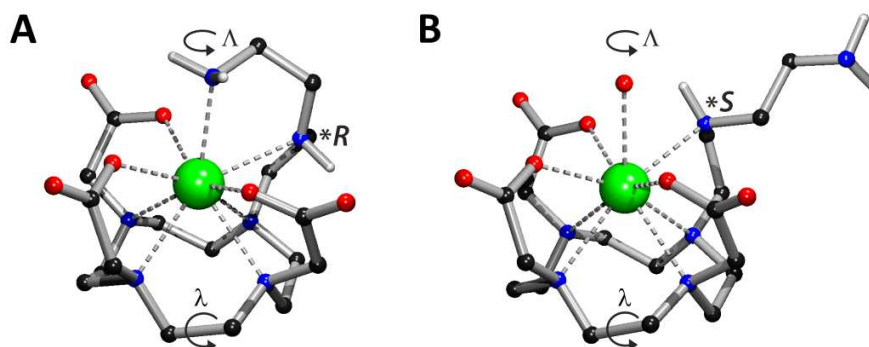


Figure 17: Tentative visualization of TSA isomers of the $[\text{Eu}(\text{do3aNN})(\text{H}_2\text{O})_{0-1}]$ complex differing in chirality of coordinated secondary amino group **A:** TSA species ($\Lambda\lambda\lambda\lambda$) with *R* chirality of the coordinated secondary amino group, enabling coordination of the primary amino group in the apical position. **B:** TSA species ($\Lambda\lambda\lambda\lambda$) with *S* chirality of the coordinated secondary amino group, disabling coordination of the primary amino group in the apical position.

Similar ^1H NMR spectra were observed also for the Yb(III) complex possessing one very broad signal of the NH_2 group at 82–104 ppm (centred at +95 ppm) which splits into two signals at 5 °C, and one narrow signal of the secondary amino group at +35 ppm (**Figure 16C**). Such a chemical shift is similar to the analogous ^1H NMR signal of the $[\text{Yb}(\text{do3a-ae})]$ complex at +42 ppm. Both these signals are not visible in D_2O (**Figure 16D**). As in the previous case, minor NH signals of another TSA isomer are observable in the ^1H NMR spectra, and minor CEST signals of exchangeable protons were detected in the Z-spectra at +17, +26 and +57 ppm.

Interesting behaviour was observed when the ^1H NMR spectra of the $[\text{Yb}(\text{H}_n\text{do3aNN})]^n$ and $[\text{Eu}(\text{H}_n\text{do3aNN})(\text{H}_2\text{O})_{0-1}]^n$ complexes were measured with bulk water presaturation. In the ^1H NMR spectra of the Eu(III) complex measured in H_2O at pH = 6.75, all three main signals of exchangeable protons of amino groups (at +22.2, +43.3 and +46.5 ppm) disappear upon presaturation of the bulk water signal (**Figure 18A**). When the same experiment was performed with the aq. solution of the Eu(III) complex at pH = 11.7, the signal at +22.2 ppm (secondary amino group) remained unaffected whilst the signals at +43.3 and +46.5 ppm (primary amino group) were decreased by the water suppression (**Figure 18B**).

Similarly, in an alkaline aq. solution of the $[\text{Yb}(\text{H}_n\text{do3aNN})]^{n-}$ complex, signal of the primary amino group was the only one affected by water presaturation. Due to a broadening of the primary amino group signal and broadening and overlapping of the signal of the secondary amino group at lower pH, suppression of these signals was not so evident as for the Eu(III) complex. In a summary, these experiments showed that exchangeable protons of both amino groups of the prepared complexes could have pH-dependent CEST effects in the physiologically relevant pH range. Based on these findings, PARACEST properties of these agents and the possibility of their use as pH-responsive probes were further investigated.

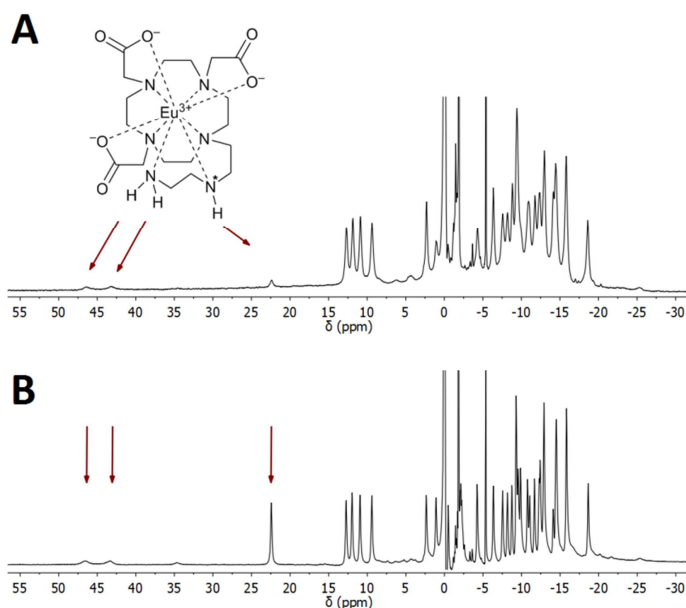


Figure 18: ^1H NMR spectra of the $[\text{Eu}(\text{H}_n\text{do3aNN})(\text{H}_2\text{O})_{0-1}]^{n-}$ complex in H_2O (90 mM, $B_0 = 7.05$ T, 25°C) at **A:** pH = 6.75 and **B:** pH = 11.70. The signal of water was saturated. Arrows show the position of exchangeable (NH) protons. Chemical shift of H_2O in the sample solution was referenced to 0 ppm.

6.2.2 PARACEST experiments

Z-spectra of the Eu(III) and Yb(III) complexes of $\text{H}_3\text{do3aNN}$ in aq. solutions were recorded over the pH range from ~ 5 to ~ 8 . These experiments revealed two CEST signals of both complexes centred at +22.2 and +44.4 ppm for the Eu(III) (**Figure 19A**) and at +35 and +95 ppm for the Yb(III) complex (**Figure 19B**). It clearly corresponds to the chemical shifts of the exchangeable protons detected and identified in the ^1H NMR spectra (**Figure 16**). The broad CEST signals at +44.4 and +95 ppm for the Eu(III) and Yb(III), respectively, correspond to exchangeable protons of the primary amino group. These broad CEST signals split into two signals of magnetically non-equivalent protons by applying a lower intensity of presaturation pulses at 25°C or at low temperatures. The CEST signals

with chemical shifts at +22.2 and +35 ppm for the Eu(III) and Yb(III) complex, respectively, represent saturation transfer between proton of the secondary amino group and those of bulk water.

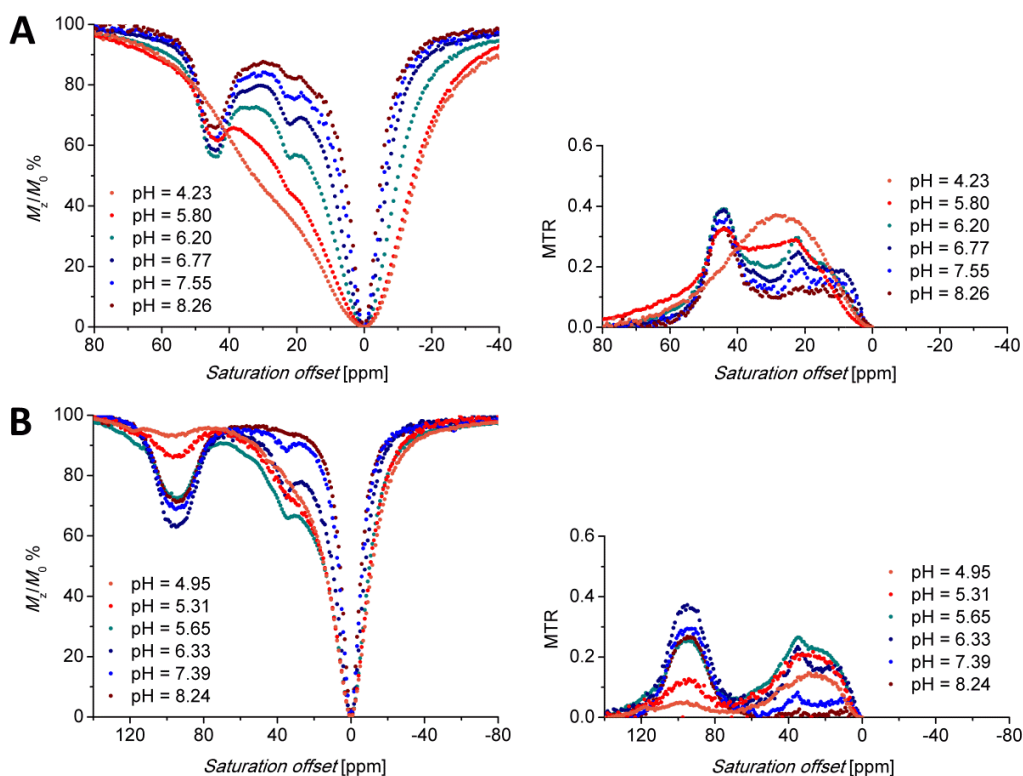


Figure 19: Z- and corresponding MTR spectra of an **A:** 83 mM and **B:** an 87 mM aq. solution of the **A:** $[\text{Eu}(\text{H}_n\text{do3aNN})(\text{H}_2\text{O})_{6-n}]^{n+}$ and **B:** $[\text{Yb}(\text{H}_n\text{do3aNN})]^{n+}$ complexes [$B_0 = 7.05$ T, $B_1 = 21.7$ μT (920 Hz), RF presaturation pulse applied for 2 s, 25 $^\circ\text{C}$].

As mentioned above (see discussion of the ^1H NMR spectra), the sets of minor signals at +10, +15 and +35 ppm for Eu(III) and at +17, +26 and +57 ppm for Yb(III) complex appear in the Z-spectra when the low saturation power was applied (**Figure 20**). These CEST signals were attributed to the less abundant TSA isomer with opposite chirality of the coordinated secondary amino group. At slightly acidic to neutral pH, all three signals were detected. However, in the alkaline region, only the couples of signals with lower chemical shifts at +10 and +15 ppm for the Eu(III) complex and at +17 and +26 ppm for the Yb(III) complex remain in the Z-spectra. This implies their assignment to the exchangeable protons of the primary amino group.

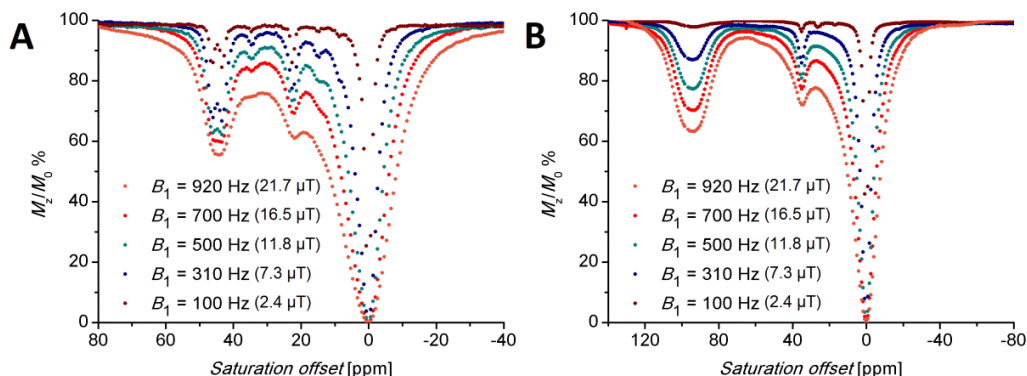


Figure 20: Z-spectra of an 87 mM aq. solution of the **A:** [Eu(H_n,do3aNN)(H₂O)₀₋₁]ⁿ complex at pH = 6.45 and **B:** [Yb(H_n,do3aNN)]ⁿ complex at pH = 6.33 at various presaturation power levels B_1 ($B_0 = 7.05$ T, RF presaturation pulse applied for 2 s, 25 °C).

The Z-spectra clearly showed that the exchangeable protons of both amino groups of the major isomer of the [Ln(H_n,do3aNN)(H₂O)₀₋₁]ⁿ complexes have significantly pH-dependent CEST effects. For detailed analysis of the CEST properties, the Z-spectra were transformed to MTR spectra (**Figure 19**). At pH < 5.5, the CEST signal of the primary amino group gradually disappear from the Z-spectra as a consequence of its protonation and decoordination [from potentiometry, the corresponding observed equilibrated protonation step has $\log K(\text{HLM}) = 6.03/6.22$ for the Eu(III)/Yb(III) complexes, respectively; see **Table 2** in Chapter 6.3.2]. Simultaneously, a new (very broad) CEST peak appears at ~25–30 ppm for both complexes. This broad signal can be attributed to the proton exchange of water with protonated amino group which is close to the paramagnetic ion and, thus, it is still shifted but this shift is much lower compared to the situation when the group is directly coordinated to the paramagnetic centre. The CEST signal of the coordinated secondary amino group was observed for the Eu(III) and Yb(III) complexes in the pH region of ~5.5–8.5 [potentiometric titrations revealed equilibrated protonation step with $\log K(\text{H}_2\text{LM}) = 5.09/5.07$ for the Eu(III)/Yb(III) complexes, respectively; see **Table 2** in Chapter 6.3.2]. In an alkaline solution (pH > 8.5), the chemical exchange of the NH proton become too slow to transfer a saturation to the bulk water signal and, thus, the CEST effect of this group cannot be detected. Such CEST behaviour is consistent with the ¹H NMR spectra measured with presaturation of the bulk water signal where the signal of the secondary amino group in

alkaline solution remains unaffected after water suppression (**Figure 18B**). This can be explained by coordination of the primary amino group and, thus, absence of a positive charge which, at $\text{pH} < 8.5$, probably helps decoordination of the secondary amine. On the other hand, an effective CEST effect of the primary amino group is detectable even in alkaline solutions. A suggested mechanism of origin of the pH-dependent CEST effects is shown in **Figure 21**.

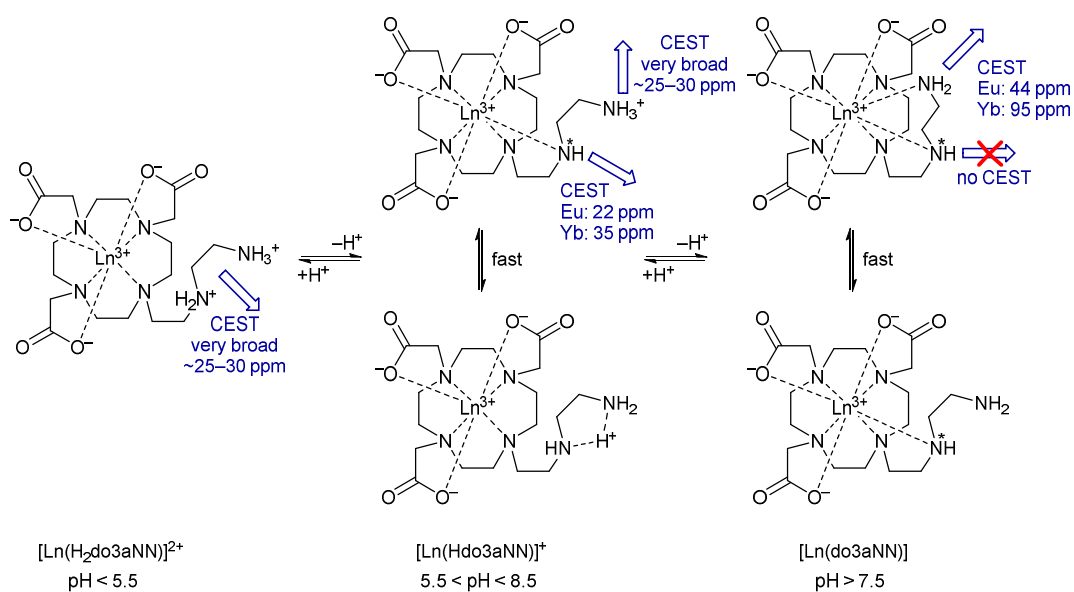


Figure 21: A suggested mechanism of origin of the pH-dependent CEST effect of the $[\text{Ln}(\text{H}_n\text{do3aNN})(\text{H}_2\text{O})_{0-1}]^{n+}$ complexes. In hepta/octa-coordinated species, binding of water molecule(s) to the central ion giving coordination number 8–9 is expected but it is not shown for the sake of clarity.

To test applicability of the prepared Eu(III) and Yb(III) complexes as pH-sensitive and concentration-independent MRI probes, the CEST effect was measured by MRI scanner for solutions in HEPES/MES buffers with different pH values and concentrations (**Figure 22**) and the ratio of MTR intensities was calculated. Then the pH-dependent function independent of a concentration of the probe was defined. Unfortunately, this function can be defined only for the Yb(III) complex of $\text{H}_3\text{do3aNN}$. It is not possible for the Eu(III) complex due to a significant overlapping of the signal of the NH proton (22.2 ppm) with the signal attributable to the protonated and uncoordinated primary amine in the acidic region. The calibration curves obtained from the MRI experiments were compared

with the curves obtained by NMR techniques (the concentration range used covers about one order of magnitude; 7.7–87 mM) and all of them were very similar (Figure 23).

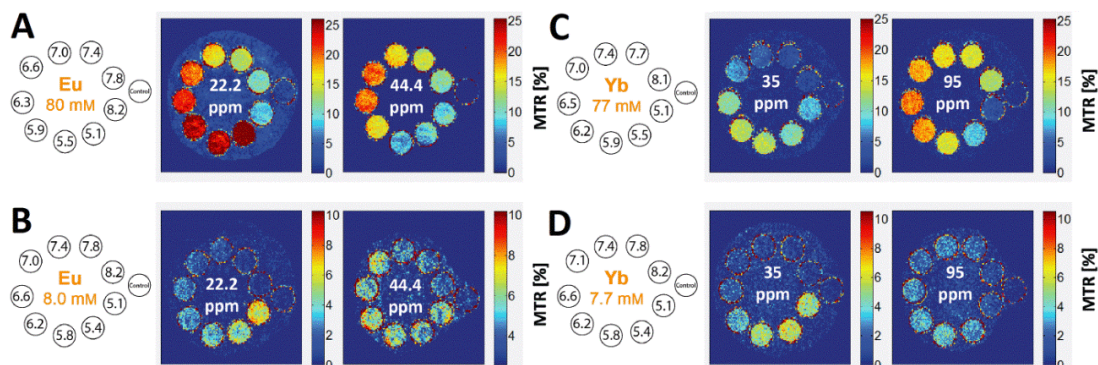


Figure 22: MRI-CEST images of phantoms consisting of one vial containing an aq. solution of MES and HEPES (1:1, 50 mM) as a standard and nine vials containing solutions of (A, B) Eu(III) or (C, D) Yb(III) complexes of $H_3do3aNN$ in the same buffer with different pH values and concentrations (in false colours). Experimental conditions: RARE pulse sequence (Rapid Acquisition with Relaxation Enhancement), $B_0 = 4.7$ T, RF presaturation pulse applied for 2 s, $T = 298$ K, $TR = 5$ s, $TE = 8.9$ ms, (B) $B_1 = 35$ μ T (1490 Hz), (A, C, D) $B_1 = 25$ μ T (1060 Hz).

The standard deviations for the low concentrated solutions measured by MRI were relatively high due to high background noise. Despite the low signal-to-noise ratio and related high standard deviations, the shape of the calibration curves enables distinguishing between the samples with $pH > 7$ and those with $pH < 6$. Such information can be useful for example in the detection of hypoxic tissues. Unfortunately, it was found that the $[Ln(do3aNN)(H_2O)_{0-1}]$ complexes are not fully kinetically inert in acidic solutions ($pH < 6$). When a solution of pre-formed complex ($pH = 7.5$) was

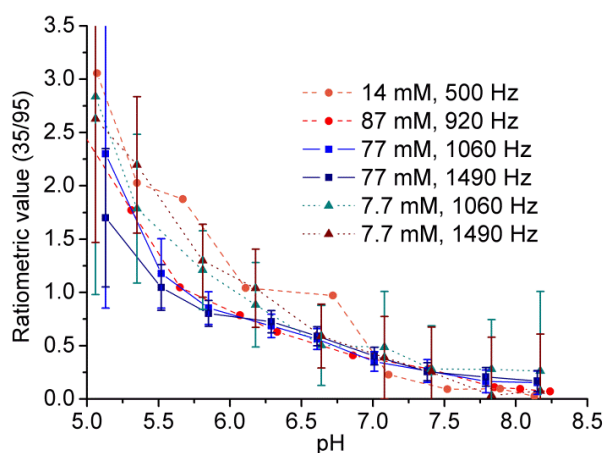


Figure 23: Ratiometric plots of the 7.7–87 mM $[Yb(H_n do3aNN)]^n$ complex, 25 $^{\circ}C$; RF presat. pulse applied for 2 s. Circles: aq. solution, $B_0 = 7.05$ T (NMR), $B_1 = 500$ Hz (11.8 μ T) or 920 Hz (21.7 μ T). Squares and triangles: 50 mM HEPES-MES, $B_0 = 4.7$ T (MRI), $B_1 = 1060$ Hz (25 μ T) or 1490 Hz (35 μ T). The ratiometric value (35/95) is the ratio of MTR intensity at 35 ppm to MTR intensity at 95 ppm.

added to slightly acidic buffered solution with pH = 5.5, a slow dissociation of the complex was observed by xylenol orange test.⁸¹ From the quantitative UV-Vis experiments, dissociation of about 10% of the complex was found after standing for one week at room temperature (**Figure 24**). Due to the dissociation, validity of the PARACEST experiments at the pH = 5–6 was tested. The innocence of the free Eu(III) aqua ion and of the free ligand was studied by independent experiments and it was shown that these do not interfere either with the ¹H or CEST measurements. It was demonstrated that the shape of the Z-/MTR spectra is not affected by a presence of the free metal ion/ligand and, therefore, conclusions drawn from the PARACEST experiments are valid even in the pH range where the complex slowly dissociates.

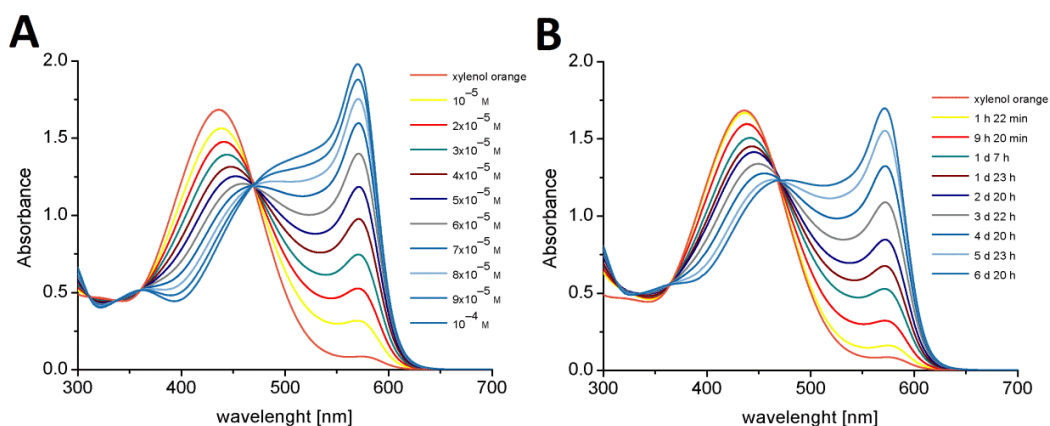


Figure 24: A: Change of the UV-Vis spectra of an aq. solution of xylenol orange (10⁻⁵ M, pH = 5.55, 0.025 M HEPES and 0.025 M MES, 25 °C) with increasing concentration of EuCl₃ (10⁻⁵–10⁻⁴ M). B: Time dependence of the UV-Vis spectra of aq. solution of xylenol orange (10⁻⁵ M, pH = 5.55, 0.025 M HEPES and 0.025 M MES, 25 °C) in presence of the [Eu(H₃do3aNN)(H₂O)₉]³⁺ complex (8·10⁻⁴ M).

6.2.3 Conclusions

A novel macrocyclic ligand H₃do3aNN was prepared and, from the pH-dependent Z-spectra, it was found that its Yb(III) and Eu(III) complexes possessed two pools of exchanging protons of amino groups that show different pH-dependences of their CEST effects in the pH range relevant for biological systems (pH ≈ 5.5–8.5). The CEST effect of the secondary amino group is observable up to pH ~ 8.5. Above this pH where the species with deprotonated primary amino group are mostly present

in solution, chemical exchange of the proton of the secondary amino group becomes too slow. On the other hand, CEST effect of the primary amino group is detectable even in alkaline solutions and, therefore, the same mechanism of the PARACEST effect as for the previously studied complexes of ligands with 2-aminoethyl pendant arm is supposed.

MTR of the Yb(III) complex with H₃do3aNN can be used for pH determination by MRI, and it is independent of the concentration of the probe (the tested concentrations were in the range 7.7–77 mM). Unfortunately, the complex cannot be used in medical applications because it is not fully kinetically inert and slowly releases the free metal ion in slightly acidic solutions. However, the proof-of-principle study shows that complexes with a linear diaminic pendant arm can be used for pH determination using MRI ratiometry. All of the results discussed above and full relevant experimental data are presented in more details in the paper⁸² reprinted in Appendix 2.

6.3 LANTHANIDE(III) COMPLEXES OF PHOSPHO-AMINO-DO3A

Based on the previous studies it is not surprising that we wanted to design and synthesize a new ligand whose complexes will be more stable than those of the H₅do3aNN and that could exhibit suitable properties for pH mapping *in vivo*. Therefore, the third goal of this Thesis was to extend PARACEST studies to Ln(III) complexes of aminophosphonate-containing DO3A analogue (H₅do3aNP; **Figure 9**). This structure was chosen because, in general, protonation constants of amino and phosphonate groups are close to the pH region relevant for living systems and, thus, complexes of the new ligand were expected to change their properties in the physiological pH range. As mentioned above, a higher kinetic inertness of the complexes was supposed. We also suggested that these phosphorus-containing molecules can be applied for pH determination using ³¹P NMR-based technique.

6.3.1 Synthesis

The target ligand H₅do3aNP was synthesized according to **Scheme 4**. The key phosphorus-containing intermediate **17** was successfully prepared by the one-step Mannich-type reaction of *N*-benzylethanolamine with diethylphosphite and paraformaldehyde and it was isolated as a brownish oil after the cation-exchange resin purification. This compound was then converted to alkylation agent **18** by reaction with methylsulfonylchloride. Alkylation of *t*Bu₃do3a·HBr by the agent **18** afforded intermediate **19**. The *t*Bu-ester groups were removed by reflux in a CF₃COOH:CHCl₃ 1:1 mixture and the ethyl-esters protection groups were removed by hydrolysis in hydrochloric acid. Hydrogenation of the deesterified compound **21** using the Pd/C catalyst produced the H₅do3aNP that was purified on cation exchange resin and was isolated by crystallization in a zwitterionic form in the overall 44% yield (based on *t*Bu₃do3a·HBr). The target ligand H₅do3aNP was structurally characterized by the single-crystal X-ray diffraction analysis.

of the phosphonate moiety. The next protonation constants $\log K(\text{H}_5\text{L}) = 4.19$ and $\log K(\text{H}_6\text{L}) = 1.90$ are associated with protonation of the acetate arms.

Table 1: Equilibrium constants ($\log K$)^[a] of $\text{H}_5\text{do3aNP}$ (0.1 M NMe_4Cl , 25 °C) obtained from potentiometric and ^{31}P NMR titrations, and comparison with related ligands.

Equilibrium	$\text{H}_5\text{do3aNP}$	$\text{H}_5\text{do3aNP}$ (^{31}P NMR)	$\text{H}_3\text{do3aNN}$ ^[b]	$\text{H}_3\text{do3a-ae}$ ^[c]	H_4dota ^[d]
$\text{H}^+ + \text{L}^{n-} \leftrightarrow \text{HL}^{1-n}$	12.56	12.52	12.62	13.19	12.9
$\text{H}^+ + \text{HL}^{1-n} \leftrightarrow \text{H}_2\text{L}^{2-n}$	10.37	10.59	10.28	10.51	9.72
$\text{H}^+ + \text{H}_2\text{L}^{2-n} \leftrightarrow \text{H}_3\text{L}^{3-n}$	9.23	9.37	9.67	8.90	4.60
$\text{H}^+ + \text{H}_3\text{L}^{3-n} \leftrightarrow \text{H}_4\text{L}^{4-n}$	6.17	5.96	8.30	3.87	4.15
$\text{H}^+ + \text{H}_4\text{L}^{4-n} \leftrightarrow \text{H}_5\text{L}^{5-n}$	4.19	–	3.30	1.27	2.29
$\text{H}^+ + \text{H}_5\text{L}^{5-n} \leftrightarrow \text{H}_6\text{L}^{6-n}$	1.90	2.05	1.58	–	1.34

[a] $K = [\text{H}_h\text{L}]/\{[\text{H}]\cdot[\text{H}_{h-1}\text{L}]\}$. [b] ref. 82. [c] ref. 74. [d] ref. 84.

The stability constant of the Eu(III) complex was obtained by an out-of-cell technique and was found to be $\log K_{\text{ML}} = 23.49$ (comparison with the stability constants of related ligands is in **Table 2**). In contrast with the $\text{Eu(III)}-\text{H}_3\text{do3aNN}$ and $\text{Gd(III)}-\text{H}_3\text{do3a-ae}$ systems, where (according to the distribution diagrams) metal complexation is not quantitative until $\text{pH} \sim 6$ and $\text{pH} \sim 5.5$, respectively,^{74,82} the distribution diagram of the $\text{Eu(III)}-\text{H}_5\text{do3aNP}$ system showed that free Eu(III) ions are not present above $\text{pH} \sim 5.0$. Equilibrated protonation of the $[\text{Eu}(\text{do3aNP})]^{2-}$ complex proceeds with $\log K(\text{HLM}) = 8.0$ and that of the $[\text{Eu}(\text{Hdo3aNP})(\text{H}_2\text{O})]^-$ occurs with $\log K(\text{H}_2\text{LM}) = 3.75$ (**Table 2**).

Table 2: Equilibrium constants ($\log K$ and $\log K_{\text{ML}}$)^[a] of the Ln(III) complexes of $\text{H}_5\text{do3aNP}$ (0.1 M NMe_4Cl , 25 °C) obtained from the potentiometric titrations, and comparison with corresponding constants reported for the complexes of related ligands.

Equilibrium	$\text{H}_5\text{do3aNP}$	$\text{H}_3\text{do3aNN}$ ^[b]	$\text{H}_3\text{do3a-ae}$ ^[d]	H_4dota ^[g]
$\text{Eu}^{3+} + \text{L}^{n-} \leftrightarrow [\text{Eu}(\text{L})]^{3-n}$	23.49	23.16/22.76 ^[c]	22.23 ^[e] /20.02 ^[f]	24.2
$\text{H}^+ + [\text{Eu}(\text{L})]^{3-n} \leftrightarrow [\text{Eu}(\text{HL})]^{4-n}$	8.00	6.03/6.22 ^[c]	5.83 ^[e] /6.06 ^[f]	–
$\text{H}^+ + [\text{Eu}(\text{HL})]^{4-n} \leftrightarrow [\text{Eu}(\text{H}_2\text{L})]^{5-n}$	3.75	5.09/5.07 ^[c]	–	–
$\text{H}^+ + [\text{Eu}(\text{H}_2\text{L})]^{5-n} \leftrightarrow [\text{Eu}(\text{H}_3\text{L})]^{6-n}$	4.35	–	–	–
$\text{H}^+ + [\text{Eu}(\text{H}_3\text{L})]^{6-n} \leftrightarrow [\text{Eu}(\text{H}_4\text{L})]^{7-n}$	3.31	–	–	–

[a] $K = [\text{H}_h\text{LM}]/\{[\text{H}]\cdot[\text{H}_{h-1}\text{LM}]\}$; $K_{\text{ML}} = [\text{ML}]/\{[\text{L}]\cdot[\text{M}]\}$. [b] ref. 82. [c] Data reported for the Yb(III) complex. [d] ref. 74. [e] Data reported for the Gd(III) complex. [f] Data reported for the La(III) complex. [g] ref. 85.

The first protonation is associated with the pendant amino group and its value ($\log K(\text{HLM}) = 8.0$) points to the promising fact that the complex could change its properties in the physiological pH range. A further three protonation steps determined from the potentiometric titrations can be attributed to simultaneous protonations of the phosphonate group and the macrocycle nitrogen atoms. Therefore, the equilibrated H_3LM and H_4LM species are expected to be *out-of-cage* complexes with protonated macrocycle amino groups as already suggested for other systems with DOTA-like ligands.⁸⁶ Moreover, an acid-base potentiometric titration of the pre-formed complex was performed (pH region 1.9–9.5) and three stepwise protonation constants were found. The first one [$\log K(\text{HLM}) = 8.29$] corresponds to protonation of the pendant amino group and the second one [$\log K(\text{H}_2\text{LM}) = 4.07$] to protonation of the phosphonate group which is coordinated. A small difference found between values obtained by titration under equilibrated conditions and on the pre-formed complex can be attributed to a partial protonation of the macrocyclic amino group in the H_2LM species under equilibrium conditions. The third protonation constant [$\log K(\text{H}_3\text{LM}) = 1.75$] is much lower than that observed in the equilibrated solutions (*out-of-cell* titration). One can assume that during the fast potentiometric titration no dissociation of the complex occurs and, thus, the third constant corresponds very probably to protonation of the coordinated carboxylate groups of the *in-cage* complex.

6.3.3 Solution structure of the Eu(III)– $\text{H}_5\text{do3aNP}$ complex

Solution structure of the Eu(III) complex of $\text{H}_5\text{do3aNP}$ was investigated by ^1H NMR spectroscopy in the pD range 6.8–9.9 (**Figure 25**). At lower pD values (pD < 7.3), one set of signals was detected in the ^1H NMR spectra pointing to the presence of only one diastereomer in solution. The signals of “axial” protons appear in the range typical for the SA isomers (20–49 ppm; **Figure 25A** and **B**). Surprisingly, when the pH was increased, the signals of the SA isomer slowly disappeared from the ^1H NMR spectra and a new set of signals appeared simultaneously. These signals can be attributed to the TSA isomer with the most shifted signals in the 7–14 ppm range (**Figure 25B** and **C**). Thus, the SA arrangement in the $[\text{Eu}(\text{Hdo3aNP})(\text{H}_2\text{O})]^-$ species is, upon deprotonation ($\text{p}K_a \sim 8$; see **Table 2**) and

coordination of the pendant secondary amino group, converted to TSA geometry in $[\text{Eu}(\text{do3aNP})]^{2-}$ ion (**Scheme 5**). Both isomers are in a slow exchange on the NMR time scale.

To support this explanation, ^{31}P NMR spectra of the Eu(III) complex were also measured (**Figure 26**). Based on the significantly shifted ^{31}P NMR resonances (SA: $\delta_{\text{P}} = -118$ ppm; TSA: $\delta_{\text{P}} = +70$ ppm; free ligand: 8–16 ppm; La(III) complex: 23–25 ppm) and short T_1 relaxation times of ^{31}P NMR signals (~ 0.2 s; La(III) complex: ~ 2 – 3 s) one can conclude that the phosphonate group is coordinated in both $[\text{Eu}(\text{Hdo3aNP})(\text{H}_2\text{O})]^- / [\text{Eu}(\text{do3aNP})]^{2-}$ species. In addition, the species are not in fast exchange as both signals are present in the ^{31}P NMR spectra in the pH range ~ 7.8 – 8.8 (**Figure 26**). A large change in the ^{31}P NMR shifts (~ 190 ppm) upon (de)protonation is unprecedented. We suppose that the coordinated phosphorus atom of the phosphonate pendant arm of protonated SA- $[\text{Eu}(\text{Hdo3aNP})(\text{H}_2\text{O})]^-$ species lies in the O_4 -plane (**Scheme 5**). After deprotonation of the secondary amino group and its coordination to the metal

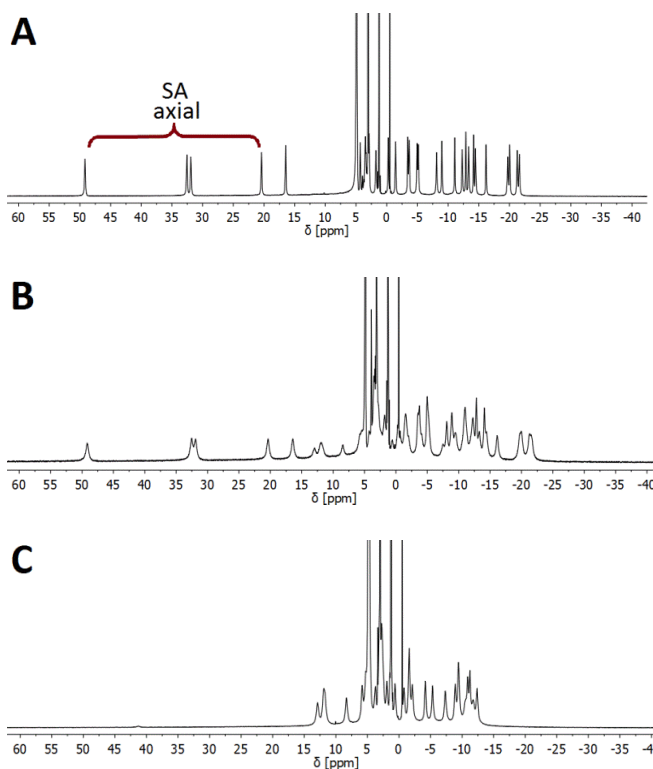
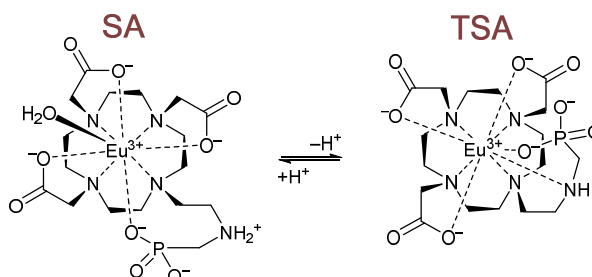


Figure 25: ^1H NMR spectra of the $[\text{Eu}(\text{Hdo3aNP})(\text{H}_2\text{O})]^- / [\text{Eu}(\text{do3aNP})]^{2-}$ species (80 mM solution in D_2O , $B_0 = 7.05$ T, 25°C) at **A:** pD = 6.8, **B:** pD = 8.4 and **C:** pD = 9.9. Chemical shift of $t\text{BuOH}$ in the sample solution was referenced to 1.25 ppm.



Scheme 5: Suggested geometry of the $[\text{Eu}(\text{do3aNP})]^{2-}$ and $[\text{Eu}(\text{Hdo3aNP})(\text{H}_2\text{O})]^-$ species. An apical coordination of a water molecule in the protonated species is expected.

centre, the phosphonate group moves up to the position capping newly formed O₃N-plane of the TSA- [Eu(do3aNP)]²⁻ species.

Surprisingly, the paramagnetic contribution to the ³¹P NMR shift of SA-[Eu(Hdo3aNP)(H₂O)]⁻ species [*i.e.* shift differences between Eu(III) and La(III) complexes of H₅do3aNP in acidic solution] is negative ($\Delta\delta_p = -143$ ppm), whereas in the Eu(III)-complexes of DOTA-like ligands having methylenephosphonate/methylenephosphinate pendant moieties with a phosphorus atom in a similar position, the paramagnetic contribution to the ³¹P NMR shift is positive (15–70 ppm).^{86,87} This contradiction can be explained by a low symmetry of the ligand field of the SA-[Eu(Hdo3aNP)]⁻ complex, which can lead to a discrepancy between principal magnetic and pseudo-C₄ axes and to significant anisotropy of magnetically induced shifts.⁸⁸ This is supported by a large difference in chemical shifts of “axial” macrocycle protons (20–49 ppm; see **Figure 25A**) pointing to different positions of pseudosymmetric-C₄ and principal magnetic axes (all “axial” protons have a similar position in respect to pseudo-C₄ symmetry and they should have a similar chemical shift when the magnetic axis is identical to the (pseudo)symmetry axis). Therefore, in the case of SA-[Eu(Hdo3aNP)]⁻ species, the phosphorus atom could fall into a space close to the principal magnetic axis direction with induced negative ³¹P NMR shifts. This hypothesis was supported by assignment of the ¹H NMR signals of both complex species in the ¹H NMR spectra. It was confirmed that the phosphorus atom moves from a space with induced negative ³¹P NMR shift in the SA isomer to a space with positive ³¹P NMR shift in the TSA isomer.

From a sigmoidal dependence (**Figure 26**) of integral intensities of the phosphorous signals on pH it is possible to calculate the protonation constant characterizing the [Eu(do3aNP)]²⁻/[Eu(Hdo3aNP)(H₂O)]⁻ equilibrium. The value of this protonation constant is strongly dependent on the concentration and type of background electrolyte ($\log K = 7.4$ – 8.5 in dependence of the ionic strength) but independent of the concentration of the complex (**Figure 26** and **Table 3**). When the ³¹P NMR spectra of the complex were measured in the presence of NaCl, CaCl₂ or MgCl₂, the value of the protonation constants dropped with increasing concentration of the salt due to the presence of the coordinable cation facilitating a deprotonation of the ligand side group. In contrast, the protonation constant is significantly higher in the presence of NMe₄Cl (**Table 3**). Such behaviour is expected. The

difference between results obtained by ^{31}P NMR titrations and potentiometry of the pre-formed complex can be attributed to a different and non-controlled ionic strength.

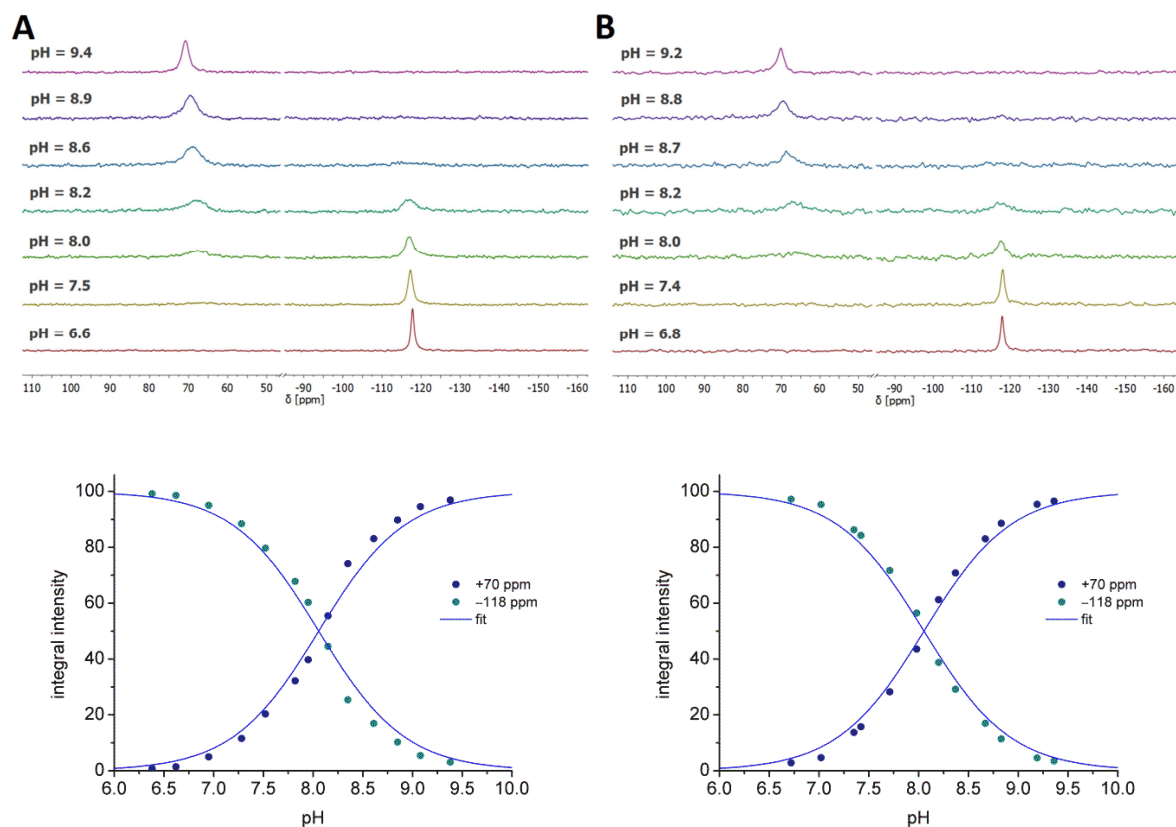


Figure 26: The pH dependence of $^{31}\text{P}\{^1\text{H}\}$ NMR spectra of SA- $[\text{Eu}(\text{Hdo3aNP})(\text{H}_2\text{O})]^-/\text{TSA}-[\text{Eu}(\text{do3aNP})]^{2-}$ complex species at different complex concentrations and corresponding pH dependencies of an integral intensity of the ^{31}P NMR signals. **A:** 50 mM solution, **B:** 10 mM solution. Conditions: H_2O , ~ 150 mM NaCl, $B_0 = 7.05$ T, 25°C . Calculated protonation constants $\log K$ **A:** 8.05, **B:** 8.06.

As the ^{31}P NMR signals of the $[\text{Eu}(\text{Hdo3aNP})(\text{H}_2\text{O})]^-/[\text{Eu}(\text{do3aNP})]^{2-}$ species provided such interesting pH dependence, the integral intensities of these signals were exploited to set up a ratiometric calibration reporting on solution pH. The logarithm-weighted ratio of the integral intensities of the ^{31}P NMR signals of both species at various experimental conditions (different concentration of the complex probe and different ionic strength) was calculated and these values were plotted against the pH in the pH range 6.5–9.5 (**Figure 27**).

Table 3: The protonation constants $\log K$ characterizing $[\text{Eu}(\text{Hdo3aNP})(\text{H}_2\text{O})]^- / [\text{Eu}(\text{do3aNP})]^{2-}$ equilibrium calculated from the ^{31}P NMR titrations at 25 °C.

Background electrolyte	Electrolyte concentration (mM)	Complex concentration (mM)	$\log K$
NaCl	60	20	8.16(3)
NaCl	120	39	8.08(2)
NaCl	154	10	8.05(2)
NaCl	154	50	8.06(3)
NaCl	250	79	7.93(3)
NaCl	1060	19	7.39(2)
NaCl	1260	85	7.40(5)
NMe_4Cl	1270	90	8.53(3)
$\text{NaCl} + \text{CaCl}_2$	190 + 65	65	7.48(3)
$\text{NaCl} + \text{MgCl}_2$	190 + 65	65	7.58(3)

The results prove the principle of the suggested method. The function is linear, slightly dependent on the ionic strength and independent of the concentration of the probe. Therefore, under the defined conditions, it is possible to use these calibration curves to determine pH irrespective of the concentration of the complex.

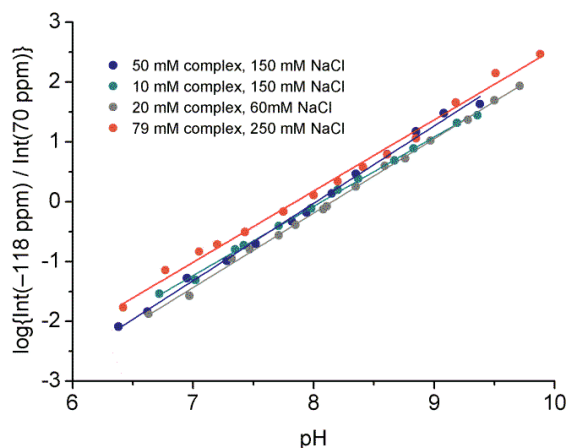


Figure 27: Dependence of $y = \log\{\text{Int}(-118 \text{ ppm}) / \text{Int}(70 \text{ ppm})\} \sim \log\{[\text{SA}] / [\text{TSA}]\}$ on pH in solutions with different concentration of the complex probe ($[\text{Eu}(\text{Hdo3aNP})(\text{H}_2\text{O})]^- / [\text{Eu}(\text{do3aNP})]^{2-}$) and at different ionic strengths relevant for physiological conditions.

6.3.4 pH mapping using ^{31}P MRS

Based on the facts summarized above, the Eu(III) complex with such a slow exchange (with respect to the NMR time-scale) between two, $[\text{Eu}(\text{Hdo3aNP})(\text{H}_2\text{O})]^-$ and $[\text{Eu}(\text{do3aNP})]^{2-}$ complex species, could be employed in the measurement of pH by ^{31}P MRI techniques. Therefore, the $[\text{Eu}(\text{Hdo3aNP})(\text{H}_2\text{O})]^-/[\text{Eu}(\text{do3aNP})]^{2-}$ system was tested as a pH probe using an MRI scanner. The localized ^{31}P NMR spectra were measured in a phantom sample consisting of one vial containing an aq. solution of H_3PO_4 (200 mM) as a reference and three vials with Eu(III)– $\text{H}_5\text{do3aNP}$ complex solutions (50 mM) having different pH values. The selected pH values were 6.4, 8.0 and 9.0. From the previous studies, it is known that the protonated $[\text{Eu}(\text{Hdo3aNP})(\text{H}_2\text{O})]^-$ and the deprotonated $[\text{Eu}(\text{do3aNP})]^{2-}$ complex species are purely present at pH = 6.4 and pH = 9.0, respectively. At pH = 8.0, both species are present in a similar abundance. The experiments performed on the MRI scanner proved the concept suggested above. The signals of the $[\text{Eu}(\text{do3aNP})]^{2-}$ and $[\text{Eu}(\text{Hdo3aNP})(\text{H}_2\text{O})]^-$ species and H_3PO_4 were clearly detected by ^{31}P MR (as shown in the localized spectra in **Figure 28**). The spectral information was then encoded into the images by MRSI. The integrals of the ^{31}P NMR signals were summed in the interval $\delta_p \pm 4$ ppm (*i.e.* 70 ± 4 , 0 ± 4 and -118 ± 4 ppm, respectively) and these were transformed into false colours. Finally, the map of distribution as a sum of all three colour-coded images was reconstructed (**Figure 28**).

As a broad spectral width (~ 250 ppm) is necessary for the measurement, the experiment requires a short excitation pulse. Due to the limitations of available hardware, a block pulse with inhomogenous excitation profile had to be used and, therefore, intensities at different frequencies may not exactly correspond to the concentrations. Due to the hardware limitations, duration of the measurement is quite long. However, it was shown that the probes having two signals of the different species in slow exchange have the prospect of being used in the ^{31}P MRI-based applications useful for pH mapping. All details on this topic are presented in the paper⁸⁹ reprinted in Appendix 3.

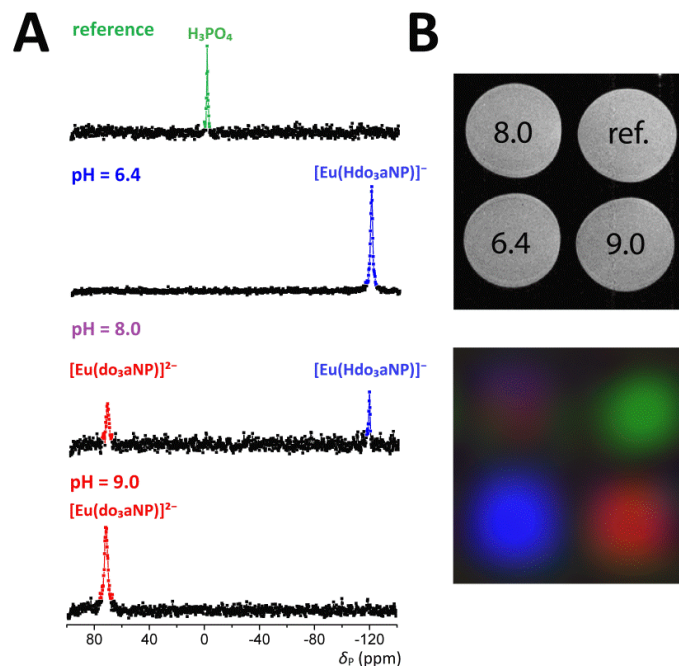


Figure 28: A: Localized ^{31}P MR spectra; B: pH map and legend (^1H MR reference image) of phantom [one vial as a reference containing an aq. solution of H_3PO_4 (~ 200 mM solution in H_2O) and three vials containing aq. solutions of Eu(III)– $\text{H}_3\text{do3aNP}$ complex at pH = 6.4, 8.0 and 9.0 (~ 50 mM solution in H_2O , ~ 150 mM NaCl), $B_0 = 4.7$ T, a single rectangular pulse: BW = 20000 Hz and duration 0.064 ms, TR = 1000 ms, $\text{TE}_{\text{eff}} = 15$ ms, measured matrix size 4×4 interpolated before Fourier transform to 32×32 by zero-filling, field of view 32×32 mm, slice thickness 10 mm, 16384 scans]. Post-processing included interpolation to spatial 256×256 matrix, integration over the selected signals and false colour coding. Colour scheme: red: signal at +70 ppm $\{[\text{Eu}(\text{do3aNP})]^{2-}\}$; blue: at -118 ppm $\{[\text{Eu}(\text{Hdo3aNP})]^{-}\}$; purple: superposition of intensities at +70/–118 ppm; green: 0 ppm (H_3PO_4).

6.3.5 PARACEST experiments

PARACEST properties of the Eu(III) complex were also investigated. First, to identify the signal of an exchangeable proton, the ^1H NMR spectra were measured in H_2O . From the pH-dependent ^1H NMR spectra, it was found that there is one signal at +36.4 ppm which is not observable up to pH ~ 7 and, when the pH is increased, the signal slowly appears (**Figure 29** and **Figure 30A**; note that all of the ^1H NMR spectra shown here have the bulk water peak set at 0 ppm). When the proton spectra are measured in D_2O (**Figure 25**) or with presaturation of the bulk water (**Figure 30B**), the signal at +36.4 ppm was not detected. As the signal is observable only at higher pH where the TSA isomer is gradually formed, one can conclude that it can be assigned to the proton of the coordinated secondary

amino group of the pendant arm. It is supported by the similarity of the chemical shift of this signal to that of one of the protons of primary amino group of the $[\text{Eu}(\text{do3a-ae})(\text{H}_2\text{O})]$ complex (+34 ppm).⁷⁴ Moreover, the signal is visible in the ^1H NMR spectrum in alkaline solutions. Thus, the possibility that it belongs to a coordinated water molecule can be excluded as those signals disappear in the alkaline region.⁷⁸

Based on these findings, PARACEST properties of the $\text{Eu}(\text{III})$ - $\text{H}_5\text{do3aNP}$ complex were investigated in an aq. solution from slightly acidic (pH \sim 6) to alkaline solutions (pH \sim 9). Surprisingly, it was found that the $\text{Eu}(\text{III})$ complex gives one CEST signal at -17 ppm at pH = 6.0 (see **Figure 31**) which slowly disappears from the Z-spectra and it is not observable above pH \sim 8. In the ^1H NMR spectra, no signal of exchangeable proton at such a chemical shift was observed. It is very probably overlapped with the signals of CH_2 protons and, therefore, it cannot be detected. As the CEST signal at -17 ppm is observed at the pH range where the presence of the $[\text{Eu}(\text{Hdo3aNP})(\text{H}_2\text{O})]^-$ species in solution is supposed, one can assume that the peak refers to the protons of protonated and uncoordinated secondary amino group

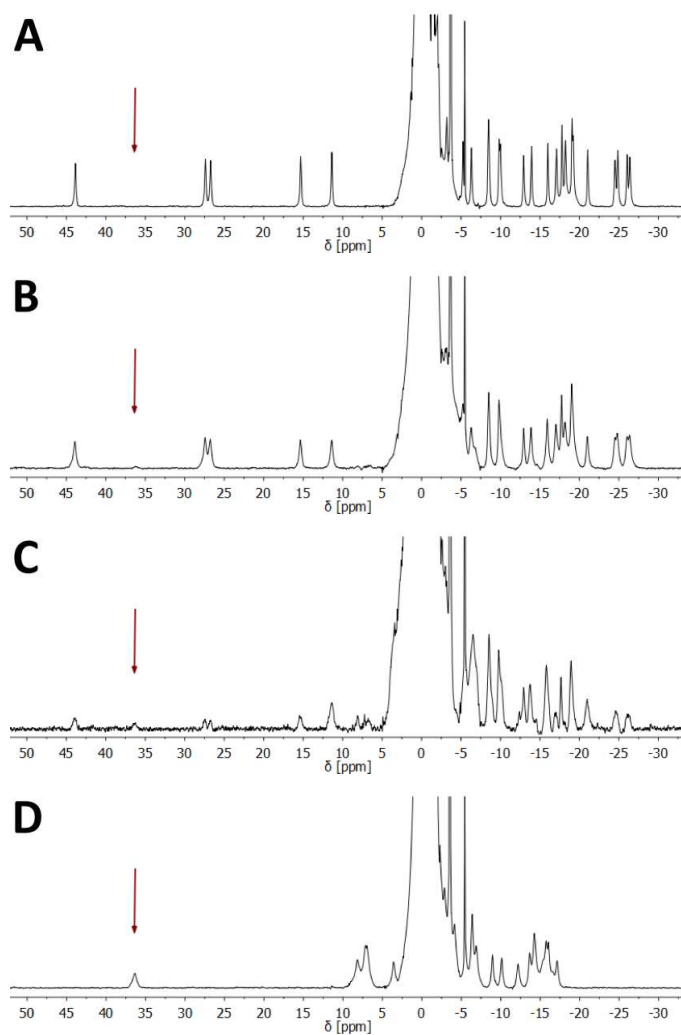


Figure 29: ^1H NMR spectra of the $[\text{Eu}(\text{Hdo3aNP})(\text{H}_2\text{O})]^-/[\text{Eu}(\text{do3aNP})]^{2-}$ species (85 mM solution in H_2O , $B_0 = 7.05$ T, 25°C) at **A:** pH = 6.5, **B:** pH = 7.4 and **C:** pH = 7.7 and **D:** pH = 8.5. Arrows show the position of the exchangeable proton. Chemical shift of H_2O in the sample solution was referenced to 0 ppm.

which is located sufficiently close to the highly paramagnetic centre. Due to a negative chemical shift of

the signal (-17 ppm), an assignment to coordinated water molecule can be excluded, as the signals of coordinated water in the Eu(III)-macrocycle complexes are typically much more shifted away from the bulk water signal and, in addition, these are in a positive chemical shifts range.^{31,90,91}

With increasing pH, the CEST signal at -17 ppm disappears from the Z-spectra as a consequence of deprotonation and coordination of pendant amino group and another signal at $+36.4$ ppm (**Figure 31**) starts to be observable. This CEST signal corresponds to the signal detected in the ^1H NMR spectra. Based on comparison with previous data obtained by the ^1H NMR experiments with this complex, it was attributed to the protons of pendant arm amino group of the $[\text{Eu}(\text{do3aNP})]^{2-}$ species. As the CEST signal is detected even in alkaline region, the mechanism

is associated with semilabile coordination of amino group analogously, as in the case of the Ln(III) complexes with $\text{H}_3\text{do3a-ae}$, $\text{H}_3\text{do3a-aeMe}$ and $\text{H}_3\text{do3aNN}$.

To validate the observed CEST spectra of the Eu(III) complex, CEST imaging was done on a 4.7 T MRI scanner using a phantom containing complex solutions at three different pH values (pH = 6.4, 7.8 and 8.6) as shown in **Figure 32**. It is evident that the CEST effect is clearly detected in the sample solution at pH = 6.4 and 7.8 when the presaturation pulse is applied at -17 ppm (**Figure 32A**), whilst by switching the presaturation frequency to $+36$ ppm, saturation transfer can be observed only in the samples at pH = 7.8 and 8.6 (**Figure 32B**). Such behaviour is consistent with the results obtained from the NMR experiments and it supports our concept of the probe with two independent proton-exchanging sites producing different dependencies of their CEST effect on pH.

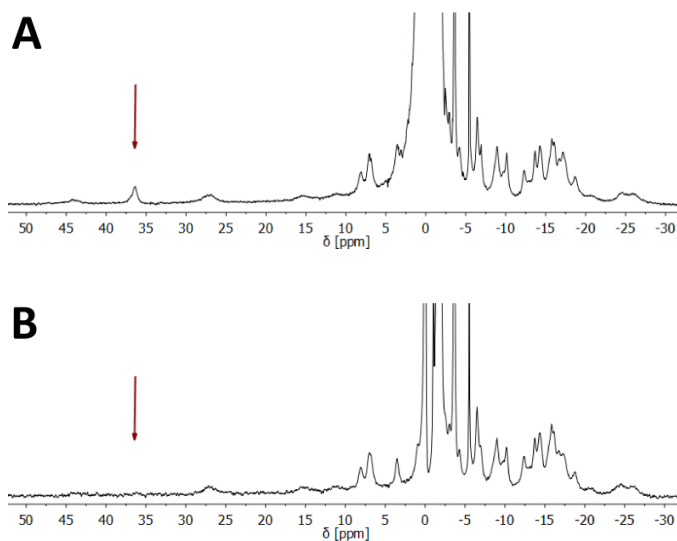


Figure 30: ^1H NMR spectra of the $[\text{Eu}(\text{Hdo3aNP})(\text{H}_2\text{O})]^- / [\text{Eu}(\text{do3aNP})]^{2-}$ species in H_2O (87 mM, $B_0 = 7.05$ T, 25 °C) at pH = 8.0 **A:** without and **B:** with presaturation of the bulk water signal. Arrows show the position of exchangeable (NH) protons. Chemical shift of H_2O in the sample solution was referenced to 0 ppm.

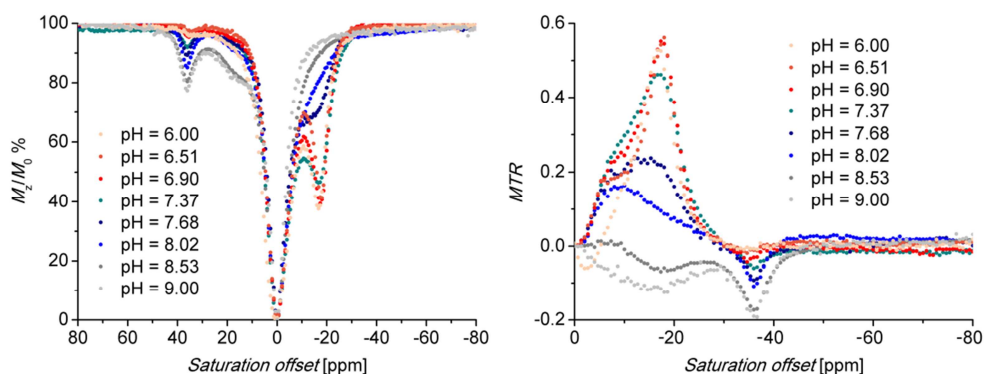


Figure 31: Z- and corresponding MTR spectra of 87 mM aq. solution of the $[\text{Eu}(\text{Hdo3aNP})(\text{H}_2\text{O})]^-$ and $[\text{Eu}(\text{do3aNP})]^{2-}$ complex species ($B_0 = 7.05 \text{ T}$, $B_1 = 16.5 \mu\text{T}$ (700 Hz), RF presaturation pulse applied for 2 s, 25 °C).

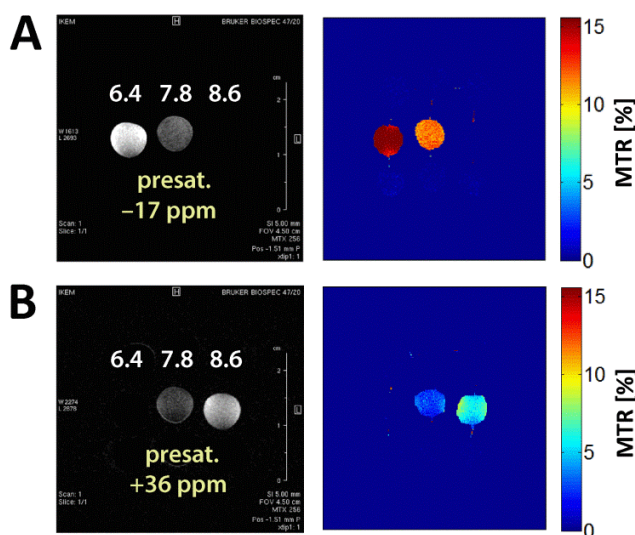


Figure 32: MRI-CEST images of phantom consisting of three vials containing aq. solutions of the Eu(III) complex of $\text{H}_5\text{do3aNP}$ (82 mM solution; ~250 mM NaCl) with different pH values (in false colours). Experimental conditions: turbo spin echo pulse sequence, $B_0 = 4.7 \text{ T}$, RF presaturation pulse applied for 2 s at **A:** -17 ppm **B:** +36 ppm; $T = 298 \text{ K}$, $\text{TR} = 5 \text{ s}$, $\text{TE} = 8.9 \text{ ms}$, $B_1 = 10 \mu\text{T}$ (425 Hz).

In the previous study it was shown that the $[\text{Ln}(\text{H}_n\text{do3aNN})(\text{H}_2\text{O})_{0-1}]^n$ complexes are not fully kinetically inert in acidic solutions ($\text{pH} < 6$).⁸² Therefore, the stability of the Eu(III) complex of the $\text{H}_5\text{do3aNP}$ was also tested. The complex solution ($\text{pD} = 5.9$) was heated for 3 weeks at 60 °C and it was

monitored by ^{31}P NMR spectroscopy and by xylenol orange test. It was found that the ^{31}P NMR spectra remain unchanged during this period and the negative xylenol orange test confirmed that the complex does not release the free metal ion. Because the complex is stable under these conditions, this probe has potential for being used as a ratiometric pH contrast agent and it is being further investigated.

6.3.6 Conclusions

The present study describes the synthesis of the new macrocyclic ligand $\text{H}_3\text{do3aNP}$ with phosphonomethyl-aminoethyl coordinating pendant arm and its coordination properties studied by potentiometry and NMR spectroscopy. NMR experiments revealed significant pH dependence of the ^{31}P NMR spectra of Eu(III) complex. It was shown that the *in-cage* complexation of the Eu(III) is finished at $\text{pH} > 5$ forming the $[\text{Eu}(\text{Hdo3aNP})(\text{H}_2\text{O})]^-$ complex species with protonated NH_3^+ group and SA arrangement and with the phosphonate group coordinated in the O_4 -plane. Upon deprotonation ($\text{p}K_a \sim 8$) and coordination of the pendant amino group, it is converted to a $[\text{Eu}(\text{do3aNP})]^{2-}$ species preferring TSA geometry with the phosphonate group capping the apical position of the newly formed O_3N -coordination plane. The ^{31}P NMR shifts of the species differ by an unprecedented value (~ 190 ppm) and both SA/TSA species are in slow exchange with respect to the NMR time scale. Therefore, it is possible to compare the integral intensities of two separate signals and use this complex as concentration independent ratiometric probe for pH determination using ^{31}P Magnetic Resonance Spectroscopic (MRS) technique. In addition, both SA- $[\text{Eu}(\text{Hdo3aNP})(\text{H}_2\text{O})]^-$ and TSA- $[\text{Eu}(\text{do3aNP})]^{2-}$ complex species are CEST-active exhibiting the CEST peaks of amino group of the aminophosphonate pendant arm at ~ -17 ppm and $+36$ ppm, respectively. These two signals have different dependencies of their CEST effect on pH. Therefore, the applicability of this complex for pH determination without complications from varying concentrations of the agent is being investigated in more detail.

7 CONCLUSIONS

In this PhD Thesis, I studied several novel macrocyclic ligands with exchangeable protons on their coordinating pendant arms that could potentially be (after the complexation with suitable paramagnetic ions) responsive CAs for MRI. My attention was focused on pH-responsive CAs because the ability to determine extracellular pH could provide information on disease progress. In an effort to develop a novel pH-responsive MRI CA with potential to be used *in vivo*, I decided to study Ln(III) complexes with exchangeable protons of amino groups.

This Thesis deals with a study of Eu(III) and Yb(III) complexes of three macrocyclic ligands with 2-aminoethyl pendant arms containing primary (H₃do3a-ae), secondary (H₃do3a-aeMe) and tertiary (H₃do3a-ae2Me) amino groups, with a view to explore their PARACEST properties. It was shown that the PARACEST effect of the Eu(III)–H₃do3a-ae/H₃do3a-aeMe and Yb(III)–H₃do3a-ae/H₃do3a-aeMe complexes was observable. In both cases, the PARACEST effect was strongly dependent on pH in the region of 4.5–7.5 where the coordination of the pendant amino group to the metal ion is expected. In more alkaline solutions, the CEST efficiency was pH-independent. Such behaviour has not yet been reported in the literature. Based on these findings, a new mechanism of the PARACEST effect associated with the semilabile coordination of the 2-aminoethyl pendant arm was suggested. Surprisingly, the Yb(III)–H₃do3a-ae2Me complex is also CEST-active. In this case, the CEST effect is caused by a magnetic saturation transfer to the bulk water protons from the protons of the uncoordinated and protonated dimethylamino group which is still located close to the paramagnetic centre. The applicability of the Eu(III)– and Yb(III)–H₃do3a-ae complexes as MRI pH probes was tested by MRI scanner in the pH region relevant for living systems. The results clearly showed the potential of these compounds.

As the second goal of my project, I decided to study another promising structure with a linear diaminic pendant arm (H₃do3aNN). Choosing this molecule was motivated by the presence of two potentially independent proton exchanging pools (primary and secondary amino groups) in the

structure. The PARACEST properties of its Eu(III) and Yb(III) complexes were studied and in both cases the experiments revealed two CEST signals of the major isomer corresponding to the primary and secondary amino groups. In addition, the shape of the Z-spectra of the $[\text{Ln}(\text{H}_n\text{do3aNN})(\text{H}_2\text{O})_{0-1}]^n$ complexes was significantly dependent on pH in a slightly acidic to neutral region (pH = 5–8). The intensity of the CEST effect was obviously dependent on the protonation state of each amino group. In addition, the CEST signal of the primary amino group exhibits different pH dependence from that of the secondary amine and the differences were clearly detectable by MRI scanner. In the case of the $[\text{Yb}(\text{H}_n\text{do3aNN})]^n$, it was possible to define the pH-dependent but concentration-independent ratiometric calibration function (the complex concentrations in the tested samples were 7.7–87 mM). Unfortunately, it was shown that the presence of linear diaminic pendant arm in the ligand structure decreases kinetic inertness of their Ln(III) complexes (the complexes slowly release the free metal ion even in slightly acidic solutions); thus, they cannot be used in medical applications. However, the present study showed the possibility of using Ln(III) complexes containing CEST-active exchangeable NH protons for pH determination using MRI ratiometry, and it was an impulse to synthesize novel complexes for this purpose.

Based on the results of the previous experiments, a novel ligand with *N*-phosphonomethyl-2-aminoethyl coordinating pendant arm ($\text{H}_5\text{do3aNP}$) was designed and prepared, and the PARACEST properties of its Ln(III) complexes and potential use of these complexes in the ^{31}P NMR/MRI-based applications were explored. It was found that the protonated $[\text{Eu}(\text{Hdo3aNP})(\text{H}_2\text{O})]^-$ complex exclusively forms a single diastereomer with square-antiprismatic (SA) geometry in solution. Upon deprotonation ($\text{p}K_a \sim 8$) and coordination of the pendant amino group, the complex rearranges to the twisted-square-antiprismatic TSA- $[\text{Eu}(\text{do3aNP})]^{2-}$ species. These complex species are in slow equilibrium on the NMR time-scale, providing two separate signals in the ^{31}P NMR spectra with a chemical shift difference of ~ 190 ppm. It was shown that the integral intensities of these signals could be used for calculation of ratiometric function in the pH range 6.5–9.5, allowing for determination of pH by MRS ratiometry. In addition, each complex species exhibits a separate CEST signal of the amino group. These CEST peaks have different dependencies on pH and, therefore, it also allows determination of pH by CEST ratiometry.

Currently, the complexes of H₅do3aNP with other Ln(III) ions are being investigated. By changing the central metal ion it is possible to influence the ³¹P NMR chemical shift of the complex species and, in addition, to affect the protonation constant characterizing equilibrium of the deprotonated/protonated secondary amino group of the pendant arm and to “modulate” properties of the PARACEST agent or agent for MRSI technique.

8 LIST OF ABBREVIATIONS

3-APP	3-aminopropylphosphonic acid
6-FPAM	6-fluoropyridoxamine
6-FPOL	6-fluoropyridoxol
BIRDS	biosensor imaging of redundant deviation in shift
BW	bandwidth
CA	contrast agent
CEST	chemical exchange saturation transfer
CSI	chemical shift imaging
DCM	dichloromethane
DMF	<i>N,N</i> -dimethylformamide
FID	free induction decay
IEPA	2-(imidazol-1-yl)-3-ethoxycarbonyl-propanoic acid
MPIO	micron-sized iron oxide particles
MRI	magnetic resonance imaging
MRS	magnetic resonance spectroscopy
MRSI	magnetic resonance spectroscopic imaging
MTR	magnetization transfer ratio
NMR	nuclear magnetic resonance
NSF	nephrogenic systemic fibrosis
PARACEST	paramagnetic chemical exchange saturation transfer
pH _e	extracellular pH
pH _i	intracellular pH
P _i	inorganic phosphate

q	number of water molecules bound in the first coordination sphere of Ln(III) ion
r_1	longitudinal relaxivity
R_1	longitudinal relaxation rate ($1/T_1$)
r_2	transversal relaxivity
R_2	transversal relaxation rate ($1/T_2$)
RARE	rapid acquisition with relaxation enhancement
RF	radiofrequency
RT	room temperature
SA	square antiprism
SPIO	super paramagnetic iron oxides
T_1	longitudinal relaxation time
T_2	transversal relaxation time
TBAB	tetrabutylammonium bromide
TE	echo time
TEA	triethylamine
TE_{eff}	effective echo time
TR	repetition time
TSA	twisted square antiprism
USPIO	ultra-small super paramagnetic iron oxides

9 DECLARATION OF CONTRIBUTION

Hereby, the author of this Thesis declares that her contribution to the work was dominant. The author performed all the chemical synthetic work (synthesis of all the studied ligands as well as their Ln(III) complexes). The author also personally performed a great deal of the characterizations and studies of the prepared ligands and complexes if she was authorized to use the equipment (HPLC purification, NMR characterization and interpretation, ^1H and ^{31}P NMR titrations, UV-Vis and PARACEST NMR experiments) or at least she prepared samples for the measurements that were performed by somebody else (MS characterization, advanced NMR experiments, PARACEST MRI and MRSI experiments). Nevertheless, she participated in the evaluation of all results. Potentiometric titrations were arranged in cooperation with J. Havlíčková or Z. Böhmová. X-ray structures were solved by I. Císařová and refined by J. Kotek on the single crystals prepared by the author. The author actively participated in preparation of all the publications.

10 ACKNOWLEDGEMENTS

First of all, I express my sincere gratitude to Honza Kotek who has supervised me during the whole time I have spent at the Faculty of Science and who has introduced me to a “scientific world”. He was an unceasing source of ideas and endless enthusiasm. Thanks for all his suggestions for the “last experiment”, even though it was never the last one. I know that without these ideas I would never be able to finish even a part of this Thesis.

I also thank Andrea, Vít and Dan from IKEM, with whom I have had a great opportunity to collaborate on scientific projects. Thanks for their help and “afternoon tea at five o’ clock”.

Furthermore, huge thanks to everyone who has participated in this research. Namely, I thank Ivana Císařová, Zdeněk Tošner, Vojta Kubíček, Petr Hermann, Honza Blahut, Jana Havlíčková and Zuzka Böhmová. Much of my experimental work would have not been completed without their assistance.

I am also very thankful to my colleagues and friends from “lab 19” and from our “small lab” for an inspiring and friendly atmosphere. It was really joyful time with them. In particular, I am grateful to Honza Blahut for our everyday fruitful discussions on (in)significant topics. He has been my faithful sports teammate and partner in “Friday experiments”, no matter what the day actually was.

Special thanks go to my friends and family who have given me their support, for which my mere expressions of thanks likewise does not suffice.

Last but not least, I thank Petr for his everyday dose of irony, personal support, patience, and for a lot of advice during the whole time I have spent at the University. Díky!

11 REFERENCES

- ¹ M. H. Levitt, *Spin Dynamics – Basics of Nuclear Magnetic Resonance*, Wiley, Chichester, United Kingdom, 2006
- ² R. R. Ernst and W. A. Anderson, *Rev. Sci. Instrum.*, 1966, **37**, 93–102
- ³ A. Kumar, *J. Indian. J. Sci.*, 2014, **94**, 363–369
- ⁴ R. V. Damadian, *Science*, 1971, **171**, 1151–1153
- ⁵ R. V. Damadian, U.S. Patent no. 3789832, 1974
- ⁶ P. C. Lauterbur, *Nature*, 1973, **242**, 190–191
- ⁷ P. C. Lauterbur, *Angew. Chem., Int. Ed.*, 2005, **44**, 1004–1011
- ⁸ G. M. Pohost, G. A. Elgavish and W. T. Evanochko, *J. Am. Col. Cardiol.*, 1986, **7**, 709–710
- ⁹ T. Geva, *J. Cardiovasc. Magn. Reson.*, 2006, **8**, 573–580
- ¹⁰ P. Hermann, J. Kotek, V. Kubiček and I. Lukeš, *Dalton Trans.*, **2008**, 3027–3047
- ¹¹ I. Tirotta, V. Dichiarante, C. Pigliacelli, G. Cavallo, G. Terreneo, F. B. Bombelli, P. Metrangolo and G. Resnati, *Chem. Rev.*, 2015, **115**, 1106–1129
- ¹² *The Chemistry of Contrast Agents in Medical Magnetic Resonance Imaging*, ed. A. Merbach, L. Helm and É. Tóth, 2nd ed., Wiley, Chichester, United Kingdom, 2013
- ¹³ T. D. Soesbe, Y. Wu and A. D. Sherry, *NMR Biomed.*, 2013, **20**, 829–838
- ¹⁴ F. L. Giesel, A. Mehndiratta and M. Essig, *Eur. Radiol.*, 2010, **20**, 2461–2474
- ¹⁵ M. Saeed, *Exp. Biol. Med.*, 2001, **226**, 367–376
- ¹⁶ (a) D. V. Hingorani, A. S. Bernstein and M. D. Pagel, *Contrast Media Mol. Imaging*, 2015, **10**, 245–265; (b) G. Angelovski, *Angew. Chem., Int. Ed.*, 2016, **55**, 7038–7046
- ¹⁷ G.-L. Davies, I. Kramberger and J. J. Davis, *Chem. Commun.*, 2013, **49**, 9704–9721
- ¹⁸ M. Port, J. M. Idée, C. Medina, C. Robic, M. Sabatou and C. Corot, *Biomaterials*, 2008, **21**, 469–490
- ¹⁹ E. P. Mayoral, V. Negri, J. S. Padrós, S. Cerdán and P. Ballesteros, *Eur. J. Radiol.*, 2008, **67**, 453–458
- ²⁰ E. Terreno, D. D. Castelli, A. Viale and S. Aime, *Chem. Rev.*, 2010, **110**, 3019–3042

- ²¹ M. Norek, E. Kampert, U. Zeitler and J. A. Peters, *J. Am. Chem. Soc.*, 2008, **130**, 5335–5340
- ²² M. Kačenka, O. Kaman, J. Kotek, L. Falteisek, J. Černý, D. Jiráček, V. Herynek, K. Zacharovová, Z. Berková, P. Jendelová, J. Kupčík, E. Pollert, P. Veverka and I. Lukeš, *J. Mater. Chem.*, 2011, **21**, 157–164
- ²³ H. B. Na, I. C. Song and T. Hyeon, *Adv. Mater.*, 2009, **21**, 2133–2148
- ²⁴ Y. X. J. Wang, *Quant. Imaging Med. Surg.*, 2011, **1**, 35–40
- ²⁵ (a) U. Liddel and N. F. Ramsey, *J. Chem. Phys.*, 1951, **19**, 1608; (b) J. T. Arnold and M. E. Packard, *J. Chem. Phys.*, 1951, **19**, 1608–1609
- ²⁶ H. M. McConnell and D. D. Thompson, *J. Chem. Phys.*, 1957, **26**, 958–959
- ²⁷ A. D. Sherry and M. Woods, *Annu. Rev. Biomed. Eng.*, 2008, **10**, 391–411
- ²⁸ S. D. Wolff and R. S. Balaban, *Magn. Reson. Med.*, 1989, **10**, 135–144
- ²⁹ S. D. Wolff and R. S. Balaban, *J. Magn. Reson.*, 1990, **86**, 164–169
- ³⁰ J. Zhou and P. C. M. van Zijl, *Prog. Nucl. Magn. Reson. Spectrosc.*, 2006, **48**, 109–136
- ³¹ S. Zhang, M. Merritt, A. E. Woessner, R. E. Lenkinski and A. D. Sherry, *Acc. Chem. Res.*, 2003, **36**, 783–790
- ³² K. M. Ward, A. H. Altras and R. S. Balaban, *J. Magn. Reson.*, 2000, **143**, 79–87
- ³³ M. Woods, D. E. Woesner and A. D. Sherry, *Chem. Soc. Rev.*, 2006, **35**, 500–511
- ³⁴ P. C. M. van Zijl, C. K. Jones, J. Ren, C. R. Malloy and A. D. Sherry, *Proc. Natl. Acad. Sci. USA*, 2007, **104**, 4359–4364
- ³⁵ S. Zhang, P. Winter, K. Wu and A. D. Sherry, *J. Am. Chem. Soc.*, 2001, **123**, 1517–1518
- ³⁶ S. Aime, A. Barge, M. Botta, A. S. De Sousa and D. Parker, *Angew. Chem., Int. Ed.*, 1998, **37**, 2673–2675
- ³⁷ S. Zhang, P. Winter, K. Wu and A. D. Sherry, *J. Am. Chem. Soc.*, 2001, **123**, 1517–1518
- ³⁸ S. Zhang and A. D. Sherry, *J. Solid State Chem.*, 2003, **171**, 38–43
- ³⁹ S. Aime, A. Barge, D. D. Castelli, F. Fedeli, A. Mortillaro, F. U. Nielsen and E. Terreno, *Magn. Reson. Med.*, 2002, **47**, 639–648
- ⁴⁰ S. Zhang, L. Michaudet, S. Burgess and A. D. Sherry, *Angew. Chem., Int. Ed.*, 2002, **41**, 1919–1921

- ⁴¹ M. Woods, D. E. Woessner, P. Zhao, A. Pasha, M.-Y. Yang, C.-H. Huang, O. Vasalitiy, J. R. Morrow and A. D. Sherry, *J. Am. Chem. Soc.*, 2006, **128**, 10155–10162
- ⁴² L. L. Chappell, D. A. Voss, Jr., W. DeW. Horrocks, Jr. and J. R. Morrow, *Inorg. Chem.*, 1998, **37**, 3989–3898
- ⁴³ S. Viswanathan, Z. Kovács, K. N. Green, A. J. Ratnakar and A. D. Sherry, *Chem. Rev.*, 2010, **110**, 1960–3018
- ⁴⁴ K. O. A. Chin, J. R. Morrow, C. H. Lake and M. R. Churchill, *Inorg. Chem.*, 1994, **33**, 656–664
- ⁴⁵ C.-H. Huang and J. R. Morrow, *Inorg. Chem.*, 2009, **48**, 7237–7243
- ⁴⁶ D. D. Castelli, E. Terreno and S. Aime, *Angew. Chem., Int. Ed.*, 2011, **123**, 1838–1840
- ⁴⁷ (a) H. Thomsen, *J. Magn. Reson. Imaging*, 2008, **28**, 284–286; (b) J. Kurtkoti, T. Snow and B. Hiremagalur, *Nephrology*, 2008, **13**, 235–241; (c) P. H. Kuo, *AJR*, 2008, **191**, 1861–1863; (d) N. M. Rofsky, A. D. Sherry and R. E. Lenkinski, *Radiology*, 2008, **247**, 608–612
- ⁴⁸ (a) S. J. Dorazio, P. B. Tsitovich, K. E. Sifers, J. A. Sperryak and J. R. Morrow, *J. Am. Chem. Soc.*, 2011, **133**, 14154–14156; (b) S. J. Dorazio, P. B. Tsitovich, S. A. Gardina and J. R. Morrow, *J. Inorg. Biochem.*, 2012, **117**, 212–219; (c) P. B. Tsitovich and J. R. Morrow, *Inorg. Chim. Acta*, 2012, **393**, 3–11; (d) S. J. Dorazio and J. R. Morrow, *Eur. J. Inorg. Chem.*, **2012**, 2006–2014; (e) S. J. Dorazio, A. O. Olatunde, P. B. Tsitovich and J. R. Morrow, *J. Biol. Inorg. Chem.*, 2014, **19**, 191–205; (f) A. O. Olatunde, C. J. Bond, S. J. Dorazio, J. M. Cox, J. B. Benedict, M. D. Daddario, J. A. Sperryak and J. R. Morrow, *Chem. - Eur. J.*, 2015, **21**, 18290–18300; (g) S. J. Dorazio and J. R. Morrow, *Inorg. Chem.*, 2012, **51**, 7448–7450
- ⁴⁹ (a) S. J. Dorazio, A. O. Olatunde, J. A. Sperryak and J. R. Morrow, *Chem. Commun.*, 2014, **49**, 10025–10027; (b) A. O. Olatunde, S. J. Dorazio, J. A. Sperryak and J. R. Morrow, *J. Am. Chem. Soc.*, 2012, **134**, 18503–18505; (c) P. B. Tsitovich, J. A. Sperryak and J. R. Morrow, *Angew. Chem., Int. Ed.*, 2013, **52**, 13997–14000
- ⁵⁰ R. J. Gillies, N. Raghunand, M. L. Garcia Martin and R. A. Gatenby, *IEEE Eng. Med. Biol.*, 2004, **23**, 57–64
- ⁵¹ S. Rockwell, T. Dobrucki, E. Y. Kim, S. T. Marrison and V. T. Vu, *Curr. Mol. Med.*, 2009, **9**, 442–458

- ⁵² B. P. Mahoney, N. Raghunand, B. Baggett and R. J. Gillies, *Biochem. Pharmacol.*, 2003, **66**, 1207–1218
- ⁵³ D. D. Castelli, G. Ferrauto, J. C. Cutrin, E. Terreno and S. Aime, *Magn. Reson. Med.*, 2014, **71**, 326–332
- ⁵⁴ (a) S. Zhang, K. Wu, A. D. Sherry, *Angew. Chem., Int. Ed.*, 1999, **38**, 3192–3194; (b) N. Raghunand, C. Howison, A. D. Sherry, S. Zhang and R. J. Gillies, *Magn. Reson. Med.*, 2003, **49**, 249–257; (c) F. K. Kálmán, M. Woods, P. Caravan, P. Jurek, M. Spiller, G. Tircsó, R. Király, E. Brücher and A. D. Sherry, *Inorg. Chem.*, 2007, **46**, 5260–5270
- ⁵⁵ M. P. Lowe, D. Parker, O. Reany, S. Aime, M. Botta, G. Castellano, E. Gianolio and R. Pagliarin, *J. Am. Chem. Soc.*, 2001, **123**, 7601–7609
- ⁵⁶ (a) G. B. Giovenzana, R. Negri, G. A. Rolla and L. Tei, *Eur. J. Inorg. Chem.*, **2012**, 2035–2039; (b) Z. Baranyai, G. A. Rolla, R. Negri, A. Forgács, G. B. Giovenzana and L. Tei, *Chem. - Eur. J.*, 2014, **20**, 2933–2944
- ⁵⁷ M. Woods, G. E. Kiefer, S. Bott, A. Castillo-Muzquiz, C. Eshelbrenner, L. Michaudet, K. McMillan, S. D. K. Mudigunda, D. Ogrin, G. Tircso, S. Zhang, P. Zhao and A. D. Sherry, *J. Am. Chem. Soc.*, 2004, **126**, 9248–9256
- ⁵⁸ J. Hall, R. Häner, S. Aime, M. Botta, S. Faulkner, D. Parker and A. S. de Sousa, *New J. Chem.*, 1998, **22**, 627–631
- ⁵⁹ L. M. de Leon-Rodriguez, A. J. M. Lubag, C. R. Malloy, G. V. Martinez, R. J. Gillies and A. D. Sherry, *Acc. Chem. Res.*, 2009, **42**, 948–957
- ⁶⁰ M. L. Garcia Matin, G. V. Martinez, N. Raghunand, A. D. Sherry, S. Zhang and R. J. Gillies, *Magn. Reson. Med.*, 2006, **55**, 309–315
- ⁶¹ S. Aime, F. Fedeli, A. Sanino and E. Terreno, *J. Am. Chem. Soc.*, 2006, **128**, 11326–11327
- ⁶² S. Aime, D. D. Castelli and E. Terreno, *Angew. Chem., Int. Ed.*, 2002, **41**, 4334–4336
- ⁶³ N. McVicar, A. X. Li, M. Suchý, R. H. E. Hudson, R. S. Menon and R. Bartha, *Magn. Reson. Med.*, 2013, **70**, 1016–1025
- ⁶⁴ (a) V. R. Sheth, Y. Li, L. Q. Chen, C. M. Howison, C. A. Flask and M. D. Pagel, *Magn. Reson. Med.*, 2012, **67**, 760–768; (b) G. Liu, Y. Li, V. R. Sheth and M. D. Pagel, *Mol. Imaging*, 2012, **11**, 47–57

- ⁶⁵ S. Posse, R. Otazo, S. R. Dager and J. Alger, *J. Magn. Reson. Imaging*, 2013, **37**, 1301–1325
- ⁶⁶ R. J. Griffiths, *Br. J. Cancer*, 1991, **64**, 425–427
- ⁶⁷ R. J. Gillies and D. L. Morse, *Annu. Rev. Biomed. Eng.*, 2005, **7**, 287–326
- ⁶⁸ S. He, R. P. Mason, V. D. Mehta, V. Arora, R. Katipally, P. V. Kulkarni and P. P. Antich, *Bioorg. Med. Chem.*, 1998, **6**, 1631–1639
- ⁶⁹ R. P. Mason, *Curr. Med. Chem.*, 1999, **6**, 481–499
- ⁷⁰ (a) R. van Sluis, Z. M. Bhujwala, N. Raghunand, P. Ballesteros, J. Alvarez, S. Cerdan, J. P. Galons and R. J. Gillies, *Magn. Reson. Med.*, 1999, **41**, 743–750; (b) M. L. Garcia Martin, G. Herigault, C. Remy, R. Farion, P. Ballesteros, J. A. Coles, S. Cerdan and A. Ziegler, *Cancer Res.*, 2001, **61**, 6524–6531
- ⁷¹ S. Aime, M. Botta, L. Milone and E. Terreno, *Chem. Commun.*, **1996**, 1265–1266
- ⁷² D. Coman, H. K. Trubel, R. E. Rycyna and F. Hyder, *NMR Biomed.*, 2009, **22**, 229–239
- ⁷³ Y. Huang, D. Coman, M. M. Ali and F. Hyder, *Contrast Media Mol. Imaging*, 2015, **10**, 51–58
- ⁷⁴ T. Krchová, J. Kotek, D. Jiráček, J. Havlíčková, I. Císařová and P. Hermann, *Dalton Trans.*, 2013, **42**, 15735–15747
- ⁷⁵ T. Krchová, Diploma Thesis, Charles University, Praha, 2012
- ⁷⁶ S. Aime, M. Botta and G. Ermondi, *Inorg. Chem.*, 1992, **31**, 4292–4299
- ⁷⁷ (a) P. Caravan, J. J. Ellison, T. J. McMurry and R. B. Lauffer, *Chem. Rev.*, 1999, **99**, 2293–2352; (b) C. F. G. C. Geraldes and S. Laurent, *Contrast Media Mol. Imaging*, 2009, **4**, 1–23
- ⁷⁸ M. Woods, A. Pasha, P. Zhao, G. Tircsó, S. Chowdhury, G. Kiefer, D. E. Woessner and A. D. Sherry, *Dalton Trans.*, 2011, **40**, 6759–6764
- ⁷⁹ A. O. Olatunde, J. M. Cox, M. D. Daddario, J. A. Sperry and J. R. Morrow, *Inorg. Chem.*, 2014, **53**, 8311–8321
- ⁸⁰ D. D. Castelli, E. Terreno and S. Aime, *Angew. Chem., Int. Ed.*, 2011, **50**, 1798–1800
- ⁸¹ A. Barge, C. Cravotto, E. Gianolio and F. Fedeli, *Contrast Media Mol. Imaging*, 2006, **1**, 184–188
- ⁸² T. Krchová, A. Gálisová, D. Jiráček, P. Hermann and J. Kotek, *Dalton Trans.*, 2016, **45**, 3486–3496
- ⁸³ I. Lukeš, J. Kotek, P. Vojtíšek and P. Hermann, *Coord. Chem. Rev.*, 2001, **216–217**, 287–312

- ⁸⁴ M. Pniok, V. Kubíček, J. Havlíčková, J. Kotek, A. Sabatie-Gogová, J. Plutnar, S. Huclier-Markai and P. Hermann, *Chem. - Eur. J.*, 2014, **20**, 7944–7955
- ⁸⁵ A. E. Martell, R. M. Smith and R. J. Motekaitis, NIST Critically Selected Stability Constants of Metal Complexes, Version 7, Texas A&M University, College Station, TX
- ⁸⁶ M. P. C. Campello, S. Lacerda, I. C. Santos, G. A. Pereira, C. F. G. C. Geraldés, J. Kotek, P. Hermann, J. Vaněk, P. Lubal, V. Kubíček, E. Tóth and I. Santos, *Chem. - Eur. J.*, 2010, **16**, 8446–8465
- ⁸⁷ (a) P. Lebdušková, P. Hermann, L. Helm, É. Tóth, J. Kotek, K. Binnemans, J. Rudovský, I. Lukeš and A. E. Merbach, *Dalton Trans.*, **2007**, 493–501; (b) T. Vitha, V. Kubíček, J. Kotek, P. Hermann, L. Vander Elst, R. N. Muller, I. Lukeš and J. A. Peters, *Dalton Trans.*, **2009**, 3204–3214; (c) J. Rudovský, P. Cígler, J. Kotek, P. Hermann, P. Vojtíšek, I. Lukeš, J. A. Peters, L. Vander Elst and R. N. Muller, *Chem. - Eur. J.*, 2005, **11**, 2373–2384; (d) J. Rudovský, J. Kotek, P. Hermann, I. Lukeš, V. Mainero and S. Aime, *Org. Biomol. Chem.*, 2005, **3**, 112–117; (e) J. Rudovský, M. Botta, P. Hermann, A. Koridze and S. Aime, *Dalton Trans.*, **2006**, 2323–2333; (f) Z. Kotková, G. A. Pereira, K. Djanashvili, J. Kotek, J. Rudovský, P. Hermann, L. Vander Elst, R. N. Muller, C. F. G. C. Geraldés, I. Lukeš and J. A. Peters, *Eur. J. Inorg. Chem.*, **2009**, 119–136; (g) G. A. Pereira, L. Ball, A. D. Sherry, J. A. Peters and C. F. G. C. Geraldés, *Helv. Chim. Acta.*, 2009, **92**, 2532–2551; (h) J. Rohovec, I. Lukeš and P. Hermann, *New J. Chem.*, 1999, **23**, 1129–1132; (i) J. Rohovec, M. Kývala, P. Vojtíšek, P. Hermann and I. Lukeš, *Eur. J. Inorg. Chem.*, **2000**, 195–203; (j) S. Aime, A. S. Batsanov, M. Botta, J. A. K. Howard, D. Parker, K. Senanayake and J. A. G. Williams, *Inorg. Chem.*, 1994, **33**, 4696–4706; (k) S. Aime, A. S. Batsanov, M. Botta, R. S. Dickins, S. Faulkner, C. E. Foster, A. Harrison, J. A. K. Howard, J. M. Moloney, T. J. Norman, D. Parker, L. Royle and J. A. G. Williams, *J. Chem. Soc., Dalton Trans.*, **1997**, 3623–3636
- ⁸⁸ (a) O. A. Blackburn, R. M. Edkins, S. Faulkner, A. M. Kenwright, D. Parker, N. J. Rogers and S. Shuvaev, *Dalton Trans.*, 2016, **45**, 6782–6800; (b) G. Cucinotta, M. Perfetti, J. Luzon, M. Etienne, P.-E. Car, A. Caneschi, G. Calvez, K. Bernot and R. Sessoli, *Angew. Chem., Int. Ed.*, 2012, **51**, 1606–1610
- ⁸⁹ T. Krchová, V. Herynek, A. Gálisová, J. Blahut, P. Hermann and J. Kotek, *Inorg. Chem.*, 2017, DOI: 10.1021/acs.inorgchem.6b02749

⁹⁰ S. Viswanathan, S. J. Ratnakar, K. N. Green, Z. Kovács, L. M. De León-Rodríguez and A. D. Sherry, *Angew. Chem., Int. Ed.*, 2009, **48**, 9330–9333

⁹¹ S. J. Ratnakar, M. Woods, A. J. M. Lubag, Z. Kovács and A. D. Sherry, *J. Am. Chem. Soc.*, 2008, **130**, 6–7

12 LIST OF APPENDICES

1. T. Krchová, J. Kotek, D. Jiráček, J. Havlíčková, I. Císařová and P. Hermann: “Lanthanide complexes of aminoethyl-DO3A as PARACEST contrast agents based on decoordination of weakly bound amino group”, *Dalton Trans.*, 2013, **42**, 15735–15747
2. T. Krchová, A. Gálisová, D. Jiráček, P. Hermann and J. Kotek: “Ln(III)-complexes of DOTA analogue with ethylenediamine pendant arm as pH-responsive PARACEST contrast agents”, *Dalton Trans.*, 2016, **45**, 3486–3496
3. T. Krchová, V. Herynek, A. Gálisová, J. Blahut, P. Hermann and J. Kotek: “Eu(III) complex with DO3A-amino-phosphonate ligand as a concentration-independent pH-responsive contrast agent for Magnetic Resonance Spectroscopy (MRS)”, *Inorg. Chem.*, 2017, DOI: 10.1021/acs.inorgchem.6b02749

APPENDIX 1

T. Krchová, J. Kotek, D. Jiráček, J. Havlíčková, I. Čiřáková and P. Hermann: “Lanthanide complexes of aminoethyl-DO3A as PARACEST contrast agents based on decoordination of weakly bound amino group”, *Dalton Trans.*, 2013, **42**, 15735–15747

Cite this: *Dalton Trans.*, 2013, **42**, 15735

Lanthanide(III) complexes of aminoethyl-DO3A as PARACEST contrast agents based on decoordination of the weakly bound amino group^a

Tereza Krchová,^a Jan Kotek,^{*a} Daniel Jiráček,^b Jana Havlíčková,^a Ivana Císařová^a and Petr Hermann^a

2-Aminoethyl DOTA analogues with unsubstituted (H_3L^1), monomethylated (H_3L^2) and dimethylated (H_3L^3) amino groups were prepared by improved synthetic procedures. Their solid-state structures exhibit an extensive system of intramolecular hydrogen bonds, which is probably present in solution and leads to the rather high value of the last dissociation constant. The protonation sequence of H_3L^1 in solution corresponds to that found in the solid state. The stability constants of the H_3L^1 complexes with La^{3+} and Gd^{3+} (20.02 and 22.23, respectively) are similar to those of DO3A and the reduction of the pK_a value of the pendant amino group from 10.51 in the free ligand to 6.06 and 5.83 in the La^{3+} and Gd^{3+} complexes, respectively, points to coordination of the amino group. It was confirmed in the solid state structure of the $[Yb(L^1)]$ complex, where disorder between the SA' and TSA' isomers was found. A similar situation is expected in solution, where a fast equilibration among the isomers hampers the unambiguous determination of the isomer ratio in solution. The PARACEST effect was observed in $Eu(III)-H_3L^1/H_3L^2$ and $Yb(III)-H_3L^1/H_3L^2$ complexes, being dependent on pH in the region of 4.5–7.5 and pH-independent in more alkaline solutions. The decrease of the PARACEST effect parallels with the increasing abundance of the complex protonated species, where the pendant amino group is not coordinating. Surprisingly, a small PARACEST effect was also observed in solutions of $Eu(III)/Yb(III)-H_3L^3$ complexes, where the pendant amino group is dimethylated. The effect is detectable in a narrow pH region, where both protonated and deprotonated complex species are present in equilibrium. The data points to the new mechanism of the PARACEST effect, where the slow coordination–decoordination of the pendant amine is coupled with the fast proton exchange between the free amino group and bulk water mediates the magnetization transfer. The pH-dependence of the effect was proved to be measurable by MRI and, thus, the complexes extend the family of pH-sensitive probes.

Received 26th July 2013,
Accepted 27th August 2013
DOI: 10.1039/c3dt52031e
www.rsc.org/dalton

Introduction

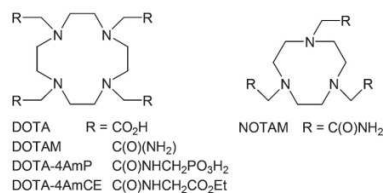
Contrast agents (CAs) that alternate the properties of bulk water have been used for a long time to improve the resolution and utilization of magnetic resonance imaging (MRI) in medicine and molecular biology. The classical molecular CAs are based on complexes of highly paramagnetic metal ions, mainly on trivalent gadolinium.¹ The complexes change the relaxation times of the bulk water protons most frequently through the exchange of the whole coordinated water molecule. Another class of CAs is based on a completely different principle, a chemical exchange saturation transfer (CEST), was introduced some time ago.² The method is based on irradiation (saturation) of protons exchangeable with bulk water protons leading, after the chemical exchange, to a decrease of the bulk water proton signal. As signals of the bulk water protons and the protons to be irradiated should be

^aDepartment of Inorganic Chemistry, Universita Karlova (Charles University), Hlavova 2030, 128 40 Prague 2, Czech Republic. E-mail: modrej@natur.cuni.cz; Fax: +420-22195-1253; Tel: +420-22195-1261

^bDepartment of Radiodiagnostic and Interventional Radiology, Magnetic Resonance Unit, Institute of Clinical and Experimental Medicine, Videnska 1958/9, 140 21 Prague 4, Czech Republic

† Electronic supplementary information (ESI) available: Crystal structures of $H_3L^2 \cdot 6H_2O$ and $H_3L^3 \cdot 3.5H_2O$, and selected geometric parameters. The distribution diagram of H_3L^1 . Chemical shift dependence of H_3L^1 on pH, and its protonation scheme. Distribution diagrams of the $Ln^{3+}:H_3L^1$ systems. Temperature dependence of the 1H NMR spectra of $[Eu(H_2O)(L^1)]$ and $[Yb(L^1)]$. Disorder of the $[Yb(L^1)]$ molecule found in the solid-state structure of $[Yb(L^1)] \cdot 5H_2O$, and its selected geometric parameters. Set of Z-spectra of the $[Eu(H_2O)(L^{1,2,3})]$ and $[Yb(L^{1,2,3})]$ complexes at different temperatures and pH. MRI-CEST images of phantoms of $[Eu(H_2O)(L^1)]$ and $[Yb(L^1)]$, and the normalized intensity of the CEST effect. 1H and $^{13}C\{^1H\}$ NMR spectra of H_3L^1 , H_3L^2 and H_3L^3 . CCDC 933967, 952384–952386. For ESI and crystallographic data in CIF or other electronic format see DOI: 10.1039/c3dt52031e

Paper



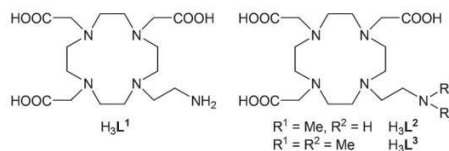
Scheme 1 Ligands discussed in the paper.

separated from each other as much as possible to reduce non-specific proton irradiation, paramagnetic complexes causing the extension of the NMR chemical shift scale were suggested (PARACEST).^{2,3} Most of these CAs are based on lanthanide(III) ions having suitable magnetic properties which are bound in macrocyclic ligands derived from DOTA (*e.g.*, DOTA-tetraamides, Scheme 1), ensuring the high thermodynamic stability and kinetic inertness of the complexes. The exchangeable protons in the complexes should be endowed with suitable properties and the most important one is the rate of their exchange with bulk water. There are two proton pools exhibiting PARACEST effects in Ln(III)-DOTA-tetraamide complexes: (i) protons of a coordinated water molecule if it is in a slow-exchange region, typically in the microsecond range (*e.g.*, [Yb(H₂O)(DOTA-4AmCE)] complex ($\tau_M = 3 \mu\text{s}$)⁴ or [Eu-(H₂O)(DOTAM)]⁵, [Eu(H₂O)(DOTA-4AmCE)]⁶ and [Eu(H₂O)(DOTA-4AmP)]⁴ complexes ($\tau_M = 55, 382$ and $67 \mu\text{s}$, respectively; for ligand structures see Scheme 1). The water molecule is bound directly to the metal ion and is close to the magnetic axis of the complexes and, thus, its protons exhibit a maximized difference in their chemical shift from the bulk water protons. (ii) Protons of *O*-coordinated amide group(s); however, these protons have their chemical shift much closer to the bulk water resonance. Nevertheless, their exchange depends on a number of external factors (*e.g.*, τ_M for [Yb-(DOTAM)]³⁺ lays, with a dependence on the pH, in the 400–5000 μs range⁷) and, therefore, the Ln(III) complexes of DOTA amide derivatives can be used as probes for various physiological parameters, such as pH, temperature, metabolite or metal ion concentrations, *etc.*^{2,3}

More recently, other PARACEST CAs based on different ligands (and, thus, on different pools of exchangeable protons) and/or metal ions have been suggested. Protons of the hydroxyl group are also labile and lanthanide(III) complexes of cyclen derivatives with alcohol pendant arms have been shown to exhibit a PARACEST effect.⁸ Some transition metal ions can also present suitable magnetic properties and complexes of high-spin iron(II) or nickel(II) with derivatives of cyclam, cyclen or 1,4,7-triazacyclononane having 2-hydroxypropyl, acetamide (*e.g.*, DOTAM and NOTAM, see Scheme 1) or (5-aminopyridine-2-yl)methyl pendant arms have been shown to have a pronounced PARACEST effect.^{9–11} Another pool of exchangeable protons, a distant non-coordinated amino group, has also been explored in some complexes of lanthanide(III)¹² as well as transition metal⁹ ions.

View Article Online

Dalton Transactions



Scheme 2 Studied ligands.

In this work, we decided to investigate the PARACEST-related properties of complexes, where the CEST-causing amino group is directly coordinated to the central lanthanide(III) ions. To ensure complex stability, the ligands are based on a macrocyclic cyclen skeleton having three acetate and one 2-aminoethyl pendant arms, which contain primary (H_3L^1), partially methylated secondary (H_3L^2) and dimethylated tertiary (H_3L^3) amino groups, see Scheme 2. Some of these ligands have already been investigated as bifunctional ligands for gadolinium(III)-based targeted MRI CAs¹³ or radio-nuclides,¹⁴ and, during work on this project, as pH-sensitive gadolinium(III)-based positive MRI CAs.¹⁵

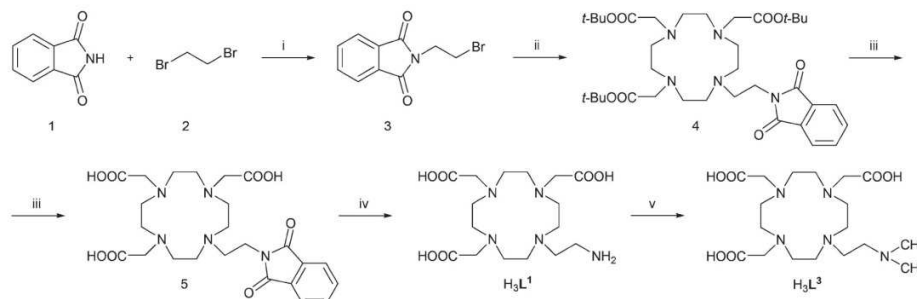
Results and discussion

Synthesis

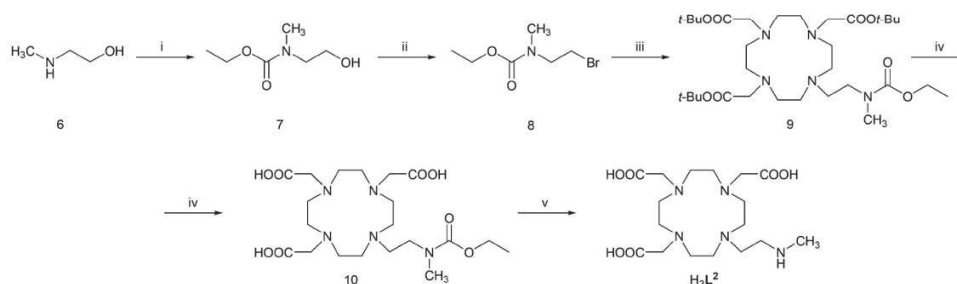
The ligands were synthesized (Schemes 3 and 4) by reaction of *t*-Bu₃DO3A with the appropriate amine-containing precursor. Alkylation of *t*-Bu₃DO3A with *N*-(2-bromoethyl)-phthalimide followed by sequential deprotection by trifluoroacetic acid and hydrazine led, after chromatography on anion exchanger, to zwitterionic H_3L^1 in 59% overall yield (Scheme 3). The synthesis is more simple compared to the previously published procedure,¹⁴ and is easily scalable and avoids HPLC purification.

To obtain ligand H_3L^2 , 2-[*N*-(ethyloxycarbonyl)-*N*-methylamino]bromoethane was used as the alkylation agent reacting with *t*-Bu₃DO3A and, after deprotection using trifluoroacetic acid and 10% aq. NaOH and chromatography on ion exchange resins, the ligand was isolated as a zwitterion in 30% overall yield (Scheme 4). Direct methylation of H_3L^1 with a formaldehyde-formic acid mixture easily produced H_3L^3 in high yield (Scheme 3); it is a significant improvement compared with the previous synthesis.¹⁵

All three studied ligands were structurally characterized in their zwitterionic forms by single-crystal X-ray diffraction analysis. Single-crystals of sufficient quality were obtained from solutions in water or aqueous ethanol. Title ligands were isolated in the form of hydrates ($\text{H}_3\text{L}^1 \cdot 5\text{H}_2\text{O}$, $\text{H}_3\text{L}^2 \cdot 6\text{H}_2\text{O}$ and $\text{H}_3\text{L}^3 \cdot 3.5\text{H}_2\text{O}$, respectively). All three molecular structures are very similar, and therefore, only the molecular structure of H_3L^1 is shown here in Fig. 1; other structures are shown in the ESI (Fig. S1 and S2[†]). In all three cases, the protonation scheme is the same – two protons are bound to the macrocycle amino groups bearing acetate moieties and are located mutually *trans*, and the third one is bound to the pendant



Scheme 3 Synthesis of studied ligands H_3L^1 and H_3L^3 : (i) DMF, K_2CO_3 , TBAB, 40 °C; (ii) $t-Bu_3DO3A-HBr$, MeCN, K_2CO_3 , 60 °C; (iii) $CF_3COOH-CHCl_3$ (1 : 1), reflux 24 h; (iv) aq. NH_2NH_2 , 90 °C, 18 h; (v) $(CH_2O)_m$, $HCOOH$, reflux 24 h.



Scheme 4 Synthesis of studied ligand H_3L^2 : (i) $CH_3CH_2OC(O)Cl$, dioxan- H_2O (1 : 1), RT, 2 h; (ii) $CBra$, PPh_3 , THF, RT, 1 h; (iii) $t-Bu_3DO3A-HBr$, K_2CO_3 , MeCN, 60 °C; (iv) $CF_3COOH-CHCl_3$ (1 : 1), reflux 24 h; (v) 10% aq. $NaOH$, 90 °C, 24 h.

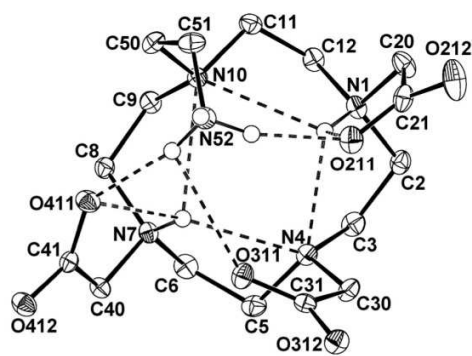


Fig. 1 Molecular structure of H_3L^1 found in the crystal structure of $H_3L^1 \cdot 5H_2O$ showing an intramolecular hydrogen bond network. The carbon-bound hydrogen atoms were omitted for clarity.

aminoethyl group. Such a protonation scheme is consistent with the form suggested on the basis of 1H NMR titration (see below, Scheme S1†). The conformation of the macrocyclic unit is (3,3,3,3)-B, as usually observed for double-protonated cyclen

rings (Table S1†).¹⁶ Such a conformation is stabilized by intramolecular hydrogen bonds between the protonated and non-protonated macrocycle amino groups. Beside these interactions, the molecular structure is stabilized by further intramolecular hydrogen bonds, including protonated amines and deprotonated oxygen atoms of the carboxylate pendant arms, and the whole crystal structure is stabilized by extended hydrogen bond networks with water solvate molecules.

Stability of the complexes

The complexing properties of the most important ligand, H_3L^1 , having a primary amino group, were investigated in detail. First, the conditions for the pendant amino group deprotonation and coordination were investigated by potentiometry. The ligand's overall protonation constants β_{n10} were determined by potentiometry and are compiled together with corresponding pK_a values in Table 1; the ligand distribution diagram is shown in Fig. S3.† As the highest protonation constant β_{110} is slightly behind the $-\log[H^+]$ range suitable for potentiometric titrations, we also performed a 1H NMR titration in the pH range 1.2–13.5 to confirm such a high value of the first protonation constant and to assign the individual protonation sites. The values of the dissociation constants

Table 1 Overall protonation constants ($\log \beta_{h10}$) of H_3L^1 and overall stability constants ($\log \beta_{h11}$) of its lanthanide(III) complexes, and corresponding $\text{p}K_{\text{A}}$ values ($l = 0.1 \text{ m (Me}_4\text{N)Cl}$, 25°C)

Stoichiometric coefficients			Constant	
h	l	M	$\log \beta_{hlm}^a$	$\text{p}K_{\text{A}}$
1	1	0	13.19(2)	13.19
2	1	0	23.70(2)	10.51
3	1	0	32.60(2)	8.90
4	1	0	36.47(2)	3.87
5	1	0	37.75(2)	1.27
La				
0	1	1	20.02(3)	—
1	1	1	26.08(2)	6.06
Gd				
0	1	1	22.23(4)	—
1	1	1	28.06(1)	5.83

$$^a \beta_{hlm} = [\text{H}_h\text{L}_l\text{M}_m] / ([\text{H}]^h [\text{L}]^l [\text{M}]^m).$$

obtained by NMR ($\text{p}K_{\text{A}} = 13.3(3)$, $11.0(3)$, $9.3(2)$, $3.8(1)$ and $1.3(3)$) are in a good agreement with those obtained by potentiometry (Table 1); the differences can be attributed to the different and non-controlled ionic strength during the NMR experiment and inaccurate (non-linear) potential–pH relationship in highly acidic/alkaline regions. However, the high value of the first protonation constant is confirmed and is clearly seen from the chemical shift dependence in the pH region 12.0–13.5 (Fig. S4†). In addition, it is possible, from pH-dependent changes of individual ^1H NMR signals, to determine also the sites of consecutive protonations (Scheme S1†): the first proton is distributed over all ring nitrogen atoms; the rather high value of the corresponding protonation constant is a consequence of intramolecular hydrogen bonds involving the ring nitrogen atoms as well as the pendant arms. Two $\text{p}K_{\text{A}}$ values can be assigned to the partly simultaneous protonation of the pendant amino group and the second nitrogen atom of the macrocyclic ring, associated with re-location of the protons bound to the ring nitrogen atoms. The same proton distribution was also found in the zwitterionic forms of all studied ligands in the solid state (see above). The last two measured constants correspond to the protonation of the pendant carboxylate groups. Further protonations of the ring nitrogen atoms take place below pH 1. Such a protonation sequence is consistent with those commonly found for all DOTA-like ligands.

The stability constants, $\log \beta_{011}$, determined for La(III) and Gd(III) ions were found to be 20.02 and 22.23, respectively (Table 1). Corresponding distribution diagrams are shown in Fig. S5 and S6.† The stability constants are lower than those reported for Ln(III)–DOTA (La(III) 22.9, Gd(III) 24.6) complexes and similar to those of Ln(III)–DO3A (Gd(III) 21.0) complexes.¹⁷ In both studied systems, protonated species with $\text{p}K_{\text{A}}$ 6.06 and 5.83 for the La(III) and Gd(III) complexes, respectively, are formed. The value for the protonation of the Gd(III)– H_3L^1 complex is in good agreement with the reported value (5.95) determined by relaxometric measurements.¹⁵ The distribution diagrams show that free lanthanide(III) ions are not present above pH 5.5. The protonation takes place on the pendant

amino group as it is the most basic site of the in-cage complex molecule and a difference of ~4–5 orders of magnitude between the constants, corresponding to its protonation in the complexes and analogous protonation in the free ligand, points to an easier deprotonation induced by coordination of the group to the metal ion. Thus, one can conclude, that studied ligands are coordinated in an octadentate fashion involving the pendant amino group in the $[\text{Ln}(\text{L}^1)]$ species, and that the amino group is de-coordinated upon protonation in the weakly acidic region. The maximum abundance of the $[\text{Gd}(\text{HL}^1)]^+$ complex species in solution is observed at pH ~5.

Structure of the complexes

To study the structure and properties of the lanthanide(III) complexes of H_3L^1 , sample solutions were prepared by dissolving LnCl_3 and the ligand in a Ln:L = 1:1.1 molar ratio, adjusting the pH with aq. LiOH to 6.0, heating the solution at 60°C overnight, re-adjusting pH to 6.5 and heating at 60°C overnight again.

The complexes of the DOTA-like ligands are usually non-coordinated (eight donor atoms coming from macrocyclic ligands and one site is occupied by a water molecule) and form two possible diastereomers – square-antiprismatic (SA) and twisted-square-antiprismatic (TSA) ones.¹ These diastereoisomers differ in the relative screwing of the macrocyclic (δ/λ) and pendant (Δ/Λ) chelate rings, giving rise to $\Delta\lambda\lambda\lambda/\Lambda\delta\delta\delta$ (SA) and $\Delta\delta\delta\delta/\Lambda\lambda\lambda\lambda$ (TSA) combinations. In the ^1H NMR spectra, the signals showing best the isomer ratio belongs to those of the “axial” protons of the macrocyclic chelate rings, which are the closest ones to the lanthanide(III) ion and to the magnetic axis of the complexes.¹⁸ In the Ln(III)–DOTA-like complexes, the TSA isomer with a larger coordination cage is strongly preferred at the beginning of the lanthanide series, with the SA one becoming dominant for heavier lanthanides.¹⁸ Although the situation is sometimes complicated by the possible presence of an octa-coordinated species (*i.e.*, without a coordinated water molecule, usually denoted as SA'/TSA'), which have a similar chemical shift range in the ^1H NMR spectra to the nona-coordinated SA/TSA species. Due to this fact, the abundance of twisted-square-antiprismatic isomers can slightly increase towards the end of the lanthanide series.^{18,19}

The solution structures of the studied complexes were investigated by variable-temperature ^1H NMR. To assure the coordination of the pendant amino group, the pH of the samples was adjusted to the weakly alkaline region. However, the spectrum of the Eu(III) complex at pH 9 (Fig. S7†) acquired at 25°C was not resolved enough to observe the required signals and to determine the isomer ratio; only very broad signals in the 17–27 ppm region (after correction for bulk magnetic susceptibility shift) were observed. Such chemical shifts are just between the regions typical for SA and TSA species, although slightly closer to the TSA one.¹⁸ Both heating up to 90°C or cooling to 0°C led to a significant broadening and visual disappearance of these signals. It points to the fact that two relatively independent fluxional processes occur, affecting

the position of the axial hydrogen atoms with respect to the lanthanide(III) ion. Therefore, we can only speculate that a mixture of the isomers is present, as it is common for most of Eu(III) complexes with DOTA-like ligands.^{18,19} A similar situation occurs for the Yb(III) complex. The ¹H NMR spectrum acquired at 25 °C and pH 8.5 (Fig. S8†) shows signals of “axial” protons as broad peaks in the 86–112 ppm region. The chemical shifts,^{18,19} signal broadening and their virtual disappearance, observed either at lower and higher temperatures, point to the presence of a SA(′)/TSA(′) exchange process.

The hypothesis of ongoing SA(′)/TSA(′) isomerism is supported by the solid-state structure of the [Yb(L¹)]·5H₂O complex (Fig. 2). The central ion is octacoordinated between mutually parallel macrocycle N₄ and pendant-arm O₃N-planes, but closer to the pendant-arm one. As a result of smaller values of the trans (“opening”) angles in the O₃N-plane (120° and 125° for O311–Yb1–N52 and O211–Yb1–O411 angles, respectively), comparing to the limiting value (~135°) for water coordination,²⁰ no water molecule is directly bound to the metal centre. During the refining of the crystal structure, the set of difference maxima in the electron density map were located close to the nitrogen and carbon atoms of the macrocycle, and pointed to some disorder in the macrocyclic unit. It was successfully modelled, leading to a calculated ratio of the SA′:TSA′ isomers of 15:85% (Fig. 2 and S9†). The structural parameters of both coordination spheres fall into regions typical for the given isomers,²⁰ with mean torsion angles between N₄ and O₃N-planes of 37.5 and 22.5°, and separation of the N₄ and O₃N-planes of 2.50 and 2.59 Å for the SA′ and TSA′ species, respectively. Further selected geometric parameters are compiled in Table S2.†

Chemical exchange saturation transfer

PARACEST experiments (measurements of so-called Z-spectra) produced the clean saturation of bulk water after irradiation of the broad regions with maxima at +19.5 and +34 ppm for the Eu(III)–H₃L¹ complex (pH = 7.67, *t* = 25 °C), and +42 ppm and +89 ppm for the Yb(III)–H₃L¹ complex (pH = 7.40, *t* = 25 °C); chemical shifts are given with respect to the signal of the bulk water protons. In the ¹H NMR spectra of the Eu(III) complex acquired in aqueous solution, a broad signal at 34 ppm is observable, and disappears on selective water pre-saturation or when acquiring the spectra in D₂O (Fig. S10†). The other signal is overlapped with C–H proton signals and, therefore, cannot be distinguished in the ¹H NMR spectra. Also in the case of the Yb(III) complex, there are C–H proton signals in the regions corresponding to the CEST effect and, thus, it prevents the direct observation of the signals.

For both complexes, the two observed CEST signals have equal intensities. With respect to the chemical structure of the complexes, the observed effect can be theoretically caused by two exchangeable pools of protons, *i.e.*, by protons of the amino group of the pendant arm and/or by protons of the coordinated water molecule. From relaxometric data, it is known that one water molecule is coordinated in the Gd(III) complex,¹⁵ and this fact is also undoubtedly valid for the

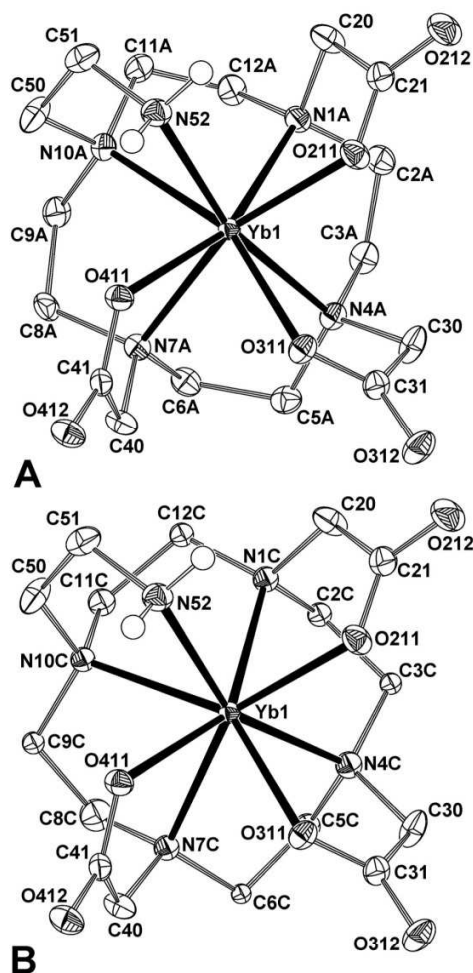


Fig. 2 Molecular structure of [Yb(L¹)] found in the crystal structure of [Yb(L¹)]·5H₂O; TSA′ (λλλλ, 85%) species (A) and SA′ (λδδδ, 15%) species (B). Carbon-bound H-atoms are omitted for clarity.

complex of the slightly larger Eu(III) ion (but it cannot be easily confirmed by the normally used luminescence measurements due to the presence of two types of quenchers, O–H and N–H, which complicates the data evaluation). However, in the case of the complex with the significantly smaller Yb(III), an anhydrous species might be expected on the basis of the solid-state structure (see above). In such cases, three possible elucidations can be considered: (i) both signals come from the amino group, (ii) one signal belongs to the coordinated water molecule and other to the amine, and (iii) both signals belong to

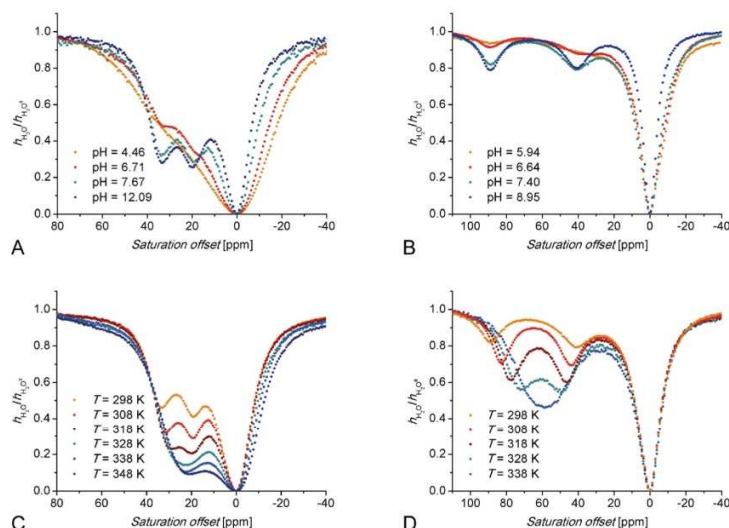


Fig. 3 Z-spectra of a 80 mM aqueous solution ($\text{H}_2\text{O}-\text{D}_2\text{O}$ 1 : 10) of $\text{Eu}(\text{III})-\text{H}_3\text{L}^1$ complex ($B_0 = 7.05$ T, satpwr = 29 dB \sim 1000 Hz, satdly = 2 s) at $T = 298$ K (A) and pH = 7.40 (C). Z-spectra of a 100 mM aqueous solution ($\text{H}_2\text{O}-\text{D}_2\text{O}$ 1 : 10) of $\text{Yb}(\text{III})-\text{H}_3\text{L}^1$ complex ($B_0 = 7.05$ T, satpwr = 29 dB \sim 1000 Hz, satdly = 2 s) at $T = 298$ K (B) and pH = 7.40 (D).

the water molecule. To distinguish between these possibilities, more detailed studies were carried out. The most interesting CEST behaviour was observed while changing the solution pH. The CEST effect started to be observable at pH \sim 6 for both of the $\text{Eu}(\text{III})$ and $\text{Yb}(\text{III})-\text{H}_3\text{L}^1$ complexes and reached a maximum at pH \sim 8, and the saturation transfer efficiency was not changed with further pH increases up to \sim 12; the mutual intensity ratio of the CEST peaks is not changed with pH. The results are shown in Fig. 3A and 3B and strongly support the first possibility, as when the CEST effect is caused by the coordinated water molecule (or by exchangeable protons of the amide⁷ or hydroxy⁸ moieties), the effect drops with increasing pH due to the faster prototropic (base-catalyzed) exchange of the corresponding protons (of the coordinated water molecule or the other mentioned pools). The behaviour reported in this work has not yet been reported in the literature. The magnitude of the CEST effect at different pH values follows an abundance of the fully deprotonated species – the CEST effect consistently disappears at lower pH with protonation and, thus, decoordination of the amino group (see potentiometric results, Table 1 and Fig. S5 and S6†). The observations mentioned above are fully consistent with the low “acidity” of the N–H bond in the studied amino derivative if compared to the generally higher acidity of the N–H proton in carboxylic amides; therefore, in the case of DOTAM complexes, base-catalysed proton exchange significantly decreases the CEST effect in alkaline solutions but, in the case of our complexes, the CEST effect remains unchanged even at very high pH.

Thus, the observed CEST signals are assigned to hydrogen atoms of the coordinated pendant amino group. Two observed signals rise from the fact that two amine hydrogen atoms become magnetically non-equivalent after the group coordination. A similar situation has been observed for the amide hydrogen atoms of DOTAM (Scheme 1).⁷ The lanthanide-induced shift of the amine hydrogen atoms is higher than that of the amide hydrogen atoms in analogous complexes, as the coordinated amine group is much closer to the metal ion and to the magnetic axis of the complexes. The possibility that two signals arise from the presence of two (SA and TSA) isomers could be excluded as both signals have an equal intensity and it would imply that the SA and TSA isomers have the same abundance for both complexes, which is very improbable due to the general trends along the lanthanide series. In addition, as both isomers should have a very similar geometry of the N_3O -plane, the NMR signals associated with the protons of the amino pendant arm should have similar chemical shifts in both the SA and TSA species; however, there is a significant difference in the chemical shifts between the signals ($\Delta\delta \sim 15$ and 50 ppm for $\text{Eu}(\text{III})$ and $\text{Yb}(\text{III})$ complexes, respectively). With increasing temperature, the saturation transfer becomes more effective and two amine hydrogen signals converge and, finally, coalesce around 55 °C and 65 °C for the $\text{Eu}(\text{III})$ and $\text{Yb}(\text{III})$ complexes, respectively (Fig. 3C and 3D). On further heating (up to 95 °C, Fig. S11†), the coalesced CEST signals approach slightly closer to signal of the bulk water but are still observable. Such a behaviour points to the dynamic averaging

of the non-equivalent amine hydrogen signals; it can originate from a faster coordination-decoordination equilibrium or from a faster geometry change.

Due to the insensitivity of the CEST effect to pH changes in the alkaline region, the process described above cannot be caused by neither hydroxide nor proton attack on the coordinated amino group. Therefore, the mechanism of the observed CEST effect is very probably associated with the (semi)labile coordination of the 2-aminoethyl pendant arm. Its coordination-decoordination is the rate-limiting step – when the pendant arm is coordinated, no exchange occurs but in the moment of the pendant arm decoordination, the exchange of protons of the free amino group with those of bulk water proceeds very quickly.

To support the hypothesis presented above, we prepared and studied complexes of mono- and dimethylated analogues, *i.e.*, with ligands H_3L^2 and H_3L^3 . The complexes of H_3L^2 showed significant CEST effects, observed as two close peaks with unequal intensity at 43 and 49.5 ppm for Eu(III) and one peak at 57 ppm for Yb(III), respectively (Fig. S12[†]). The two signals in the Z-spectra, observed in the case of the Eu(III) complex, can be attributed to two modes of coordination of the methylamino group, in which the methyl and hydrogen occupy equatorial/axial or reverse positions. In the case of the complex with the smaller Yb(III) ion, one of these possibilities is probably strongly preferred due to the larger steric strain around the methyl group, leading to only one observable signal in the Z-spectra. However, to our surprise, the Yb(III)- H_3L^3 complex also exhibits a CEST effect at 26 ppm, although the CEST peak has a small intensity and is observable only in a narrow pH range 6–8.5 (Fig. 4 and S13[†]). In this pH region, the protonation-deprotonation of the $-NMe_2$ group is supposed (accordingly to the corresponding $\log K_A \sim 7.8$ reported previously for its Gd(III) complex¹³). Thus, an equilibrium between the deprotonated (and mostly coordinated) and protonated (and uncoordinated) amino group in the complex is present. Therefore, the observation of the CEST effect can be explained by the protonation-deprotonation of the uncoordinated dimethylamino group, which is still located sufficiently close to the highly paramagnetic centre to mediate the saturation transfer to the bulk water through this process. Such an

explanation is consistent with the fact that the observed CEST effect disappears at a relatively low temperature ~ 65 °C, which is probably due to the much faster chemical exchange process (Fig. S13[†]), contrary to the complexes of H_3L^1 where the analogous signal disappearance cannot be reached even at 95 °C (see above). In the case of the Eu(III)- H_3L^3 complex, a slight CEST effect was also observed, causing some asymmetric broadening of the water signal in the Z-spectra (Fig. S13[†]). This feature can be explained in a similar way to the above.

To test the applicability of the complexes as MRI pH probes, the CEST effect was measured in phantoms containing Eu(III)- H_3L^1 and Yb(III)- H_3L^1 complex solutions having different pH and concentrations. The final CEST images were obtained after irradiation at the CEST and symmetrical negative frequencies and subtracting the images (Fig. 5 and S14[†]). Normalized signal intensities are shown in Fig. S15 and S16[†]. The results clearly show that the prepared complexes can be successfully employed as CEST probes in the pH region relevant to living systems.

Experimental

Materials and methods

Commercially available chemicals had synthetic purity and were used as received. Deionized water, used for the synthesis of the ligands and their complexes, was prepared using a deionization water system ROWAPUR 200/100. Water used for potentiometric titrations was prepared by a Milli-Q (Millipore).

t-Bu₃DO3A-HBr [1,4,7-tris(*t*-butylcarboxymethyl)-1,4,7,10-tetraazacyclododecane hydrobromide] was prepared according to the published procedure.²¹ Dry solvents were prepared by the standard purification procedures²² and stored over molecular sieves under an argon atmosphere: dry MeCN was obtained by distillation from P₂O₅, THF was dried by refluxing with potassium and distilled under an argon atmosphere.

The ESI-MS spectra were acquired on a Bruker ESQUIRE 3000 spectrometer equipped with an electrospray ion source and ion-trap detection. Measurements were carried out in the positive and negative modes. NMR characterization data (1D: ¹H, ¹³C; 2D: HSQC, HMBC, ¹H-¹H COSY) were recorded on VNMR300, Varian^{UNITY} INOVA 400 or Bruker Avance III 600, using 5-mm sample tubes. Chemical shifts δ are given in ppm and coupling constants J are reported in Hz. For the ¹H and ¹³C measurements in D₂O, *t*-BuOH was used as the internal standard ($\delta_H = 1.25$, $\delta_C = 30.29$). For the measurements in CDCl₃, TMS was used as the internal standard ($\delta_H = 0.00$, $\delta_C = 0.00$). Abbreviations s (singlet), t (triplet), q (quartet), m (multiplet) and br (broad) are used in order to express the signal multiplicities. Elemental analysis was performed at the Institute of Macromolecular Chemistry of the Academy of Science of the Czech Republic (Prague).

Synthesis

N-(2-Bromoethyl)phthalimide (3). Compound 3 was prepared according to a modified published procedure.²³ To a

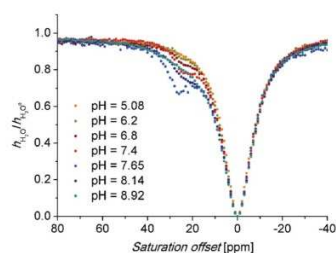


Fig. 4 Z-spectra of a 50 mM aqueous solution (H_2O-D_2O 1:10) of the Yb(III)- H_3L^3 complex ($B_0 = 7.05$ T, $T = 298$ K, $\text{satpwr} = 29$ dB ~ 1000 Hz, $\text{satdly} = 2$ s).

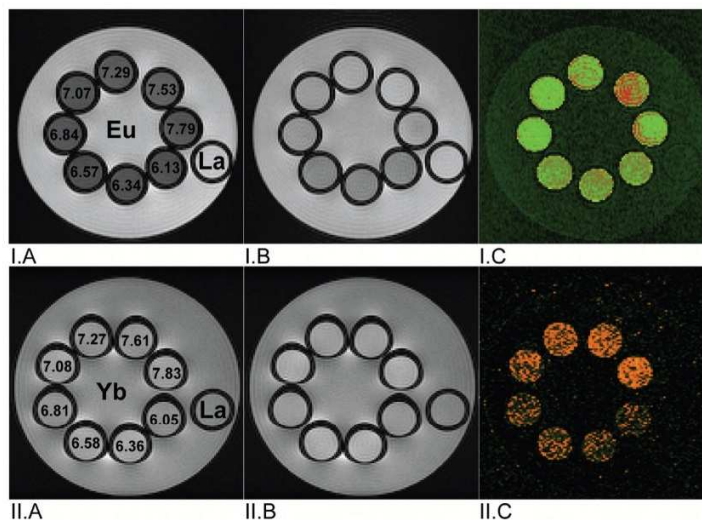


Fig. 5 MRI-CEST images of phantoms consisting of one vial containing 80 mM aq. solution of $[\text{La}(\text{H}_2\text{O})(\text{L}^1)]$ as a diamagnetic standard and eight vials containing 80 mM aq. solutions of $[\text{Eu}(\text{H}_2\text{O})(\text{L}^1)]$ and $[\text{Yb}(\text{L}^1)]$ with different pH values; pH is shown in figures A. Experimental conditions: MSME pulse sequence, $B_0 = 4.7 \text{ T}$, $B_1 = 20 \mu\text{T}$, $T = 293 \text{ K}$, satdly = 2 s, TR = 5 s, TE = 8.9 ms, scan time = 8 min. I.A: T_1 -weighted image, satfrq = 34 ppm from the bulk water signal. I.B: T_1 -weighted image, satfrq = -34 ppm from the bulk water signal. I.C: The difference between images I.A and I.B in false colours. II.A: T_1 -weighted image, satfrq = 89 ppm from the bulk water signal. II.B: T_1 -weighted image, satfrq = -89 ppm from the bulk water signal. II.C: The difference between images II.A and II.B in false colours.

well-stirred suspension of K_2CO_3 (9.40 g, 68 mmol), 1,2-dibromoethane **2** (11.7 ml, 136 mmol) and tetrabutylammonium bromide (TBAB, 0.70 g) in DMF (20 ml), was added phthalimide **1** (5.00 g, 34 mmol) and the reaction mixture was stirred for 18 h at 40 °C. Next, the mixture was poured into water (150 ml) and the product **3** was extracted with ethylacetate ($4 \times 25 \text{ ml}$). The organic portion was concentrated *in vacuo*. The product was purified by crystallization from hot EtOH to give **3** (7.61 g, 88%).

^1H NMR (299.9 MHz, CDCl_3): δ 3.59 (2H, t, $^3J_{\text{HH}} = 6.6$, $\text{NCH}_2\text{CH}_2\text{Br}$); 4.09 (2H, t, $^3J_{\text{HH}} = 6.6$, $\text{NCH}_2\text{CH}_2\text{Br}$); 7.70–7.73 (2H, m, arom.); 7.84–7.86 (2H, m, arom.).

$^{13}\text{C}\{^1\text{H}\}$ NMR (75.4 MHz, CDCl_3): δ 28.55 (1C, $\text{NCH}_2\text{CH}_2\text{Br}$); 39.70 (1C, $\text{NCH}_2\text{CH}_2\text{Br}$); 123.93 (2C, arom.); 132.23 (2C, arom. quaternary); 134.63 (2C, arom.); 168.22 (2C, CO).

Elemental analysis: found (calcd for $\text{C}_{10}\text{H}_8\text{BrNO}_2$, $M_r = 254.1$) C: 47.68 (47.27), H: 3.07 (3.17), N: 5.32 (5.51), Br: 31.15 (31.45).

1,4,7-Tris(carboxymethyl)-10-(2-aminoethyl)-1,4,7,10-tetraazacyclododecane ($\text{H}_3\text{L}^1 \cdot 3\text{H}_2\text{O}$). Compound **4** was prepared *in situ* according to a modified published procedure.¹⁴ To a well-stirred suspension of K_2CO_3 (2.40 g, 17.4 mmol) and *t*-Bu₃DO3A-HBr (2.59 g, 4.37 mmol) in dry MeCN (40 ml), alkylating reagent **3** (1.22 g, 4.80 mmol) was gradually added over 30 min and the reaction mixture was stirred for 24 h at 60 °C. The solids were filtered off and the filtrate was evaporated on a rotary evaporator. The oily residue was dissolved in CHCl_3 (20 ml) and extracted with distilled water ($4 \times 10 \text{ ml}$). The

organic portion was dried over anhydrous Na_2SO_4 and concentrated *in vacuo* to give 3.40 g of yellow oil containing compound **4** contaminated with phthalhydrazide and an excess of alkylating reagent **3**. The by-product and alkylating reagent were not removed, and the crude product **4** was used in the next step without purification (only a small amount of the crude product **4** was purified for characterization purposes using HPLC).

A portion (3.35 g) of this mixture containing compound **4** was dissolved in CF_3COOH and CHCl_3 (30 ml, 1 : 1); the resulting solution was refluxed for 24 h. After evaporation to dryness the oily residue was dissolved in a small amount of distilled water and then loaded onto a strong cation exchange column (Dowex 50, 50–100 mesh, H^+ -form, $2 \times 9 \text{ cm}$). Acidic impurities were removed by elution with water and the product **5** was eluted with 5% aq. NH_3 . Fractions containing the product (TLC check) were combined and evaporated to give 2.82 g of yellow oil containing compound **5**. The crude product **5** was used in the next step without purification.

The portion (2.80 g) of the crude product **5** was dissolved in 80% aq. $\text{NH}_2\text{NH}_2 \cdot \text{H}_2\text{O}$ (15 ml); the resulting mixture was then heated for 18 h at 90 °C and concentrated *in vacuo*. The residue was dissolved in a small amount of distilled water. Then the solution was filtered and loaded onto a strong anion exchange column (Dowex 1, OH^- -form, $1.25 \times 8 \text{ cm}$). Impurities were removed by elution with water and the product H_3L^1 was eluted with 5% aq. CH_3COOH . Fractions containing the pure product (TLC and ^1H NMR check) were combined and

evaporated to give H_3L^1 (1.90 g) as a yellow oil. The crude product was purified by crystallization from hot EtOH to give $H_3L^1 \cdot 3H_2O$ (1.15 g, 59%) as a white powder.

Compound 4. HPLC: Solvent: A = CH_3CN , B = 0.1% of CF_3COOH in H_2O , C = H_2O . Gradient: A: 20–50%, 0–24 min; 50%, 24–40 min; 50–20%, 40–41 min; 20%, 41–61 min. B: 20%, 0–61 min. t_R = 17.0 min.

1H NMR (299.9 MHz, $CDCl_3$): δ 1.45–1.48 (27H, m, $C(CH_3)_3$); 3.15–3.43 (18H, m, CH_2); 3.53 (4H, s, CH_2CO_2); 3.86 (2H, s, CH_2CO_2); 4.02 (2H, br, CH_2); 7.73–7.76 (2H, m, arom.); 7.84–7.87 (2H, m, arom.).

$^{13}C\{^1H\}$ NMR (150.9 MHz, $CDCl_3$): δ 27.92 (9C, $C(CH_3)_3$); 32.58, 48.97, 49.92, 50.13, 51.17, 51.86, 54.77 (13C, CH_2); 82.96 (2C, $C(CH_3)_3$); 84.28 (1C, $C(CH_3)_3$); 123.58 (2C, arom.); 131.65 (2C, arom. quaternary); 134.37 (2C, arom.); 167.85 (3C, CH_2CO_2); 169.22 (2C, NCO).

MS-ESI: (+): 688.5 ($[M + H]^+$, calcd 688.4); 710.4 ($[M + Na]^+$; calcd 710.4).

Compound 5. MS-ESI: (–): 518.0 ($[M - H]^-$, calcd 518.2).

$H_3L^1 \cdot 3H_2O$. 1H NMR (600.2 MHz, D_2O , pD = 5.4, Fig. S17[†]): 2.85–2.89 (4H, m, CH_2NCH_2CO); 2.94 (2H, br, $CH_2CH_2NH_2$); 3.02–3.04 (4H, m, $CH_2N(CH_2)_2NH_2$); 3.06 (2H, t, $^3J_{HH} = 5.1$, CH_2NH_2); 3.13 (2H, s, CH_2CO); 3.33–3.37 (2H, m, CH_2NCH_2CO); 3.40–3.45 (2H, m, CH_2NCH_2CO); 3.54–3.58 (2H, m, CH_2NCH_2CO); 3.71–3.77 (2H, m, CH_2NCH_2CO); 3.90 (4H, AB-multiplet, CH_2CO).

$^{13}C\{^1H\}$ NMR (150.9 MHz, D_2O , pD = 5.4, Fig. S18[†]): δ 37.01 (1C, CH_2NH_2); 48.90 (2C, $CH_2N(CH_2)_2NH_2$); 48.99 (2C, CH_2NCH_2CO); 50.82 (1C, $CH_2CH_2NH_2$); 51.00 (2C, CH_2NCH_2CO); 53.06 (2C, CH_2NCH_2CO); 55.85 (1C, CH_2CO); 58.07 (2C, CH_2CO); 171.02 (2C, CH_2CO); 178.77 (1C, CH_2CO).

MS-ESI: (+): 412.0 ($[M + Na]^+$, calcd 412.2); 428.0 ($[M + K]^+$, calcd 428.2). (–): 425.8 ($[M + K - 2H]^-$, calcd 426.2).

Elemental analysis: found (calcd for $C_{16}H_{37}N_5O_9$, $M_r = 443.5$) C: 43.17 (43.33), H: 8.40 (8.41), N: 15.39 (15.79).

2-[N-(Ethoxyxycarbonyl)-N-methylamino]ethanol (7). To a solution of **6** (2.64 g, 35.2 mmol) in a mixture of dioxane and H_2O (30 ml, 1 : 1), ethoxyxycarbonylchloride (0.96 g, 8.85 mmol) was added dropwise. The solution was stirred at room temperature for 2 h and concentrated *in vacuo*. The oily residue was dissolved in CH_2Cl_2 (30 ml) and extracted with H_2O (3 \times 15 ml) and 3% aq. HCl (1 \times 15 ml). The organic portion was dried over Na_2SO_4 and concentrated *in vacuo* to give 1.10 g of **7** as a colourless oil.

1H NMR (299.9 MHz, $CDCl_3$): δ 1.24 (3H, t, $^3J_{HH} = 7.2$, CH_2CH_3); 2.94 (3H, s, NCH_3); 3.41 (2H, br, NCH_2); 3.73 (2H, br, CH_2OH); 4.11 (2H, q, $^3J_{HH} = 7.2$, CH_2CH_3).

$^{13}C\{^1H\}$ NMR (75.4 MHz, $CDCl_3$): δ 14.85 (1C, CH_2CH_3); 35.42 (1C, NCH_3); 51.92 (1C, CH_2CH_2OH); 61.40 (1C, CH_2OH); 61.74 (1C, CH_2CH_3); 158.17 (1C, CO).

MS-ESI: (+): 148.5 ($[M + H]^+$, calcd 148.1); 170.4 ($[M + Na]^+$, calcd 170.1).

2-[N-(Ethoxyxycarbonyl)-N-methylamino]bromoethane (8). To a well-stirred solution of **7** (1.09 g, 7.41 mmol) in dry THF (40 ml), in a flask equipped with a drying tube, CBr_4 (3.68 g, 11.1 mmol) and PPh_3 (2.92 g, 11.1 mmol) were added.

The reaction mixture was stirred for 1 h at room temperature, filtered and then evaporated on a rotary evaporator. The oily residue was dissolved in small amount of CH_2Cl_2 and purified by chromatography (SiO_2 , 18 \times 3.5 cm). Impurities were removed by elution with CH_2Cl_2 , the pure product was eluted using a mixture of acetone and CH_2Cl_2 (1 : 9). Fractions containing the product **8** (TLC check) were combined and evaporated to give **8** (1.32 g) as a colourless oil.

1H NMR (299.9 MHz, $CDCl_3$): δ 1.26 (3H, t, $^3J_{HH} = 6.9$, CH_2CH_3); 2.97 (3H, s, NCH_3); 3.45 (2H, br, NCH_2); 3.62 (2H, br, CH_2Br); 4.14 (2H, q, $^3J_{HH} = 6.9$, CH_2CH_3).

$^{13}C\{^1H\}$ NMR (75.4 MHz, $CDCl_3$): δ 14.89 (1C, CH_2CH_3); 29.50 (1C, CH_2Br); 35.60 (1C, NCH_3); 51.30 (1C, CH_2CH_2Br); 61.76 (1C, CH_2CH_3); 156.31 (1C, CO).

1,4,7-Tris(carboxymethyl)-10-[2-(N-methylamino)ethyl]-1,4,7,10-tetraazacyclododecane ($H_3L^2 \cdot 5.5H_2O$). To a well-stirred suspension of K_2CO_3 (3.30 g, 23.9 mmol) and *t*-Bu₃DO3A-HBr (2.89 g, 4.85 mmol) in dry MeCN (30 ml), a solution of alkylating reagent **8** (1.32 g, 6.28 mmol) in dry MeCN (10 ml) was added dropwise. The reaction mixture was stirred for 24 h at 60 °C, filtered, and the filtrate was evaporated on a rotary evaporator. The oily residue was dissolved in $CHCl_3$ (20 ml) and extracted with distilled water (4 \times 10 ml). The organic portion was dried over Na_2SO_4 and concentrated *in vacuo* to give 3.82 g of yellow oil containing compound **9** contaminated with an excess of alkylating reagent **8**. The alkylating reagent was not removed, and the crude product **9** was used in the next step without purification.

A portion (3.80 g) of the mixture containing compound **9** was dissolved in a mixture of CF_3COOH and $CHCl_3$ (30 ml, 1 : 1); the resulting solution was refluxed for 24 h and evaporated on a rotary evaporator. The oily residue was dissolved in a small amount of distilled water and evaporated (this procedure was then repeated three more times) to give 5.00 g of yellow oil containing compound **10** (it was used in the next step without purification).

The crude product **10** (5.00 g) was dissolved in 10% aq. NaOH (50 ml) and stirred for 24 h at 90 °C. Then the solution was loaded onto a strong anion exchange column (Dowex 1, OH^- -form, 1.25 \times 20 cm). Impurities were removed by elution with water and the product H_3L^2 was eluted with 5% aq. CH_3COOH . Fractions containing the product (TLC and 1H NMR check) were combined and evaporated to give H_3L^2 (1.97 g) as a brownish oil. The crude product was dissolved in small amount of distilled water and anhydrous EtOH was added dropwise. Crystallization started after a few minutes, and the suspension was left overnight. The white crystalline solid was filtered off and dried under a vacuum to give $H_3L^2 \cdot 5.5H_2O$ (0.66 g, 30%) as a white powder.

Compound 9. MS-ESI: (+): 644.5 ($[M + H]^+$, calcd 644.5); 666.4 ($[M + Na]^+$; calcd 666.5).

Compound 10. MS-ESI: (–): 474.1 ($[M - H]^-$, calcd 474.3); 512.0 ($[M + K - 2H]^-$, calcd 512.0).

$H_3L^2 \cdot 5.5H_2O$. 1H NMR (299.9 MHz, D_2O , pD = 1.15): δ 2.63 (3H, s, NCH_3); 2.80–3.15 (12H, m, CH_2); 3.20–3.63 (10H, m, CH_2); 3.97 (4H, br, CH_2CO_2).

^1H NMR (299.9 MHz, D_2O , pD = 5.3, Fig. S19[†]): δ 2.77 (3H, s, NCH_3); 2.80–2.91 (4H, m, CH_2); 2.94–3.08 (8H, m, CH_2); 3.13 (2H, s, CH_2CO_2); 3.31–3.46 (4H, m, CH_2); 3.52–3.60 (2H, m, CH_2); 3.70–3.76 (2H, m, CH_2); 3.89 (4H, AB-multiplet, CH_2CO_2).

$^{13}\text{C}\{^1\text{H}\}$ NMR (150.9 MHz, D_2O , pD = 5.6, Fig. S20[†]): δ 34.93 (1C, NCH_3); 46.89 (1C, CH_2NCH_3); 48.89 (2C, CH_2); 49.03 (2C, CH_2); 50.42 (1C, $\text{CH}_2\text{CH}_2\text{NCH}_3$); 51.04 (2C, CH_2); 53.10 (2C, CH_2); 55.68 (1C, CH_2CO_2); 58.16 (2C, CH_2CO_2); 171.08 (2C, CH_2CO_2); 178.63 (1C, CH_2CO_2).

MS-ESI: (+): 404.3 ([M + H]⁺, calcd 404.2); 426.9 ([M + Na]⁺, calcd 426.2); 442.8 ([M + K]⁺, calcd 442.2).

Elemental analysis: found (calcd for $\text{C}_{17}\text{H}_{44}\text{N}_5\text{O}_{11.5}$, $M_r = 502.6$): C: 40.84 (40.63), H: 9.27 (9.22), N: 13.80 (13.84).

1,4,7-Tris(carboxymethyl)-10-[2-(*N,N*-dimethylamino)ethyl]-1,4,7,10-tetraazacyclododecane ($\text{H}_3\text{L}^3\cdot 4\text{H}_2\text{O}$). To a well-stirred solution of $\text{H}_3\text{L}^3\cdot 3\text{H}_2\text{O}$ (100 mg, 0.225 mmol) in 10% aq. HCOOH (10 ml), paraformaldehyde (26.5 mg, 0.88 mmol) was added; the reaction mixture was refluxed for 5 h and analysed by ^1H NMR. To the reaction mixture, more paraformaldehyde (26.5 mg, 0.88 mmol) was added and the reaction mixture was refluxed for 5 h (this procedure was then repeated once more). After the reaction was completed, the solution was filtered and the filtrate was concentrated *in vacuo*. The residue was dissolved in a small amount of distilled water and evaporated under reduced pressure (this procedure was then repeated three more times) to give H_3L^3 (95 mg) as a yellow oil. The crude product was purified by crystallization from hot EtOH to give $\text{H}_3\text{L}^3\cdot 4\text{H}_2\text{O}$ (78 mg, 71%) as a white powder.

^1H NMR (600.2 MHz, D_2O , pD = 4.8, Fig. S21[†]): δ 2.87–2.90 (2H, m, CH_2); 2.93 (6H, s, $\text{N}(\text{CH}_3)_2$); 2.96 (2H, t, $^3J_{\text{HH}} = 6.0$ Hz, $\text{NCH}_2\text{CH}_2\text{N}(\text{CH}_3)_2$); 3.05–3.08 (4H, m, CH_2); 3.13–3.17 (2H, m, CH_2); 3.27 (2H, t, $^3J_{\text{HH}} = 6.0$ Hz, $\text{CH}_2\text{N}(\text{CH}_3)_2$); 3.36 (2H, s, CH_2CO_2); 3.38–3.40 (2H, m, CH_2); 3.47–3.56 (6H, m, CH_2); 3.88 (4H, AB-multiplet, CH_2CO_2).

$^{13}\text{C}\{^1\text{H}\}$ NMR (150.9 MHz, D_2O , pD = 4.8, Fig. S22[†]): δ 44.32 (2C, $\text{N}(\text{CH}_3)_2$); 48.08 (1C, CH_2 , $\text{NCH}_2\text{CH}_2\text{N}(\text{CH}_3)_2$); 48.70 (2C, CH_2); 49.14 (2C, CH_2); 51.32 (2C, CH_2); 52.68 (2C, CH_2); 55.63 (1C, CH_2CO_2); 56.08 (1C, $\text{CH}_2\text{N}(\text{CH}_3)_2$); 57.49 (2C, CH_2CO_2); 170.51 (2C, CH_2CO_2); 177.96 (1C, CH_2CO_2).

MS-ESI: (+): 456.9 ([M + K]⁺, calcd 456.2).

Elemental analysis: found (calcd for $\text{C}_{18}\text{H}_{43}\text{N}_5\text{O}_{10}$, $M_r = 489.6$): C: 44.29 (44.16), H: 8.86 (8.85), N: 14.14 (14.31).

Syntheses of Ln(III) complexes. The Ln(III) complexes of H_3L^1 , H_3L^2 and H_3L^3 for NMR, NMR CEST and MRI CEST experiments were prepared by mixing the lanthanide(III) chloride (Eu^{3+} , Yb^{3+} , La^{3+}) with 1.1 equiv. of the ligand in a small amount of distilled water, adjusting to pH 6 with 1 M aq. LiOH, and stirring overnight at 60 °C. Then the pH was re-adjusted to 6.5 with 1 M aq. LiOH and the solution was stirred overnight at 60 °C.

$\text{Eu}^{3+}\text{-H}_3\text{L}^1$. MS-ESI: (+): 540.1 ([M + H]⁺, calcd 540.2); 562.1 ([M + Na]⁺; calcd 562.1). (–): 573.9 ([M + Cl][–], calcd 574.1).

$\text{Yb}^{3+}\text{-H}_3\text{L}^1$. MS-ESI: (+): 561.1 ([M + H]⁺, calcd 561.2); 683.1 ([M + Na]⁺; calcd 683.2). (–): 594.9 ([M + Cl][–], calcd 595.1).

$\text{Eu}^{3+}\text{-H}_3\text{L}^2$. MS-ESI: (+): 553.6 ([M + H]⁺, calcd 554.2). (–): 587.7 ([M + Cl][–], calcd 588.1).

$\text{Yb}^{3+}\text{-H}_3\text{L}^2$. MS-ESI: (+): 581.8 ([M + Li]⁺, calcd 581.2). (–): 609.6 ([M + Cl][–], calcd 609.1).

$\text{Eu}^{3+}\text{-H}_3\text{L}^3$. MS-ESI: (+): 574.7 ([M + Li]⁺, calcd 574.2). (–): 602.6 ([M + Cl][–], calcd 602.1).

$\text{Yb}^{3+}\text{-H}_3\text{L}^3$. MS-ESI: (+): 595.8 ([M + Li]⁺, calcd 595.2). (–): 623.6 ([M + Cl][–], calcd 623.1).

X-Ray diffraction

Single-crystals of $\text{H}_3\text{L}^1\cdot 5\text{H}_2\text{O}$ were prepared by slow evaporation of the aqueous solution. The crystals of $\text{H}_3\text{L}^2\cdot 6\text{H}_2\text{O}$ were prepared by evaporation of the ethanolic solution, and the crystals of $\text{H}_3\text{L}^3\cdot 3.5\text{H}_2\text{O}$ were prepared by the slow cooling of a saturated hot ethanolic solution. The $\text{Yb}^{3+}\text{-H}_3\text{L}^1$ complex for crystallization was prepared by mixing the ligand with 1.1 equiv. of the YbCl_3 in a small amount of distilled water. The pH was adjusted to ~6 with 1 M NaOH, and the mixture was stirred overnight at 60 °C. Then the pH was re-adjusted to 6.5 and the solution was stirred overnight at 60 °C. The complex was purified on a Al_2O_3 column by chromatography. The pure product was eluted using a mixture of EtOH– H_2O –conc. aq. NH_3 (10 : 8 : 1). Single crystals of $[\text{Yb}(\text{L}^1)]\cdot 5\text{H}_2\text{O}$ were prepared from a concentrated aqueous solution of the complex by slow diffusion of the THF vapours.

The diffraction data were collected by employing a ApexII CCD diffractometer using Mo- $\text{K}\alpha$ radiation ($\lambda = 0.71073$ Å) at 150(1) K and analyzed using the SAINT V8.27B (Bruker AXS Inc., 2012) program package. The structures were solved by direct methods (SHELXS97²⁴) and refined by full-matrix least-squares techniques (SHELXL97²⁵). The relevant data for the structures have been provided.†

Crystal data

$\text{H}_3\text{L}^1\cdot 5\text{H}_2\text{O}$: $\text{C}_{16}\text{H}_{41}\text{N}_5\text{O}_{11}$, $M = 479.54$, monoclinic, $a = 7.80380(10)$, $b = 16.7236(3)$, $c = 17.8081(3)$ Å, $\beta = 92.1431(12)^\circ$, $U = 2322.47(6)$ Å³, space group $P2_1/c$, $Z = 4$, 5358 total reflections, 4408 intense reflections, $R_1[I > 2\sigma(I)] = 0.0344$, $wR_2(\text{all data}) = 0.0873$. CCDC 952386.† All non-hydrogen atoms were refined anisotropically. Although all hydrogen atoms could be found in the electron difference map, those bound to carbon atom were fixed in theoretical positions using a riding model with $U_{\text{eq}}(\text{H}) = 1.2U_{\text{eq}}(\text{C})$ to keep the number of refined parameters low. Hydrogen atoms bound to nitrogen or oxygen atoms were fully refined.

$\text{H}_3\text{L}^2\cdot 6\text{H}_2\text{O}$: $\text{C}_{17}\text{H}_{45}\text{N}_5\text{O}_{12}$, $M = 511.58$, monoclinic, $a = 9.4479(7)$, $b = 17.7199(14)$, $c = 15.5379(9)$ Å, $\beta = 106.573(2)^\circ$, $U = 2493.2(3)$ Å³, space group $P2_1/n$, $Z = 4$, 5723 total reflections, 4765 intense reflections, $R_1[I > 2\sigma(I)] = 0.0415$, $wR_2(\text{all data}) = 0.1129$. CCDC 952384.† The strategy of refinement was the same as that described in the previous case. Beside this, several solvate water molecules were refined as twisted in two positions with some disordered hydrogen atoms in two positions with half-occupancy.

$\text{H}_3\text{L}^3\cdot 3.5\text{H}_2\text{O}$: $\text{C}_{18}\text{H}_{42}\text{N}_5\text{O}_{9.50}$, $M = 480.57$, monoclinic, $a = 7.4798(2)$, $b = 15.9561(4)$, $c = 20.0951(6)$ Å, $\beta = 91.5670(10)^\circ$,

$U = 2397.42(11) \text{ \AA}^3$, space group $P2_1/n$, $Z = 4$, 5503 total reflections, 4686 intense reflections, $R_1[I > 2\sigma(I)] = 0.0370$, $wR_2(\text{all data}) = 0.0952$. CCDC 952385.† The refining strategy was the same as described above.

$[\text{Yb}(\text{L}^1)] \cdot 5\text{H}_2\text{O}$: $\text{C}_{16}\text{H}_{38}\text{N}_5\text{O}_{11}\text{Yb}$, $M = 649.55$, monoclinic, $a = 16.8708(7)$, $b = 7.5238(4)$, $c = 18.4880(9) \text{ \AA}$, $\beta = 90.4230(10)^\circ$, $U = 2346.7(2) \text{ \AA}^3$, space group $P2_1/c$, $Z = 4$, 5374 total reflections, 5160 intense reflections, $R_1[I > 2\sigma(I)] = 0.0137$, $wR_2(\text{all data}) = 0.0306$. CCDC 933967.† Preliminary refinement revealed a number of different maxima of the electronic density, which were located close to the carbon and nitrogen atoms of the macrocyclic part of the molecule. It pointed to a disorder of the macrocycle in a similar way as already reported in the literature (see, e.g., ref. 20c, Fig. S9†). It was successfully modelled using the anisotropic refinement of atoms occupying positions with a higher occupancy, whilst the less occupied part was refined in isotropic mode. All other non-hydrogen atoms were refined anisotropically. Although hydrogen atoms could be found in the electron difference map, they were fixed in theoretical (C–H) or original (N–H, O–H) positions using the riding model with $U_{\text{eq}}(\text{H}) = 1.2U_{\text{eq}}(\text{X})$ to keep the number of refined parameters low.

HPLC

The analytical HPLC system consisted of a gradient pump Beta 10 (ECOM) equipped with a mixer Knauer A0285 and dual UV-detector (ECOM). Analysis was performed on a LunaPHC8 column ($150 \times 4.6 \text{ mm}$, Phenomenex, the flow rate 1 ml min^{-1}). The mobile phase was continuously vacuum degassed in a DG 3014 degasser (ECOM) and it was mixed in the gradient pump from the stock solutions. The detector wavelengths were set to 210 and 254 nm. Injection volumes were $20 \mu\text{l}$ (concentrations of the samples were 1 mg ml^{-1}).

The preparative HPLC system was composed of a gradient pump LCD 50 K (ECOM) and UV-Vis detector LCD 2083 (ECOM). Preparation was performed on a LunaPHC8 ($250 \times 21.1 \text{ mm}$, Phenomenex, the flow rate was maintained at 20 ml min^{-1}). The detector wavelengths were set to 210 nm. The mobile phase was prepared separately and degassed using an ultrasound probe (Cole-Parmer 750-Watt Ultrasonic Homogenizer). Injection volumes were 1 ml. The collection and processing of the data was performed using Clarity (DataApex) software.

Potentiometry

Potentiometric titrations²⁶ were carried out in a vessel thermostatted at $25.0 \pm 0.1 \text{ }^\circ\text{C}$, at a constant ionic strength ($I = 0.1 \text{ M}$ (Me_4N)Cl) using a PHM 240 pH-meter, a GK 2401B combined glass electrode and a 2 ml ABU 900 automatic piston burette (all Radiometer). The initial volume was ca. 5 ml and the ligand concentration in the titration vessel was ca. 0.004 M. An inert atmosphere was provided by the constant passage of argon saturated with the vapour of the solvent [0.1 M (Me_4N)Cl]. Extra HCl was added to the starting solution to run titrations in the $-\log[\text{H}^+]$ range 2.0–12.0 (for protonation constants) and 1.8–6.0 for the Gd^{3+} and La^{3+} stability constants.

Titration were performed with a (Me_4N)OH solution. Titrations with metal ions were performed at metal-to-ligand molar ratios of 1 : 1. Ligand titrations consisted of about 40 points per titration and were run in triplicate. As the complexation was too slow for conventional titration, the “out-of-cell” method was used;²⁶ about 25 points per titration, two parallel titrations, three weeks at room temperature for equilibration. To calculate the protonation constants of the ligand and the stability constants of the complexes, the OPIUM²⁷ software package was used.

The overall protonation constants β_{h10} are concentration constants defined as $\beta_{h10} = [\text{H}_h\text{L}]/([\text{H}]^h \cdot [\text{L}])$ (they can be transferred into stepwise dissociation constants as $\text{p}K_{\text{A}}(\text{H}_h\text{L}) = \log \beta_h - \log \beta_{h-1}$). The concentration stability constants β_{hlm} are generally defined by $\beta_{hlm} = [\text{H}_h\text{L}_m\text{M}_m]/([\text{H}]^h \cdot [\text{L}]^l \cdot [\text{M}]^m)$. The value of $\text{p}K_{\text{w}}$ used was 13.81.

¹H NMR titrations

The ¹H NMR titration over the whole pH region (31 points), for determination of the protonation constants, was performed at 25 °C (ligand concentration: 0.05 M; no ionic strength control) in H₂O on a Bruker Avance (III) 600 ($B_0 = 14.1 \text{ T}$), using 5 mm sample tubes. ¹H NMR spectra were measured without pre-saturation of the water signal. A coaxial capillary with D₂O (for the lock) and *t*-BuOH (as external standard; $\delta_{\text{H}} = 1.25 \text{ ppm}$) was used. The solution pH (0.5–13.5) was adjusted with aqueous HCl or NMe₄OH solutions and measured with a combined glass electrode (Mettler Toledo) and pH-meter (3505 pH Meter, JENWAY) calibrated with standard buffers. Protonation constants were calculated with the OPIUM software package.²⁷

CEST experiments

All Z-spectra were recorded on a VNMR5300 operating at 299.9 MHz ($B_0 = 7.05 \text{ T}$), using 5 mm sample tubes and a coaxial capillary with D₂O and *t*-BuOH as the external standard. Samples were of 25–100 mM concentration in the mixture of H₂O and D₂O (1 : 10) or in H₂O; pH was adjusted with aqueous HCl or LiOH solutions. Standard pulse sequences for pre-saturation experiments were used. Saturation offsets were set using the array-function (increment 200–250 Hz). Other measurement parameters are listed below each figure.

MRI CEST images were measured with phantoms consisting of one vial containing an aqueous solution of the La^{3+} -complex as a control and eight (resp. five) vials containing aqueous solution of Eu^{3+} or Yb^{3+} -complexes with different pH values or concentrations. All MRI CEST images were acquired on a 4.7 T scanner (Bruker BioSpec, Germany) using RARE (Rapid Acquisition with Refocused Echoes) or MSME (Multi Slice Multi Echo) pulse sequences with pre-saturation pulse. Experimental conditions: TR = 5000 ms, TE = 8.9 ms, resolution $0.35 \times 0.35 \times 2 \text{ mm}$, turbo factor = 4 (in RARE sequence). Other measurement parameters are listed below each figure. Parameters of pre-saturation pulse: $B_1 = 20 \mu\text{T}$, $\text{satdly} = 2 \text{ s}$. For all MR experiments, the resonator coil was used.

All MR images were processed using an in-house program, written in Matlab (The Mathworks Inc, USA), where the signal intensity was normalized to unit slope and receiver gain. Then the difference image between the images acquired with negative and positive frequency offset of the saturation frequency was calculated. Difference images were analysed using ImageJ software (NIH, USA), regions of interest were outlined manually.

Conclusions

We prepared 2-aminoethyl derivatives of DO3A and showed that the coordinated amino group mediates NMR saturation transfer to the bulk water. We suggest a new mechanism for the PARACEST effect, consisting of the coordination-decoordination of the amino group having an optimal rate, combined with the very fast protonation-deprotonation of the group while the group is non-bound to the paramagnetic metal ion. The pH-dependence of the saturation transfer parallels with the abundance of the species with the coordinated amino group. This novel type of PARACEST agent broadens the arsenal of pH-sensitive probes for possible *in vivo* pH measurements by MRI.

Acknowledgements

We thank J. Plutnar and Z. Tošner for their help with the setting of the CEST pulse sequences. The financial support of the Ministry of Education of the Czech Republic (no. MSM0021620857), the Grant Agency of the Czech Republic (no. 207/11/1437) and the Grant Agency of the Charles University (no. 110213) is acknowledged.

Notes and references

- (a) P. Caravan, J. J. Ellison, T. J. McMurphy and R. B. Lauffer, *Chem. Rev.*, 1999, **99**, 2293–2352; (b) P. Hermann, J. Kotek, V. Kubiček and I. Lukeš, *Dalton Trans.*, 2008, 3027–3047; (c) C. F. G. C. Geraldes and S. Laurent, *Contrast Media Mol. Imaging*, 2009, **4**, 1–23.
- (a) J. Zhou and P. C. M. van Zijl, *Prog. Nucl. Magn. Reson. Spectrosc.*, 2006, **48**, 109–136; (b) Y. Wu, M. Evbuomwan, M. Melendez, A. Opina and A. D. Sherry, *Future Med. Chem.*, 2010, **2**, 351–366; (c) E. Terreno, D. D. Castelli and S. Aime, *Contrast Media Mol. Imaging*, 2010, **5**, 78–98; (d) P. C. M. van Zijl and N. N. Yadav, *Magn. Reson. Med.*, 2011, **65**, 927–948; (e) G. Liu, X. Song, K. W. Y. Chan and M. T. McMahon, *NMR Biomed.*, 2013, **26**, 810–828.
- (a) S. Zhang, M. Merritt, D. E. Woessner, R. E. Lenkinski and A. D. Sherry, *Acc. Chem. Res.*, 2003, **36**, 783–790; (b) M. Woods, D. E. Woessner and A. D. Sherry, *Chem. Soc. Rev.*, 2006, **35**, 500–511; (c) S. Viswanathan, Z. Kovács, K. N. Green, S. J. Ratnakar and A. D. Sherry, *Chem. Rev.*, 2010, **110**, 2960–3018; (d) T. C. Soesbe, Y. Wu and A. D. Sherry, *NMR Biomed.*, 2013, **26**, 829–838.
- S. Zhang and A. D. Sherry, *J. Solid State Chem.*, 2003, **171**, 38–43.
- M. Woods, A. Pasha, P. Zhao, G. Tireso, S. Chowdhury, G. Kiefer, D. E. Woessner and A. D. Sherry, *Dalton Trans.*, 2011, **40**, 6759–6764.
- S. Zhang, K. Wu, M. C. Biewer and A. D. Sherry, *Inorg. Chem.*, 2001, **40**, 4284–4290.
- S. Zhang, L. Michaudet, S. Burgess and A. D. Sherry, *Angew. Chem., Int. Ed.*, 2002, **41**, 1919–1921.
- (a) C.-H. Huang and J. R. Morrow, *Inorg. Chem.*, 2009, **48**, 7237–7243; (b) C.-H. Huang and J. R. Morrow, *J. Am. Chem. Soc.*, 2009, **131**, 4206–4207; (c) C.-H. Huang, J. Hammell, S. J. Ratnakar, A. D. Sherry and J. R. Morrow, *Inorg. Chem.*, 2010, **49**, 5963–5970; (d) J. Hammell, L. Buttarazzi, C.-H. Huang and J. R. Morrow, *Inorg. Chem.*, 2011, **50**, 4857–4867; (e) D. D. Castelli, E. Terreno and S. Aime, *Angew. Chem., Int. Ed.*, 2011, **50**, 1798–1800.
- S. J. Dorazio, P. B. Tsitovich, K. E. Sifers, J. A. Sperryak and J. R. Morrow, *J. Am. Chem. Soc.*, 2011, **133**, 14154–14156.
- (a) S. J. Dorazio and J. R. Morrow, *Inorg. Chem.*, 2012, **51**, 7448–7450; (b) S. J. Dorazio, P. B. Tsitovich, S. A. Gardina and J. R. Morrow, *J. Inorg. Biochem.*, 2012, **117**, 212–219; (c) P. B. Tsitovich and J. R. Morrow, *Inorg. Chim. Acta*, 2012, **393**, 3–11.
- A. O. Olatunde, S. J. Dorazio, J. A. Sperryak and J. R. Morrow, *J. Am. Chem. Soc.*, 2012, **134**, 18503–18505.
- (a) B. Yoo and M. D. Pagel, *J. Am. Chem. Soc.*, 2006, **128**, 14032–14033; (b) G. Liu, Y. Li and M. D. Pagel, *Magn. Reson. Med.*, 2007, **58**, 1249–1256; (c) T. Chauvin, P. Durand, M. Bernier, H. Meudal, B.-T. Doan, F. Noury, B. Badet, J.-C. Beloeil and É. Tóth, *Angew. Chem., Int. Ed.*, 2008, **47**, 4370–4372; (d) T. Chauvin, S. Torres, R. Rosseto, J. Kotek, B. Badet, P. Durand and É. Tóth, *Chem.–Eur. J.*, 2012, **18**, 1408–1418; (e) V. R. Sheth, G. Liu, Y. Li and M. D. Pagel, *Contrast Media Mol. Imaging*, 2012, **7**, 26–34; (f) V. R. Sheth, Y. Li, L. Q. Chen, C. M. Howison, C. A. Flask and M. D. Pagel, *Magn. Reson. Med.*, 2012, **67**, 760–768.
- (a) J. A. Duimstra, F. J. Femia and T. J. Meade, *J. Am. Chem. Soc.*, 2005, **127**, 12847–12855; (b) A. Mishra, J. Pfeuffer, R. Mishra, J. Engelmann, A. K. Mishra, K. Ugurbil and N. K. Logothetis, *Bioconjugate Chem.*, 2006, **17**, 773–780.
- A. K. Mishra and J.-F. Chatal, *New J. Chem.*, 2001, **25**, 336–339.
- G. B. Giovenzana, R. Negri, G. A. Rolla and L. Tei, *Eur. J. Inorg. Chem.*, 2012, 2035–2039.
- M. Meyer, V. Dahaoui-Gindrey, C. Lecomte and R. Guillard, *Coord. Chem. Rev.*, 1998, **178–180**, 1313–1405.
- K. Kumar, C. A. Chang, L. C. Francesconi, D. D. Dischino, M. F. Malley, J. Z. Gougoutas and M. F. Tweedle, *Inorg. Chem.*, 1994, **33**, 3567–3575.
- S. Aime, M. Botta, M. Fasano, M. P. M. Marques, C. F. G. C. Geraldes, D. Pubanz and A. E. Merzbach, *Inorg. Chem.*, 1997, **36**, 2059–2068.
- (a) J. Rudovský, P. Cígler, J. Kotek, P. Hermann, P. Vojtišek, I. Lukeš, J. A. Peters, L. Vander Elst and R. N. Muller, *Chem.–Eur. J.*, 2005, **11**, 2373–2384; (b) P. Lebdušková,

- P. Hermann, L. Helm, É. Tóth, J. Kotek, K. Binnemans, J. Rudovský, I. Lukeš and A. E. Merbach, *Dalton Trans.*, 2007, 493–501; (c) T. Vitha, V. Kubiček, J. Kotek, P. Hermann, L. Vander Elst, R. N. Muller, I. Lukeš and J. A. Peters, *Dalton Trans.*, 2009, 3201–3214; (d) D. D. Castelli, M. C. Caligara, M. Botta, E. Terreno and S. Aime, *Inorg. Chem.*, 2013, 52, 7130–7138.
- 20 (a) I. Lukeš, J. Kotek, P. Vojtíšek and P. Hermann, *Coord. Chem. Rev.*, 2001, 216–217, 287–312; (b) P. Vojtíšek, P. Cígler, J. Kotek, J. Rudovský, P. Hermann and I. Lukeš, *Inorg. Chem.*, 2005, 44, 5591–5599; (c) J. Kotek, J. Rudovský, P. Hermann and I. Lukeš, *Inorg. Chem.*, 2006, 45, 3097–3102.
- 21 (a) A. Dadabhoy, S. Faulkner and P. G. Sammes, *J. Chem. Soc., Perkin Trans. 2*, 2002, 348–357; (b) D. A. Moore, *Org. Synth.*, 2008, 85, 10–14.
- 22 D. D. Perrin and W. L. F. Armarego, *Purification of Laboratory Chemicals*, Pergamon Press, Oxford, 3rd edn, 1988.
- 23 N. Cesari, C. Biancalani, C. Vergelli, V. Dal Piaz, A. Graziano, P. Biagini, C. Ghelardini, N. Galeotti and M. P. Giovannoni, *J. Med. Chem.*, 2006, 49, 7826–7835.
- 24 G. M. Sheldrick, *SHELXS97, Program for Crystal Structure Solution from Diffraction Data*, University of Göttingen, Göttingen, 1997.
- 25 G. M. Sheldrick, *SHELXL97, Program for Crystal Structure Refinement from Diffraction Data*, University of Göttingen, Göttingen, 1997.
- 26 (a) P. Táborský, P. Lubal, J. Havel, J. Kotek, P. Hermann and I. Lukeš, *Collect. Czech. Chem. Commun.*, 2005, 70, 1909–1942; (b) M. Försterová, I. Svobodová, P. Lubal, P. Táborský, J. Kotek, P. Hermann and I. Lukeš, *Dalton Trans.*, 2007, 535–549.
- 27 M. Kývala and I. Lukeš, International Conference Chemo-metrics 95, p. 63, Pardubice, Czech Republic, 1995. Full version of "OPIUM" available (free of charge) on: <http://web.natur.cuni.cz/~kyvala/opium.html>.

Electronic supplementary information (ESI)
for

Lanthanide(III) complexes of aminoethyl-DO3A as PARACEST contrast agents based on decoordination of the weakly bound amino group

Tereza Kechová,^a Jan Kočík,^{a*} Daniel Dřelák,^b Jana Havlíčková,^a Věra Čistáková,^a Petr Herrmann^a^a Department of Inorganic Chemistry, University Karlova (Charles University), Hlavova 2030, 128 40 Prague 2, Czech Republic. Tel: +420-22195-1201. Fax: +420-22195-1253. E-mail: inodict@natur.cuni.cz^b Department of Radiodiagnostic and Interventional Radiology, Magdalenic Resonance Unit, Institute of Clinical and Experimental Medicine, Vřátovská 159/899, 140 21 Prague 4, Czech Republic

Content:

Fig. S1 Molecular structure of H_2L^2 found in the crystal structure of $\text{H}_2\text{L}^2 \cdot 6\text{H}_2\text{O}$.	Page
Fig. S2 Molecular structure of H_2L^2 found in the crystal structure of $\text{H}_2\text{L}^2 \cdot 3,5\text{H}_2\text{O}$.	2
Table S1 Torsion angles in the macrocyclic units found in the crystal structures of $\text{H}_2\text{L}^2 \cdot 5\text{H}_2\text{O}$, $\text{H}_2\text{L}^2 \cdot 6\text{H}_2\text{O}$ and $\text{H}_2\text{L}^2 \cdot 3,5\text{H}_2\text{O}$.	2
Fig. S3 The distribution diagram of H_2L^2 .	3
Fig. S4 ^1H NMR chemical shifts dependence of H_2L^2 on pH.	3
Scheme S1 Protonation scheme of H_2L^2 .	4
Fig. S5 Distribution diagram of the $\text{La}^{3+} \cdot 3\text{H}_2\text{L}^2$ system.	4
Fig. S6 Distribution diagram of the $\text{Gd}^{3+} \cdot 3\text{H}_2\text{L}^2$ system.	5
Fig. S7 ^1H NMR spectra of $[\text{Eu}(\text{H}_2\text{O})_9(\text{L}^2)]$ at different temperatures.	5
Fig. S8 ^1H NMR spectra of $[\text{Yb}(\text{L}^2)]$ at different temperatures.	6
Fig. S9 Disorder of the $[\text{Yb}(\text{L}^2)]$ molecule found in the solid-state structure of $[\text{Yb}(\text{L}^2)] \cdot 5\text{H}_2\text{O}$.	7
Table S2 Selected geometric parameters found in the structure of $[\text{Yb}(\text{L}^2)] \cdot 5\text{H}_2\text{O}$.	8
Fig. S10 ^1H NMR spectra of $[\text{Eu}(\text{H}_2\text{O})_9(\text{L}^2)]$ in H_2O , in H_2O with pressurization of the bulk water signal and in D_2O .	8
Fig. S11 Z-spectra of an solution of $[\text{Eu}(\text{H}_2\text{O})_9(\text{L}^2)]$ and $[\text{Yb}(\text{L}^2)]$ complexes at different temperatures (85 °C, 95 °C).	9
Fig. S12 Z-spectra of an solution of $[\text{Eu}(\text{H}_2\text{O})_9(\text{L}^2)]$ and $[\text{Yb}(\text{L}^2)]$ complexes at different pH and temperatures.	10
Fig. S13 Z-spectra of an solution of $[\text{Eu}(\text{H}_2\text{O})_9(\text{L}^2)]$ and $[\text{Yb}(\text{L}^2)]$ complexes at different pH and temperatures.	10
Fig. S14 MRI-CEST images of phantoms containing aq. solutions of $[\text{Eu}(\text{H}_2\text{O})_9(\text{L}^2)]$ and $[\text{Yb}(\text{L}^2)]$ with different concentrations.	11
Fig. S15 pH dependence of normalized intensity of the CEST effect of phantoms containing aqueous solutions of $[\text{Eu}(\text{H}_2\text{O})_9(\text{L}^2)]$ and $[\text{Yb}(\text{L}^2)]$.	12
Fig. S16 Concentration dependence of normalized intensity of the CEST effect of phantoms containing aqueous solutions of $[\text{Eu}(\text{H}_2\text{O})_9(\text{L}^2)]$ and $[\text{Yb}(\text{L}^2)]$.	13
Fig. S17 ^1H NMR spectrum of H_2L^2 .	13
Fig. S18 $^{13}\text{C}\{^1\text{H}\}$ NMR spectrum of H_2L^2 .	14
Fig. S19 ^1H NMR spectrum of H_2L^2 .	14
Fig. S20 $^{13}\text{C}\{^1\text{H}\}$ NMR spectrum of H_2L^2 .	15
Fig. S21 ^1H NMR spectrum of H_2L^2 .	16
Fig. S22 $^{13}\text{C}\{^1\text{H}\}$ NMR spectrum of H_2L^2 .	16

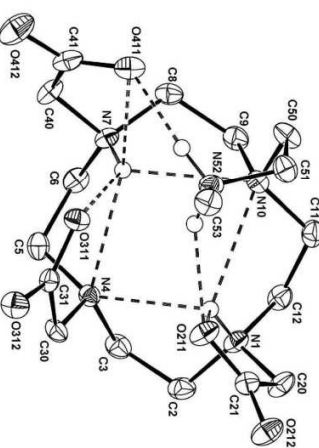


Fig. S1 Molecular structure of H_2L^2 found in the crystal structure of $\text{H}_2\text{L}^2 \cdot 6\text{H}_2\text{O}$. Dashed lines show system of intramolecular hydrogen bonds. Carbon-bound hydrogen atoms are omitted for sake of clarity.

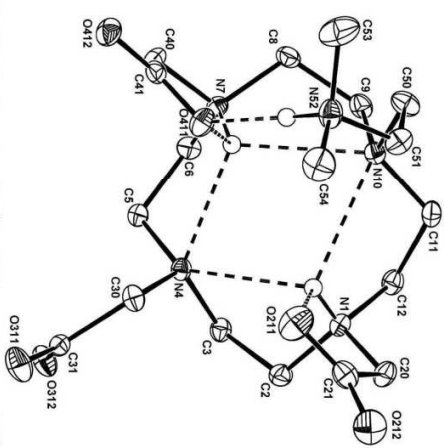


Fig. S2 Molecular structure of H_2L^2 found in the crystal structure of $\text{H}_2\text{L}^2 \cdot 3,5\text{H}_2\text{O}$. Dashed lines show system of intramolecular hydrogen bonds. Carbon-bound hydrogen atoms are omitted for sake of clarity.

Table S1 Torsion angles in the macrocyclic units found in the crystal structures of H_3L^+ ·5H₂O, H_3L^+ ·6H₂O and H_3L^+ ·3.5H₂O.

Torsion angle, °	H_3L^+	H_3L^+	H_3L^+
N1-C2-C3-N4	-49.71(13)	-47.30(16)	-53.54(13)
C2-C3-N4-C5	170.56(10)	168.61(12)	166.59(9)
C3-N4-C5-C6	-88.19(11)	-90.39(14)	-90.36(11)
N4-C5-C6-N7	-63.19(12)	-64.59(15)	-58.02(12)
C5-C6-N7-C8	153.42(10)	154.47(11)	159.90(9)
C6-N7-C8-C9	-73.45(12)	-73.59(14)	-76.06(12)
N7-C8-C9-N10	-58.24(13)	-55.17(16)	-58.50(13)
C8-C9-N10-C11	167.89(10)	167.82(12)	163.69(9)
C9-N10-C11-C12	-78.57(12)	-78.52(14)	-80.67(11)
N10-C11-C12-N1	-62.61(12)	-67.48(14)	-68.79(12)
C11-C12-N1-C2	159.05(9)	158.99(11)	160.83(9)
C12-N1-C2-C3	-76.48(12)	-73.82(15)	-66.10(12)

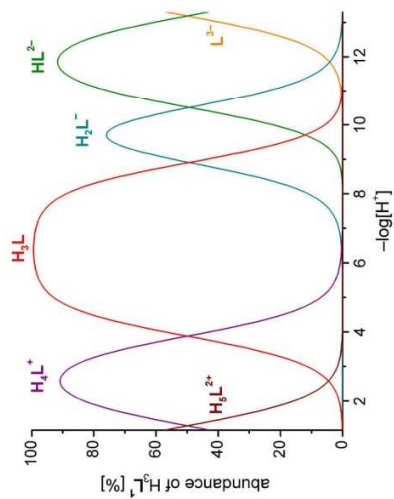


Fig. S3 The distribution diagram of H_3L^+ .

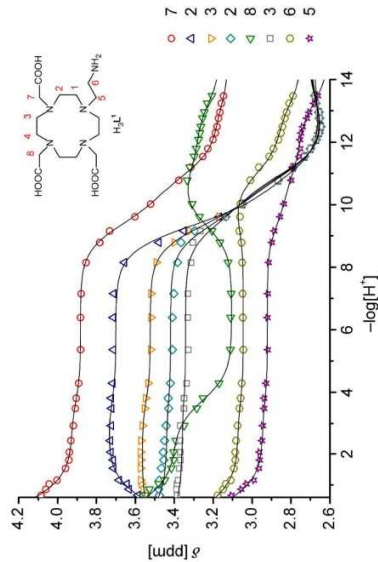
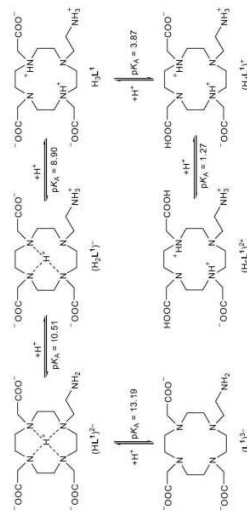


Fig. S4 pH dependence of δ_c of H_3L^+ ($B_c = 14.1$ T, 25 °C). Dependence of chemical shifts of protons 1 and 4 were not included as they are overlapping with other signals. At pH below 9, individual protons of CH₂ groups 2 and 3 became nonequivalent resulting in two signals for each of groups.



Scheme S1 Consecutive protonation scheme of H_3L^+ .

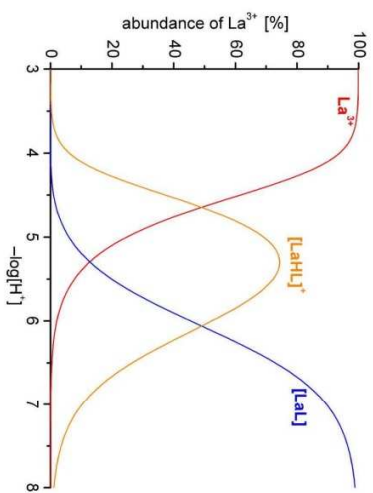


Fig. S5 Distribution diagram of the $\text{La}^{3+}\text{-H}_2\text{L}^+$ ($\alpha_{\text{M}} = \alpha_{\text{L}} = 0.004$ M) system ($l = 0.1$ M (NMe)₂Cl, 25 °C); determined by potentiometry, $L = (\text{L})^{3-}$.

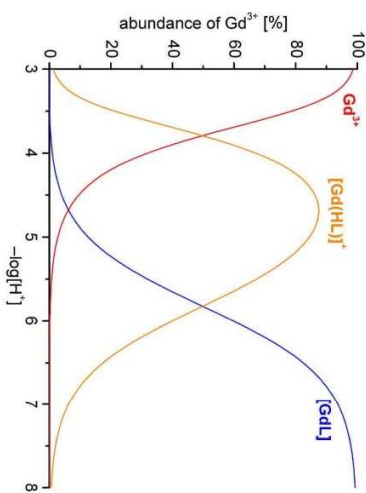


Fig. S6 Distribution diagram of the $\text{Gd}^{3+}\text{-H}_2\text{L}^+$ ($\alpha_{\text{M}} = \alpha_{\text{L}} = 0.004$ M) system ($l = 0.1$ M (NMe)₂Cl, 25 °C); determined by potentiometry, $L = (\text{L})^{3-}$.

5

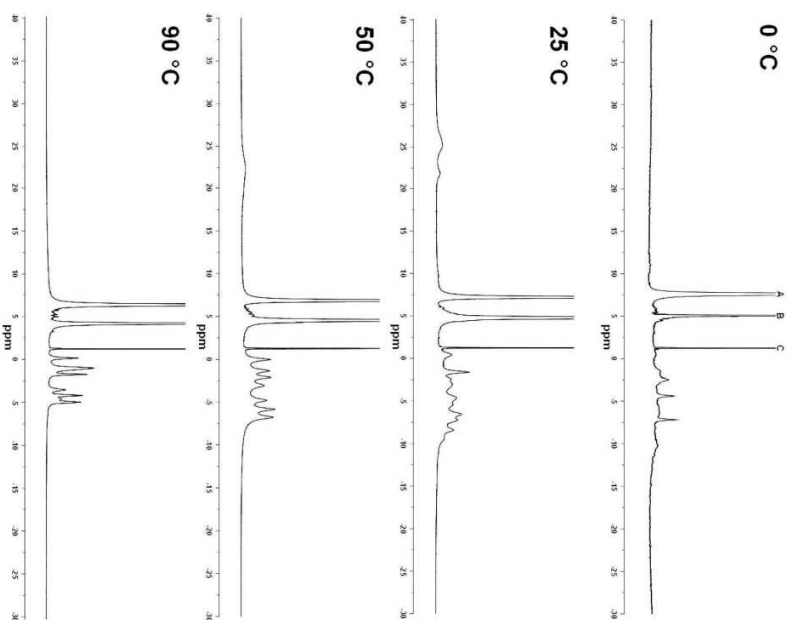


Fig. S7 ^1H NMR spectra of $[\text{Eu}(\text{H}_2\text{O})(\text{L})]$ (0.1 M) solution in D_2O , $\delta_{\text{A}} = 7.05$ T for 25, 50 and 90 °C and 9.4 T for 0 °C; $\text{pD} = 9.0$. A coaxial capillary with D_2O and $t\text{-BuOH}$ was used as external standard ($\delta_{\text{H}} = 1.25$ ppm). Signals assignment: A = H₂O in sample solution, B = H₂O in capillary, C = $t\text{-BuOH}$ in capillary

6

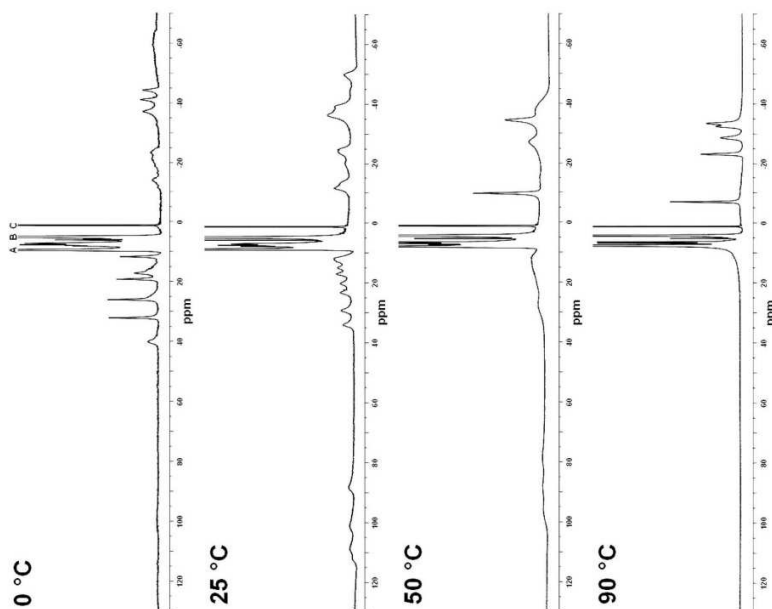


Fig. S8 ^1H NMR spectra of $[\text{Yb}(\text{L}')]$ (0.1 M solution in D_2O , $B_0 = 7.05$ T for 25, 50 and 90 °C and 9.4 T for 0 °C, $\text{pD} = 8.5$). A coaxial capillary with D_2O and $t\text{-BuOH}$ was used as external standard ($\delta_{\text{H}} = 1.25$ ppm). Signals assignment: A = HDO in sample solution, B = HDO in capillary, C = $t\text{-BuOH}$ in capillary.

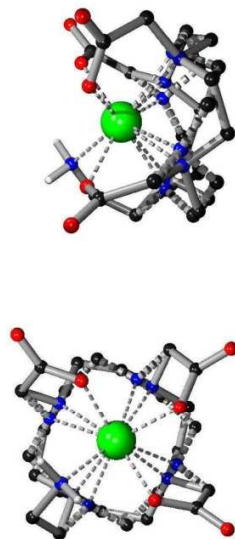
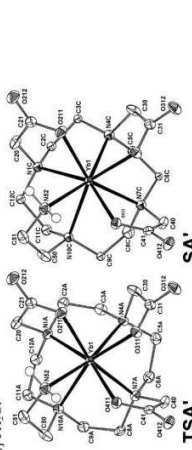


Fig. S9 Disorder of the $[\text{Yb}(\text{L}')]$ molecule found in the solid-state structure of $[\text{Yb}(\text{L}')] \cdot 5\text{H}_2\text{O}$. Figure shows overlay of both disordered complex species, more abundant (85 %) TSA' isomer is represented using solid bonds and less abundant (15 %) SA' isomer using dashed bonds. A: Top view, B: Side view. Carbon-bound hydrogen atoms are omitted for clarity reasons. Colour code: Yb – green; N – blue; O – red; C – black; H – grey.

Table S2 Geometric parameters of coordination sphere of Yb^{3+} ion in the crystal structure of $[\text{Yb}(\text{L}')] \cdot 5\text{H}_2\text{O}$.



TSA'		SA'	
Coordination distances, Å			
Ni plane of TSA' unit		NQA-OQ	2.5919
Yb1-N1A	2.519(2)	NQC-OQ	2.5042
Yb1-N4A	2.562(2)	Yb1-NQA	1.482(2)
Yb1-N7A	2.516(2)	Yb1-NQC	1.396(2)
Yb1-N10A	2.553(2)	Yb1-OQ	1.111(2)
Dihedral angles of pendants in TSA' unit, °			
Ni plane of SA' unit		N1A-NQA-OQ-O211	-23.47(8)
Yb1-N1C	2.535(13)	N4A-NQA-OQ-O311	-23.90(8)
Yb1-N4C	2.466(13)	N7A-NQA-OQ-O411	-23.46(8)
Yb1-N7C	2.498(13)	N10A-NQA-OQ-N52	-19.15(8)
Yb1-N10C	2.525(12)		
Dihedral angles of pendants in SA' unit, °			
O1N plane		N1C-NQC-OQ-O211	-38.5(4)
Yb1-O211	2.2707(12)	N4C-NQC-OQ-O311	-38.8(4)
Yb1-O311	2.2564(12)	N7C-NQC-OQ-O411	-38.8(4)
Yb1-O411	2.2764(12)	N10C-NQC-OQ-N52	-34.3(4)
Yb1-N52	2.4485(15)		

NQA – the centroid of the N-plane in TSA arrangement; NQC – the centroid of the N-plane in SA arrangement; OQ – the centroid of the O_3N -plane.

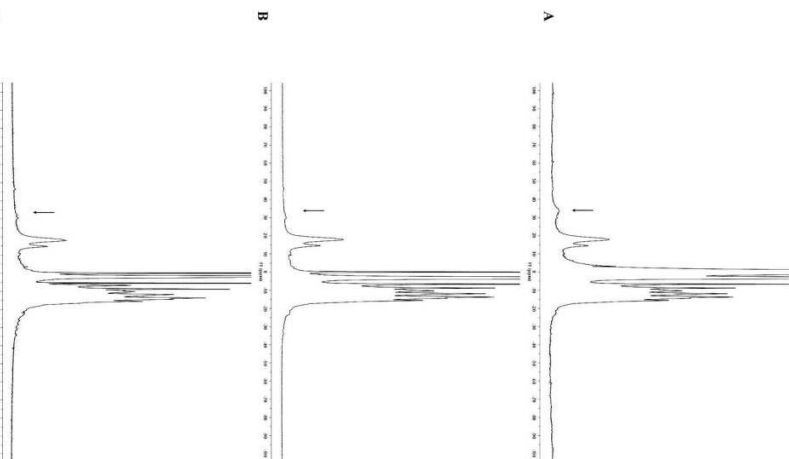


Fig. S10 A: ^1H NMR spectrum of $[\text{Eu}(\text{H}_2\text{O})_{12}]^{3+}$ (1 M solution in H_2O , $B_0 = 7.05$ T, 25 °C, pH = 7.9).
B: ^1H NMR spectrum of $[\text{Eu}(\text{H}_2\text{O})_{12}]^{3+}$ (1 M solution in H_2O , $B_0 = 7.05$ T, 25 °C, pH = 7.9), water signal was saturated. C: ^1H NMR spectrum of $[\text{Eu}(\text{H}_2\text{O})_{12}]^{3+}$ (1 M solution in D_2O , $B_0 = 7.05$ T, 25 °C, pH = 7.9). In all spectra, a coaxial capillary with D_2O and $t\text{-BuOH}$ was used. Chemical shift of H_2O in solution was referenced to 0 ppm.

9

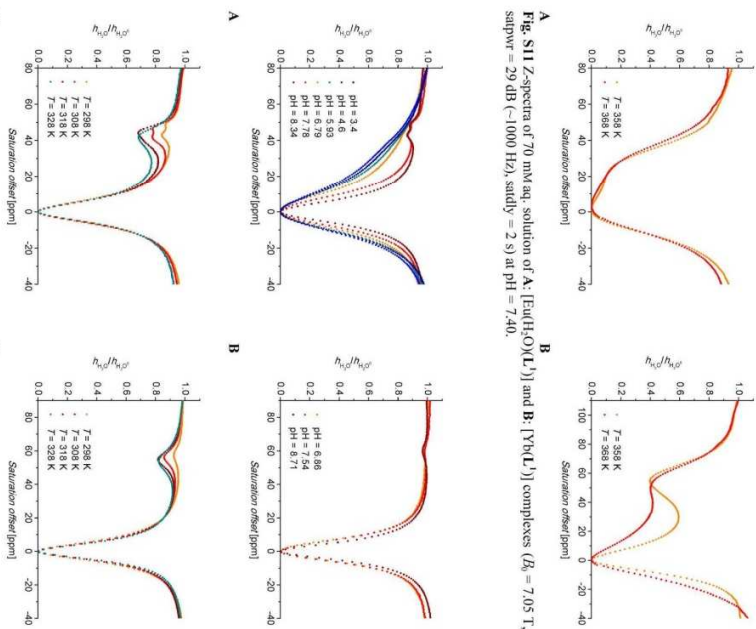


Fig. S12 A: Z-spectra of 25 mM aq. solution ($\text{H}_2\text{O}/\text{D}_2\text{O}$ 1:10) of $[\text{Eu}(\text{H}_2\text{O})_{12}]^{3+}$ complex ($B_0 = 7.05$ T, satpw = 29 dB, 1000 Hz, satdy = 2 s). A: $T = 298$ K, C: pH = 8.16. B, D: Z-spectra of a 25 mM (B) or 50 mM (D) aq. solution ($\text{H}_2\text{O}/\text{D}_2\text{O}$ 1:10) of $[\text{Yb}(\text{L})]$ complex ($B_0 = 7.05$ T, satpw = 29 dB, 1000 Hz, satdy = 2 s). B: $T = 298$ K. D: pH = 8.35.

Fig. S12 A-C: Z-spectra of a 25 mM aq. solution ($\text{H}_2\text{O}/\text{D}_2\text{O}$ 1:10) of $[\text{Eu}(\text{H}_2\text{O})_{12}]^{3+}$ complex ($B_0 = 7.05$ T, satpw = 29 dB, 1000 Hz, satdy = 2 s). A: $T = 298$ K, C: pH = 8.16. B, D: Z-spectra of a 25 mM (B) or 50 mM (D) aq. solution ($\text{H}_2\text{O}/\text{D}_2\text{O}$ 1:10) of $[\text{Yb}(\text{L})]$ complex ($B_0 = 7.05$ T, satpw = 29 dB, 1000 Hz, satdy = 2 s). B: $T = 298$ K. D: pH = 8.35.

10

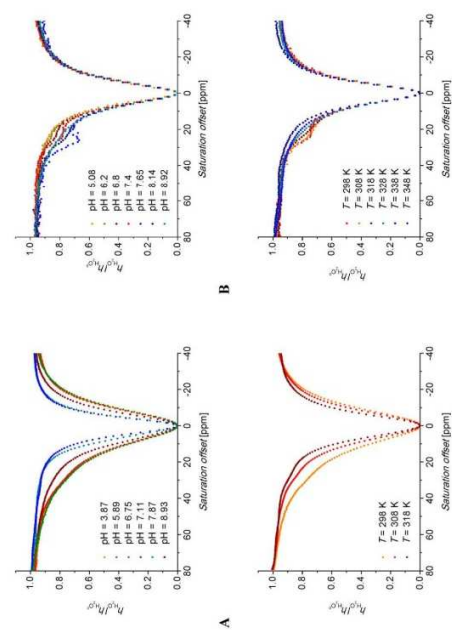


Fig. S13 A, C: Z-spectra of 25 mM aq. solution (H₂O:D₂O, 1:10) of [Eu(H₂O)₉(L⁻)₃] complex ($B_0 = 7.05$ T, satpwr = 29 dB (~1000 Hz), satdy = 2 s); A: T = 298 K. C: pH = 5.40. B, D: Z-spectra of 50 mM aq. solutions (H₂O:D₂O 1:10) of the [Yb(L⁻)₃] complex ($B_0 = 7.05$ T, satpwr = 29 dB (~1000 Hz), satdy = 2 s); B: T = 298 K. D: pH = 7.72.

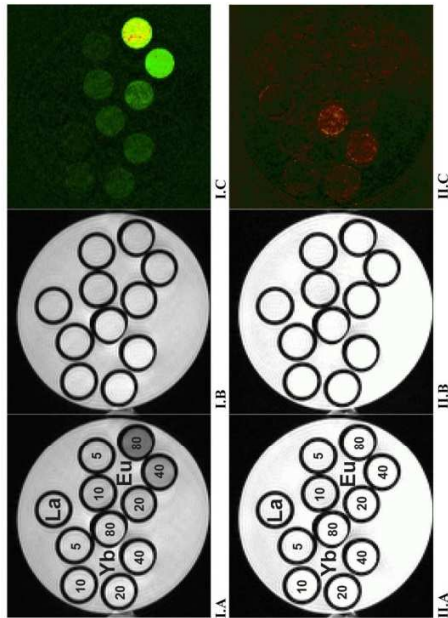


Fig. S14 MRI-CEST images of phantom consisting of one vial containing 80 mM aq. solution of [La(H₂O)₉(L⁻)₃] as a standard and five vials containing aqueous solution of [Eu(H₂O)₉(L⁻)₃] and [Yb(L⁻)₃] with different concentrations; pH = 7.4; concentrations (mM) are given as labels in figures A, B. Experimental conditions: RARE pulse sequence, $B_0 = 4.7$ T, $B_1 = 20$ μ T, T = 293 K, satdy = 2 s, TR = 5 s, TE = 8.9 ms, scan time = 2 min. I.A: T₁-weighted image, satfrq = 34 ppm from the bulk water signal. I.B: T₂-weighted image, satfrq = -34 ppm from the bulk water signal. I.C: The difference between images I.A and I.B in false colours. II.A: T₁-weighted image, satfrq = 89 ppm from the bulk water signal. II.B: T₂-weighted image, satfrq = -89 ppm from the bulk water signal. II.C: The difference between images II.A and II.B in false colours.

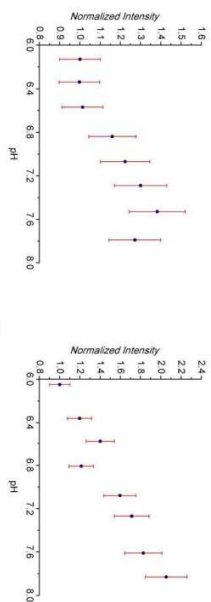


Fig. S15 pH dependence of normalized intensity of the CEST effect (20 μ T, MRI 4.7 T). A: [Eu(DH-O)(L)], data from Fig. S11C. B: [Yb(L)], data from Fig. S11C.

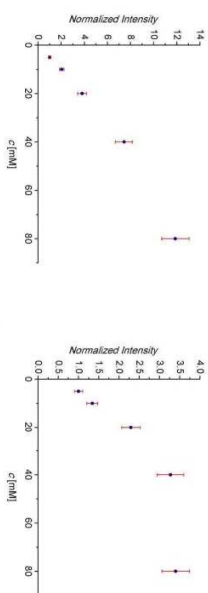


Fig. S16 Concentration dependence of normalized intensity of the CEST effect (20 μ T, MRI 4.7 T). A: [Eu(DH-O)(L)], data from Fig. S141C. B: [Yb(L)], data from Fig. S141C.

Characterization ^1H and $^{13}\text{C}\{^1\text{H}\}$ NMR spectra of the ligands

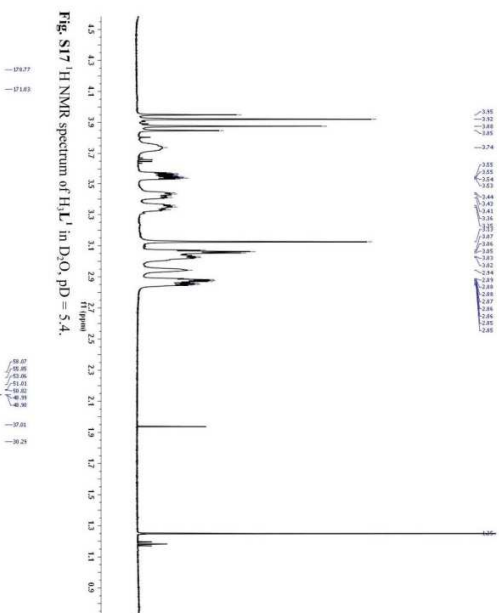


Fig. S17 ^1H NMR spectrum of H_2L^1 in D_2O , pH = 5.4.

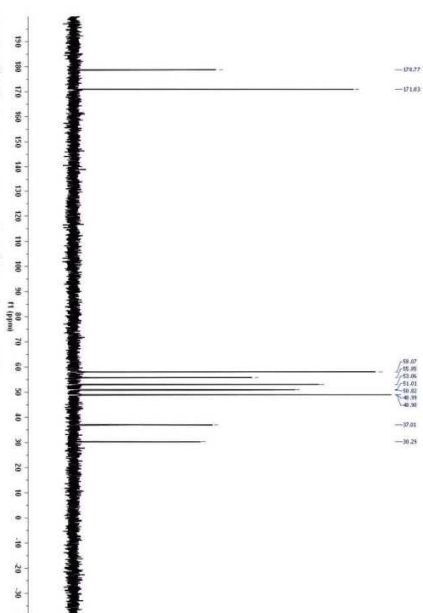
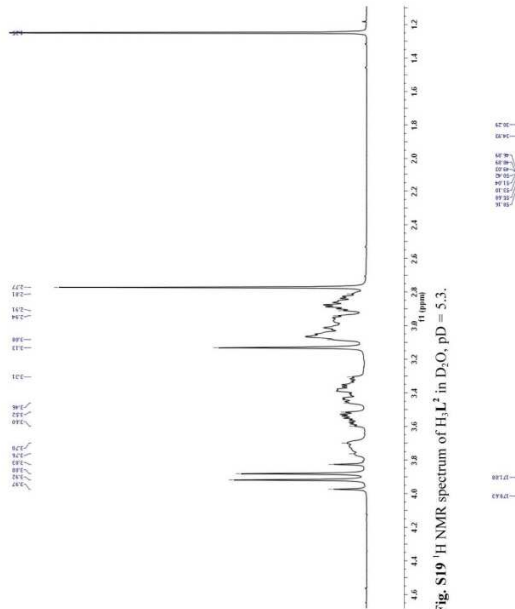
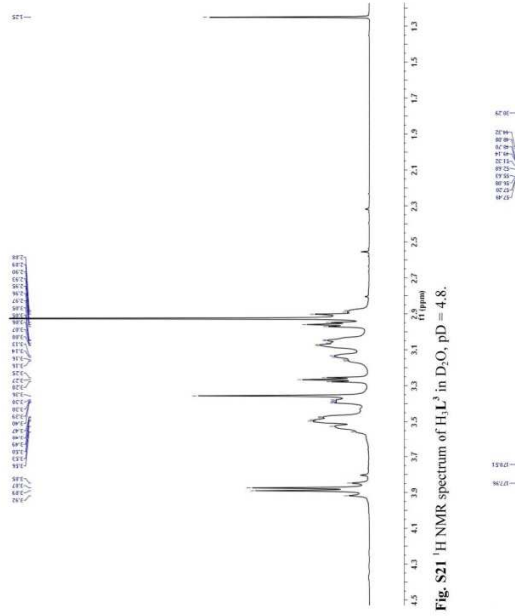


Fig. S18 $^{13}\text{C}\{^1\text{H}\}$ NMR spectrum of H_2L^1 in D_2O , pH = 5.4.



15



16

Fig. S20 ^{13}C (^1H) NMR spectrum of H_3L^2 in D_2O , pH = 4.8.

APPENDIX 2

T. Krchová, A. Gálisová, D. Jiráček, P. Hermann and J. Kotek: “Ln(III)-complexes of DOTA analogue with ethylenediamine pendant arm as pH-responsive PARACEST contrast agents”, *Dalton Trans.*, 2016, **45**, 3486–3496



Cite this: *Dalton Trans.*, 2016, **45**, 3486

Ln(III)-complexes of a DOTA analogue with an ethylenediamine pendant arm as pH-responsive PARACEST contrast agents†

T. Krchová,^a A. Gálisová,^b D. Jiráček,^{b,c} P. Hermann^a and J. Kotek^{*a}

A novel macrocyclic DO3A derivative containing a linear diamine pendant arm, H₃do3aNN, was prepared and its protonation and complexation properties were studied by means of potentiometry. It determined ligand consecutive protonation constants $\log K_{A_n} = 12.62, 10.28, 9.67, 8.30, 3.30$ and 1.58 and stability constants of selected lanthanide (Eu(III), Yb(III)) complexes $\log K_{EuL} = 23.16$ and $\log K_{YbL} = 22.76$. The complexes could be protonated on the pendant amino group(s) with $\log K(HLM) \approx 5.6$ and $\log K(H_2LM) \approx 4.8$. Solution structures of both complexes were studied by NMR spectroscopy. The study revealed that the complex species exist exclusively in the form of twisted-square-antiprismatic (TSA) isomers. The complexes show significant pH dependence of the Chemical Exchange Saturation Transfer (CEST) between their amino groups and the bulk water molecules in the pH range of 5–8. Thus, the pH dependence of the magnetization transfer ratio of CEST signals can be used for pH determination using magnetic resonance imaging techniques in a pH range relevant for *in vivo* conditions.

Received 11th November 2015.

Accepted 11th January 2016

DOI: 10.1039/c5dt04443j

www.rsc.org/dalton

Introduction

Magnetic resonance imaging (MRI), due to its non-invasive character and spatial resolution (down to a mm³ at clinical magnetic fields), is currently one of the most important diagnostic methods used in clinical medicine.¹ Relevant diagnostic information from MRI images can be obtained even with the natural contrast between various tissues. However, for further improvement of image contrast and resolution, exogenous contrast agents (CAs) based on complexes of highly paramagnetic metal ions or superparamagnetic nanocrystalline materials altering the relaxation times of bulk water are widely used.^{1,2} In addition to common MRI T₁- and T₂-contrast agents, which shorten the longitudinal (T₁) and transversal (T₂) relaxation

times,² a new class of CAs based on a Chemical Exchange Saturation Transfer (CEST) mechanism was introduced in the past decade.^{3,4}

The principle of the CEST effect is based on saturation of the proton signal of the contrast agent molecule by a selective radiofrequency pulse. This saturation is transferred to the surrounding water molecules *via* chemical exchange of the labile protons between the contrast agent and bulk water resulting in a decrease in the water signal intensity and, therefore, darkening of the corresponding area in the MR image. To reduce any nonspecific water proton irradiation and to increase the sensitivity of the CEST CAs, paramagnetic complexes (PARACEST agents) are used to shift the resonance frequency of the exchangeable protons far away from that of bulk water.^{4–6} These agents contain a paramagnetic metal ion chelated by a multidentate ligand. Most often, Ln(III) complexes of ligands derived from DOTA (thus ensuring high stability and kinetic inertness of the complexes) have been used.^{6,7} As alternatives, complexes of transition metal ions having suitable magnetic properties, such as Ni(II), Fe(II) or Co(II), with ligands based on cyclam, cyclen, 1,4,7-triazacyclononane or 1,4,10-trioxa-7,13-diazacyclopenta-decane, *etc.* have also been reported (Fig. 1).⁸

One of the major advantages of CEST agents is the possibility to modulate water signal intensity by a selective pre-saturation pulse and, therefore, image contrast produced by these CAs can be switched “on” or “off” at will by selecting the appropriate irradiation frequency. This fact makes it possible to detect several agents in the same sample.⁹ Another advan-

^aDepartment of Inorganic Chemistry, Faculty of Science, Universita Karlova (Charles University), Hlavova 2030, 128 43 Prague 2, Czech Republic.

E-mail: modrej@natur.cuni.cz; Fax: +420-221951253; Tel: +420-221951261

^bDepartment of Radiodiagnostic and Interventional Radiology, Magnetic Resonance Unit, Institute for Clinical and Experimental Medicine, Videňská 1958/9, Prague 4, 140 21, Czech Republic

^cInstitute of Biophysics and Informatics, 1st Faculty of Medicine, Universita Karlova (Charles University), Salmovská 1, 120 00 Prague 2, Czech Republic

† Electronic supplementary information (ESI) available: X-ray diffraction data, temperature- and pH-dependence of NMR spectra of studied compounds, additional Z-spectra and magnetization transfer ratio spectra of studied complexes, protonation and stability constants of studied ligand and its complexes, tentative structures of isomeric complex species with different protonation. CCDC 1430249. For ESI and crystallographic data in CIF or other electronic format see DOI: 10.1039/c5dt04443j

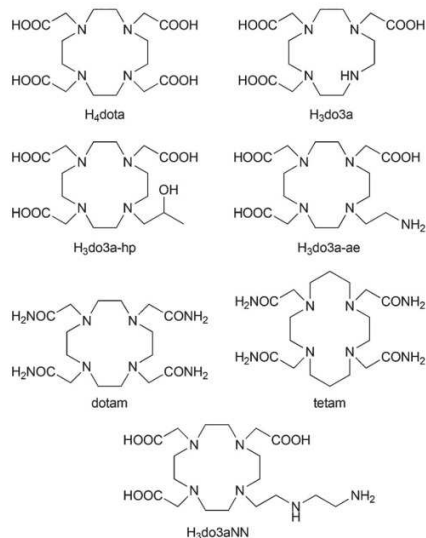


Fig. 1 Structural formulas of the ligands discussed in the text.

tage lies in the sensitivity of the proton exchange rate (k_{ex}) to a number of external factors and, thus, the CEST complexes are suitable for measuring various physiological parameters, such as temperature, pH, metabolite or metal ion concentration, etc.^{4c,5,6}

Recently, a lot of effort has been invested into developing MRI CAs capable of reporting on *in vivo* changes of pH in a tissue as they could serve as valuable biomarkers of disease progression or indicators for the choice of treatment.¹⁰ Several studies have demonstrated the unique ability of PARACEST CAs to act as pH sensors and nowadays ratiometric methods are being explored to make the assessments independent of the local concentration of the CAs.¹¹ For example, a Yb(III) analogue of the clinically approved MRI CA [Gd(do3a-hp)] (ProHance®, ligand shown in Fig. 1) shows two independent well-resolved PARACEST peaks at 71 and 99 ppm originating from the protons of the coordinated alcohol group of individual complex isomers.^{11a} The ratio of these two PARACEST signals is pH-dependent, which can be used to develop a concentration-independent method of pH measurement, and the Yb(III) complex has been already tested for measuring extracellular pH in murine melanoma.^{11b} Similarly, the PARACEST peaks of a Co(II) complex of tetam (Fig. 1) have distinct pH dependencies and the two most shifted signals (at 95 and 112 ppm) were shown to be suitable for pH mapping.^{8e}

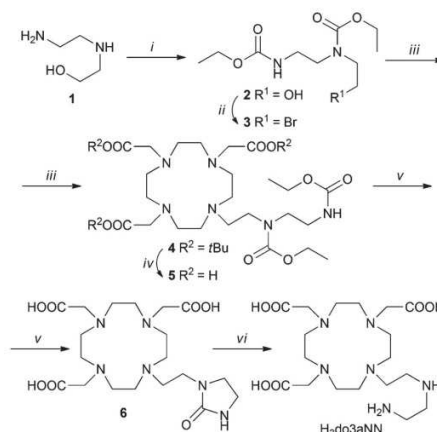
It was shown that Ln(III) complexes of cyclen derivatives with pendant arms containing an amido-amine pendant arm,^{11g,h} or a (semi)coordinating amino group¹² produced a pH-sensitive PARACEST effect in the pH region relevant for

living systems. Based on these findings, we decided to synthesize a new macrocyclic ligand H₃do3aNN (Fig. 1) containing a semi-labile coordinating pendant arm with two (primary and secondary) amino groups (as two potentially independent proton exchanging pools), and to investigate the PARACEST properties of its Ln(III) complexes.

Results and discussion

Synthesis

The synthesis of H₃do3aNN is shown in Scheme 1. The alkylation agent 3 was prepared by CBr₄/PPh₃ bromination of ethyl-carbamate-protected *N*-(2-aminoethyl)ethanolamine 2. The alkylation of *t*Bu₃do3a-HBr was performed using a slight excess of the alkylation agent as, under the reaction conditions, the alkylation agent undergoes elimination of HBr. The *t*Bu-ester groups were removed by reflux in a CF₃CO₂H : CHCl₃ 1 : 1 mixture and the ethyl-carbamate protection groups were removed by hydrolysis in 10% aq. NaOH. Surprisingly, in this reaction step, preferential formation of the urea-derivative 6 was observed, with only trace amounts of the required compound H₃do3aNN. However, the intermediate 6 can be isolated by crystallization in a zwitterionic form with 42% overall yield (based on *t*Bu₃do3a). The identity of the intermediate 6 was confirmed by a single-crystal X-ray diffraction study (see ESI and Fig. S1†). Hydrolysis of 6 with aq. HCl produced H₃do3aNN with a high yield. The best way to obtain the product in the solid form was trituration of the evaporated reaction mixture in dry THF or EtOH overnight. However, the resulting off-white solid is very hygroscopic and has to be



Scheme 1 Synthesis of H₃do3aNN. (i) CH₃CH₂OC(O)Cl, dioxane : H₂O (1 : 1), RT, 2 h; (ii) CBr₄, PPh₃, THF, RT, 1 h; (iii) *t*Bu₃do3a-HBr, K₂CO₃, MeCN, 60 °C, 24 h; (iv) CF₃CO₂H : CHCl₃ (1 : 1), reflux 18 h; (v) 10% aq. NaOH, 90 °C, 24 h; (vi) aq. HCl (1 : 1), 95 °C, 7 d.

stored in a desiccator over P₂O₅. All other attempts (different organic solvents used for trituration or crystallization) led to the isolation of the title ligand as oil. To prevent possible esterification by EtOH, the use of THF was preferred for trituration.

Thermodynamic behaviour of H₃do3aNN and its Ln(III) complexes

Potentiometric titrations of the ligand performed in the pH range of 1.6–12.2 revealed six consecutive protonation processes in this region (Tables 1 and S1†). Based on comparison with the literature data,^{12,13} the first protonation step ($\log K_p(\text{HL}) = 12.6$) can be attributed to the protonation of one of (or to sharing of a proton over several of) the macrocycle amino groups. The next three protonation steps proceed in part simultaneously due to the similarity of the constants ($\log K_p(\text{H}_2\text{L}) = 10.3$, $\log K_p(\text{H}_3\text{L}) = 9.7$ and $\log K_p(\text{H}_4\text{L}) = 8.3$) and occur on one other macrocycle amino group and two amino groups of the pendant *N*-(2-aminoethyl)-2-aminoethyl moiety (the value reported for analogous protonation of a 2-aminoethyl pendant moiety for H₃do3a-ae is $\log K_p = 8.9$).¹² Further protonations of H₃do3aNN proceed on the carboxylate groups and lie in the usual range.

Stability constants of [Ln(do3aNN)]³⁻ (23.16 and 22.76 for the Eu(III) and Yb(III) complexes, respectively, Tables 1 and S2†) were obtained by the out-of-cell titration technique. The values are slightly lower compared with those reported for H₄dota itself, but lie in the expected range, as can be seen from a comparison with the values reported for the related ligand H₃do3a-ae – although, in that case, stability constants were determined for other lanthanides: La(III), $\log K_{\text{LaL}} = 20.02$, and Gd(III), $\log K_{\text{GdL}} = 22.23$.¹² However, according to the distribution diagram of the Eu(III)–H₃do3aNN system shown in Fig. 2, the metal complexation is not quantitative until pH ≈ 6 due to a combination of low affinity of the amino groups for Ln(III) ions and high donor-site basicity.

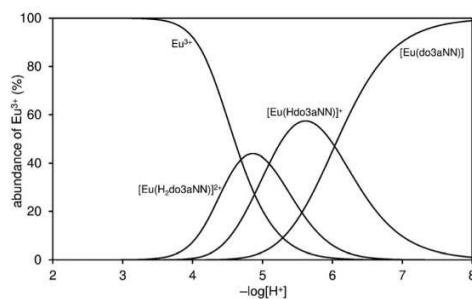


Fig. 2 Distribution diagram of metal-containing species in the Eu(III)–H₃do3aNN system ($c_M = c_L = 0.004$ M, 25 °C, $I = 0.1$ MMe₄Cl).

Equilibrated protonation steps of [Ln(do3aNN)] proceed with $\log K_p(\text{HLM}) = 6.03/6.22$ and those of the [Ln(Hdo3aNN)]⁺ species occur with $\log K_p(\text{H}_2\text{LM}) = 5.09/5.07$ for the Eu(III)/Yb(III) complexes, respectively (Tables 1 and S2†). They are close to the values of analogous protonation constants reported for [Ln(do3a-ae)] complexes ($\log K_p(\text{HLM}) = 6.06$ and 5.83 for La(III)/Gd(III) systems).¹² The observed values are slightly higher than the protonation constants found for the pre-formed complexes under “non-equilibrium” conditions: in such experiments, complexes were pre-formed at pH ≈ 7 and were titrated employing the standard (“fast”) acid–base titration method. The corresponding observed protonation constants were $\log K_p(\text{HLM}) = 5.57$ and 5.67, and $\log K_p(\text{H}_2\text{LM}) = 4.84$ and 4.85 for Eu(III)/Yb(III), respectively (Table S3†). From these slight differences between the protonation constants, one can conclude that, during out-of-cell titrations, protons in the [Ln(Hdo3aNN)]⁺ and [Ln(H₂do3aNN)]²⁺ species are probably located not only on the amine pendant arm but, at least

Table 1 Equilibrium constants ($\log K_p$ and $\log K_{\text{ML}}^0$)^a of H₃do3aNN (0.1 M NMe₄Cl, 25 °C) and its complexes, and the comparison with corresponding constants reported for related ligands

Equilibrium	H ₃ do3aNN	H ₃ do3a-ae ^b	H ₄ dota	H ₃ do3a-hp ^c	H ₃ do3a ^c
$\text{H}^+ + \text{L}^{n-} \leftrightarrow \text{HL}^{(n-1)-}$	12.62(2)	13.19	11.74 ^c	11.17	12.46
$\text{H}^+ + \text{L}^{(n-1)-} \leftrightarrow \text{H}_2\text{L}^{(n-2)-}$	10.28(2)	10.51	9.76 ^c	9.33	9.49
$\text{H}^+ + \text{L}^{(n-2)-} \leftrightarrow \text{H}_3\text{L}^{(n-3)-}$	9.67(2)	8.90	4.68 ^c	4.99	4.26
$\text{H}^+ + \text{L}^{(n-3)-} \leftrightarrow \text{H}_4\text{L}^{(n-4)-}$	8.30(3)	3.87	4.11 ^c	3.80	3.51
$\text{H}^+ + \text{L}^{(n-4)-} \leftrightarrow \text{H}_5\text{L}^{(n-5)-}$	3.30(3)	1.27	2.37 ^c	2.84	1.97
$\text{H}^+ + \text{L}^{(n-5)-} \leftrightarrow \text{H}_6\text{L}^{(n-6)-}$	1.58(3)	—	—	—	—
$\text{Eu}^{3+} + \text{L}^{n-} \leftrightarrow [\text{Eu}(\text{L})]^{(3-n)-}$	23.16(5)	—	24.2 ^d	—	—
$\text{H}^+ + [\text{Eu}(\text{L})]^{(3-n)-} \leftrightarrow [\text{Eu}(\text{HL})]^{(4-n)-}$	6.03(5)	—	—	—	—
$\text{H}^+ + [\text{Eu}(\text{HL})]^{(4-n)-} \leftrightarrow [\text{Eu}(\text{H}_2\text{L})]^{(5-n)-}$	5.09(7)	—	—	—	—
$\text{Yb}^{3+} + \text{L}^{n-} \leftrightarrow [\text{Yb}(\text{L})]^{(3-n)-}$	22.76(4)	—	24.0 ^d	—	—
$\text{H}^+ + [\text{Yb}(\text{L})]^{(3-n)-} \leftrightarrow [\text{Yb}(\text{HL})]^{(4-n)-}$	6.22(4)	—	—	—	—
$\text{H}^+ + [\text{Yb}(\text{HL})]^{(4-n)-} \leftrightarrow [\text{Yb}(\text{H}_2\text{L})]^{(5-n)-}$	5.07(4)	—	—	—	—
$\text{Gd}^{3+} + \text{L}^{n-} \leftrightarrow [\text{Gd}(\text{L})]^{(3-n)-}$	—	22.23	24.67 ^c	24.5	22.02

^a $K_p = [\text{H}_n\text{L}]/([\text{H}][\text{H}_{n-1}\text{L}])$ or $[\text{H}_n\text{LM}]/([\text{H}][\text{H}_{n-1}\text{LM}])$; $K_{\text{ML}} = [\text{ML}]/([\text{L}][\text{M}])$. ^b Ref. 12. ^c Ref. 13. ^d Ref. 14.

partly, also on the macrocycle amino groups. The suggested structures of individual species with tentative protonation sites are shown in Schemes S1 and S2.†

Unfortunately, the $[\text{Ln}(\text{do3aNN})]$ complexes are not fully kinetically inert, and slowly dissociate at $\text{pH} < 6$. This was confirmed by a xylenol orange test: after the addition of a solution of the pre-formed complex (at $\text{pH} = 7.5$) to a buffered solution of xylenol orange at $\text{pH} = 5.5$, the colour gradually changed on standing from orange to orange-violet as a result of free metal appearance in the solution. A quantitative measurement revealed the dissociation of about 9–10% of the complex after standing for one week at room temperature (compare Fig. S16 and S17†). From a thermodynamic point of view, the extent of complex dissociation should be less than 20% at $\text{pH} = 5$ (see the distribution diagram shown in Fig. 2). It was confirmed by independent experiments that neither the free metal aqua ion nor the free ligand interferes with the ^1H NMR or CEST measurements. Therefore, conclusions drawn from PARACEST experiments (see below) are fully valid even at $\text{pH} 5\text{--}6$.

Solution structure of the $[\text{Ln}(\text{H}_n\text{do3aNN})]^\ddagger$ complexes

It is well-known that in $\text{Ln}(\text{III})$ complexes of DOTA-like ligands the central $\text{Ln}(\text{III})$ is coordinated between two planes – one formed by the macrocycle amino groups (N_4 -plane), and the other by the oxygen atoms of the carboxylate pendant moieties (O_4 -plane), and these species exhibit two types of isomerisms in solution.¹⁵ The first type is connected with the conformation of the macrocycle ethylene bridges, *i.e.* with the sign of the torsion angle around the C–C bond (δ/λ), and the second one is related to the direction of rotation of the pendant arms (Δ/Λ). A combination of these isomerisms leads to the formation of two diastereomeric pairs of enantiomers (*i.e.* four isomers): $\Delta\lambda\lambda\lambda/\Lambda\delta\delta\delta$ (SA, square-antiprismatic) and $\Delta\delta\delta\delta/\Lambda\lambda\lambda\lambda$ (TSA, twisted-square-antiprismatic).² The isomer ratio in solution can be determined from the ^1H NMR spectra using the “axial” protons of the macrocyclic chelate ring, which are the ones closest to the $\text{Ln}(\text{III})$ ion and to the principal magnetic axis, and usually can be easily found in the ^1H NMR spectra.¹⁶ Therefore, the solution structures of the $[\text{Eu}(\text{do3aNN})]$ and $[\text{Yb}(\text{do3aNN})]$ complexes were investigated by variable-temperature ^1H NMR spectroscopy (Fig. S2 and S3†). The pD of the samples in D_2O was adjusted to the alkaline region to ensure full deprotonation and coordination of the pendant amino group. In both complexes, only one set of signals was detected pointing to the presence of only one diastereomer. The signals of “axial” protons appear in the range typical for the TSA isomers ($\text{Eu}(\text{III})$: 9–13 ppm, $\text{Yb}(\text{III})$: 45–62 ppm; with respect to the signal of bulk water referenced to 0 ppm). No ^1H NMR signals of “axial” CH_2 protons attributable to an SA isomer were observed (such signals typically lie in the chemical shift regions of 25–40 ppm and 100–150 ppm for $\text{Eu}(\text{III})$ and $\text{Yb}(\text{III})$ complexes, respectively).^{16,17} Thus, based on the ^1H NMR data,

† Such a formula is used when more species differing in protonation are present in a solution. For the range of n refer to the distribution diagram shown in Fig. 2.

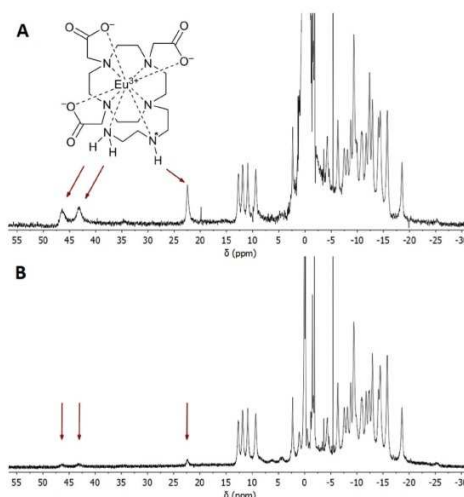


Fig. 3 (A) ^1H NMR spectrum of the $[\text{Eu}(\text{H}_n\text{do3aNN})]$ complex (0.09 M solution in H_2O , $B_0 = 7.05$ T, 25 °C, $\text{pH} = 6.75$). (B) The same sample, the signal of water was saturated. Arrows show the positions of exchangeable (N–H) protons. The chemical shift of H_2O in the sample solution was referenced to 0 ppm.

exclusive formation of the TSA isomer is expected. With increasing temperature, the ^1H NMR signals become broader, pointing to the occurrence of a conformational change of the complex molecules (Fig. S2 and S3†).

To identify the signals of exchangeable (N–H) protons in the ^1H NMR spectra, samples of the $[\text{Eu}(\text{H}_n\text{do3aNN})]$ and $[\text{Yb}(\text{H}_n\text{do3aNN})]$ complexes were investigated in H_2O at 25 and 5 °C (Fig. 3, 4, S4 and S5†). In the ^1H NMR spectra of the $[\text{Eu}(\text{H}_n\text{do3aNN})]$ complex recorded in H_2O at $\text{pH} = 6.75$ (Fig. 3A), three main signals of exchangeable protons (one narrow signal at 22.2 and two broad signals at 43.3 and 46.5 ppm; with respect to the bulk water signal) can be observed, which disappear upon bulk water presaturation (Fig. 3B). Of these, only the signals at 43.3 and 46.5 ppm are influenced by water presaturation at $\text{pH} = 11.7$, whilst the signal at 22.2 ppm remains unaffected (Fig. 4A and B). When recording ^1H NMR spectra in a D_2O solution ($\text{pD} = 10.7$), none of the three signals are observable (Fig. 4C and S2†). Based on this behaviour, the narrow signal at 22.2 ppm is attributed to the coordinated secondary amino group. The assignment is supported by the similarity of the chemical shift of this signal to that of one of the $-\text{NH}_2$ protons of the $[\text{Eu}(\text{do3a-ae})]$ complex (19.5 ppm).¹² The two broad signals are attributed to the coordinated primary amino group and this assignment is supported by their coalescence at higher temperatures (Fig. S6†).

The primary amino group is expected to be coordinated in a position capping the O_3N -plane formed by the pendant

Paper

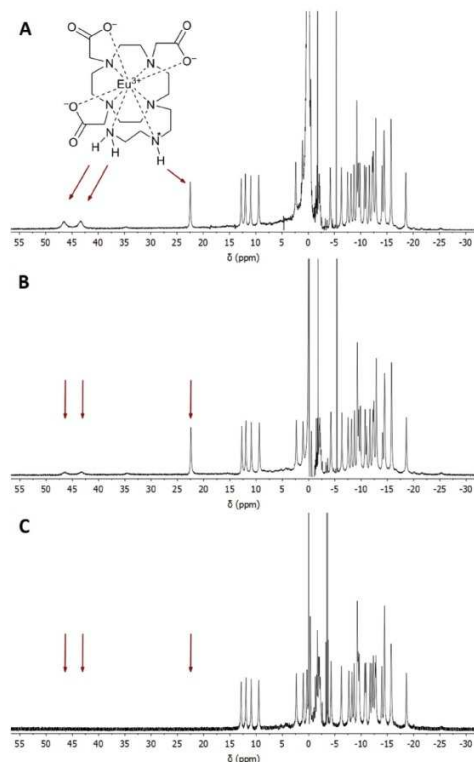


Fig. 4 (A) ^1H NMR spectrum of the $[\text{Eu}(\text{do3aNN})]$ complex in H_2O (0.09 M, $B_0 = 7.05$ T, 25 $^\circ\text{C}$, pH = 11.70). (B) The same sample, the signal of water was saturated. (C) ^1H NMR spectrum of the $[\text{Eu}(\text{do3aNN})]$ complex in D_2O (0.04 M, $B_0 = 7.05$ T, 25 $^\circ\text{C}$, pD = 10.73). Arrows show the positions of exchangeable (N–H) protons. The chemical shifts of $\text{H}_2\text{O}/\text{HDO}$ in the sample solutions were referenced to 0 ppm.

donor atoms and, thus, close to the magnetic axis of the complex. Therefore, the corresponding protons are markedly influenced by the paramagnetic ion and their chemical shifts lie in the range typical for a coordinated water molecule.^{5,18} However, the presence of these signals in ^1H NMR spectra also in an alkaline solution (and the presence of a corresponding CEST effect in Z-spectra at alkaline pH, see below) clearly excludes the possibility that these signals belong to a coordinated water molecule, the signal of which disappears in the alkaline region.¹⁹ In slightly acidic solutions where protonation of the uncoordinated primary amino group (and thus, its decoordination) is expected, even a proton of the secondary amino group is exchanged with bulk water on an NMR time scale. In contrast, in an alkaline solution, only the exchange of the terminal primary amino group protons is observable.

View Article Online

Dalton Transactions

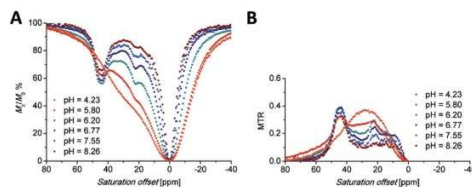


Fig. 5 (A) Z-Spectra of an 83 mM aqueous solution of the $[\text{Eu}(\text{H},\text{do3aNN})]$ complex ($B_0 = 7.05$ T, $B_1 = 21.7$ μT (920 Hz), RF pre-saturation pulse applied for 2 s, 25 $^\circ\text{C}$). (B) Corresponding MTR spectra.

Besides the three signals of exchangeable protons of the $[\text{Eu}(\text{do3aNN})]$ complex discussed above, a small signal at ≈ 35 ppm was found in the ^1H NMR spectra (Fig. 3 and 4), better seen at a lower temperature (37.5 ppm, Fig. S5A \dagger).

At this chemical shift, a minor exchangeable pool of protons was found also in the CEST experiments (see discussion of Z-spectra below), accompanied by two other peaks in Z-spectra lying at 10 and 15 ppm, which are visible especially at low saturation power (Fig. 5 and S7A \dagger). Due to the absence of any ^1H NMR signals of “axial” CH_2 protons attributable to the SA isomer, the presence of this isomer in the solution can be excluded. Therefore, these minor exchangeable proton pools were attributed to another TSA isomer that originates from the chirality of the nitrogen atom of the secondary amino group caused by coordination of this group. Judging by the similarity of the chemical shift of the exchangeable proton pool at 35 ppm to one of the signals attributed to the coordinated amino group in $[\text{Eu}(\text{do3a-ae})]$ (34 ppm),¹² one can suggest that this signal belongs to the secondary amino group of the TSA isomer with reverse orientation of H vs. the $\text{CH}_2\text{CH}_2\text{NH}_2$ substituents (*i.e.* with opposite chirality of the coordinated secondary amine). The results of simple molecular modelling shown in Fig. S9 \dagger suggest that apical coordination of the primary amino group is possible only in the $\Delta\delta\delta\delta\text{-S}/\Lambda\lambda\lambda\lambda\text{-R}$ enantiomeric pair, and thus, this isomer is suggested to be the major one, leaving the $\Delta\delta\delta\delta\text{-R}/\Lambda\lambda\lambda\lambda\text{-S}$ species as the minor isomer. In the case of this low-abundance isomer, the position of the primary amino group is not suitable for coordination close to the magnetic axis and, therefore, the signals of the primary amino group in Z-spectra are significantly closer (at 10 and 15 ppm, Fig. S7 \dagger) to the free water signal. As both protons of the primary amino group have individual signals, their resolution triggered by coordination or by fixing in an intramolecular hydrogen bond system is expected.

A similar behaviour was observed also for the $[\text{Yb}(\text{do3aNN})]$ complex. In an alkaline solution, there are two signals disappearing in D_2O , see Fig. S4 \dagger – a narrow signal of the proton of the secondary amino group at 35 ppm (this assignment is supported by the similarity of the chemical shift of the analogous ^1H NMR signal of $[\text{Yb}(\text{do3a-ae})]$, 42 ppm)¹² and a very broad signal of NH_2 protons at 82–104 ppm (the signals cannot be distinguished at 25 $^\circ\text{C}$, but split at 5 $^\circ\text{C}$, Fig. S5B \dagger). As in the previous case, only the signal attributable to the primary

amino group is affected by water presaturation in an alkaline solution, Fig. S4B†. Minor signals of another TSA isomer are also observable in ^1H NMR spectra, and minor exchangeable pools of protons were found in CEST experiments at low saturation power (three other peaks in Z-spectra at 17, 26 and 57 ppm, Fig. S7B†).

CEST experiments

Saturation transfer experiments in solutions ranging from slightly acidic to slightly alkaline (pH 5.7–8.3) revealed two signals in the ^1H Z-spectra of each complex. These signals are centred at +22.2 and +44.4 ppm for the Eu(III) complex (Fig. 5A) and +35 and +95 ppm for the Yb(III) complex (Fig. 6A).

The broad signals at the higher chemical shifts (44.4 and 95 ppm for the Eu(III) and Yb(III) complex, respectively) correspond to the averaged signals of the primary amino group. This broad signal splits into two distinct signals of magnetically non-equivalent protons at a lower intensity of presaturation pulses and at low temperatures (Fig. S7A†), similar to the behaviour of this group found in ^1H NMR spectra (Fig. 3, 4, S5 and S6†). The Z-spectra signals with lower chemical shifts (22.2 and 35 ppm for the Eu(III) and Yb(III) complex, respectively) were attributed to the signal of the proton of the secondary amino group. Thus, the Z-spectra of both complexes clearly confirm the presence of proton-exchanging pools that belong to the protons of the primary and secondary amino groups as they were identified in the ^1H NMR spectra (see above).

Besides the signals attributable to the major isomer, a set of minor signals (at 10, 15 and 35 ppm, distinguishable especially when low saturation power was applied) appears in the Z-spectra of the $[\text{Eu}(\text{H}_r\text{do3aNN})]$ complex (Fig. S7A†). At slightly acidic to neutral pH, all three Z-signals are apparent. In contrast, in the alkaline region only the signals at 10 and 15 ppm remain in the Z-spectra, implying their assignment to the primary amino group, with the last one (at 35 ppm) belonging to the secondary amino group. These signals belong to the less abundant isomer with opposite chirality of the coordinated secondary amino group (see discussion of ^1H NMR spectra above). A similar set of minor signals (at 17, 26 and 57 ppm) appears also in the Z-spectra of the $[\text{Yb}(\text{H}_r\text{do3aNN})]$ complex (Fig. S7B†).

The shape of the Z-spectra of the $[\text{Ln}(\text{H}_r\text{do3aNN})]$ complexes (Ln = Eu, Yb) has significant pH dependence in slightly

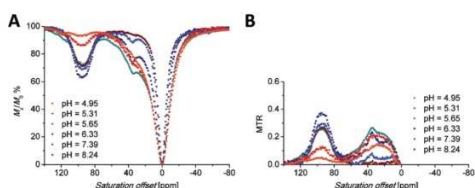
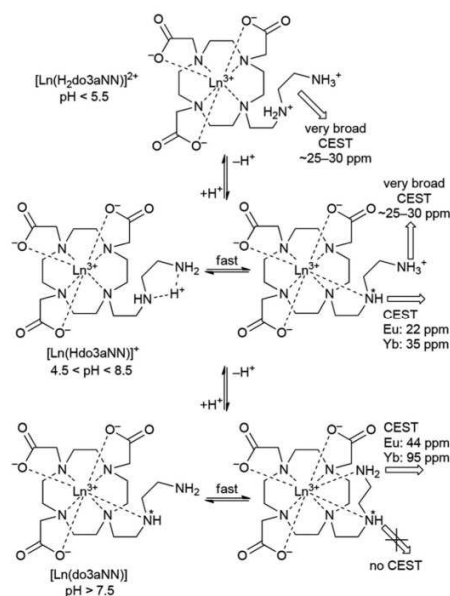


Fig. 6 (A) Z-Spectra of an 87 mM aqueous solution of the $[\text{Yb}(\text{H}_r\text{do3aNN})]$ complex ($B_0 = 7.05$ T, $B_1 = 21.7$ μT (920 Hz), RF presaturation pulse applied for 2 s, 25 $^\circ\text{C}$). (B) Corresponding MTR spectra.

acidic to neutral regions (Fig. 5A and 6A). To see the differences in Z-spectra more clearly, the magnetization transfer ratio (MTR) spectra were constructed (Fig. 5B and 6B). At pH < 5.5, the CEST effect of the coordinated primary amino group gradually disappears as a consequence of protonation and decoordination of the group. Simultaneously, a new, very broad CEST signal appears centred at ≈ 25 –30 ppm for both complexes. Although partial dissociation of the complexes occurs in this pH region (see above for discussion of thermodynamic properties), the free metal aqua ions as well as the free ligand are CEST-silent (as proved by an independent experiment) and, therefore, these new signals can be attributed to the chemical exchange of the protonated primary amino group of the complex. Such a group – whilst uncoordinated – is still paramagnetically shifted, but not as much as when the group is coordinated. On the other hand, an effective CEST of the secondary amino group was detected for the Eu(III) and Yb(III) complexes in the pH region of ≈ 5.5 –8.5. At higher pH values, the chemical exchange of the NH proton becomes too slow to transfer saturation to bulk water and, thus, the CEST effect of the secondary amino group is not observable (Fig. 5A, 6A and S8†). It is consistent with the ^1H NMR spectra of the studied complexes (Fig. 4 and S4†), where the signals of secondary amino groups are observable even in alkaline solutions



Scheme 2 A suggested mechanism of origin of pH-dependent CEST effects on $[\text{Ln}(\text{H}_r\text{do3aNN})]$ complexes. In hepta/octa-coordinated species, binding of a water molecule(s) to the central ion giving the coordination number to 8–9 is expected, but it is not shown for the sake of clarity.

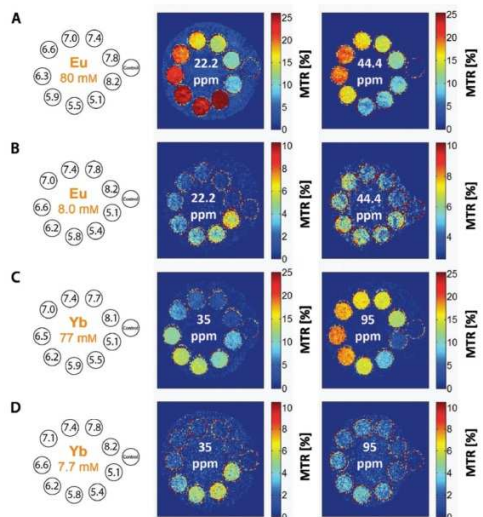


Fig. 7 MRI-CEST images of phantoms consisting of one vial containing an aq. solution of MES and HEPES (1:1, 50 mM) as a standard and nine vials containing solutions of (A, B) the $[\text{Eu}(\text{H}_7\text{do3aNN})]$ or (C, D) $[\text{Yb}(\text{H}_7\text{do3aNN})]$ complexes in the same buffer with different pH values and concentrations. Experimental conditions: RARE pulse sequence, $B_0 = 4.7$ T, RF presaturation pulse applied for 2 s, $T = 298$ K, $\text{TR} = 5$ s, $\text{TE} = 8.9$ ms, (B) $B_1 = 35$ μT (1490 Hz), (A, C, D) $B_1 = 25$ μT (1060 Hz).

($\text{pH} > 11$) (*i.e.* their chemical exchange with bulk water is slow) and remain unaffected after water presaturation. A graphical representation of the suggested processes giving rise to the peaks in Z -spectra is shown in Scheme 2.

It is evident that the two pools of exchanging amine protons show different dependences of their CEST effects in the pH range relevant to the physiological conditions. The applicability of the $[\text{Eu}(\text{H}_7\text{do3aNN})]$ and $[\text{Yb}(\text{H}_7\text{do3aNN})]$ complexes as pH-sensitive MRI probes was tested for solutions with different pH values (HEPES/MES buffers) and concentrations of the complex (Fig. 7).

To define the pH-dependent but concentration-independent function, the ratio of MTR intensities was calculated. However, this ratio can be defined reasonably only for the Yb(III) complex (35/95 ppm), as in the case of the Eu(III) complex there is a significant overlap of the low-shift signal of the coordinated secondary amino group (22.2 ppm) with the new signal appearing in the acidic region (attributable to the protonated and uncoordinated primary amine, Fig. 5B).

To prove the suggested concept of ratiometric pH determination, samples of $[\text{Yb}(\text{H}_7\text{do3aNN})]$ with different complex concentrations and different pH values were measured by both NMR and MRI techniques. The concentration range used covers about one order of magnitude (7.7–8.7 mM). All calibration curves were very similar (see Fig. 8 and S10[†]), although

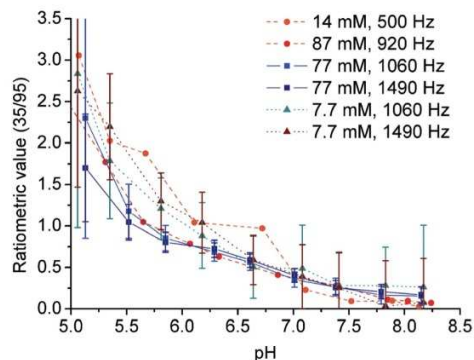


Fig. 8 Ratiometric plots of the 7.7–8.7 mM $[\text{Yb}(\text{H}_7\text{do3aNN})]$ complex, 25 °C; RF presaturation pulse applied for 2 s. Circles: aq. solution, $B_0 = 7.05$ T (NMR), $B_1 = 500$ Hz (11.8 μT) or 920 Hz (21.7 μT). Squares and triangles: 50 mM HEPES–MES, $B_0 = 4.7$ T (MRI), $B_1 = 1060$ Hz (25 μT) or 1490 Hz (35 μT). The ratiometric value (35/95) is the ratio of MTR intensity at 35 ppm to MTR intensity at 95 ppm.

standard deviations of the data points from MRI experiments acquired for the low concentration were relatively high due to a high background noise and, thus, a low signal-to-noise ratio was obtained under these conditions. The final curves are compiled in Fig. 8. Although the method has high ESDs with respect to the determination of an exact pH value, the shape of calibration curves enables distinguishing between samples with $\text{pH} > 7$ and those with $\text{pH} < 6$. Such a finding is relevant for the design of contrast agents useful *e.g.* for distinguishing between normal and hypoxic tissues.

Experimental

Materials and methods

All reagents and solvents were commercially available, had synthetic purity and were used as received. Water used for potentiometric titrations was deionized by using a Milli-Q (Millipore).

1,4,7-Tris(*tert*-butylcarboxymethyl)-1,4,7,10-tetraazacyclododecane hydrobromide ($t\text{Bu}_3\text{do3a-HBr}$) was prepared according to the published procedure.²⁰ THF was dried by the standard method²¹ and stored over molecular sieves under an argon atmosphere. Anhydrous MeCN and EtOH were from commercial sources.

NMR characterization data (1D: ^1H , $^{13}\text{C}\{^1\text{H}\}$; 2D: HSQC, HMBC, ^1H – ^1H COSY) were recorded on a VNMR5300 or Bruker Avance III 600, using 5-mm sample tubes. Chemical shifts are reported as δ values and are given in ppm. Coupling constants J are reported in Hz. Unless stated otherwise, NMR experiments were performed at 25 °C. For samples dissolved in D_2O , the pD value was calculated by correcting the pH-electrode reading by +0.4, *i.e.* pD = pH reading + 0.4. For the ^1H and ^{13}C

NMR measurements of diamagnetic compounds in D_2O , *t*BuOH was used as an internal standard ($\delta_H = 1.25$, $\delta_C = 30.29$). For the measurements in $CDCl_3$, TMS was used as an internal standard ($\delta_H = 0.00$, $\delta_C = 0.00$). In the case of paramagnetic complexes, chemical shifts were referenced to the water signal of the sample ($\delta_H = 0.00$) to keep the chemical shift values in 1H NMR spectra consistent with the scale of Z-spectra. The abbreviations s (singlet), t (triplet), q (quartet), m (multiplet) and br (broad) are used in order to express the signal multiplicities. Lanthanide(III) concentrations in solutions were determined by measurement of the bulk magnetic susceptibility (BMS) shifts.²² The ESI-MS spectra were recorded on a Bruker ESQUIRE 3000 spectrometer equipped with an electrospray ion source and ion-trap detection. Measurements were carried out in both the positive and negative modes. UV-Vis solution spectra were recorded using a SPECORD® 50 PLUS (ANALYTIC JENA AG) spectrophotometer at 25 °C in the range of 300–1000 nm with data intervals of 0.2 nm and integration time of 0.04 s. Elemental analysis was performed at the Institute of Macromolecular Chemistry of the Czech Academy of Sciences (Prague, Czech Republic).

Synthesis

Synthesis of 2. Ethyl chloroformate (8.02 g, 73.9 mmol, 2.2 eq.) was added dropwise to a well-stirred solution of **1** (3.5 g, 33.6 mmol) in a mixture of dioxane (30 ml) and H_2O (30 ml), and the reaction mixture was stirred for 2 h at room temperature. In the next step, conc. aq. NH_3 (≈ 10 ml) was added and the reaction mixture was stirred for 15 min. The mixture was concentrated *in vacuo*, poured into H_2O (50 ml) and extracted with CH_2Cl_2 (3×30 ml). The organic layer was dried over anhydrous Na_2SO_4 and concentrated *in vacuo* to yield 4.50 g (54%) of **2** as a colourless oil.

1H NMR (600 MHz, $CDCl_3$): δ 1.15–1.19 (6H, m, CH_2CH_3); 3.28 (2H, br, $NHCH_2$); 3.36 (4H, br, CH_2NCH_2); 3.63–3.69 (2H, br, CH_2OH); 4.02–4.08 (4H, m, OCH_2).

$^{13}C\{^1H\}$ NMR (150.9 MHz, $CDCl_3$): δ 14.61, 14.65 (2C, CH_2CH_3); 40.03, 40.18 (1C, $NHCH_2$); 48.45, 48.74 (1C, CH_2); 51.11, 51.51 (1C, CH_2); 60.91 (1C, OCH_2); 61.15, 61.40 (1C, CH_2OH); 61.66 (1C, OCH_2); 157.30 (2C, CO). All four backbone carbon atoms show two ^{13}C NMR signals due to rigid conformations of the molecule locked by different orientations of the amide groups.

MS-ESI: (+) 270.8 ($[M + Na]^+$, calcd 271.1).

Synthesis of 3. CBR_4 (4.11 g, 12.4 mmol, 1.5 eq.) and PPh_3 (3.25 g, 12.4 mmol, 1.5 eq.) were added to a well-stirred solution of **2** (2.05 g, 8.25 mmol) in dry THF (70 ml) in a flask equipped with a drying tube. The reaction mixture was stirred for 1 h at room temperature, filtered and then evaporated in a rotary evaporator. The oily residue was dissolved in a small amount of CH_2Cl_2 and purified by chromatography (silica, 25×3.5 cm). Impurities were removed by elution with CH_2Cl_2 , and the pure product was eluted using acetone : CH_2Cl_2 (1 : 9). Fractions containing the pure product **3** (as checked by NMR) were combined and evaporated to give compound **3** (2.24 g, 87%) as a colourless oil.

1H NMR (600 MHz, $CDCl_3$): δ 1.16–1.18 (3H, br, CH_2CH_3); δ 1.22 (3H, t, $^3J_{HH} = 7.2$, CH_2CH_3); 3.28 (2H, br, CH_2); 3.39–3.45 (4H, br, CH_2); 3.58 (2H, br, CH_2Br); 4.04–4.08 (2H, m, CH_2CH_3); 4.10 (2H, q, $^3J_{HH} = 7.2$, CH_2CH_3).

$^{13}C\{^1H\}$ NMR (150.9 MHz, $CDCl_3$): δ 14.78, 14.84 (2C, CH_2CH_3); 29.28, 29.53 (1C, CH_2Br); 40.04 (1C, $NHCH_2$); 48.11 (1C, CH_2); 49.74, 50.41 (1C, CH_2); 61.05, 62.02 (2C, OCH_2); 156.41, 157.09 (2C, CO). Two of the backbone carbon atoms show two ^{13}C NMR signals due to rigid conformations of the molecule locked by different orientations of the amide groups.

Synthesis of 4. A solution of the alkylating reagent **3** (1.79 g, 5.75 mmol, 1.35 eq.) in dry MeCN (10 ml) was added dropwise to a well-stirred suspension of K_2CO_3 (2.94 g, 21.3 mmol, 5 eq.) and *t*Bu₃do3a-HBr (2.54 g, 4.26 mmol) in dry MeCN (40 ml) at room temperature. The reaction mixture was stirred at 60 °C for 24 h, filtered, and the filtrate was evaporated in a rotary evaporator. The oily residue was dissolved in $CHCl_3$ (25 ml) and extracted with distilled water (4×10 ml). The organic layer was dried over anhydrous Na_2SO_4 and concentrated *in vacuo* to yield a yellow oil (3.76 g) containing a crude compound **4** contaminated with an excess of the alkylating reagent **3**. The excess alkylating reagent was not removed, and the crude product **4** was used in the next step without purification.

MS-ESI: (+) 745.3 ($[M + H]^+$, calcd 745.5); 767.2 ($[M + Na]^+$, calcd 767.5).

Synthesis of 5. A portion (3.70 g) of the crude compound **4** obtained above was dissolved in a mixture of CF_3CO_2H and $CHCl_3$ (1 : 1, 30 ml). The resulting solution was refluxed for 18 h and evaporated in a rotary evaporator. The oily residue was dissolved in a small amount of distilled water and evaporated (this procedure was then repeated three more times) to produce a yellow oil (3.10 g) containing compound **5**, which was used in the next step without purification.

MS-ESI: (+) 577.0 ($[M + H]^+$, calcd 577.3). (–) 574.9 ($[M - H]^-$; calcd 575.3).

Synthesis of 6. The crude product **5** (3.00 g) was dissolved in 10% aq. NaOH (50 ml) and stirred for 24 h at 90 °C. Then, the solution was loaded onto a strong anion exchange column (Dowex 1, OH^- -form, 1.5×20 cm). Impurities were removed by elution with water and the product **6** was eluted with 5% aq. AcOH. Fractions containing the product (as checked by 1H NMR) were combined, filtered and evaporated to give compound **6** (2.21 g) as a brownish oil. The crude product was dissolved in a water : MeOH mixture (1 : 5, v : v, ≈ 5 ml) and overlaid with EtOH (≈ 5 ml) and the mixture was left to stand for 2 d. After this period, the solid product was filtered off and dried under vacuum to yield **6**·2.5 H_2O (900 mg, 42% based on *t*Bu₃do3a) as a white powder.

1H NMR (600 MHz, D_2O , pD = 5.88): δ 3.05 (2H, br, CH_2CH_2NCO); 3.16 (4H, br, $(CH_2)_2NCH_2CH_2NCO$); 3.20–3.29 (4H, m, $(CH_2)_2NCH_2CO$); 3.33–3.44 (12H, br, CH_2CH_2NCO , CH_2CH_2NH , $(CH_2)_2NCH_2CO$); 3.52 (2H, br s, CH_2CO); 3.57 (2H, t, $^3J_{HH} = 8.1$, CH_2NH); 3.70 (4H, br s, CH_2CO).

$^{13}C\{^1H\}$ NMR (150.9 MHz, D_2O , pD = 5.88): δ 38.69 (1C, NCH_2CH_2NH); 39.45 (1C, CH_2CH_2NCO); 46.05 (1C, CH_2NH);

49.05 (2C, (CH₂)₂NCH₂CH₂NCO); 49.95 (2C, (CH₂)₂NCH₂CO); 50.17 (1C, CH₂CH₂NCO); 51.14 (2C, (CH₂)₂NCH₂CO); 51.79 (2C, (CH₂)₂NCH₂CO); 56.21 (1C, CH₂CO); 57.43 (2C, CH₂CO); 165.09 (1C, NCONH); 173.25 (2C, CH₂CO); 175.78 (1C, CH₂CO).

MS-ESI: (+) 480.9 ([M + Na]⁺, calcd 481.2). (–) 456.8 ([M – H][–], calcd 457.3).

Elemental analysis: found (calcd for 6·2.5H₂O, C₁₉H₃₉N₆O_{9.5}, M_r = 503.6) C: 45.30 (45.32), H: 7.85 (7.81), N: 16.12 (16.69).

Synthesis of H₃do3aNN. Compound 6·2.5H₂O (415 mg, 0.824 mmol) was dissolved in aq. HCl (10 ml, 1 : 1) and the resulting solution was stirred for 7 d at 95 °C and evaporated in a rotary evaporator. The oily residue was dissolved in a small amount of distilled water and evaporated to dryness, leaving a glassy solid, which was triturated in dry THF overnight. Next, the product was collected by filtration, and stored in a desiccator (P₂O₅) to give H₃do3aNN in the form of a hydrochloride hydrate (500 mg, 95%) as a white powder.

Mother liquors after crystallization of the intermediate 6 can be also used for the preparation of the title ligand. After acid hydrolysis of impure 6, the crude H₃do3aNN was converted to its ammonium salt by chromatography on a strong cation exchanger (Dowex 50, 50–100 mesh, H⁺-form). Acids were eluted with water and the crude product was collected by 5% aq. ammonia. After evaporation of volatiles, the oily residue was dissolved in water and poured onto a column of a weak cation exchanger (Amberlite CG50, 200–400 mesh, H⁺-form). Impurities were eluted with water and the H₃do3aNN compound was collected by 3% aq. HCl. Fractions containing the product were combined and evaporated to dryness leaving a glassy solid, which was triturated as described above.

¹H NMR (600 MHz, D₂O, pD = 6.07, 55 °C, Fig. S11†): δ 2.85–2.87 (4H, m, macrocyclic CH₂); 3.01–3.09 (6H, br m, NCH₂CH₂NH, macrocyclic CH₂); 3.11 (2H, s, CH₂CO₂); 3.19 (2H, t, ³J_{FH} = 5.1, NCH₂CH₂NH); 3.30–3.36 (2H, br m, macrocyclic CH₂); 3.42–3.45 (2H, br m, macrocyclic CH₂); 3.47–3.49 (2H, br t, NHCH₂CH₂NH₂); 3.54–3.56 (2H, br t, NHCH₂CH₂NH₂); 3.57–3.61 (2H, m, macrocyclic CH₂); 3.74–3.80 (2H, br, macrocyclic CH₂); 3.92 (2H, AB-multiplet, CH₂CO₂).

¹³C{¹H} NMR (150.9 MHz, D₂O, pD = 6.07, 55 °C, Fig. S12†): δ 37.07 (1C, NHCH₂CH₂NH₂); 46.04 (1C, NCH₂CH₂NH); 46.99 (1C, NHCH₂CH₂NH₂); 48.84 (4C, macrocyclic CH₂); 50.45 (1C, NCH₂CH₂NH); 51.23 (2C, macrocyclic CH₂); 53.30 (2C, macrocyclic CH₂); 55.55 (1C, CH₂CO₂); 58.34 (2C, CH₂CO₂); 171.24 (2C, CH₂CO₂); 179.41 (1C, CH₂CO₂).

MS-ESI: (+) 432.9 ([M + H]⁺, calcd 433.3). (–) 430.8 ([M – H][–], calcd 431.3).

Elemental analysis: found (calcd for H₃do3aNN·5HCl·1.5H₂O, C₁₈H₄₄Cl₅N₆O_{7.5}, M_r = 641.8) C: 34.18 (33.68), H: 7.13 (6.91), N: 12.75 (13.09), Cl: 27.57 (27.62).

Synthesis of [Ln(H₃do3aNN)] complexes. The Ln(III) complexes of H₃do3aNN for NMR, NMR CEST and MRI CEST experiments were prepared by mixing the lanthanide(III) chloride hydrate (Eu³⁺, Yb³⁺) with 1.1 equiv. of the ligand in a small amount of distilled water, adjusting the pH to ≈7 with 1 M aq.

LiOH, and stirring overnight at 60 °C. Then, the pH was re-adjusted to ≈7 with 1 M aq. LiOH and the solution was again stirred overnight at 60 °C.

All the prepared samples were checked using a xylenol orange test (acetate buffer, pH = 5.7) to exclude the presence of free Ln(III) ions. The exact concentration of the Ln(III) complexes in the solution was determined using Evans's method.²²

[Eu(H₃do3aNN)]

MS-ESI: (+) 588.9 ([M + Li]⁺, calcd 589.2). (–) 616.7 ([M + Cl][–], calcd 617.2).

[Yb(H₃do3aNN)]

MS-ESI: (+) 609.9 ([M + Li]⁺, calcd 610.2). (–) 637.7 ([M + Cl][–], calcd 638.2).

PARACEST experiments

All Z-spectra were recorded using a VNMR300 spectrometer operating at 299.9 MHz (B₀ = 7.05 T); 5 mm sample tubes and a coaxial capillary with D₂O and tBuOH as an external standard were used. Solutions of the complexes for PARACEST NMR experiments were prepared in pure water with the pH adjusted using aq. HCl/LiOH solutions and had concentrations in the range of 14–87 mM. Standard pulse sequences for presaturation experiments were used. Saturation offsets were set using the array function (increment 200–250 Hz). Data from the PARACEST experiments were plotted as the dependence of normalized water signal intensity (M_z/M₀%) on saturation offset. Here, M₀ represents the magnetization (*i.e.* intensity) of the water signal without RF saturation and M_z corresponds to the water signal when a presaturation pulse is applied. Other experimental parameters are specified in the figure captions.

The magnetization transfer ratio (MTR) was calculated using $MTR = M_{\Delta\omega}/M_0 - M_{-\Delta\omega}/M_0$ in which M_{±Δω} is the magnetization (*i.e.* intensity) of the water signal with the use of a presaturation frequency ±Δω away from the bulk water signal.

MRI PARACEST images were measured with a phantom consisting of one vial containing an aqueous solution of buffers [a mixture of 0.025 M 2-(N-morpholino)ethanesulfonic acid (MES) and 0.025 M 4-(2-hydroxyethyl)-1-piperazineethanesulfonic acid (HEPES)] as a standard and nine vials containing solutions of the Eu³⁺ or Yb³⁺-complexes dissolved in buffers (0.025 M MES and 0.025 M HEPES) with different pH values and concentrations. The innocence of the chosen buffers was confirmed by silence of pure buffer solutions in the CEST experiment (*i.e.*, no signal in the Z-spectra of the pure buffers was found). All MRI PARACEST images were acquired on a 4.7 T scanner (Bruker BioSpec, Germany) using a modified spin-echo sequence (Rapid Acquisition with Refocused Echoes – RARE). Experimental conditions: repetition time (TR) = 5000 ms, echo time (TE) = 8.9 ms, resolution 0.35 × 0.35 × 2 mm³, turbo factor = 4. Other experimental parameters are specified in the figure captions. For all MR experiments, a resonator coil with an inner diameter of 70 mm was used. MTR maps were normalized to the signal acquired at a frequency offset –Δω and reconstructed from a manually outlined region of interest on a pixelwise basis using a custom script

written in Matlab (Mathworks, Natick, MA, USA). MTR maps were visualized on a false-colour scale in percentage units.

Potentiometry

Potentiometric titrations^{2,3} were carried out in a thermostatted vessel at 25.0 ± 0.1 °C at a constant ionic strength $I(\text{NMe}_4\text{Cl}) = 0.1$ M. The measurements were taken with an HCl excess added to the initial mixture and the mixtures were titrated with a stock NMe_4OH solution. An inert atmosphere was maintained by constant passage of argon saturated with water vapour. The ligand concentration in the titration vessel was ≈ 0.004 M.

Ligand protonation constants were determined by standard potentiometric titrations performed in the pH range of 1.6–12.2 (80 points per titration, titrations were carried out four times).

In the cases of the $\text{Ln(III)}\text{-H}_3\text{do3aNN}$ systems, the equilibria were established slowly and, therefore, the out-of-cell technique was used in the pH range of 1.6–7.2 (two titrations per system, 25 points per titration). The metal:ligand ratio was 1:1 in all cases. The waiting time was 7 weeks. Then, the potential at each titration point (tube) was determined with a freshly calibrated electrode.

Pre-formed complexes for the determination of their protonation constants were prepared in the following way: in an ampoule, equimolar molar amounts of the ligand and metal stock solutions were mixed and a calculated amount (based on the out-of-cell titration data) of a stock solution of NMe_4OH was gradually added to reach $\text{pH} \approx 7$, which corresponds to full complexation according to the out-of-cell titration. Ampoules were flame-sealed and left at 55 °C for 3 d. Aliquots were taken from the final solution, a defined amount of an HCl stock solution was added into these samples and the mixtures were immediately titrated by an NMe_4OH stock solution in a way analogous to the procedure described above for the determination of ligand protonation constants in the pH range of 2.3–12.1. The initial volumes were ≈ 5 cm³ for the conventional titrations and ≈ 1 cm³ for the out-of-cell ones, respectively.

The constants with their standard deviations were calculated by using the OPIUM program package.²⁴ Overall protonation constants are defined as $\beta_h = [\text{H}_h\text{L}]/([\text{H}]^h[\text{L}])$, and they can be transferred to the consecutive protonation constants $\log K_p$ by $\log K_p(\text{H}_h\text{L}) = \log \beta_h - \log \beta_{(h-1)}$; it should be noted that $\log K_p = \text{p}K_A$ of the corresponding protonated species H_hL . The overall stability constants β_{hlm} are concentration constants defined as $\beta_{hlm} = [\text{H}_h\text{L}_m\text{M}_m]/([\text{H}]^h[\text{L}]^m[\text{M}]^m)$. The water ion product used in the calculations was $\text{p}K_w = 13.81$. Stability constants of metal hydroxido complexes were taken from the literature.¹⁴ In the text, pH means $-\log[\text{H}^+]$. The best fits of experimental data are shown in Fig. S13–S15† and the results are compiled in Tables S1–S3.†

Conclusions

The present study revealed significant pH dependence of the Chemical Exchange Saturation Transfer (CEST) effect of

selected Ln(III) complexes with the novel macrocyclic ligand $\text{H}_3\text{do3aNN}$ containing a linear diamine pendant arm. The pH dependence is substantial in the pH range relevant for biological systems ($\text{pH} \approx 5.5\text{--}8.5$). Based on these findings, we have shown that the magnetization transfer ratio of CEST signals of the complexes can be used for pH determination by MRI, and it is independent of the concentration of the probes.

Unfortunately, the studied complexes are not fully kinetically inert in acidic solutions and slowly release the free metal ions, which excludes their direct use in medical applications. However, the study brings proof-of-principle of possibility to use a linear diamine fragment for pH determination using MRI ratiometry.

Acknowledgements

This work was supported by the Czech Science Foundation (P207-11-1437), by the Grant Agency of the Charles University (no. 110213) and by the project of the Ministry of Health, Czech Republic, for the development of a research organization IN00023001 (Institutional support, Institute for Clinical and Experimental Medicine). We thank Z. Böhmová for potentiometric measurements, I. Čiřáková for collection of X-ray diffraction data and nH. Blahut for his help with some NMR experiments and for Fig. S9.†

References

- 1 *The Chemistry of Contrast Agents in Medical Magnetic Resonance Imaging*, ed. A. Merbach, L. Helm and É. Tóth, 2nd edn, Wiley, Chichester, United Kingdom, 2013.
- 2 (a) P. Caravan, J. J. Ellison, T. J. McMurry and R. B. Lauffer, *Chem. Rev.*, 1999, **99**, 2293–2352; (b) P. Hermann, J. Kotek, V. Kubiček and I. Lukeš, *Dalton Trans.*, 2008, 3027–3047; (c) C. F. G. C. Geraldes and S. Laurent, *Contrast Media Mol. Imaging*, 2009, **4**, 1–23.
- 3 K. M. Ward, A. H. Aletras and R. S. Balaban, *J. Magn. Reson.*, 2000, **143**, 7987.
- 4 (a) J. Zhou and P. C. M. van Zijl, *Prog. Nucl. Magn. Reson. Spectrosc.*, 2006, **48**, 109–136; (b) Y. Wu, M. Evbuomwan, M. Melendez, A. Opina and A. D. Sherry, *Future Med. Chem.*, 2010, **2**, 351–366; (c) E. Terreno, D. D. Castelli and S. Aime, *Contrast Media Mol. Imaging*, 2010, **5**, 78–98; (d) P. C. M. van Zijl and N. N. Yadav, *Magn. Reson. Med.*, 2011, **65**, 927–948; (e) G. Liu, X. Song, K. W. Y. Chan and M. T. McMahon, *NMR Biomed.*, 2013, **26**, 810–828.
- 5 S. Zhang, M. Merritt, D. E. Woessner, R. E. Lenkinski and A. D. Sherry, *Acc. Chem. Res.*, 2003, **36**, 783–790.
- 6 (a) M. Woods, D. E. Woessner and A. D. Sherry, *Chem. Soc. Rev.*, 2006, **35**, 500–511; (b) S. Viswanathan, Z. Kovács, K. N. Green, S. J. Ratnakar and A. D. Sherry, *Chem. Rev.*, 2010, **110**, 2960–3018; (c) T. C. Soesbe, Y. Wu and A. D. Sherry, *NMR Biomed.*, 2013, **26**, 829–838.
- 7 (a) M. Woods, D. E. Woessner, R. Zhao, A. Pasha, M.-Y. Yang, C.-H. Huang, O. Vasalitiy, J. R. Morrow and

- A. D. Sherry, *J. Am. Chem. Soc.*, 2006, **128**, 10155–10162; (b) C.-H. Huang and J. R. Morrow, *Inorg. Chem.*, 2009, **48**, 7237–7243.
- 8 (a) S. J. Dorazio, P. B. Tsitovich, K. E. Sisters, J. A. Sperry and J. R. Morrow, *J. Am. Chem. Soc.*, 2011, **133**, 14154–14156; (b) A. O. Olatunde, S. J. Dorazio, J. A. Sperry and J. R. Morrow, *J. Am. Chem. Soc.*, 2012, **134**, 18503–18505; (c) S. J. Dorazio, A. O. Olatunde, P. B. Tsitovich and J. R. Morrow, *J. Biol. Inorg. Chem.*, 2014, **19**, 191–205; (d) P. B. Tsitovich and J. R. Morrow, *Inorg. Chem.*, 2014, **53**, 8311–8321; (e) S. J. Dorazio, A. O. Olatunde, J. A. Sperry and J. R. Morrow, *Chem. Commun.*, 2013, **49**, 10025–10027; (f) P. B. Tsitovich and J. R. Morrow, *Inorg. Chim. Acta*, 2012, **393**, 3–11; (g) S. J. Dorazio, P. B. Tsitovich, S. A. Gardina and J. R. Morrow, *J. Inorg. Biochem.*, 2012, **117**, 212–219.
- 9 (a) S. Aime, C. Carrera, D. D. Castelli, S. G. Crich and E. Terreno, *Angew. Chem., Int. Ed.*, 2005, **44**, 1813–1815; (b) G. Ferrauto, D. D. Castelli, E. Terreno and S. Aime, *Magn. Reson. Med.*, 2013, **69**, 1703–1711; (c) E. Gianolio, R. Stefania, E. D. Gregorio and S. Aime, *Eur. J. Inorg. Chem.*, 2012, 1934–1944.
- 10 D. V. Hingorani, A. S. Bernstein and M. D. Pagel, *Contrast Media Mol. Imaging*, 2015, **10**, 245–265.
- 11 (a) D. D. Castelli, E. Terreno and S. Aime, *Angew. Chem.*, 2011, **123**, 1838–1840; (b) D. D. Castelli, G. Ferrauto, J. C. Cutrin, E. Terreno and S. Aime, *Magn. Reson. Med.*, 2014, **71**, 326–332; (c) S. Aime, A. Barge, D. D. Castelli, F. Fedeli, A. Mortillaro, F. U. Nielsen and E. Terreno, *Magn. Reson. Med.*, 2002, **47**, 639–648; (d) Y. Wu, T. C. Soesbe, G. E. Kiefer, P. Zhao and A. D. Sherry, *J. Am. Chem. Soc.*, 2010, **132**, 14002–14003; (e) D. L. Longo, P. Z. Sun, L. Concolino, F. C. Michelotti, F. Uggeri and S. Aime, *J. Am. Chem. Soc.*, 2014, **136**, 14333–14336; (f) D. L. Longo, W. Dastrú, G. Diglio, J. Keupp, S. Langereis, S. Lanzardo, S. Prestigio, O. Steinbach, E. Terreno, F. Uggeri and S. Aime, *Magn. Reson. Med.*, 2011, **65**, 202–211; (g) V. R. Sheth, Y. Li, L. Q. Chen, C. M. Howison, C. A. Flask and M. D. Pagel, *Magn. Reson. Med.*, 2012, **67**, 760–768; (h) G. Liu, Y. Li, V. R. Sheth and M. D. Pagel, *Mol. Imaging*, 2012, **11**, 47–57; (i) N. McVicar, A. X. Li, M. Suchý, R. H. E. Hudson, R. S. Menon and R. Bartha, *Magn. Reson. Med.*, 2013, **70**, 1016–1025.
- 12 T. Krchová, J. Kotek, D. Jirá, J. Havlíčková, I. Císařová and P. Hermann, *Dalton Trans.*, 2013, **42**, 15735–15747.
- 13 A. Bianchi, L. Calabi, C. Giorgi, P. Losi, P. Mariani, P. Paoli, P. Rossi, B. Valtancoli and M. Virtuani, *J. Chem. Soc., Dalton Trans.*, 2000, 697–705.
- 14 A. E. Martell, R. M. Smith and R. J. Motekaitis, *NIST Critically Selected Stability Constants of Metal Complexes, Version 7*, Texas A&M University, College Station, TX, 2003.
- 15 S. Aime, M. Botta and G. Ermondi, *Inorg. Chem.*, 1992, **31**, 4291–4299.
- 16 S. Aime, M. Botta, M. Fasano, M. P. M. Marques, C. F. G. C. Geraldès, D. Pubanz and A. E. Merbach, *Inorg. Chem.*, 1997, **36**, 2059–2068.
- 17 (a) T. Vitha, V. Kubiček, J. Kotek, P. Hermann, L. V. Elst, R. N. Muller, I. Lukeš and J. A. Peters, *Dalton Trans.*, 2009, 3204–3214; (b) M. Polášek, J. Kotek, P. Hermann, I. Císařová, K. Binnemans and I. Lukeš, *Inorg. Chem.*, 2009, **48**, 455–465.
- 18 (a) S. Viswanathan, S. J. Ratnakar, K. N. Green, Z. Kovács, L. M. De Leónrodríguez and A. D. Sherry, *Angew. Chem., Int. Ed.*, 2009, **48**, 9330–9333; (b) S. J. Ratnakar, M. Woods, A. J. M. Lubag, Z. Kovács and A. D. Sherry, *J. Am. Chem. Soc.*, 2008, **130**, 6–7.
- 19 M. Woods, A. Pasha, P. Zhao, G. Tirso, S. Chowdhury, G. Kiefer, D. E. Woessner and A. D. Sherry, *Dalton Trans.*, 2011, **40**, 6759–6764.
- 20 B. Jagadish, G. L. Brickert-Albrecht, G. S. Nichol, E. A. Mash and N. Raghunand, *Tetrahedron Lett.*, 2011, **52**, 2058–2061.
- 21 D. D. Perrin and W. L. F. Armarego, *Purification of Laboratory Chemicals*, Pergamon Press, Oxford, 3rd edn, 1988.
- 22 D. M. Corsi, C. Platas-Iglesias, H. van Bekkum and J. A. Peters, *Magn. Reson. Chem.*, 2001, **39**, 723–726.
- 23 (a) P. Táborský, P. Lubal, J. Havel, J. Kotek, P. Hermann and I. Lukeš, *Collect. Czech. Chem. Commun.*, 2005, **70**, 1909–1942; (b) M. Försterová, I. Svobodová, P. Lubal, P. Táborský, J. Kotek, P. Hermann and I. Lukeš, *Dalton Trans.*, 2007, 535–549.
- 24 (a) M. Kývala and I. Lukeš, International Conference Chemometrics 1995 (Pardubice, Czech Republic), July 3–7, 1995, p. 63; (b) M. Kývala, P. Lubal and I. Lukeš, *IX. Solution Equilibria Analysis with the OPIUM Computer Program; Spanish-Italian and Mediterranean Congress on Thermodynamics of Metal Complexes (SIMEC 98) (Girona, Spain)*, June 2–5, 1998, The full version of the OPIUM program is available (free of charge) on <http://www.natur.cuni.cz/~kyvala/opium.html>.

Electronic Supplementary Material (ESI) for Dalton Transactions.
This journal is © The Royal Society of Chemistry 2016

Electronic Supporting Information

for

Ln(III)-complexes of a DOTA analogue with an ethylenediamine pendant arm as pH-responsive PARACEST contrast agents

Terza Krehov^a, Andrea Galisová^b, Daniel Jirák^{b,c}, Petr Hermann^c, Jan Kočí^e

^a Department of Inorganic Chemistry, Faculty of Science, Universita Karlova (Charles University), Hlavova 2030, 128 43 Prague 2, Czech Republic. Tel.: +420-221951261; Fax: +420-221951253; E-mail: andrea@natur.cuni.cz

^b Department of Radiodiagnostic and Interventional Radiology, Magnetic Resonance Unit, Institute for Clinical and Experimental Medicine, Vidětská 1958/9, Prague 4, 140 21 Czech Republic.

^c Institute of Biophysics and Informatics, 1st Faculty of Medicine, Universita Karlova (Charles University), Salmovská 1, 120 00 Prague 2, Czech Republic.

Contents

X-Ray diffraction.....	2
Temperature dependence of ¹ H NMR spectra of [Eu(d03aNN)] in D ₂ O.....	3
Temperature dependence of ¹ H NMR spectra of [Yb(d03aNN)] in D ₂ O.....	4
pH dependence of ¹ H NMR spectra of [Yb(d03aNN)].....	5
Low-temperature ¹ H NMR spectra of [Eu(d03aNN)] and [Yb(d03aNN)] in H ₂ O.....	6
Temperature dependence of NMR spectra of [Eu(H ₄ d03aNN)] in H ₂ O.....	7
Dependence of Z-spectra of [Eu(H ₄ d03aNN)] and [Yb(H ₄ d03aNN)] on presaturation intensity.....	8
Tentative visualization of TSA isomers differing in chirality of coordinated secondary amino group.....	10
pH dependence of MTR of [Eu(H ₄ d03aNN)] complex.....	11
¹ H and ¹³ C/ ¹ H NMR spectra of H ₄ d03aNN.....	12
Potentiometric studies – protonation and stability constants of H ₄ d03aNN and its Eu(III)/Yb(III) complexes.....	13
Schemes – suggested protonation sites of complex species.....	16
UV-Vis spectrophotometry.....	17
References.....	18

X-Ray diffraction

The single-crystal of **6**·2H₂O was prepared from concentrated aqueous solution of the compound **6** by a slow diffusion of EtOH vapours. The diffraction data were collected employing ApexII CCD diffractometer using Mo-K α radiation ($\lambda = 0.71073$ Å) at 150(1) K and analysed using the SAINT V8.27B (Bruker AXS Inc., 2012) program package. The structures were solved by direct methods (SHELXS97¹) and refined by full-matrix least-squares techniques (SHELXL97¹). All non-hydrogen atoms were refined anisotropically. Carbon atoms of the ethylene group of amine pendant arm were found to be disordered in two positions with relative occupancy 56:44. Hydrogen atoms attached to carbon atoms were fixed in theoretical positions using a riding model with $L_{\text{C}}(\text{H}) = 1.2 L_{\text{C}}(\text{C})$, and those belonging to the oxygen or nitrogen atoms were fully refined.

Crystal data

6·2H₂O, C₂₄H₄₈N₆O₆, $M_r = 494.55$, monoclinic, $a = 7.7686(3)$, $b = 15.4411(5)$, $c = 19.4703(7)$ Å, $\beta = 93.165(2)^\circ$, $V = 2332.01(14)$ Å³, space group $F2_1/c$, $Z = 4$, 4582 total reflections, 3599 intense reflections, $R_{\text{int}}[I > 2\sigma(I)] = 0.0596$, $wR_{\text{ref}}(\text{all data}) = 0.1757$, CCDC-1430249.

The found protonation scheme (Figure S1) is similar to those found previously for related 2-aminooethyl analogues³ – two protons are bound to the mutually *trans* macrocyclic amino groups bearing acetate moieties and the third one belongs to the “odd” acetate moiety. The conformation of the macrocyclic unit is (3,3,3)-B, as usually observed for the double-protonated cyclen rings.⁴ Such a conformation is stabilized by the intramolecular hydrogen bonds between the protonated and non-protonated macrocyclic amino groups. The whole crystal structure is stabilized by the extended hydrogen bonds network between ligand and the water solvate molecules.

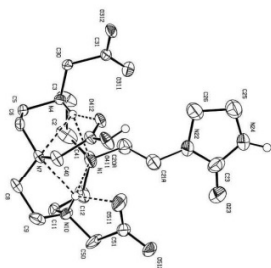


Figure S1 Molecular structure of **6** found in the crystal structure of **6**·2H₂O. Carbon-bound hydrogen atoms are omitted for clarity reasons. Hydrogen bonds are dashed.

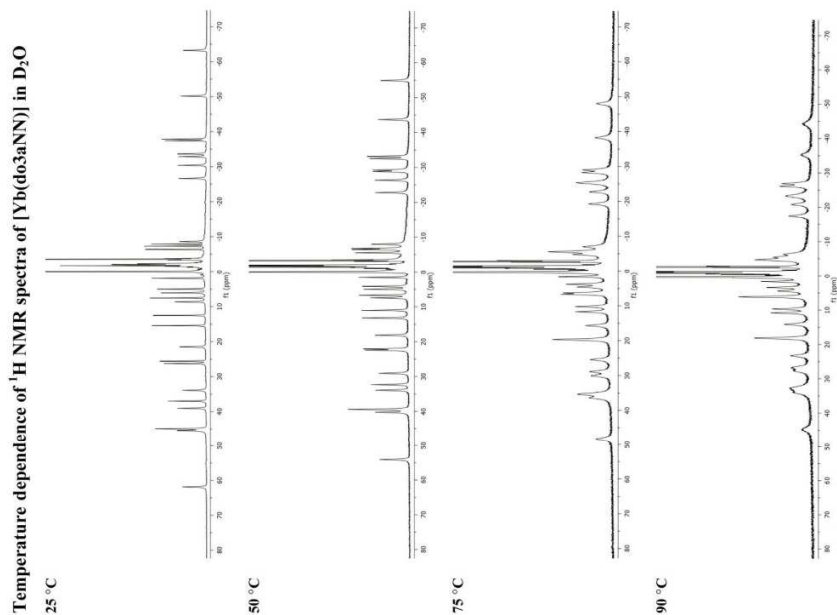


Figure S3 ^1H NMR spectra of the $[\text{Yb}(\text{do}3\text{aNN})]$ complex (~ 0.08 M solution in D_2O , $B_0 = 7.05$ T, $\text{pD} = 11.3$) at different temperatures. The chemical shift of HDO in the sample solution was referenced to 0 ppm.

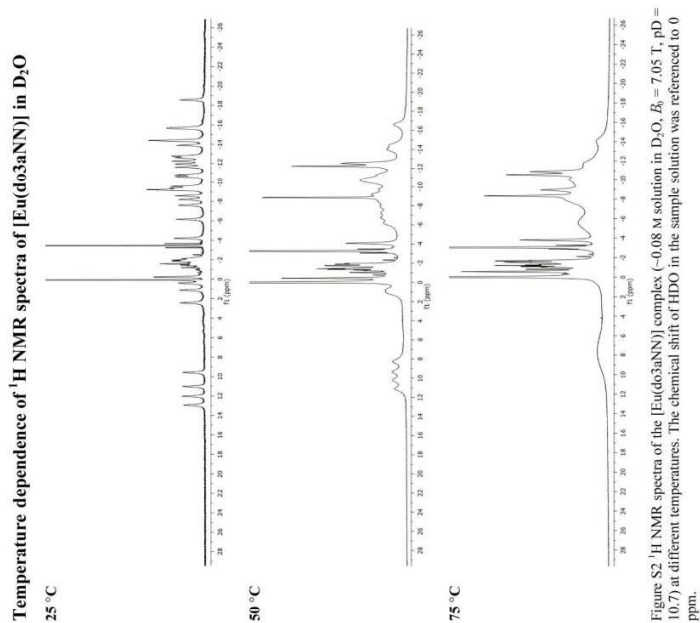


Figure S2 ^1H NMR spectra of the $[\text{Eu}(\text{do}3\text{aNN})]$ complex (~ 0.08 M solution in D_2O , $B_0 = 7.05$ T, $\text{pD} = 10.7$) at different temperatures. The chemical shift of HDO in the sample solution was referenced to 0 ppm.

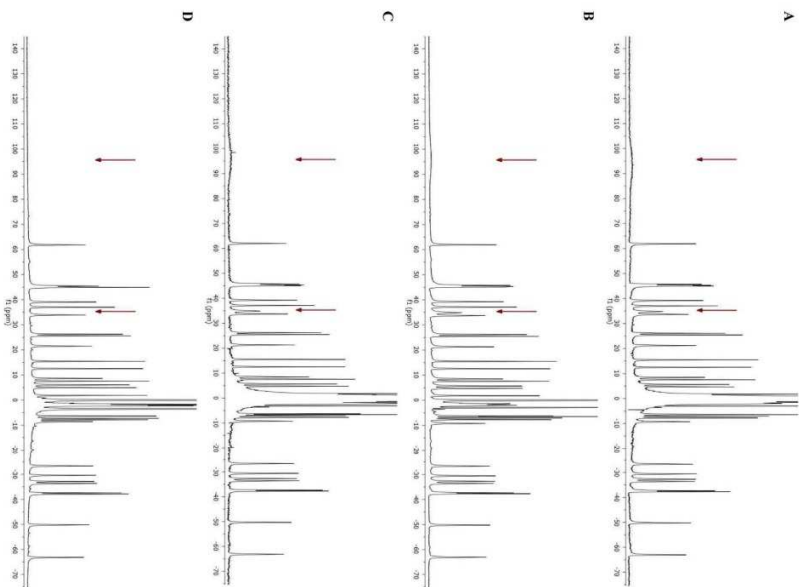
pH dependence of ^1H NMR spectra of $[\text{Yb}(\text{do}3\text{aNN})]$ 

Figure S4 A: ^1H NMR spectrum of the $[\text{Yb}(\text{do}3\text{aNN})]$ complex, 0.09 M solution in H_2O , $B_0 = 7.05$ T, 25 $^\circ\text{C}$, pH = 9.38. B: the same sample, water signal was saturated. C: the same sample, pH was re-adjusted to 11.3. D: 0.04 M solution in D_2O , $B_0 = 7.05$ T, 25 $^\circ\text{C}$, pH = 11.34. Arrows show the positions of exchangeable (N-H) protons. The chemical shifts of $\text{H}_2\text{O}/\text{HDO}$ in the sample solutions were referenced to 0 ppm.

5

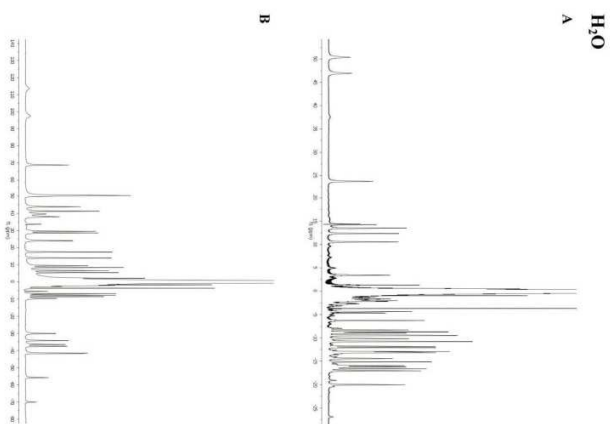
Low-temperature ^1H NMR spectra of $[\text{Eu}(\text{do}3\text{aNN})]$ and $[\text{Yb}(\text{do}3\text{aNN})]$ in H_2O 

Figure S5 A: ^1H NMR spectrum of the $[\text{Eu}(\text{do}3\text{aNN})]$ complex, 47 mM solution in H_2O , $B_0 = 14.1$ T, 5 $^\circ\text{C}$, pH = 9.5. B: ^1H NMR spectrum of the $[\text{Yb}(\text{do}3\text{aNN})]$ complex, 45 mM solution in H_2O , $B_0 = 14.1$ T, 5 $^\circ\text{C}$, pH = 9.6. The chemical shifts of H_2O in the sample solutions were referenced to 0 ppm.

6

Dependence of Z-spectra of [Eu(H₄d03aNN)] and [Yb(H₄d03aNN)] on presaturation intensity

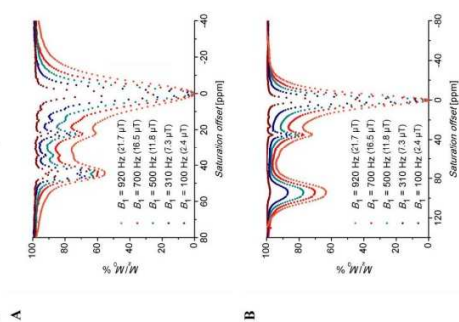


Figure S7 A: Z-spectra of an 87 mM aqueous solution of the [Eu(H₄d03aNN)] complex ($B_0 = 7.05$ T, RF presaturation pulse applied for 2 s, pH = 6.45, 25 °C). B: Z-spectra of an 87 mM aqueous solution of the [Yb(H₄d03aNN)] complex ($B_0 = 7.05$ T, RF presaturation pulse applied for 2 s, pH = 6.33, 25 °C).

Temperature dependence of NMR spectra of [Eu(H₄d03aNN)] in H₂O

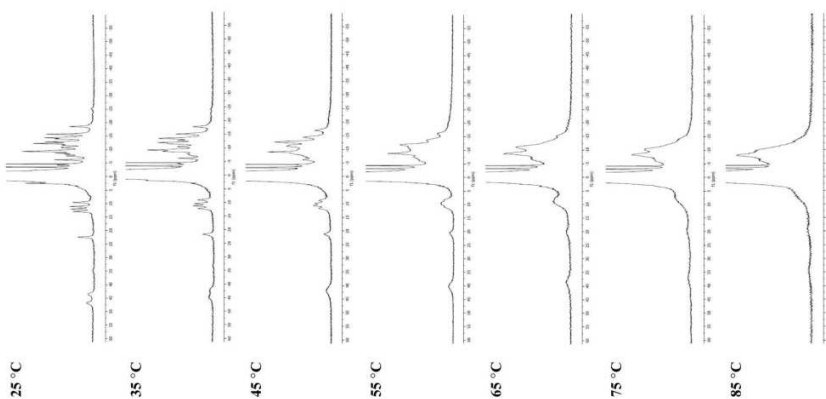


Figure S6 ¹H NMR spectra of the [Eu(H₄d03aNN)] complex (~0.05 M solution in H₂O, $B_0 = 7.05$ T, pH = 6.75) at different temperatures. The chemical shift of H₂O in the sample solution was referenced to 0 ppm.

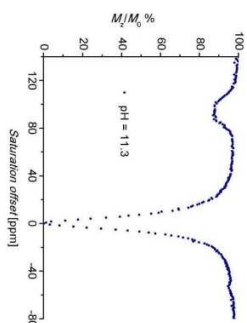


Figure S8 A: Z-spectra of an 87 mM aqueous solution of the [Yb(dob3aNN)] complex at pH = 11.3 ($f_0 = 7.05$ T, $B_1 = 21.7$ μ T (920 Hz), RF presaturation pulse applied for 2 s, 25 $^{\circ}$ C).

Tentative visualization of TSA isomers differing in chirality of coordinated secondary amino group

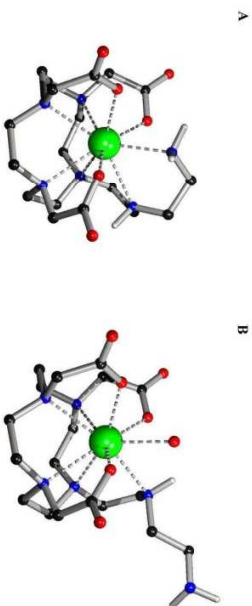


Figure S9 A: TSA A2222 species with R chirality of the secondary amino group, enabling coordination of the primary amino group in the apical position. B: TSA A2222 species with S chirality of the secondary amino group, disallowing coordination of the primary amino group in the apical position. It should be noted that the primary amino group has to be fixed in position close to the central ion, as its protons have resolved the 1 H NMR signals and are still somewhat paramagnetically shifted. Such finding points to a some weak coordination of this group to the metal ion or its participation in an intramolecular hydrogen bond system.

Both structures were optimised with Gaussian package (Gaussian 09, Revision D.01),⁵ using DFT method with M06 functional⁶ and 6-31(G(d,p)) base set for all atoms but europium, where large core pseudopotential of Dolg et al. together with appropriate base set were used.⁷ Default value for integration grid ("Fine") and SCF convergence criteria 10^{-8} were used. The stationary points found on the potential energy surfaces as a result of the geometry optimizations have been tested to represent energy minima *via* frequency analysis. Solvent effects were evaluated using the polarizable continuum model (PCM) as implemented in Gaussian.

pH dependence of MTR of [Eu(H_2O_3aNN)] complex

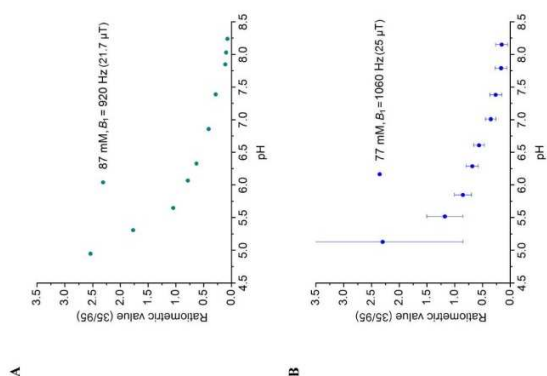


Figure S10 A: Ratiometric plot of an 87 mM aq. solution of the [Yb(H_2O_3aNN)] complex, at 25 °C taken by NMR; $B_1 = 7.05$, $B_2 = 21.7$ μ T (920 Hz), RF presaturation pulse applied for 2 s. **B:** Ratiometric plot of a 77 mM solution of the [Yb(H_2O_3aNN)] complex in 50 mM HEPES-MES (1-1) at 25 °C taken by MRI; RARE pulse sequence, TR = 5 s, TE = 8.9 ms, $B_1 = 4.7$ T, $B_2 = 25$ μ T (1060 Hz), RF presaturation pulse applied for 2 s. The ratiometric value (35/95) is the ratio of the MTR intensity at 35 ppm to the MTR intensity at 95 ppm.

1H and $^{13}C\{^1H\}$ NMR spectra of H_2O_3aNN

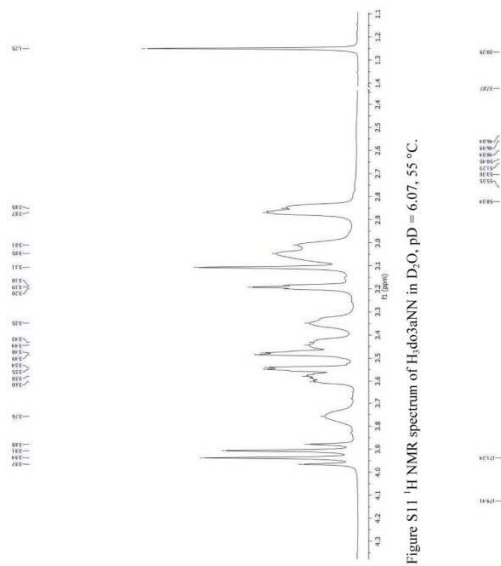


Figure S11 1H NMR spectrum of H_2O_3aNN in D_2O , pH = 6.07, 55 °C.

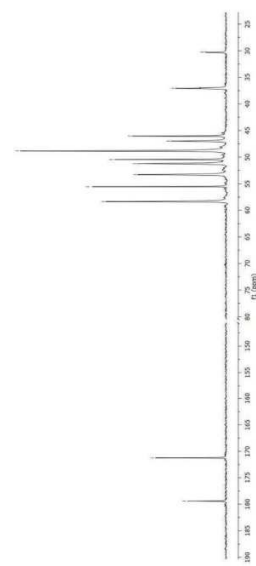


Figure S12 $^{13}C\{^1H\}$ NMR spectrum of H_2O_3aNN in D_2O , pH = 6.07, 55 °C.

Potentiometric studies – protonation and stability constants of H₄d₃aNN and its Eu(III)/Yb(III) complexes

Table S1 Overall protonation constants ($\log\beta_n^{\text{H}}$) of H₄d₃aNN (0.1 M NaMeCl, 25 °C).

n	$\log\beta_n^{\text{H}}$
1	12.62(2)
2	22.90(2)
3	32.57(2)
4	40.87(3)
5	44.17(3)
6	45.78(3)

$^{\text{H}}\beta_n = [\text{H}_n\text{L}]/([\text{H}]^n[\text{L}])$

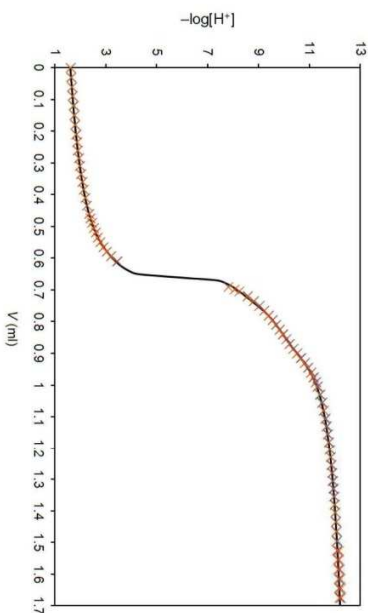


Figure S13 Titration data of the acid-base titration of the free ligand H₄d₃aNN showing the best fit calculated using the protonation constants from Table S1 ($c_{\text{L}} = 0.004$ M, 0.1 M NaMeCl, 25 °C).

13

Table S2 Overall stability constants ($\log\beta_{\text{MLn}}^{\text{H}}$) of [Ln(H₄d₃aNN)] complexes (0.1 M NaMeCl, 25 °C).

n	l	m	$\log\beta_{\text{MLn}}^{\text{H}}$	
			Eu	Yb
0	1	1	23.16(5)	22.76(4)
1	1	1	29.19(4)	28.98(3)
2	1	1	34.28(7)	34.05(4)

$^{\text{H}}\beta_{\text{MLn}} = [\text{H}_n\text{L}_m\text{M}]/([\text{H}]^n[\text{L}]^m[\text{M}]^n)$

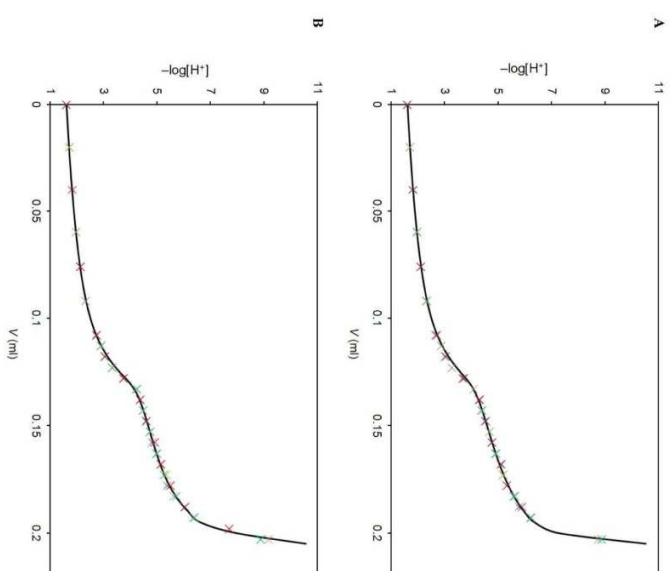


Figure S14 Titration data of the out-of-cell titration of Ln(II)-H₄d₃aNN systems showing the best fit calculated using the stability constants from Table S2 ($c_{\text{Ln}} = c_{\text{L}} = 0.004$ M, 0.1 M NaMeCl, 25 °C, equilibration time = 7 weeks). A: Eu(II)-H₄d₃aNN system. B: Yb(II)-H₄d₃aNN system.

14

Table S3 Overall protonation constants ($\log \beta_{011}^{\text{H}}$) of [Ln(d03aNN)] complexes (0.1 M NNMe_2Cl , 25 °C).

<i>n</i>	$\log \beta_{011}^{\text{H}}$	$\log \beta_{011}^{\text{H}, \text{b}}$
1	5.57(3)	5.67(1)
2	10.41(2)	10.52(1)

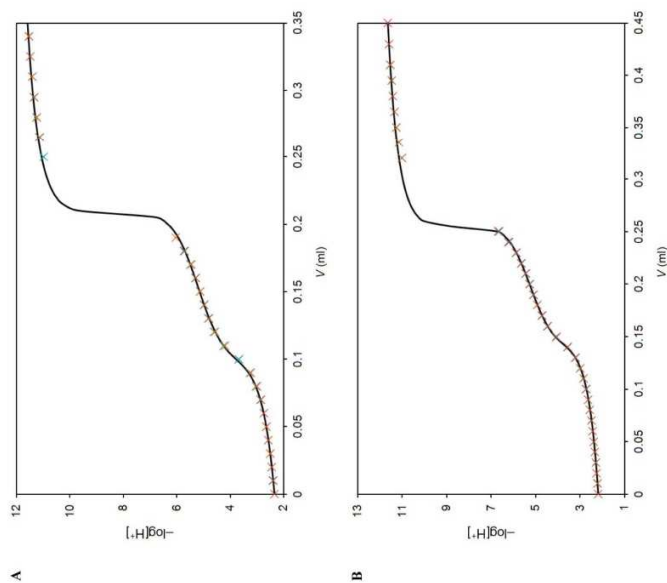
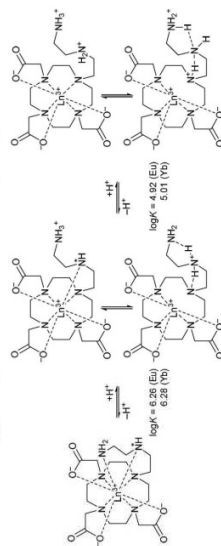
$$-\log \beta_{011}^{\text{H}} = [\text{H}_2\text{L}][\text{M}]^2 / [\text{H}]^2 [\text{LM}]$$


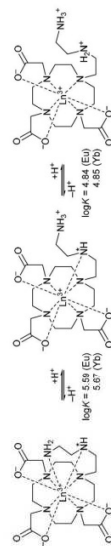
Figure S15 Titration data of the acid-base titration of the pre-formed [Ln(d03aNN)] complexes with the best fits calculated using the protonation constants from Table S3 ($c_{\text{Ln}} = 0.003 \text{ M}$, $0.1 \text{ M NNMe}_2\text{Cl}$, 25 °C). **A:** $\text{H}^+ - [\text{Eu}(\text{d03aNN})]$ system. **B:** $\text{H}^+ - [\text{Yb}(\text{d03aNN})]$ system.

15

Schemes – suggested protonation sites of complex species



Scheme S1 Suggested species with the tentative protonation sites present in the protonation equilibrium of Ln(III)- $\text{H}_2\text{d03aNN}$ mixtures during out-of-cell titration. In the protonated species, binding of the water molecule(s) to the central ion filling its coordination sphere to the coordination number 8-9 is expected, but it is not shown for the sake of clarity



Scheme S2 Suggested species occurring during the non-equilibrium potentiometric acid-base titration of pre-formed [Ln(d03aNN)] complexes. In the hepta/octa-coordinated species, binding of the water molecule(s) to the central ion filling its coordination sphere to the coordination number 8-9 is expected, but it is not shown for the sake of clarity.

16

UV-Vis spectrophotometry

UV-Vis solution spectra were obtained on a SPECORD® 50 PLUS (ANALYTIC JENA AG) spectrophotometer at 25 °C in the range of 300–1000 nm with the data intervals of 0.2 nm and the integration time of 0.04 s.

The samples for UV-Vis spectra of xylenol orange- Eu^{3+} complex were prepared by the following way: 100 μl of xylenol orange solution (10^{-4} M) in buffer (mixture of 0.025 M aq. HEPES and 0.025 M aq. MES; pH = 5.55) was added to 898 μl of the same buffer (pH = 5.55). Gradually, 2.2 μl portions of aq. solution of EuCl_3 in H_2O (4.46 mM) were added, and the UV-Vis spectrum was acquired after each addition (Figure S16).

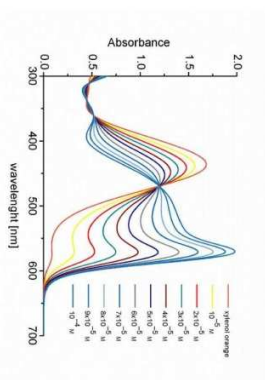


Figure S16 Change of UV-Vis spectra of aq. solution of xylenol orange (10^{-4} M, pH = 5.55, 0.025 M HEPES and 0.025 M MES, 25 °C) with increasing concentration of EuCl_3 (10^{-4} – 10^{-2} M).

Kinetic stability of $[\text{Eu}(\text{H}_2\text{d}03\text{aNN})]$ complex was studied by following procedure: 100 μl of aq. solution of $[\text{Eu}(\text{d}03\text{aNN})]$ complex (8 mM, pH = 7.5) was added to the mixture of 800 μl of buffer solution (mixture of 0.025 M aq. HEPES and 0.025 M aq. MES, pH = 5.55) with 100 μl of xylenol orange solution (10^{-4} M) in the same buffer (pH = 5.55). The evaluation of the absorption spectra with time was measured and is shown in Figure S17.

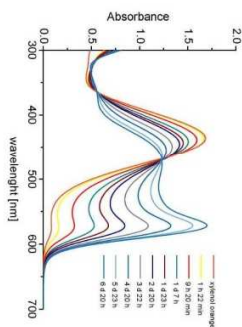


Figure S17 Time dependence of UV-Vis spectra of aq. solution of xylenol orange (10^{-4} M, pH = 5.55, 0.025 M HEPES and 0.025 M MES, 25 °C) in the presence of the $[\text{Eu}(\text{H}_2\text{d}03\text{aNN})]$ complex ($8 \cdot 10^{-4}$ M).

References

- G. M. Sheldrick, SHELSX97, Program for Crystal Structure Solution from Diffraction Data, University of Göttingen, Göttingen, 1997.
- G. M. Sheldrick, SHEXLX97, Program for Crystal Structure Refinement from Diffraction Data, University of Göttingen, Göttingen, 1997.
- T. Krelková, J. Koček, D. Jiřík, J. Havlíčková, I. Cisarová and P. Hermann, *Dalton Trans.* 2013, **42**, 15735–15747.
- M. Meyer, V. Dahnout-Gindrey, C. Lecomte and R. Guillard, *Coord. Chem. Rev.*, 1998, **178–180**, 1313–1405.
- M. J. Frisch, G. W. Trucks, H. B. Schlegel, G. E. Scuseria, M. A. Robb, J. R. Cheeseman, G. Scalmani, V. Barone, B. Mennucci, G. A. Petersson and et al., Gaussian 09, Revision D01, Gaussian, Inc.: Wallingford.
- Y. Zhao and D. G. Truhlar, *Theor. Chem. Acc.*, 2008, **120**, 215–241.
- M. Dolg, H. Stoll and H. Preuss, *Theor. Chim. Acta*, 1993, **85**, 441–450.

APPENDIX 3

T. Krchová, V. Herynek, A. Gálisová, J. Blahut, P. Hermann and J. Kotek: “Eu(III) complex with DO3A-amino-phosphonate ligand as a concentration-independent pH-responsive contrast agent for Magnetic Resonance Spectroscopy (MRS)”, *Inorg. Chem.*, 2017, DOI: 10.1021/acs.inorgchem.6b02749

Eu(III) Complex with DO3A-amino-phosphonate Ligand as a Concentration-Independent pH-Responsive Contrast Agent for Magnetic Resonance Spectroscopy (MRS)

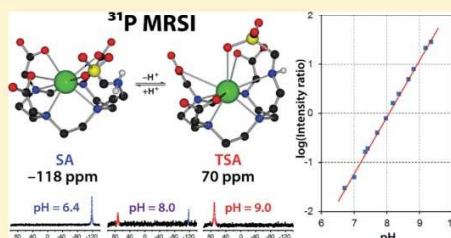
Tereza Krchová,[†] Vít Herynek,[‡] Andrea Gálišová,[‡] Jan Blahut,[†] Petr Hermann,[†] and Jan Kotek^{*,†,‡}

[†]Department of Inorganic Chemistry, Faculty of Science, Charles University, Hlavova 2030, Prague 2 128 43, Czech Republic

[‡]Department of Radiodiagnostic and Interventional Radiology, Magnetic Resonance Unit, Institute for Clinical and Experimental Medicine, Videňská 1958/9, Prague 4 140 21, Czech Republic

Supporting Information

ABSTRACT: A new DOTA-like ligand H₃do3aNP with a 2-[amino(methylphosphonic acid)]ethyl-coordinating pendant arm was prepared, and its coordinating properties were studied by NMR spectroscopy and potentiometry. The study revealed a rare slow exchange (on the ¹H and ³¹P NMR time scale) between protonated and unprotonated complex species with a corresponding acidity constant pK_a ~ 8.0. This unusually slow time scale associated with protonation is caused by a significant geometric change from square-antiprismatic (SA) arrangement observed for protonated complex SA-[Eu(Hdo3aNP)]⁻ to twisted-square-antiprismatic (TSA) arrangement found for deprotonated complex TSA-[Eu(do3aNP)]²⁻. This behavior results in simultaneous occurrence of the signals of both species in the ³¹P NMR spectra at approximately -118 and +70 ppm, respectively. Such an unprecedented difference in the chemical shifts between species differing by a proton is caused by a significant movement of the principal magnetic axis and by a change of phosphorus atom position in the coordination sphere of the central Eu(III) ion (i.e., by relative movement of the phosphorus atom with respect to the principal magnetic axis). It changes the sign of the paramagnetic contribution to the ³¹P NMR chemical shift. The properties discovered can be employed in the measurement of pH by MRS techniques as presented by proof-of-principle experiments on phantoms.



INTRODUCTION

Over the past two decades, the ability to provide essential information about variations in tissue pH has become increasingly important. Therefore, it is not surprising that magnetic resonance imaging (MRI), as one of the most widely used diagnostic methods in clinical medicine,¹ has been proposed as a suitable technique for this purpose. The tumor extracellular microenvironment is often slightly more acidic than healthy tissue due to increased anaerobic glycolysis and a related accumulation of lactic acid, reduced passive buffering capacity, and poor tissue perfusion.² For example, the extracellular pH in solid tumors typically ranges between 6.5 and 7.2.³ Therefore, measurement of extracellular pH using noninvasive techniques is important not only for early detection of disease or metabolic disorder, but also for suggesting the most efficient treatment and for monitoring the effects of pH-altering therapies.² Nowadays, several strategies (and appropriate contrast agents, CAs) to measure tissue pH are intensively investigated.⁴ Previous studies have suggested relaxation-based MRI CAs with longitudinal relaxivity (*r*₁) dependent on pH.⁵ The Gd(III) complexes investigated were based on a variation in the number of inner-sphere water molecules (*q*), for example, caused by the

presence of *β*-arylsulfonamide⁶ or *p*-nitrophenol⁷ groups on the chelate species. The deprotonation and coordination of these groups is associated with removal of the inner-sphere water molecule, and such a change in *q* leads to a change in relaxivity *r*₁. Similarly, in the case of Gd(III) complexes of H₃do3a with 2-aminoethyl pendant arms, such as H₃do3a-ae (Figure 1), a change in the protonation state of the amino group causes a (de)coordination of the pendant arm, and thus, it also leads to changes in relaxivity.⁸ Interesting results have been obtained by Hall et al., who studied the Gd(III) complex with terpyridine-containing macrocycle.⁹ The authors demonstrated a significant decrease of relaxivity with increasing pH and attributed it to a decrease in *q* from 3 to 0 due to formation of the hydroxido species and hydroxido-bridged dimer connected with a negligible exchange rate of coordinated OH⁻ ions.⁹ However, for quantification of pH using these relaxation-based CAs, knowledge of the actual agent concentration is needed.¹⁰ This is the reason why new methods employing ratiometric approaches are developed, as they remove dependence of the observed signal on the local concentration of CAs. For example,

Received: November 17, 2016

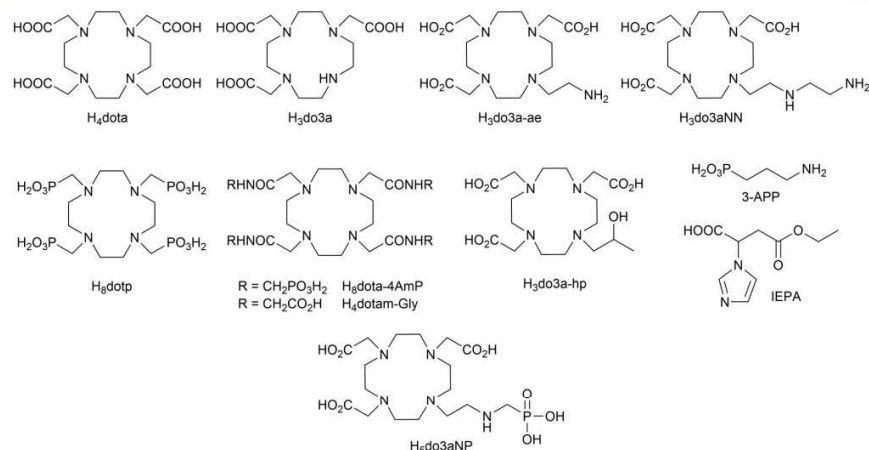


Figure 1. Structural formulas of the ligands discussed in the text.

Gillies and co-workers developed a “dual-injection” relaxivity-based method employing administration of two compounds (pH-sensitive $[\text{Gd}(\text{dota-4AmP})]^{5-}$ and pH-insensitive $[\text{Gd}(\text{dotp})]^{5-}$; for structures of both ligands, see Figure 1) with a comparable biodistribution and pharmacokinetics, allowing determination of the concentration of the first agent from the concentration of the second one. It was shown that this approach allowed pH mapping both *in vitro* and *in vivo*.^{5b,10,11} An alternative approach was introduced by Aime et al. They investigated the possibility of measuring the ratio of transversal and longitudinal relaxation rates of water protons (R_2/R_1) after injecting a single paramagnetic Gd(III) complex of DOTA-functionalized polypeptide (poly-L-ornithine).¹² Recently, the paramagnetic MRI contrast agents that are detected via the chemical exchange saturation transfer (CEST) effect, so-called PARACEST CAs, have also been used to ratiometrically estimate *in vitro/in vivo* pH by utilizing a ratio of two different CEST signals.^{3,13} These can originate from the exchangeable protons of the same molecule, as in the case of paramagnetic $\text{H}_4\text{dotam-Gly}$ (Figure 1) complexes with some Ln(III) ions (Pr, Nd, and Eu) where the protons of a coordinated water molecule and amide protons of the macrocyclic ligand represent two CEST-active exchanging pools.¹⁴ Similarly, the Yb(III) complex of $\text{H}_3\text{do3aNN}$ (Figure 1) with two proton-exchanging pools of the primary and secondary amino groups has been shown to be suitable for this purpose.¹⁵ Two different CEST signals can also originate from two conformations of the same molecule generating CEST signals at different chemical shifts, as was shown for Yb(III)-analogue of the clinically used $[\text{Gd}(\text{do3a-hp})(\text{H}_2\text{O})]$ (ProHance; Figure 1).^{13e,16}

An alternative approach to *in vivo* pH measurement is the MRS (magnetic resonance spectroscopy) technique. In general, MRS provides information about abundance and concentration of tissue metabolites, and it can help to characterize many pathologies, including neurological, psychiatric, and metabolic diseases.¹⁷ In addition, spectral information on a metabolite/compound with a particular chemical shift can be encoded into the image, and a map of its spatial distribution can be reconstructed by a method called magnetic resonance

spectroscopic imaging (MRSI). Several methods for pH mapping by MRS using different endogenous or exogenous compounds have been used, and these are generally based on a difference in chemical shifts between pH-dependent and pH-independent resonances. Application of MRS to measure pH began early on with the acquisition of the ^{31}P MR spectra of inorganic phosphate (P_i) because its resonance frequency is pH-dependent. The majority of P_i resonance comes from intracellular phosphate,¹⁸ and thus, the chemical shift of the P_i generally reflects the intracellular pH.^{2,11,19} To determine the extracellular pH of tumors in animal models, nontoxic exogenous reporter 3-aminopropylphosphonic acid (3-APP; Figure 1) with chemical shift dependence ~ 1 ppm per pH unit has been used.^{2,19} Tissue pH can also be detected *in vivo* using diamagnetic ^1H MRS probes with the pH-sensitive signal of ^1H nucleus. Exogenously administered 2-imidazol-1-yl-3-ethoxycarbonyl-propionic acid (IEPA; Figure 1) has been employed for this purpose. The chemical shift of the imidazole ring C-2 hydrogen atom is in the 7–9 ppm range and is pH-sensitive. This compound has been used for imaging extracellular pH in breast or brain tumors.²⁰ However, the disadvantage of using diamagnetic compounds as pH probes is the fact that their signal can be overlapped with the resonances of other compounds present *in vivo*. Therefore, complexes of paramagnetic metal ions are studied due to the expanded chemical shift scale of NMR-active nuclei. In particular, Ln(III) complexes with macrocyclic ligands have been used because they are stable under *in vivo* conditions. The Yb(III) complex of H_8dotp (Figure 1) has been introduced as a prototype of a new class of pH indicators because stepwise protonation of the complex is accompanied by variations in the protons' chemical shifts (6 resonances in ^1H NMR spectrum); this enables creation of a calibration curve for pH determination.²¹ Simultaneous determination of pH and temperature by Tm(III) complexes of H_8dotp using three proton chemical shifts was studied by a three-dimensional chemical shift method called biosensor imaging of redundant deviation in shift (BIRDS).²² The Ln(III) complexes of two metal ions (Tm and Yb) with phosphonate ligand $\text{H}_8\text{dota-4AmP}$ (Figure 1)

also exhibit suitable pH-sensitivities for BIRDS detection using chemical shift difference between two proton resonances. Moreover, these agents are also CEST-active, and thus, the CEST effect observed together with BIRDS opens the way toward high-resolution and quantitative pH imaging.^{2,3}

To contribute to the fields described above, we prepared a new macrocyclic ligand H₅do3aNP (Figure 1). The amino-phosphonate-coordinating pendant arm was chosen because, in general, protonation constants of amino and phosphonate groups are close to the physiological pH; thus, the complexes of the new ligand were expected to change their properties in the pH region relevant for living systems. In addition, the presence of a phosphorus atom could be potentially employed in ³¹P NMR-based applications. In this work, we report on ligand synthesis and the unusual ¹H and ³¹P NMR properties of its europium(III) complex which are employable in ³¹P MRS/MRSI for determination of pH. In addition, potentiometric and NMR studies found high stability for the studied complex in solution, which is promising for potential *in vivo* use of related compounds.

EXPERIMENTAL SECTION

Materials and Methods. Unless stated otherwise, commercially available chemicals and solvents were used without further purification. Water used for potentiometric titrations was deionized by the Milli-Q device (Millipore).

1,4,7-Tris(*tert*-butylcarboxymethyl)-1,4,7,10-tetraazacyclododecane hydrobromide (tBu₃do3a-HBr)²⁴ and *N*-benzylethanolamine²⁵ were prepared according to the published procedures. Dichloromethane (DCM) was dried by the standard procedure²⁶ and stored over molecular sieves under an argon atmosphere.

NMR characterization data (1D: ¹H, ¹³C; 2D: HSQC, HMBC, ¹H-¹H COSY, ¹H-¹H EXSY, ³¹P-³¹P EXSY) were recorded on VNMR300, Bruker Avance III 400, or Bruker Avance III 600 spectrometers, using 5 mm sample tubes. The longitudinal relaxation times *T*₁'s of ³¹P were measured on the VNMR300 by inversion recovery pulse sequence (15 or 10 increments on d2 exponentially sampled) with the spectrometer offset identical to the compound signal and properly calibrated pulse length. Selectively ¹H-decoupled ¹³C NMR spectra were obtained on the Bruker Avance III 600 spectrometer by standard one-pulse ¹³C measurement with low-power continuous-wave ¹H decoupling at the desired frequency offset. Exchange rates were measured using a selective ³¹P-³¹P EXSY pulse sequence with the mixing-time changing from 20 μs to 500 ms exponentially. Exchange rates of isomer interchange were determined by numerical fitting of the mixing-time-dependent ³¹P NMR integral value with the Bloch-McConnell equation using Matlab.²⁷ Unless stated otherwise, NMR experiments were performed at 25 °C. The pD value means a reading of the freshly calibrated pH electrode of the sample dissolved in D₂O corrected by +0.4. Chemical shifts δ are given in ppm, and coupling constants *J* are reported in Hz. For ¹H and ¹³C{¹H} measurements of diamagnetic compounds in D₂O, *t*BuOH was used as the internal standard (δ_H = 1.25, δ_C = 30.29). For the measurements in CDCl₃, TMS was used as the internal standard (δ_H = 0.00, δ_C = 0.00). For ³¹P measurements, 85% H₃PO₄ in H₂O was used as the external standard (δ_P = 0.00). In the case of paramagnetic complexes, ¹H chemical shifts were referenced to the *t*BuOH signal of the sample (δ_H = 1.25). Abbreviations [s (singlet), d (doublet), t (triplet), m (multiplet), and br (broad)] are used in order to express the signal multiplicities. Lanthanide(III) concentrations in solutions were determined by measuring bulk magnetic susceptibility (BMS) shifts.²⁸

The ESI-MS spectra were run on the Bruker ESQUIRE 3000 spectrometer equipped with an electrospray ion source and ion-trap detection. The measurements were carried out in both positive and negative modes.

Luminescence spectra were acquired on a Luminescence Thermo Spectronic spectrometer AMINCO Bowman Series 2. The luminescence spectra were obtained after excitation at the Eu(III) ⁵L₆ ← ⁷F₀ band (λ = 396 nm).

Syntheses. **Synthesis of 1.** Paraformaldehyde (4.00 g, 133 mmol) was added to a well-stirred solution of *N*-benzylethanolamine (4.00 g, 26.5 mmol) and diethyl-phosphite (17.2 mL, 134 mmol) in dry MeCN (30 mL). The reaction mixture was stirred at 60 °C for 2 days, filtered, and then evaporated on a rotary evaporator. The oily residue was dissolved in a small amount of EtOH, and then the solution was loaded onto a strong cation exchanger column (Dowex 50, H⁺-form, 4 cm × 20 cm, in EtOH). Impurities were removed by elution with EtOH, and product **1** was eluted with concentrated aqueous NH₃/EtOH (1/5). The fractions containing product **1** (TLC and ¹H NMR check) were combined, evaporated, redissolved in absolute EtOH, and evaporated to give compound **1** (7.62 g, 95.6%) as a brownish oil.

¹H NMR (299.9 MHz, CD₃OD): δ 1.34 (6H, t, ³J_{HH} = 7.0, CH₂CH₃); 2.80 (2H, t, ³J_{HH} = 6.0, CH₂CH₂OH); 3.07 (2H, d, ²J_{HP} = 10.0, PCH₂N); 3.67 (2H, t, ³J_{HH} = 6.0, CH₂CH₂OH); 3.85 (2H, s, CH₂Ph); 4.13 (4H, dq, ³J_{HH} = ³J_{PH} = 7.0, CH₂CH₃); 7.25–7.41 (5H, m, arom). ¹³C{¹H} NMR (75.4 MHz, CD₃OD): δ 17.64 (2C, d, ³J_{CP} = 6.0, OCH₂CH₃); 51.09 (1C, d, ¹J_{CP} = 162, PCH₂N); 58.89 (1C, d, ³J_{CP} = 8.0, CH₂); 61.9 (1C, CH₂); 62.24 (1C, ³J_{CP} = 7.5, CH₂); 64.39 (2C, ²J_{CP} = 7.0, OCH₂CH₃); 129.16 (1C, arom); 130.18 (2C, arom); 131.02 (2C, arom); 140.83 (1C, arom quaternary). ³¹P{¹H} NMR (121.4 MHz, CD₃OD): δ 27.17 (1P, s). ³¹P NMR (121.4 MHz, CD₃OD): δ 27.17 (1P, m). MS-ESI: (+) 323.7 ([M + Na]⁺, calcd 324.1).

Synthesis of 2. A solution of CH₃SO₂Cl (1.14 g, 9.96 mmol, 1.2 equiv) in dry CH₂Cl₂ (10 mL) was dropwise added to a well-stirred solution of **1** (2.50 g, 8.30 mmol) and Et₃N (1.68 g, 16.6 mmol, 2 equiv) in dry CH₂Cl₂ (70 mL) with cooling (ice bath). The reaction mixture was then stirred for 20 min. Next, saturated aqueous NaHCO₃ (50 mL) was added, and the mixture was stirred for 10 min. The organic layer was separated, washed with saturated aqueous NaHCO₃ (2 × 30 mL) and H₂O (2 × 30 mL), dried over Na₂SO₄, and concentrated *in vacuo* to give 3.05 g (97%) of **2** as a brownish oil. Compound **2** is not stable and must be immediately used for further synthesis.

¹H NMR (299.9 MHz, CDCl₃): δ 1.31 (6H, t, ³J_{HH} = 7.0, CH₂CH₃); 2.98 (2H, d, ²J_{HP} = 11.0, PCH₂N); 2.99 (3H, s, CH₃); 3.08 (2H, t, ³J_{HH} = 6.0, OCH₂CH₂N); 3.85 (2H, s, CH₂Ph); 4.09 (4H, dq, ³J_{HH} = ³J_{PH} = 7.0, CH₂CH₃); 4.29 (2H, t, ³J_{HH} = 6.0, S(O)₂CH₂CH₂N); 7.23–7.35 (5H, m, arom). ¹³C{¹H} NMR (75.4 MHz, CDCl₃): δ 16.60 (2C, d, ³J_{CP} = 6.0, OCH₂CH₃); 37.50 (1C, S(O)₂CH₂); 49.67 (1C, d, ¹J_{CP} = 159, PCH₂N); 53.62 (1C, d, ³J_{CP} = 6.0, CH₂); 60.40 (1C, ³J_{CP} = 9.0, CH₂); 62.03 (2C, ²J_{CP} = 7.0, OCH₂CH₃); 68.19 (1C, CH₂); 127.56 (1C, arom); 128.49 (2C, arom); 129.11 (2C, arom); 138.17 (1C, arom quaternary). ³¹P{¹H} NMR (121.4 MHz, CDCl₃): δ 24.80 (1P, s). ³¹P NMR (121.4 MHz, CDCl₃): δ 24.80 (1P, m).

Synthesis of 3. A solution of alkylating reagent **2** (2.71 g, 7.14 mmol, 1.70 equiv) in dry MeCN (30 mL) was dropwise added to a well-stirred suspension of tBu₃do3a-HBr (2.50 g, 4.20 mmol) and K₂CO₃ (1.15 g, 8.3 mmol, 2 equiv) in dry MeCN (45 mL). The reaction mixture was stirred at room temperature for 1 day and filtered, and the filtrate was evaporated on a rotary evaporator. The oily residue was dissolved in CHCl₃ (30 mL) and extracted with distilled water (4 × 15 mL). The organic layer was dried over Na₂SO₄ and concentrated *in vacuo* to give 4.50 g of a yellow oil containing crude compound **3** contaminated with an excess of the alkylating reagent **2** and the products of its degradation. Crude product **3** was used in the next step without purification.

³¹P{¹H} NMR (121.4 MHz, CDCl₃, 25 °C): δ 25.89 (1P, s). ³¹P NMR (121.4 MHz, CDCl₃): δ 25.89 (1P, m). MS-ESI: (+) 797.8 ([M + H]⁺, calcd 798.5); 819.9 ([M + Na]⁺, calcd 820.5).

Synthesis of 4. The total amount of crude compound **3** obtained above (4.50 g) was dissolved in a mixture of CF₃CO₂H and CHCl₃ (40 mL, 1:1 v/v). The resulting solution was refluxed for 18 h and then evaporated on a rotary evaporator. The oily residue was dissolved in a

small amount of distilled water and evaporated, and this procedure was repeated three more times. The oily residue was dissolved in a small amount of distilled water, and the solution was loaded onto a strong cation exchanger column (Dowex 50, H⁺-form, 4 cm × 15 cm). The impurities were removed by elution with water, and product 4 was eluted with aq NH₃ (5%). The fractions containing product 4 (¹H NMR check) were combined. After evaporation of volatiles, the oily residue was dissolved in water and poured onto a column of a weak cation exchanger (Amberlite CG50, 200–400 mesh, 4 cm × 15 cm). The impurities were eluted with water, and product 4 was collected by 20% aq CH₃COOH. The fractions containing product 4 were combined and evaporated to give 2.30 g of brownish oil, which was used in the next step without further purification.

When crude product 4 prepared in another batch was left to stand for several days, it solidified on standing. The sample for elemental analysis was isolated by washing this solid with ethanol, filtering, and then equilibrating the solid in ambient air.

¹H NMR (600 MHz, D₂O, 50 °C, pD = 6.74, Figure S1): δ 1.33 (6H, t, ³J_{HH} = 7.0, CH₂CH₃); 2.94 (2H, t, ³J_{HH} = 6.0, CH₂NCH₂Ph); 3.01–3.85 (6H, br, CH₂CH₂NCH₂Ph + macrocyclic CH₂); 3.11–3.16 (6H, br, NCH₂P + macrocyclic CH₂); 3.18–3.22 (4H, br m, macrocyclic CH₂); 3.29–3.34 (4H, br m, macrocyclic CH₂); 3.45 (4H, br s, CH₂CO); 3.58 (2H, br s, CH₂CO); 3.81 (2H, s, NCH₂Ph); 4.14 (4H, m, CH₂CH₃); 7.38–7.47 (5H, m, arom). ¹³C{¹H} NMR (150.9 MHz, D₂O, 50 °C, pD = 6.74, Figure S2): δ 16.30 (2C, OCH₂CH₃); 49.69 (1C, d, ¹J_{CP} = 160, PCH₂N); 49.69 (1C, d, ³J_{CP} = 8.0, CH₂NCH₂Ph); 49.91 (2C, macrocyclic CH₂); 50.71 (2C, macrocyclic CH₂); 50.86 (1C, CH₂CH₂NCH₂Ph); 51.11 (4C, macrocyclic CH₂); 56.40 (1C, CH₂CO); 57.47 (2C, CH₂CO); 60.66 (1C, d, ³J_{CP} = 8.5, CH₂Ph); 64.22 (1C, d, ²J_{CP} = 6.5, OCH₂CH₃); 128.52 (1C, arom); 129.34 (2C, arom); 13.21 (2C, arom); 138.44 (1C, arom quaternary); 173.73 (1C, CH₂CO); 174.94 (2C, CH₂CO). ³¹P{¹H} NMR (121.4 MHz, D₂O, pD = 6.74, Figure S3): δ 28.39 (1P, s). ³¹P NMR (121.4 MHz, D₂O, pD = 6.74, Figure S4): δ 28.39 (1P, m). MS-ESI: (+) 629.3 ([M + H]⁺, calcd 630.0); 652.0 ([M + Na]⁺, calcd 652.3); (–) 627.8 ([M – H][–], calcd 628.3). Elemental analysis found (calcd for 4·4H₂O, C₂₈H₄₆N₆O₁₃P, M_r = 701.8): C, 47.90 (47.92); H, 7.54 (8.04); N, 9.76 (9.98); P, 3.94 (4.41).

Synthesis of 5. The total amount of crude product 4 obtained above (2.30 g) was dissolved in concentrated aqueous HCl (20 mL) and stirred at 95 °C for 24 h. Then, the solution was evaporated on a rotary evaporator, dissolved in a small amount of water, and loaded onto a strong cation exchanger column (Dowex 50, H⁺-form, 4 cm × 15 cm). The impurities were removed by elution with water, and product 5 was eluted with 5% aq NH₃. The fractions containing the product were combined, filtered, and evaporated to give compound 5 (1.35 g) as a brownish oil which was used in the next step without further purification.

³¹P{¹H} NMR (121.4 MHz, D₂O, pD = 3.9): 7.68 (1P, s). ³¹P NMR (121.4 MHz, D₂O, pD = 3.9): 7.68 (1P, t, ³J_{HP} = 12.5). MS-ESI: (+) 574.0 ([M + H]⁺, calcd 574.3); 611.9 ([M + K]⁺, calcd 612.2); 633.9 ([M + Na + K – H]⁺, calcd 634.2); (–) 571.8 ([M – H][–], calcd 572.3); 609.8 ([M + K – 2H][–], calcd 610.2).

Synthesis of H₂do3aNP. Crude product 5 (1.30 g) was dissolved in 20% aq CH₂CO₂H (50 mL). Next, Pd/C catalyst (10%, 0.26 g) was added, and the flask was evacuated and filled by H₂. The mixture was stirred under a hydrogen atmosphere (using a rubber balloon) for 48 h at room temperature (RT). Then, the catalyst was removed by filtration, and all volatiles were evaporated *in vacuo*. The product H₂do3aNP was purified by chromatography on a strong cation exchanger column (Dowex 50, H⁺-form, 3 cm × 15 cm). Impurities were removed by elution with water, and the product H₂do3aNP was eluted with 5% aq pyridine. The fractions containing the product were combined, filtered, and evaporated to dryness leaving a glassy solid which was dissolved in a small amount of water and crystallized by standing for 2 h. The white crystalline solid was isolated by filtration, washed with EtOH, and air-dried to give a white powder of hydrate H₂do3aNP·4.5H₂O (1050 mg, 44% based on tBu₃do3a-HBr).

¹H NMR (600 MHz, D₂O, pD = 5.81, Figure S5): δ 2.86–2.94 (4H, br m, macrocyclic CH₂); 3.00–3.05 (4H, br, NCH₂CH₂NH +

macrocyclic CH₂); 3.07–3.10 (2H, br m, macrocyclic CH₂); 3.20 (2H, br s, CH₂CO₂); 3.23 (2H, d, ³J_{HP} = 12.0, NCH₂P); 3.30 (2H, br t, ³J_{HH} = 5.0, NCH₂CH₂NH); 3.30–3.37 (2H, br m, macrocyclic CH₂); 3.42–3.45 (2H, br m, macrocyclic CH₂); 3.53–3.56 (2H, br m, macrocyclic CH₂); 3.69–3.72 (2H, br m, macrocyclic CH₂); 3.88 (4H, AB-multiplet, CH₂CO₂). ¹³C{¹H} NMR (150.9 MHz, D₂O, pD = 5.81, Figure S6): δ 45.78 (1C, d, ¹J_{CP} = 136, NCH₂P); 46.54 (1C, d, ³J_{CP} = 3.5, CH₂NCH₂P); 48.97 (2C, macrocyclic CH₂); 49.00 (2C, macrocyclic CH₂); 50.36 (1C, CH₂CH₂NCH₂P); 51.08 (2C, macrocyclic CH₂); 53.02 (2C, macrocyclic CH₂); 55.71 (1C, CH₂CO); 57.83 (2C, CH₂CO); 170.92 (2C, CH₂CO); 178.98 (1C, CH₂CO). ³¹P{¹H} NMR (121.4 MHz, D₂O, pD = 5.81, Figure S7): δ 9.37 (1P, s). ³¹P NMR (121.4 MHz, D₂O, pD = 5.81, Figure S8): δ 9.37 (1P, s, ²J_{HP} = 12.0). MS-ESI: (+) 483.6 ([M + H]⁺, calcd 484.2); 505.6 ([M + Na]⁺, calcd 506.2); (–) 481.3 ([M – H][–], calcd 482.2); 519.1 ([M + Cl][–], calcd 518.2). Elemental analysis found (calcd for H₂do3aNP·4.5H₂O, C₁₇H₄₃N₆O_{13.5}P, M_r = 564.4): C, 36.22 (36.17); H, 8.09 (7.68); N, 12.17 (12.41); P, 5.61 (5.49).

Synthesis of Eu(III)–H₂do3aNP Complex. Three procedures for preparation of the Eu(III) complex of H₂do3aNP for NMR and MRI experiments were used. In the first one, EuCl₃·6H₂O was mixed with 1.05 equiv of the ligand in a small amount of distilled water. The pH was adjusted to 7 with 1 M aq NaOH, and the solution was stirred overnight at 60 °C. Then, the pH was readjusted to 7 with 1 M aq NaOH, and the solution was again stirred overnight at 60 °C.

In the second case, the Eu(III) complex was prepared by mixing the ligand with 1 equiv of Eu(III) acetate stock solution (concentration was determined by measuring BMS shifts)²⁸ in a small amount of distilled water. The pH was adjusted to ~8 with concentrated aq NH₃, and the mixture was stirred overnight at 60 °C. Then, the solution was filtered and evaporated to dryness leaving a glassy solid, which was dissolved in distilled water and evaporated on a rotary evaporator at 90 °C to remove ammonium acetate (this procedure was then repeated five more times).

In the third case, the Eu(III) complex was prepared by mixing EuCl₃·6H₂O with 1.05 equiv of the ligand in a small amount of distilled water. The pH was adjusted to ~8 with 0.8 M aq (NMe₄)OH, and the mixture was stirred overnight at 60 °C.

All prepared samples were checked using the xylenol orange test (acetate buffer, pH = 5.7) to exclude the presence of free Eu(III) ions. The exact concentration of Eu(III) complex in solution was determined using Evans' method.²⁸

Eu(III)–H₂do3aNP MS-ESI: (–) 631.6 with appropriate isotopic pattern ([M – H][–], calcd 632.1).

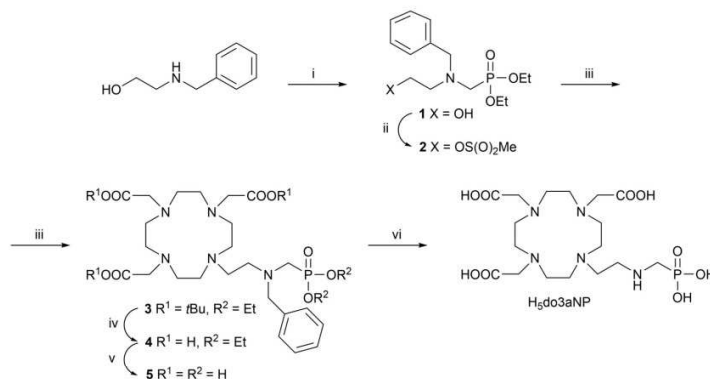
X-ray Diffraction Study. Single crystals of H₂do3aNP·4.75H₂O were prepared by slow evaporation of the aqueous solution of H₂do3aNP. Diffraction data were collected by employing an ApexII CCD diffractometer using Mo K α radiation (λ = 0.71073 Å) at 150(1) K and analyzed using the SAINT V8.27B (Bruker AXS Inc., 2012) program package. The structures were solved by direct methods (SHELXS97)²⁹ and refined by full-matrix least-squares techniques (SHELXL97).³⁰ Relevant data for the structures have been deposited at the Cambridge Crystallographic Data Centre. The structure was solved in space group *P*1, where the independent unit consists of two ligand molecules which have very similar conformations. However, higher symmetry (*c*/2) is prevented by disorder of the phosphonate moiety of one of the units. The 10 highest isolated electronic maxima were attributed to the water solvate molecules, one of them half-occupied due to collision with one position of disordered phosphonate oxygen atoms. All non-hydrogen atoms were refined anisotropically, and hydrogen atoms were fixed in theoretical (C–H, N–H) or original (O–H) positions using a riding model $U_{11} = 1.2U_x$.

Crystal data follow: H₂do3aNP·4.75H₂O, C₁₇H_{43.5}N₆O_{13.75}P, M_r = 569.04, triclinic, $a = 11.0215(3)$ Å, $b = 12.3502(3)$ Å, $c = 19.0688(6)$ Å, $\alpha = 84.311(1)^\circ$, $\beta = 80.106(1)^\circ$, $\gamma = 81.467(1)^\circ$, $V = 2521.46(12)$ Å³, space group *P*1, $z = 4$, 11576 total reflections, 8615 intense reflections, $R_1 [I > 2\sigma(I)] = 0.0535$, $wR_2(\text{all data}) = 0.1543$. CCDC-1500120.

Potentiometry. Potentiometric titrations were carried out in a thermostated (25.0 ± 0.1 °C) vessel at a constant ionic strength [I =

D

DOI: 10.1021/acs.inorgchem.6b02749
Inorg. Chem. XXXX, XXX, XXX–XXX

Scheme 1. Synthesis of H₅do3aNP^a

^a(i) HP(O)(OEt)₂, (CH₂O)_n, dry MeCN, 60 °C, 2 days; (ii) CH₃SO₂Cl, Et₃N, dry CH₂Cl₂, 0 °C–RT, 20 min; (iii) *t*Bu₃do3a-HBr, K₂CO₃, dry MeCN, RT, 24 h; (iv) CF₃COOH:CHCl₃ (1:1), reflux 18 h; (v) conc aq HCl, 95 °C, 24 h; (vi) H₂, Pd/C, 20% aq CH₃COOH, RT, 2 days.

0.1 M (Me₄N)Cl]. Measurements were taken with an excess of HCl stock solution added to the initial mixture, and the mixtures were titrated with stock solution of (NMe₄)OH. The ligand concentration in the titration vessel was ca. 0.004 M. An inert atmosphere was provided by a constant passage of argon saturated with water vapor. Before and after each titration, calibrations [titrations of HCl stock solution with (NMe₄)OH stock solution] were performed for determination of electrode calibration parameters as described previously.³¹

For determination of the ligand protonation constants, a standard technique was used,³¹ with the initial volume ca. 5 cm³ and in the pH range 1.9–12.1. Four titrations were carried out with ~70 points per titration.

Titrations of the Eu(III)–H₅do3aNP system were performed by an out-of-cell technique³¹ as the equilibrium was established slowly. In the experiments, the metal-to-ligand molar ratio was 1.00:1.04, and the starting volume of each titration point [before addition of (NMe₄)OH] was ca. 1 cm³. In total, two titration sets in the pH range 1.8–9.0 were prepared with 30 points per titration, and ampoules with solutions were flame-sealed. After 4 weeks (waiting time for equilibration), the potential of each solution was determined with a freshly calibrated electrode, with measurement of odd and even data points separately affording four independent data series of 15 data points.

A preformed Eu(III) complex for determination of its protonation constants was prepared in the following way: in the ampoule, equimolar amounts of the ligand and metal stock solutions were mixed, and a calculated amount (based on out-of-cell titration data) of (NMe₄)OH stock solution was gradually added to reach pH ca. 6, which corresponds to full complexation according to the out-of-cell titration. Ampoules were flame-sealed and left at 55 °C for 3 days. From the final solution, aliquot volumes were pipetted, a defined amount of HCl stock solution was added into these samples, and the mixtures were immediately titrated by (NMe₄)OH stock solution in an analogous way as described above for the determination of the ligand protonation constants; the concentration of the complex in the titration vessel was ca. 0.003 M. The pH range used in these titrations was 1.9–9.5, and the titrations were carried out four times with 30 points per titration.

The OPIUM program package³² was used for calculation of the ligand protonation constants and stability/protonation constants of the Eu(III) complex. All constants are concentration constants. Calculated protonation constants are defined as $\beta_h = [H_hL]/\{[H]^h[L]\}$, and they can be transferred to consecutive protonation constants $\log K$ by $\log K(H_hL) = \log \beta_h - \log \beta_{h-1}$. Calculated stability constants β_{hlm} are defined by $\beta_{hlm} = [H_hL]_m/[H]^h[L]^m$.

Calculated constants with their standard deviations are compiled in Tables S8–S10, and the fits of titration data are shown in Figures S27, S31, and S32. The water ion product used in all calculations was $pK_w = 13.81$.³³

³¹P and ¹H NMR Titration of H₅do3aNP and Its Eu(III) Complex. ³¹P and ¹H NMR spectra were performed on a VNMR300 (B₀ = 7.05 T) using 5 mm sample tubes. A coaxial capillary with 85% H₃PO₄ in H₂O ($\delta_p = 0$) or with *t*BuOH in D₂O ($\delta_H = 1.25$) as the external standard was used. Solution pH was measured with a combined glass electrode (Spinrode Hamilton) employing a pH meter (3505 pH Meter, JENWAY) calibrated with standard buffers. Protonation constants were calculated with the OPIUM software package.³²

³¹P NMR titration (46 points) for determination of protonation constants and sites of H₅do3aNP was performed at 25 °C (0.05 M ligand concentration; no ionic strength control) in H₂O. The solution pH (0.1–13.6) was adjusted with aq HCl or aq (NMe₄)OH solutions. The fit is shown in Figure S28.

¹H NMR titration of H₅do3aNP in the alkaline region (14 points) was performed at 25 °C (0.05 M ligand concentration; no ionic strength control) in H₂O. Solution pH (7.9–12.0) was adjusted with aq HCl or aq KOH solutions. The fit is shown in Figure S29.

³¹P NMR titration in acidic region (14 points) of preformed Eu(III)–H₅do3aNP complex was performed at 25 °C (0.038 M complex concentration; ~150 mM NaCl) in H₂O. Solution pH (from 7.0 to 2.0) was adjusted with aq HCl solutions. The fit is shown in Figure S20.

MRS Experiments. A phantom consisting of one vial containing an aq solution of H₃PO₄ as a reference and three vials containing ~50 mM aq solutions of the Eu(III)–H₅do3aNP complex (~150 mM NaCl) with different pH values (6.4, 8.0, and 9.0) was prepared for MRS experiments. At these pH values, the once protonated complex [Eu(Hdo3aNP)][−] and the fully deprotonated species [Eu(do3aNP)]^{2−} are present, with the former predominant at pH = 6.4 and the latter at pH = 9.0. At pH = 8.0, both species are present in similar abundance (see distribution diagram in Figure 6).

All MRS experiments were performed on a 4.7 T MR scanner BioSpec (Bruker BioSpin, Germany) using a dual ¹H/³¹P surface coil with a diameter of 5 cm (Bruker BioSpin, Germany). Nonlocalized ³¹P MRS spectra of the phantom were acquired by using a single rectangular pulse with 0.064 ms duration and 20000 Hz bandwidth (BW); the other measurement parameters were the following: acquisition delay 0.05 ms, repetition time (TR) = 1000 ms, number of acquisitions (NA) = 512, and scan time 8.5 min. For ¹H reference

E

DOI: 10.1021/acs.inorgchem.6b02749
Inorg. Chem. XXXX, XXX, XXX–XXX

images, a turbo spin echo sequence was used with the following parameters: TR/TE = 3000 ms/12 ms, turbo factor = 8, matrix size of 256 × 256, field of view (FOV) = 35 mm × 35 mm, slice thickness 1 mm, and scan time 5 min. ³¹P MRSI spectra localized from 4 × 4 voxels covering the whole phantom volume were acquired by chemical shift imaging sequence using the same rectangular pulse as for the nonlocalized ³¹P MR spectra. Spectral width 20 kHz (246.44 ppm) was sampled by 8192 points. The spectra were acquired by 16384 accumulations from the volume with field of view = 32 mm × 32 mm and slice thickness 10 mm; the other parameters were TR = 1000 ms, effective echo time (TE_{eff}) = 15 ms, and scan time 4.5 h. Raw data were interpolated to a matrix 32 × 32 × 8192 by zero-filling, and Fourier transform provided a three-dimensional matrix of numbers containing information about signal amplitude spatially encoded in *x*- and *y*-axis; frequency chemical shift was encoded in *z*-axis.

³¹P MRSI data were processed using ImageJ software (version 1.46r, National Institutes of Health). First, the data were interpolated into a matrix size of 256 × 256 × 256. Then, the images acquired within an interval of 70 ± 4 ppm were summed (to obtain an integral signal) as well as the images in the interval of 0 ± 4 ppm and -118 ± 4 ppm, and were finally false color coded.

RESULTS AND DISCUSSION

Synthesis. The target ligand H₃do3aNP was prepared following the multistep synthesis outlined in Scheme 1. The key phosphorus-containing intermediate **1** was obtained by Mannich-type reaction of *N*-benzyl-ethanolamine with diethylphosphite and paraformaldehyde and was isolated after cation-exchange chromatography. It was converted to alkylation agent **2** by reaction with methanesulfonyl chloride, and compound **2** was used in the reaction with *t*Bu₃do3a, affording intermediate **3**. After sequential deprotection of *t*Bu-ester and ethyl-ester groups using trifluoroacetic acid and aq hydrochloric acid, respectively, the de-esterified compound **5** was hydrogenated using the Pd/C catalyst to give the target ligand H₃do3aNP that was purified by cation-exchange chromatography and was isolated in the zwitterionic form in the overall 44% yield (based on *t*Bu₃do3a-HBr).

The target ligand H₃do3aNP was structurally characterized by single-crystal X-ray diffraction analysis. In the crystal structure of H₃do3aNP·4.75H₂O, two independent ligand molecules are present, but both adopt a very similar conformation. Therefore, only one of them is shown in Figure 2. A zwitterionic molecule is protonated on two nitrogen atoms of the macrocycle (those bearing the “*trans*” acetate groups) and the nitrogen atom of the side arm. The remaining protons are located on the phosphonate and on the “odd” acetate groups. Molecular conformation is stabilized by medium-strength intramolecular hydrogen bonds (Table S1), and the whole structure is stabilized through a wide system of intermolecular hydrogen bonds involving water molecules.

Solution Structure of the Eu(III)–H₃do3aNP Complex. Ln(III) complexes of the DOTA-like ligands are typically present in a solution as a mixture of square-antiprismatic (SA) and twisted-square-antiprismatic (TSA) isomers.³⁴ These isomers differ in conformation of the five-membered chelate rings of the macrocycle (δ/λ) and course of rotation of the pendant arms (Δ/Λ). Combination of the macrocycle and pendant conformations results in two diastereomeric pairs of the enantiomers (Figure S9). The pair $\Delta\lambda\lambda\lambda/\Lambda\delta\delta\delta$ forms the SA arrangement while the $\Delta\delta\delta\delta/\Lambda\lambda\lambda\lambda$ enantiomers correspond to the TSA structure.³⁵ Typically, two diastereomers are in a slow exchange with respect to the time scale of an NMR experiment, giving rise to two sets of ¹H NMR signals. Therefore, both isomers can be distinguished, and their relative

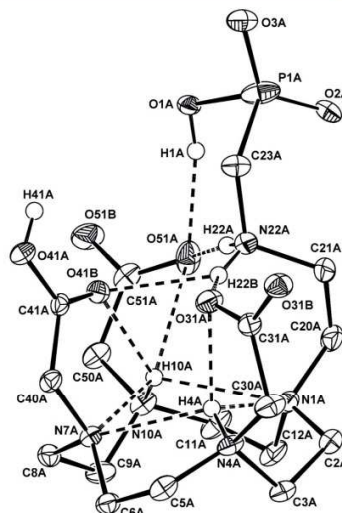


Figure 2. Molecular structure of H₃do3aNP found in the crystal structure of H₃do3aNP·4.75H₂O. Intramolecular hydrogen bonds are dashed (Table S1).

abundance in solution can be easily determined. Isomerism evaluation mostly uses signals of “axial” protons of the macrocyclic ring (Figure S9) because these are the closest ones to the Ln(III) ion and to the principal magnetic axis; thus, they are shifted away from the other signals in the ¹H NMR spectra. Typically, “axial” signals of the TSA species of Eu(III) complexes with DOTA-like ligands are found in the ~7–28 ppm range whereas those of the SA isomers appear in the ~25–40 ppm region.³⁶

Solution structure of the Eu(III) complex species was investigated by ¹H NMR spectroscopy in the pD range 6.8–9.9 (Figure 3 and Figure S10). At pD < 7.3, only one set of signals was observed in the ¹H NMR spectra, where the signals of the most positively shifted “axial” protons of the complex species appear in the range typical for the SA isomer (20–49 ppm). At higher temperatures, the ¹H NMR signals somewhat shift and broaden due to faster conformational changes of the complex molecule (Figure S11). With increasing pD, ¹H NMR signals of the SA isomer gradually disappear with a simultaneous appearance of peaks attributable to the TSA isomer with the most shifted signals in the 7–14 ppm range (Figure 3 and Figure S10). Thus, one can suggest that both SA and TSA species are present in the pD range 7.5–9.0 (Figures S10, S12, and S13). At pD > 9.0, only signals of pure TSA species were detected. Heating of the alkaline solution also led to a significant broadening of signals of the TSA isomer, pointing to conformational change of the complex molecule (Figures S12 and S14). On the basis of these observations, one can suggest that two differently protonated species are present in the pD range 7.5–9.0; so, the pK_A of the deprotonation process lies in this range, and thus, the deprotonation obviously occurs on the pendant amino group. The protonated form of the complex exists exclusively in the SA isomer, whereas the pure TSA species is formed upon deprotonation.

F

DOI: 10.1021/acs.inorgchem.6b02749
Inorg. Chem. XXXX, XXX, XXX–XXX

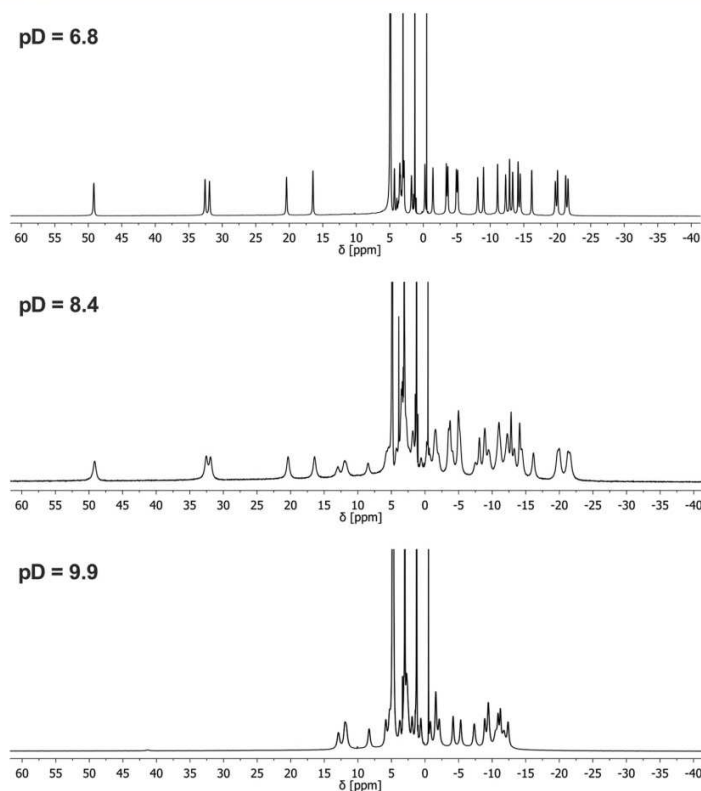


Figure 3. ^1H NMR spectra of $\text{SA}[\text{Eu}(\text{Hdo3aNP})]^-/\text{TSA}[\text{Eu}(\text{do3aNP})]^{2-}$ (~ 0.08 M solution in D_2O , $B_0 = 7.05$ T) at different pD values.

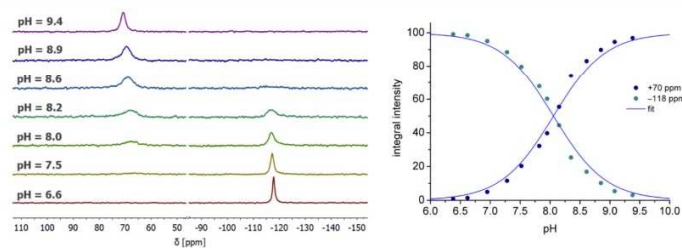


Figure 4. $^{31}\text{P}\{^1\text{H}\}$ NMR spectra of $\text{SA}[\text{Eu}(\text{Hdo3aNP})]^-/\text{TSA}[\text{Eu}(\text{do3aNP})]^{2-}$ complex species at various pH values and corresponding pH dependence of an integral intensity of ^{31}P NMR signals (50 mM solution in H_2O , ~ 150 mM NaCl, $B_0 = 7.05$ T, 25°C).

^{31}P NMR spectroscopic study also revealed a slow chemical exchange between both complex species with respect to the time scale of the NMR experiment (Figure 4 and Figures S16 and S18) as the signals of both species are present in the ^{31}P NMR spectra acquired in the pH range 7.5–8.9; their chemical shifts remain nearly constant with pH change. ^{31}P NMR 1D-EXSY revealed a rate for isomer interconversions on a

millisecond scale (rate constants $191(8) \text{ s}^{-1}$ for $\text{SA} \rightarrow \text{TSA}$ and $156(7) \text{ s}^{-1}$ for $\text{TSA} \rightarrow \text{SA}$ rearrangements, respectively, 25°C , pD = 8.6). In addition, an extreme chemical shift difference (by ~ 190 ppm) between signals of the SA and TSA species was observed. In both species, the phosphonate group is obviously coordinated, as evidenced by a significantly influenced ^{31}P NMR chemical shift (+70 ppm for the TSA and -118 ppm for

G

DOI: 10.1021/acs.inorgchem.6b02749
Inorg. Chem. XXXX, XXX, XXX–XXX

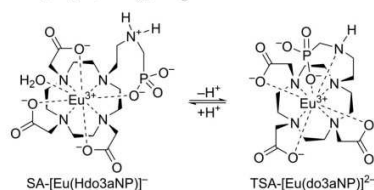
the SA species, respectively, Figure 4) compared to that for the diamagnetic La(III) complex ($\delta = 25.3$ ppm at pD = 7.0 and $\delta = 22.7$ ppm at pD = 10.1). The coordination of the phosphonate group was also confirmed by measurement of T_1 relaxation times of ^{31}P NMR signal, which are $T_1 = 0.207(4)$ s for the SA species (measured at pD = 6.8) and $T_1 = 0.202(11)$ s for the TSA species (pD = 9.6), respectively, whereas the La(III) complex relaxes much slower with $T_1 = 1.84(8)$ s (pD = 7.0) and $T_1 = 3.09(10)$ s (pD = 10.1).

The dependence of integral intensities of these signals on pH is sigmoidal and, in accordance with the suggestion stated above, could be successfully modeled by the suggestion stated above, involving just one (de)protonation step (Figure 4 and Figures S16–S18), affording the protonation constant $\log K(=pK_a) = 7.4\text{--}8.5$ with dependence on ionic strength, see Table S2. The ^{31}P chemical shifts of both species (Figures S16 and S18) and derived protonation constants (Table S2) are independent of complex concentration; therefore, intermolecular coordination of the phosphonate to the metal ion belonging to a different complex molecule and the formation of polynuclear complexes can be excluded. Furthermore, the protonated complex was found to be fully stable at pD = 5.9 (Figure S19). The value of the protonation constant $\log K$ is dependent on the quality and concentration of a background electrolyte: in the presence of NaCl, the value drops with increasing concentration of the salt because the presence of a coordinating metal ion generally facilitates a deprotonation of the donor atoms. In contrast, when ^{31}P NMR titration was performed with the use of $(\text{NMe}_2)\text{Cl}$ as the background electrolyte, the value of the protonation constant was significantly higher (Table S2). In the presence of CaCl₂ and MgCl₂, i.e., in the presence of stronger coordinating metal ions (Figure S18), the chemical shifts in ^{31}P NMR spectra remain unaffected, and $\log K$'s are lower than those calculated in the case of NaCl-containing solutions (Table S2).

On the basis of the value of $\log K$, the protonation process obviously occurs on the pendant arm amino group, and thus, one can conclude that the equilibrium involves monodeprotonated and fully deprotonated complex species; thus, the complex species are $\text{SA}[\text{Eu}(\text{Hdo3aNP})]^-$ and $\text{TSA}[\text{Eu}(\text{do3aNP})]^{2-}$. To confirm such an assignment, the ^1H NMR spectra were also measured in H_2O solution. In a slightly acid region, no difference between the spectra of $\text{SA}[\text{Eu}(\text{Hdo3aNP})]^-$ acquired in D_2O and H_2O was found (Figure S15A,B). At this pH, the side amino group is protonated (and thus uncoordinated), and the hydrogen atoms are exchanged with the solvent (D_2O) or overlaid with others; on the basis of chemical exchange saturation transfer experiments, chemical shift of these hydrogen atoms is -17 ppm if referenced as $\delta(\text{H}_2\text{O}) = 0$.³⁷ In contrast, in a slightly alkaline region, a new signal at 36.4 ppm (if referenced as $\delta(\text{H}_2\text{O}) = 0$) appeared in the spectra of $\text{TSA}[\text{Eu}(\text{do3aNP})]^{2-}$ acquired in H_2O (Figure S15C,D). This peak can be attributed to a hydrogen atom bound in the coordinated pendant secondary amino group, where this hydrogen atom is not in fast exchange with the solvent. This assignment is also supported by a similarity in the chemical shift of this signal to the values observed for structurally related compounds $[\text{Eu}(\text{do3a-ae})]$ and $[\text{Eu}(\text{do3aNN})]$ (Figure 1), respectively; one of the ^1H NMR signals of the coordinated primary amino group in $[\text{Eu}(\text{do3a-ae})]$ lies at 34 ppm,⁴⁴ and the signal of one of the isomers of $[\text{Eu}(\text{do3aNN})]$ with a coordinated secondary amino group is located at 35 ppm.¹⁵

With mononuclearity of the complex species taken into account, electrostatic repulsion of the central metal ion and the protonated pendant amino group, as well as general steric hindrances, the phosphonate group should be in the protonated $\text{SA}[\text{Eu}(\text{Hdo3aNP})]^-$ species coordinated in the O_4 -plane (Scheme 2). In such a case, it opens a space for coordination of

Scheme 2. Suggested Geometry of the $\text{SA}[\text{Eu}(\text{Hdo3aNP})]^-$ and $\text{TSA}[\text{Eu}(\text{do3aNP})]^{2-}$ Species^a



^aA water molecule in the protonated species is expected to be coordinated in the apical position.

a water molecule in an O_4 -capping apical position. Luminescence lifetimes of Eu(III) ion were measured, giving $\tau = 697 \mu\text{s}$ for $\text{SA}[\text{Eu}(\text{Hdo3aNP})]^-$ species in H_2O (pH = 6.4) and $\tau = 2.21$ ms when this sample was evaporated and dissolved in D_2O , consistent with the assumption of water coordination.³⁸ After deprotonation, coordination of the secondary amino group occurs and forms an O_3N -coordination plane in the $\text{TSA}[\text{Eu}(\text{do3aNP})]^{2-}$ species. The phosphonate group very probably moves to the position capping this O_3N -plane (Scheme 2). However, although the geometry discussed above is the sole possibility making chemical sense, it is a bit contradictory in a comparison of the ^{31}P NMR shift of $\text{SA}[\text{Eu}(\text{Hdo3aNP})]^-$ species with that of Eu(III) complexes of DOTA-like ligands having methylenephosphonate/phosphinate pendant moieties, which have a phosphorus atom in a similar spatial position as that expected for $\text{SA}[\text{Eu}(\text{Hdo3aNP})]^-$. To the best of our knowledge, in all Eu(III) complexes of phosphinate/phosphonate ligands reported previously, the paramagnetic contribution to the ^{31}P NMR shift is positive, giving signals with 15–70 ppm higher chemical shift compared to that of the free ligands or diamagnetic La(III) complexes (Table S3).^{36b,c,e,f,39,40} Contrary to these values, when comparing ^{31}P NMR shift differences between Eu(III) and La(III) complexes of $\text{H}_3\text{do3aNP}$ in acid media, the paramagnetic contribution to chemical shift of $\text{SA}[\text{Eu}(\text{Hdo3aNP})]^-$ is $\Delta\delta = -143$ ppm.

The origin of this contradiction probably lies in the low symmetry of the ligand field of the $\text{SA}[\text{Eu}(\text{Hdo3aNP})]^-$ complex, which can lead to a discrepancy between principal magnetic and pseudo- C_4 axes and to significant anisotropy of magnetically induced shifts.⁴¹ Typically, the complexes of DOTA-like ligands have (pseudo)- C_4 symmetry, and it is usually suggested that the principal magnetic axis is identical with (or very close to) the (pseudo)symmetry C_4 axis. In such axially symmetric systems, the phosphorus atoms lie outside the McConnell cone, which defines a sign of paramagnetic contribution to the chemical shift [in relevant crystal structures, angle between (pseudo)- C_4 axis and Ln–P vector is $73\text{--}89^\circ$ (Figure S22 and Table S4),^{36c,b,40,42} whereas the McConnell critical angle is 54.7°]. It should be noted that, for historical reasons, the direction of upfield–downfield shifts differs for ^1H

H

DOI: 10.1021/acs.inorgchem.6b02749
Inorg. Chem. XXXX, XXX, XXX–XXX

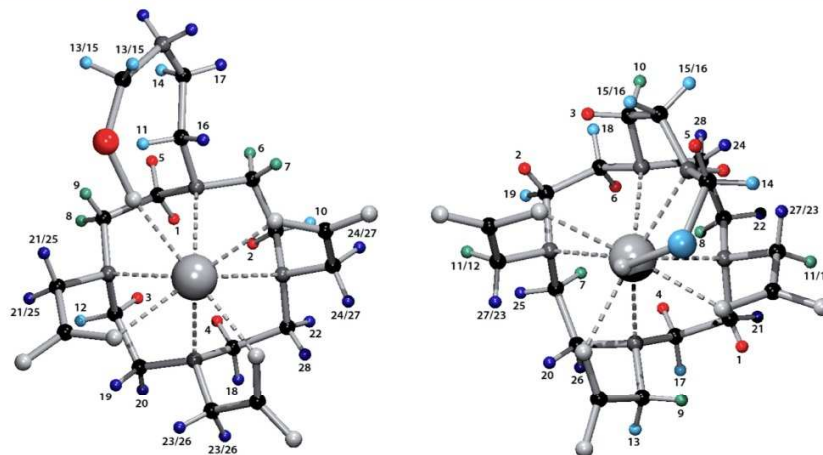


Figure 5. Assignment of the ^1H NMR spectra of $\text{SA}[\text{Eu}(\text{Hdo3aNP})]^-/\text{TSA}[\text{Eu}(\text{do3aNP})]^{2-}$ complex species. Geometry of the complex species is tentative and was not optimized. Atoms are labeled by order numbers from the spectra going from left to right according to Figure S24. For better visualization, protons with positive paramagnetic contribution are red, those with small negative contribution are pale blue, those with large negative contribution dark blue, and those which are not influenced are green. For phosphorus atom, the red color indicates a negative ^{31}P NMR shift contribution (i.e., position in space with positive ^1H NMR shift contribution), and blue indicates a positive ^{31}P NMR shift contribution (i.e., space with negative ^1H NMR shift contribution).

Table 1. Equilibrium Constants ($\log K$ and $\log K_{\text{ML}}^{\text{st}}$) of $\text{H}_3\text{do3aNP}$ (0.1 M NMe_4Cl , 25 $^\circ\text{C}$) and Its Eu(III) Complexes and Comparison with Corresponding Constants Reported for Related Ligands

equilibrium	$\text{H}_3\text{do3aNP}$ potentiometry	$\text{H}_3\text{do3aNP}$ ^{31}P NMR	$\text{H}_3\text{do3aNN}^b$	$\text{H}_3\text{do3a-ae}^c$	H_4dota
$\text{H}^+ + \text{L}^{n-} \leftrightarrow \text{HL}^{(n-1)-}$	12.56(1)	12.52(17)	12.62	13.19	12.9 ^e
$\text{H}^+ + \text{HL}^{(n-1)-} \leftrightarrow \text{H}_2\text{L}^{(n-2)-}$	10.37(1)	10.59(3)	10.28	10.51	9.72 ^e
$\text{H}^+ + \text{H}_2\text{L}^{(n-2)-} \leftrightarrow \text{H}_3\text{L}^{(n-3)-}$	9.23(1)	9.37(8)	9.67	8.90	4.60 ^e
$\text{H}^+ + \text{H}_3\text{L}^{(n-3)-} \leftrightarrow \text{H}_4\text{L}^{(n-4)-}$	6.17(1)	5.96(8)	8.30	3.87	4.15 ^e
$\text{H}^+ + \text{H}_4\text{L}^{(n-4)-} \leftrightarrow \text{H}_5\text{L}^{(n-5)-}$	4.19(1)		3.30	1.27	2.29 ^e
$\text{H}^+ + \text{H}_5\text{L}^{(n-5)-} \leftrightarrow \text{H}_6\text{L}^{(n-6)-}$	1.90(1)	2.05(9)	1.58		1.34 ^e
$\text{Eu}^{3+} + \text{L}^{n-} \leftrightarrow [\text{Eu}(\text{L})]^{(3-n)-}$	23.49(3)		23.16	22.23 ^d	24.2 ^f
$\text{H}^+ + [\text{Eu}(\text{L})]^{(3-n)-} \leftrightarrow [\text{Eu}(\text{HL})]^{(4-n)-}$	8.00(3)		6.03	5.83 ^d	
$\text{H}^+ + [\text{Eu}(\text{HL})]^{(4-n)-} \leftrightarrow [\text{Eu}(\text{H}_2\text{L})]^{(5-n)-}$	3.75(4)		5.09		
$\text{H}^+ + [\text{Eu}(\text{H}_2\text{L})]^{(5-n)-} \leftrightarrow [\text{Eu}(\text{H}_3\text{L})]^{(6-n)-}$	4.35(4)				
$\text{H}^+ + [\text{Eu}(\text{H}_3\text{L})]^{(6-n)-} \leftrightarrow [\text{Eu}(\text{H}_4\text{L})]^{(7-n)-}$	3.31(4)				

^a $K = [\text{H}_n\text{L}]/\{[\text{H}][\text{H}_{(n-1)}\text{L}]\}$ or $[\text{H}_n\text{LM}]/\{[\text{H}][\text{H}_{(n-1)}\text{LM}]\}$; $K_{\text{ML}} = [\text{ML}]/\{[\text{L}][\text{M}]\}$. ^bRef 15. ^cRef 44. ^dData reported for Gd(III) complex. ^eRef 45. ^fRef 33.

and ^{31}P NMR scales; therefore, in the same space, the ^{31}P NMR paramagnetic induced shift contribution is positive whereas that of ^1H NMR is negative (and *vice versa*). However, in the case of the $\text{SA}[\text{Eu}(\text{Hdo3aNP})]^-$ complex, there is a large difference in chemical shifts of "axial" macrocycle protons [these protons have a similar position with respect to pseudo- C_4 symmetry defined by the central ion and the barycenter of the N_4 -plane, and thus, they should have a similar chemical shift when the magnetic axis is identical to the (pseudo)symmetry axis]; this points to some difference between positions of pseudosymmetric- C_4 and principal magnetic axes. Therefore, the phosphorus atom could fall into a space close to the principal magnetic axis direction with induced positive ^1H /negative ^{31}P NMR shifts. To confirm this assumption, the signals found in ^1H NMR spectra of both $\text{SA}[\text{Eu}(\text{Hdo3aNP})]^-$ and $\text{TSA}[\text{Eu}(\text{do3aNP})]^{2-}$ complexes were assigned on the basis of ^1H

COSY and ^1H EXSY experiments and ^{13}C NMR spectra with selectively tuned ^1H decoupling (Figure S23–S26 and Tables S5–S7). The assignment is shown in Figure 5 (for detailed description see S1). This assignment confirmed that the position of the phosphorus atom moves from a space with induced positive ^1H /negative ^{31}P NMR shifts in $\text{SA}[\text{Eu}(\text{Hdo3aNP})]^-$ to an area with negative ^1H /positive ^{31}P NMR shifts in $\text{TSA}[\text{Eu}(\text{do3aNP})]^{2-}$ complexes, respectively. Another surprising finding is the fact that the most shifted signals in ^1H NMR spectra of $\text{TSA}[\text{Eu}(\text{do3aNP})]^{2-}$ species are not the "axial" ones. In this case, the direction of the most positive ^1H induced shift probably lies almost parallel in respect to the N_4 -plane, so the principal magnetic axis should be almost perpendicular to the pseudo- C_4 axis. The phosphorus atom falls outside this direction, and so, its induced ^{31}P paramagnetic shift is positive in the ^{31}P NMR scale.

1

DOI: 10.1021/acs.inorgchem.6b02749
Inorg. Chem. XXXX, XXX, XXX–XXX

Further acidification of the solution of the SA-[Eu(Hdo3aNP)]⁻ species leads to a gradual change of the ³¹P chemical shift from -118 ppm at pH = 7 to -156 ppm at pH = 2 (Figure S20). Obviously, as the chemical shift is very affected in the whole of this pH region, the phosphonate group is still coordinated, and the gradual change of the chemical shift corresponds to formation of the SA-[Eu(H₂do3aNP)] species. From the ³¹P NMR data, log *K* = 3.40(1) was calculated which confirms this assignment because the protonation constant of the free phosphonate group (log *K* ~ 5–7) drops to the log *K* ~ 3–4 range upon coordination to the metal ion.⁴³ Formation of the SA-[Eu(H₂do3aNP)] species was also supported by the ¹H NMR spectra of the complex in acidic solution (Figure S21).

Thermodynamic Behavior of H₂do3aNP and Its Eu(III) Complex. To obtain information on thermodynamic stability of the studied Eu(III) complex and confirm the conclusions stated above, potentiometric studies of the H₂do3aNP, equilibrated Eu(III)–H₂do3aNP system and preformed Eu(III)–H₂do3aNP complex were performed.

The potentiometric titrations of H₂do3aNP performed in the pH range 1.9–12.1 revealed six consecutive protonation processes (Table 1 and Table S8; fit shown in Figure S27); the ligand distribution diagram is shown in Figure S30. Five of these constants could also be calculated from the pH dependence of the ³¹P NMR spectra (Table 1 and Table S8, fit shown in Figure S28). On the basis of comparison with the literature data,⁴³ the first protonation step (log *K*(HL) = 12.56) can be attributed to a proton shared by the macrocycle amino groups. This assignment of the protonation site is consistent with a relatively small change (+0.5 ppm) of the ³¹P NMR shift and a large change of the ¹H chemical shift of the α-acetate protons (+0.21 and +0.28 ppm for “double” and “odd” acetates, respectively) compared to that of the NCH₂P group (+0.05 ppm), see Table S8 and Figure S29. According to the highest change (~6 ppm) in ³¹P chemical shift during the NMR titration, the second protonation step (log *K*(H₂L) = 10.37) obviously occurs on the amino group belonging to the pendant moiety. It is also consistent with changes observed in ¹H NMR spectra; change of δ(¹H) of NCH₂P is 0.25 ppm, much higher than the δ(¹H) changes of the acetate groups (0.11 and 0.08 ppm, respectively, see Table S8). The value of the protonation constant is higher than the value reported for the analogous protonation of the 2-aminoethyl arm for H₂do3a-ae (log *K* = 8.90)⁴⁴ due to the positive induction effect of the phosphonate moiety.⁴³ Analogous protonation of H₂do3aNN occurs in this pH region, although in that case it was not possible to assign an exact value due to a number of protonation steps occurring with similar log *K*'s.¹⁵ The third protonation (log *K*(H₃L) = 9.23) corresponds to the second protonation of the macrocycle amino groups. The log *K*(H₃L) is somewhat lower than the second ring-amine protonation of related ligands due to electrostatic repulsion with a protonated pendant amino group. The third protonation locks two protons on the macrocycle nitrogen atoms bearing “trans” acetate groups due to mutual electrostatic repulsion, as evidenced by change of δ(¹H) (+0.38 and -0.26 ppm for “double” and “odd” acetates, respectively, see Figure S29). The fourth protonation with log *K*(H₄L) = 6.17 occurs on the phosphonate moiety, as evidenced by a reverse change of the ³¹P NMR shift (Figure S28). The next one (log *K*(H₅L) = 4.19) is associated with the protonation of the acetate *trans* to the aminophosphonate arm, and it has no influence on the chemical shift of the ³¹P NMR

signal due to a long distance between these groups, so this constant cannot be calculated from ³¹P NMR data. The last (sixth) protonation occurs on one of the remaining acetate arms or macrocycle amino groups. The suggested protonation scheme is fully consistent with the molecular structure found in the solid state (see above).

The stability constant of the [Eu(do3aNP)]²⁻ complex (log *K*_{ML} = 23.49, Table 1) was obtained by an out-of-cell titration technique. The value falls into the expected range, as can be seen from a comparison with the stability constants reported for the related ligands (Table 1). According to the distribution diagrams of the Eu(III)–H₂do3aNP system shown in Figure 6, the metal ion complexation is quantitative at pH ~ 4.5.

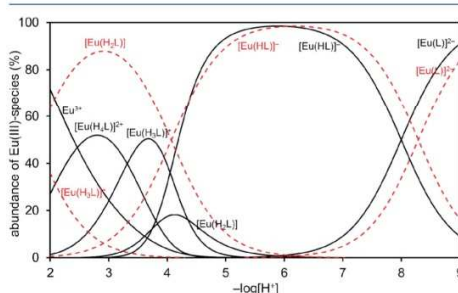


Figure 6. Distribution diagram of metal-containing species in the Eu(III)–H₂do3aNP system (black solid lines, *c*_M = *c*_L = 0.004 M) and of species present in acid–base titration of the preformed [Eu(do3aNP)]²⁻ complex (red dashed lines) Conditions: 25 °C, *I* = 0.1 M NMe₄Cl.

The first protonation of the fully deprotonated species, [Eu(do3aNP)]²⁻, proceeds with log *K*(HLM) = 8.0. In the analysis of the NMR spectra (see above), this protonation was suggested to occur on the side arm secondary amino group. The protonation constant of this group in the free ligand has the value log *K*(H₂L) = 10.37, and so a significant metal-induced decrease of this value confirms coordination of the deprotonated amino group to the central Eu(III) ion.

A further three protonation steps in the equilibrated solutions occur with log *K*'s in a narrow range ~3–4 (Table 1). These processes occur at pH higher than that corresponding to protonation of the coordinated acetate group and, thus, can be attributed to simultaneous protonations of the phosphonate group and the macrocycle nitrogen atoms. Therefore, the equilibrated species H₃LM and H₄LM are expected to be out-of-cage complexes with double-protonated macrocycle amino groups similar to those suggested for other systems with DOTA-like ligands.⁴⁰

To support the conclusions stated above, an acid–base titration of the preformed complex was performed. In this case, only three stepwise protonation constants were found: log *K*(HLM) = 8.29(2), log *K*(H₂LM) = 4.07(3), and log *K*(H₃LM) = 1.75(3) (see Table S10 and distribution diagram in Figure 6). According to the interpretation above, the first constant corresponds to a protonation of the pendant amino group, and this value is consistent with the results of ³¹P NMR and out-of-cell potentiometric studies. The second constant is assigned to protonation of the coordinated phosphonate group, consistent with the ³¹P NMR data presented above. The

J

DOI: 10.1021/acs.inorgchem.6b02749
Inorg. Chem. XXXX, XXX, XXX–XXX

differences between values obtained by the ^{31}P NMR and potentiometric titrations can be attributed to a difference in ionic strength, different methods of pH electrode calibration, and temperature of the pH measurement. The third constant calculated for the preformed complex is significantly lower compared to constants observed in the equilibrated solutions (out-of-cell titration). One can assume that during the short time scale of the potentiometric titration only the in-cage complex is present (i.e., no dissociation of macrocycle–Eu(III) bonds occurs) due to relative kinetic inertness of the complexes with DOTA-like ligands,¹ and therefore, this constant corresponds very probably to the protonation of a coordinated carboxylate group.

Overall, the results of the potentiometric study are fully consistent with the results of ^{31}P NMR studies discussed above and support the interpretation shown in Scheme 2.

pH Mapping Using MRS. To address possible pH determination from ^{31}P NMR data, the logarithm-weighted ratio of integral intensity of the ^{31}P NMR signals of TSA-[Eu(do3aNP)]²⁻ and SA-[Eu(Hdo3aNP)]⁻ was calculated. This function is linear in the pH range 6.5–9.5, as shown in Figure 7, proving the principle of the suggested method (the data were observed at various experimental conditions).

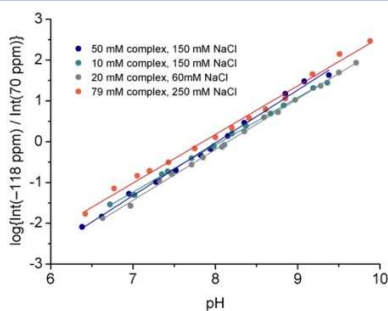


Figure 7. Dependence of $y = \log\{\text{[SA]}/\text{[TSA]}\}$ on pH in solutions with different concentrations of the complex probe and at different ionic strengths relevant for physiologic conditions.

Finally, we tested the applicability of the [Eu(do3aNP)]²⁻/[Eu(Hdo3aNP)]⁻ system as a pH probe for MRI. However, this experiment had some limitations due to the accessible hardware. The broad spectral width (20 kHz/246 ppm) necessary for the experiment required a short excitation pulse. Due to hardware limitations, a block pulse (instead of modulated one) had to be used for excitation to reach sufficient pulse intensity. As the excitation profile of the block pulse is inhomogeneous, intensities at different frequencies may not exactly correspond to the concentrations. The space-localized ^{31}P MR spectra were measured in the phantom consisting of four vials: a vial containing an aqueous solution of H_3PO_4 as a reference and three vials containing the Eu(III)– $\text{H}_3\text{do3aNP}$ complex solutions having different pH values (6.4, 8.0, and 9.0). The localized spectra and intensity of individual signals from different parts of the phantom are shown in Figure 8, and the results clearly show a spatial resolution of areas with different pH values, proving the suggested concept.

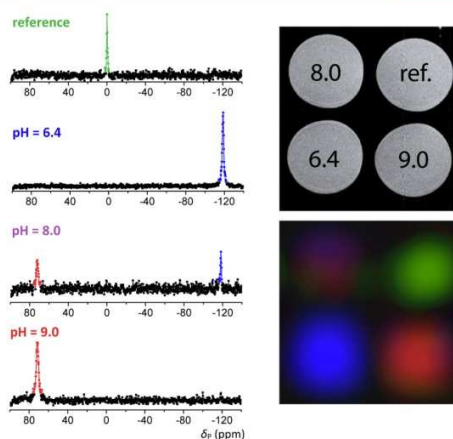


Figure 8. Left: localized ^{31}P MR spectra. Right: pH map and legend (^1H MR reference image) of phantom consisting of one vial containing aqueous H_3PO_4 as a reference and three vials containing aqueous solutions of the Eu(III)– $\text{H}_3\text{do3aNP}$ complex with different pH values. Postprocessing included interpolation to a spatial 256×256 matrix, integration over the selected signals, and false color coding. Color scheme: red, signal at +70 ppm; blue, –118 ppm; purple color results from red/blue superposition; green, 0 ppm.

CONCLUSIONS

New ligand $\text{H}_3\text{do3aNP}$ with a 2-[amino(methylphosphonic acid)]ethyl pendant arm was synthesized, and its coordination properties were studied by potentiometry and NMR spectroscopy. Full in-cage complexation of Eu(III) is finished at $\text{pH} > 4.5$, forming the protonated SA-[Eu(Hdo3aNP)]⁻ complex with square-antiprismatic (SA) geometry. Upon deprotonation with $\text{p}K_A \sim 8$, the twisted-square-antiprismatic TSA-[Eu(do3aNP)]²⁻ complex is formed. Both complexes are in a slow equilibrium on the NMR time scale, and their ^{31}P NMR shifts differ by ~ 190 ppm due to significant movement of the principal magnetic axis leading to different paramagnetic contributions to the ^{31}P NMR shift. To the best of our knowledge, such a strict change of the coordination geometry with (de)protonation has not been observed before.

The existence of two separate signals in the ^{31}P NMR spectra allows ratiometric determination of pH by MRS. As both signals belong to the same compound (differing just by its protonation state), this ensures the same biodistribution of both species, and the ratiometric approach brings the advantage of independence of the measured data on the probe concentration. Unfortunately, the $\text{p}K_A$ of the studied complex lies somewhat outside the region optimal for *in vivo* use; nevertheless, this parameter can be altered by a suitably designed ligand, and thus, the discovered principle shows promising potential for *in vivo* applications.

ASSOCIATED CONTENT

Supporting Information

The Supporting Information is available free of charge on the ACS Publications website at DOI: 10.1021/acs.inorgchem.6b02749.

K

DOI: 10.1021/acs.inorgchem.6b02749
Inorg. Chem. XXXX, XXX, XXX–XXX

NMR spectra and studies, hydrogen bond lengths, and potentiometric results (PDF)
Crystal data (CIF)

AUTHOR INFORMATION

Corresponding Author

*E-mail: modrej@natur.cuni.cz. Phone: +420-221951261. Fax: +420-221951253.

ORCID

Jan Kotek: 0000-0003-1777-729X

Notes

The authors declare no competing financial interest.

ACKNOWLEDGMENTS

We thank Z. Böhmová for the potentiometric measurements and Dr. I. Čiśářová for the X-ray diffraction study. Support from the Grant Agency of the Czech Republic (Project 16-03156S) is acknowledged. We really appreciate remarks from the referees regarding the spatial dependence of the paramagnetic contribution to chemical shift.

REFERENCES

- (1) *The Chemistry of Contrast Agents in Medical Magnetic Resonance Imaging*, 2nd ed.; Merbach, A., Helm, L., Tóth, E., Eds.; Wiley: Chichester, United Kingdom, 2013.
- (2) Gillies, R. J.; Raghunand, N.; Garcia-Martin, M. L.; Gatenby, R. A. pH imaging: A review of pH measurement methods and applications in cancers. *IEEE Eng. Med. Biol.* **2004**, *23*, 57–64.
- (3) Hingorani, D. V.; Bernstein, A. S.; Pagel, M. D. A review of responsive MRI contrast agents: 2005–2014. *Contrast Media Mol. Imaging* **2015**, *10*, 245–265.
- (4) Zhu, L.; Yang, Y.; Farquhar, K.; Wang, J.; Tian, C.; Ranville, J.; Boyes, S. G. Surface Modification of Gd Nanoparticles with pH-Responsive Block Copolymers for Use As Smart MRI Contrast Agents. *ACS Appl. Mater. Interfaces* **2016**, *8*, 5040–5050.
- (5) (a) Zhang, S.; Wu, K.; Sherry, A. D. A Novel pH-Sensitive MRI Contrast Agent. *Angew. Chem., Int. Ed.* **1999**, *38*, 3192–3194. (b) Raghunand, N.; Howison, C.; Sherry, A. D.; Zhang, S.; Gillies, R. J. Renal and systemic pH imaging by contrast-enhanced MRI. *Magn. Reson. Med.* **2003**, *49*, 249–257. (c) Kálmán, F. K.; Woods, M.; Caravan, P.; Jurek, P.; Spiller, M.; Tircso, G.; Kiraly, R.; Brücher, E.; Sherry, A. D. Potentiometric and Relaxometric Properties of Gadolinium-based MRI Contrast Agent for Sensing Tissue pH. *Inorg. Chem.* **2007**, *46*, 5260–5270.
- (6) Lowe, M. P.; Parker, D.; Reany, O.; Aime, S.; Botta, M.; Castellano, G.; Gianolio, E.; Pagliarini, R. pH-dependent modulation of relaxivity and luminescence in macrocyclic gadolinium and europium complexes based on reversible intramolecular sulfonamide ligation. *J. Am. Chem. Soc.* **2001**, *123*, 7601–7609.
- (7) Woods, M.; Kiefer, G. E.; Bott, S.; Castillo-Muzquiz, A.; Eshelbrenner, C.; Michaudet, L.; McMillan, K.; Mudigunda, S. D. K.; Ogrin, D.; Tircso, G.; Zhang, S.; Zhao, P.; Sherry, A. D. Synthesis, Relaxometric and Photophysical Properties of a New pH-Responsive MRI Contrast Agent: The Effect of Other Ligating Groups on Dissociation of a *p*-Nitrophenolic Pendant Arm. *J. Am. Chem. Soc.* **2004**, *126*, 9248–9256.
- (8) (a) Giovenzana, G. B.; Negri, R.; Rolla, G. A.; Tei, L. Gd-Aminoethyl-DO3A Complexes: A Novel Class of pH-Sensitive MRI Contrast Agents. *Eur. J. Inorg. Chem.* **2012**, *2012*, 2035–2039. (b) Baranyai, Z.; Rolla, G. A.; Negri, R.; Forgács, A.; Giovenzana, G. B.; Tei, L. Comprehensive Evaluation of the Physicochemical Properties of Ln^{III} Complexes of Aminoethyl-DO3A as pH-Responsive T₁-MRI Contrast Agents. *Chem. - Eur. J.* **2014**, *20*, 2933–2944.
- (9) Hall, J.; Haner, R.; Aime, S.; Botta, M.; Faulkner, S.; Parker, D.; de Sousa, A. S. Relaxometric and luminescence behaviour of triaquaheptamacrocylic complexes, the gadolinium complex dis-

playing a high relaxivity with a pronounced pH dependence. *New J. Chem.* **1998**, *22*, 627–631.

(10) de Leon-Rodriguez, L. M.; Lubag, A. J. M.; Malloy, C. R.; Martinez, G. V.; Gillies, R. J.; Sherry, A. D. Responsive MRI agents for sensing metabolism *in vivo*. *Acc. Chem. Res.* **2009**, *42*, 948–957.

(11) Garcia-Martin, M. L.; Martinez, G. V.; Raghunand, N.; Sherry, A. D.; Zhang, S.; Gillies, R. J. High resolution pH(e) imaging of rat glioma using pH-dependent relaxivity. *Magn. Reson. Med.* **2006**, *55*, 309–315.

(12) Aime, S.; Fedeli, F.; Sanino, A.; Terreno, E. R₂/R₁ Ratiometric Procedure for a Concentration-Independent, pH-Responsive, Gd(III)-Based MRI Agent. *J. Am. Chem. Soc.* **2006**, *128*, 11326–11327.

(13) (a) Soesbe, T. C.; Wu, Y.; Sherry, A. D. Advantages of paramagnetic CEST complexes having slow-to-intermediate water exchange properties as responsive MRI agents. *NMR Biomed.* **2013**, *26*, 829–838. (b) Dorazio, S. J.; Olatunde, A. O.; Sperry, J. A.; Morrow, J. R. CoCEST: cobalt(II) amide-appended paraCEST MRI contrast agents. *Chem. Commun.* **2013**, *49*, 10025–10027. (c) Sheth, V. R.; Li, Y.; Chen, L. Q.; Howison, C. M.; Flask, C. A.; Pagel, M. D. Measuring *in vivo* tumor pH with CEST-FISP MRI. *Magn. Reson. Med.* **2012**, *67*, 760–768. (d) Liu, G.; Li, Y.; Sheth, V. R.; Pagel, M. D. Imaging *in vivo* extracellular pH with a single paramagnetic chemical exchange saturation transfer magnetic resonance imaging contrast agent. *Mol. Imaging* **2012**, *11*, 47–57. (e) Castelli, D. D.; Ferrauto, G.; Cutrin, J. C.; Terreno, E.; Aime, S. *In vivo* maps of extracellular pH in murine melanoma by CEST-MRI. *Magn. Reson. Med.* **2014**, *71*, 326–332.

(14) Aime, S.; Castelli, D. D.; Terreno, E. Novel pH-reporter MRI contrast agents. *Angew. Chem., Int. Ed.* **2002**, *41*, 4334–4336.

(15) Krchová, T.; Gálišová, A.; Jiráček, D.; Hermann, P.; Kotek, J. Ln(III)-complexes of a DOTA analogue with an ethylenediamine pendant arm as pH-responsive PARACEST contrast agents. *Dalton Trans.* **2016**, *45*, 3486–3496.

(16) Castelli, D. D.; Terreno, E.; Aime, S. YbIII-HPDO3A: A Dual pH- and Temperature-Responsive CEST Agent. *Angew. Chem.* **2011**, *123*, 1838–1840.

(17) Posse, S.; Otazo, R.; Dager, S. R.; Alger, J. MR spectroscopic imaging: principles and recent advances. *J. Magn. Reson. Imaging* **2013**, *37*, 1301–1325.

(18) Griffiths, R. J. Are cancer cells acidic? *Br. J. Cancer* **1991**, *64*, 425–427.

(19) Gillies, R. J.; Morse, D. L. *In vivo* magnetic resonance spectroscopy in cancer. *Annu. Rev. Biomed. Eng.* **2005**, *7*, 287–326.

(20) (a) van Sluis, R.; Bhujwala, Z. M.; Raghunand, N.; Ballesteros, P.; Alvarez, J.; Cerdan, S.; Galons, J. P.; Gillies, R. J. *In vivo* imaging of extracellular pH using ¹H MRSI. *Magn. Reson. Med.* **1999**, *41*, 743–750. (b) Garcia-Martin, M. L.; Herigault, G.; Remy, C.; Farion, R.; Ballesteros, P.; Coles, J. A.; Cerdan, S.; Ziegler, A. Mapping Extracellular pH in Rat Brain Gliomas *In Vivo* by H Magnetic Resonance Spectroscopic Imaging: Comparison with Maps of Metabolites. *Cancer Res.* **2001**, *61*, 6524–6531.

(21) Aime, S.; Botta, M.; Milone, L.; Terreno, E. Paramagnetic complexes as novel NMR pH indicators. *Chem. Commun.* **1996**, 1265–1266.

(22) Coman, D.; Trubel, H. K.; Rycyna, R. E.; Hyder, F. Brain temperature and pH measured by (1)H chemical shift imaging of a thulium agent. *NMR Biomed.* **2009**, *22*, 229–239.

(23) Huang, Y.; Coman, D.; Ali, M. M.; Hyder, F. Lanthanide ion (III) complexes of 1,4,7,10-tetraazacyclododecane-1,4,7,10-tetraaminophosphonate (DOTA-4AmP⁵⁻) for dual biosensing of pH with CEST (chemical exchange saturation transfer) and BIRDS (biosensor imaging of redundant deviation in shifts). *Contrast Media Mol. Imaging* **2015**, *10*, 51–58.

(24) Jagadish, B.; Brickert-Albrecht, G. L.; Nichol, G. S.; Mash, E. A.; Raghunand, N. On the Synthesis of 1,4,7-Tris(tert-butoxycarbonylmethyl)-1,4,7,10-tetraazacyclododecane. *Tetrahedron Lett.* **2011**, *52*, 2058–2061.

(25) Jiang, X.-J.; Lo, P.-Ch.; Tsang, Y.-M.; Yeung, S.-L.; Fong, W.-P.; Ng, D. K. P. Phthalocyanine–Polyamine Conjugates as pH-Controlled

L

DOI: 10.1021/acs.inorgchem.6b02749
Inorg. Chem. XXXX, XXX, XXX–XXX

Photosensitizers for Photodynamic Therapy. *Chem. - Eur. J.* **2010**, *16*, 4777–4783.

(26) Perrin, D. D.; Armarego, W. L. F. *Purification of Laboratory Chemicals*, 3rd ed.; Pergamon Press: Oxford, 1988.

(27) *MATLAB R2015b*; The MathWorks Inc.: Natick, MA, 2000.

(28) Corsi, D. M.; Platas-Iglesias, C.; van Bekkum, H.; Peters, J. A. Determination of paramagnetic lanthanide (III) concentrations from bulk magnetic susceptibility shifts in NMR spectra. *Magn. Reson. Chem.* **2001**, *39*, 723–726.

(29) Sheldrick, G. M. *SHELXS97, Program for Crystal Structure Solution from Diffraction Data*; University of Göttingen: Göttingen, Germany, 1997.

(30) Sheldrick, G. M. *SHELXL97, Program for Crystal Structure Refinement from Diffraction Data*; University of Göttingen: Göttingen, Germany, 1997.

(31) (a) Táborský, P.; Lubal, P.; Havel, J.; Kotek, J.; Hermann, P.; Lukeš, I. Thermodynamic and Kinetic Studies of Lanthanide(III) Complexes with H₂do3ap (1,4,7,10-Tetraazacyclododecane-1,4,7-triacetic-10-(methylphosphonic Acid)), a Monophosphonate Analogue of H₂do4. *Collect. Czech. Chem. Commun.* **2005**, *70*, 1909–1942. (b) Fürstrová, M.; Svobodová, I.; Lubal, P.; Táborský, P.; Kotek, J.; Hermann, P.; Lukeš, I. Thermodynamic study of lanthanide(III) complexes with bifunctional monophosphonic acid analogues of H₂do4 and comparative kinetic study of yttrium(III) complexes. *Dalton Trans.* **2007**, 535–549.

(32) Kývala, M.; Lukeš, I. *International Conference Chemometrics 95*; Pardubice, Czech Republic, 1995; p 63. Full version of *OPIUM* available (free of charge) on <http://web.natur.cuni.cz/~kyvala/opium.html>.

(33) Martell, A. E.; Smith, R. M.; Motekaitis, R. J. *NIST Critically Selected Stability Constants of Metal Complexes (Version 7)*; Texas A&M University: College Station, TX.

(34) Aime, S.; Botta, M.; Ermondi, G. NMR study of solution structures and dynamics of lanthanide(III) complexes of DOTA. *Inorg. Chem.* **1992**, *31*, 4291–4299.

(35) (a) Caravan, P.; Ellison, J. J.; McMurry, T. J.; Lauffer, R. B. Gadolinium(III) Chelates as MRI Contrast Agents: Structure, Dynamics, and Applications. *Chem. Rev.* **1999**, *99*, 2293–2352. (b) Hermann, P.; Kotek, J.; Kubiček, V.; Lukeš, I. Gadolinium(III) complexes as MRI contrast agents: ligand design and properties of the complexes. *Dalton Trans.* **2008**, 3027–3047. (c) Geraldes, C. F. G. C.; Laurent, S. Classification and basic properties of contrast agents for magnetic resonance imaging. *Contrast Media Mol. Imaging* **2009**, *4*, 1–23.

(36) (a) Aime, S.; Botta, M.; Fasano, M.; Marques, M. P. M.; Geraldes, C. F. G. C.; Pubanz, D.; Merbach, A. E. Conformational and Coordination Equilibria on DOTA Complexes of Lanthanide Metal Ions in Aqueous Solution Studied by (1)H-NMR Spectroscopy. *Inorg. Chem.* **1997**, *36*, 2059–2068. (b) Lebdušková, P.; Hermann, P.; Helm, L.; Tóth, É.; Kotek, J.; Binnemans, K.; Rudovský, J.; Lukeš, I.; Merbach, A. E. Gadolinium(III) Complexes of Mono- and Diethyl Esters of Monophosphonic Acid Analogue of DOTA as Potential MRI Contrast Agents: Solution Structures and Relaxometric Studies. *Dalton Trans.* **2007**, 493–501. (c) Vitha, T.; Kubiček, V.; Kotek, J.; Hermann, P.; Vander Elst, L.; Müller, R. N.; Lukeš, I.; Peters, J. A. Gd(III) complex of a monophosphate-bis(phosphonate) DOTA analogue with a high relaxivity; Lanthanide(III) complexes for imaging and radiotherapy of calcified tissues. *Dalton Trans.* **2009**, 3204–3214. (d) Castelli, D. D.; Caligara, M. C.; Botta, M.; Terreno, E.; Aime, S. Combined high resolution NMR and H-1 and O-17 relaxometric study sheds light on the solution structure and dynamics of the Lanthanide(III) complexes of HPDO3A. *Inorg. Chem.* **2013**, *52*, 7130–7138. (e) Rudovský, J.; Cigler, P.; Kotek, J.; Hermann, P.; Vojtišek, P.; Lukeš, I.; Peters, J. A.; Vander Elst, L.; Müller, R. N. Lanthanide (III) complexes of a mono (methylphosphonate) analogue of H₂do4: The influence of protonation of the phosphonate moiety on the TSAP/SAP isomer ratio and the water exchange rate. *Chem. - Eur. J.* **2005**, *11*, 2373–2384. (f) Rudovský, J.; Kotek, J.; Hermann, P.; Lukeš, I.; Mainero, V.; Aime, S. Synthesis of a Bifunctional

Monophosphonic Acid DOTA Analogue Ligand and Its Lanthanide-(III) Complexes. A Gadolinium(III) Complex Endowed with an Optimal Water Exchange Rate for MRI Applications. *Org. Biomol. Chem.* **2005**, *3*, 112–117.

(37) Krchová, T.; Kotek, J. Unpublished results.

(38) Beeby, A.; Clarkson, I. M.; Dickins, R. S.; Faulkner, S.; Parker, D.; Royle, L.; de Sousa, A. S.; Williams, J. A. G.; Woods, M. Non-radiative deactivation of the excited states of europium, terbium and ytterbium complexes by proximate energy-matched OH, NH and CH oscillators: an improved luminescence method for establishing solution hydration states. *J. Chem. Soc., Perkin Trans. 2* **1999**, 493–504.

(39) (a) Rudovský, J.; Botta, M.; Hermann, P.; Koridze, A.; Aime, S. Relaxometric and solution NMR structural studies on ditopic lanthanide(III) complexes of a phosphinate analogue of DOTA with a fast rate of water exchange. *Dalton Trans.* **2006**, 2323–2333. (b) Kotková, Z.; Pereira, G. A.; Djanashvili, K.; Kotek, J.; Rudovský, J.; Hermann, P.; Vander Elst, L.; Müller, R. N.; Geraldes, C. F. G. C.; Lukeš, I.; Peters, J. A. Lanthanide(III) Complexes of Phosphonic Acid Analogues of H₂DOTA as Model Compounds for the Evaluation of the Second-Sphere Hydration. *Eur. J. Inorg. Chem.* **2009**, 2009, 119–136. (c) Pereira, G. A.; Ball, L.; Sherry, A. D.; Peters, J. A.; Geraldes, C. F. G. C. NMR Characterization of Lanthanide(3+) Complexes of Tetraazatetrakisphosphinato and Tetraazatetrakisphosphonato Ligands. *Helv. Chim. Acta* **2009**, *92*, 2532–2551. (d) Rohovec, J.; Lukeš, I.; Hermann, P. Lanthanide complexes of a cyclen derivative with phenylphosphonic pendant arms for possible ¹H and ³¹P MRI temperature sensitive probes. *New J. Chem.* **1999**, *23*, 1129–1132.

(e) Rohovec, J.; Kývala, M.; Vojtišek, P.; Hermann, P.; Lukeš, I. Synthesis, Crystal Structures, and Solution Properties of N-Methylene-(phenyl)phosphonic Acid Derivatives of Cyclen and Cyclam. *Eur. J. Inorg. Chem.* **2000**, 2000, 195–203. (f) Aime, S.; Batsanov, A. S.; Botta, M.; Howard, J. A. K.; Parker, D.; Senanayake, K.; Williams, J. A. G. Solution and Solid-state Characterization of Highly Rigid, Eight-Coordinate Lanthanide(III) Complexes of a Macrocyclic Tetraazacyclododecane Phosphinate. *Inorg. Chem.* **1994**, *33*, 4696–4706. (g) Aime, S.; Batsanov, A. S.; Botta, M.; Dickins, R. S.; Faulkner, S.; Foster, C. E.; Harrison, A.; Howard, J. A. K.; Moloney, J. M.; Norman, T. J.; Parker, D.; Royle, L.; Williams, J. A. G. Nuclear magnetic resonance, luminescence and structural studies of lanthanide complexes with octadentate macrocyclic ligands bearing benzylphosphinate groups. *J. Chem. Soc., Dalton Trans.* **1997**, 3623–3636.

(40) Campello, M. P. C.; Lacerda, S.; Santos, I. C.; Pereira, G. A.; Geraldes, C. F. G. C.; Kotek, J.; Hermann, P.; Vaněk, J.; Lubal, P.; Kubiček, V.; Tóth, E.; Santos, I. Lanthanide(III) complexes of 4,10-bis(phosphonomethyl)-1,4,7,10-tetraazacyclododecane-1,7-diacetic acid (trans-H₂do2a2p) in solution and in the solid state: structural studies along the series. *Chem. - Eur. J.* **2010**, *16*, 8446–8465.

(41) (a) Blackburn, O. A.; Edkins, R. M.; Faulkner, S.; Kenwright, A. M.; Parker, D.; Rogers, N. J.; Shuvaev, S. Electromagnetic susceptibility anisotropy and its importance for paramagnetic NMR and optical spectroscopy in lanthanide coordination chemistry. *Dalton Trans.* **2016**, 45, 6782–6800. (b) Cucinotta, G.; Perfetti, M.; Luzon, J.; Etienne, M.; Car, P.-E.; Caneschi, A.; Calvez, G.; Bernot, K.; Sessoli, R. Magnetic Anisotropy in a Dysprosium/DOTA Single-Molecule Magnet: Beyond Simple Magneto-Structural Correlations. *Angew. Chem., Int. Ed.* **2012**, *51*, 1606–1610.

(42) (a) Rohovec, J.; Vojtišek, P.; Hermann, P.; Mosinger, J.; Žák, Z.; Lukeš, I. Synthesis, crystal structures and NMR and luminescence spectra of lanthanide complexes of 1,4,7,10-tetraazacyclododecane with N-methylene(phenyl)phosphonic acid pendant arms. *J. Chem. Soc., Dalton Trans.* **1999**, 3585–3592. (b) Avcella, F.; Peters, J. A.; Geraldes, C. F. G. C. X-ray Crystal Structure of a Sodium Salt of [Gd(DOTP)]⁵⁻: Implications for Its Second-Sphere Relaxivity and the ²³Na NMR Hyperfine Shift Effects of [Tm(DOTP)]⁵⁻. *Eur. J. Inorg. Chem.* **2003**, 2003, 4179–4186. (c) Vojtišek, P.; Cigler, P.; Kotek, J.; Rudovský, J.; Hermann, P.; Lukeš, I. Crystal Structures of Lanthanide-(III) Complexes with Cyclen Derivative Bearing Three Acetate and One Methylphosphonate Pendants. *Inorg. Chem.* **2005**, *44*, 5591–5599. (d) Luck, R. L.; Maupin, C. L.; Parker, D.; Riehl, J. P.; Williams,

J. A. G. Circularly polarized luminescence and structural studies of a dysprosium(III) complex with an octadentate macrocyclic ligand bearing benzylphosphinate groups. *Inorg. Chim. Acta* **2001**, *317*, 331–337.

(43) Lukeš, I.; Kotek, J.; Vojtíšek, P.; Hermann, P. Tetraazacycles with Methylphosphinic/phosphonic Acid Pendant Arms. A Comparison with their Acetic Acid Analogues. *Coord. Chem. Rev.* **2001**, *216–217*, 287–312.

(44) Krchová, T.; Kotek, J.; Jiráček, D.; Havlíčková, J.; Čisarová, I.; Hermann, P. Lanthanide(III) complexes of aminoethyl-DO3A as PARACEST contrast agents based on decoordination of the weakly bound amino group. *Dalton Trans.* **2013**, *42*, 15735–15747.

(45) Pniok, M.; Kubíček, V.; Havlíčková, J.; Kotek, J.; Sabatie-Gogova, A.; Plutnar, J.; Huclier-Markai, S.; Hermann, P. Thermodynamic and kinetic study of scandium(III) complexes of DTPA and DOTA: a step toward scandium radiopharmaceuticals. *Chem. - Eur. J.* **2014**, *20*, 7944–7955.

Electronic supplementary information for:

**Eu(III) Complex with DO3A-amino-phosphonate Ligand as a
Concentration-Independent pH-Responsive Contrast Agent for Magnetic
Resonance Spectroscopy (MRS)**

Terезa Krehova,^a Vlt Herynek,^b Andrea Galisova,^b Jan Blahut,^a Petr Hermann,^a Jan Kocik^a

^a Department of Inorganic Chemistry, Faculty of Science, Charles University, Hlavova 20/30, 128 43 Prague 2, Czech Republic. Tel.: +420-221951261. Fax: +420-221951253. E-mail: modest@natur.cuni.cz

^b Department of Radiodiagnostic and Interventional Radiology, Magnetic Resonance Unit, Institute for Clinical and Experimental Medicine, Videlska 1958/9, Prague 4, 140 21 Czech Republic.

Contents

¹ H and ¹³ C{ ¹ H} NMR spectra of compound 4	2
³¹ P and ³¹ P{ ¹ H} NMR spectra of compound 4	3
¹ H and ¹³ C{ ¹ H} NMR spectra of H4d03aNP	4
³¹ P and ³¹ P{ ¹ H} NMR spectra of H4d03aNP	5
Selected hydrogen bonds found in the crystal structure of H4d03aNP 4.75H2O	6
¹ H NMR studies of Eu(III) complex of H4d03aNP	7
³¹ P NMR studies of Eu(III) complex of H4d03aNP	14
Overview of ³¹ P NMR shifts of the ligands having methylenephosphonate or methylphosphinate pendant moieties and their Eu(III)/La(III) complexes	20
Overview of complex geometries found in the solid state	23
Assignment of hydrogen atom signals in ¹ H NMR spectra of Eu(III)-H4d03aNP complexes	26
Potentiometric, ¹ H and ³¹ P NMR studies – protonation and stability constants of H4d03aNP and its Eu(III) complex	33

¹H and ¹³C{¹H} NMR spectra of compound 4

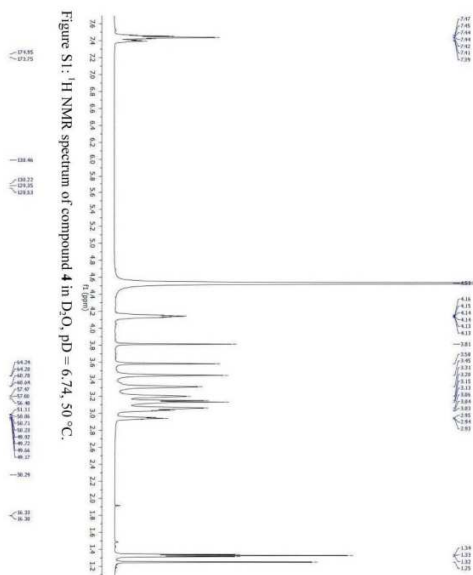


Figure S1: ¹H NMR spectrum of compound 4 in D₂O, pH = 6.74, 50 °C.

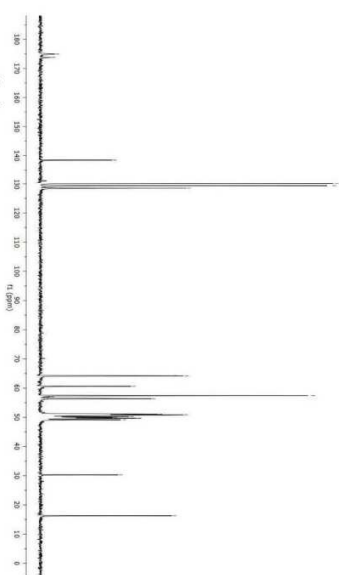


Figure S2: ¹³C{¹H} NMR spectrum of compound 4 in D₂O, pH = 6.74, 50 °C.

³¹P and ³¹P{¹H} NMR spectra of compound 4

Figure S3

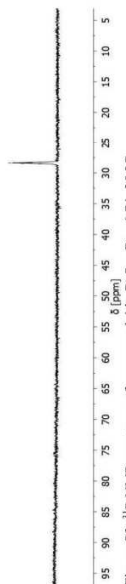


Figure S3: ³¹P NMR spectrum of compound 4 in D₂O, pD = 6.74, 25 °C.

Figure S4

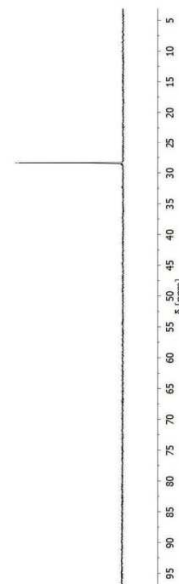


Figure S4: ³¹P{¹H} NMR spectrum of compound 4 in D₂O, pD = 6.74, 25 °C.

¹H and ¹³C{¹H} NMR spectra of H₄do.3aNP

Figure S5

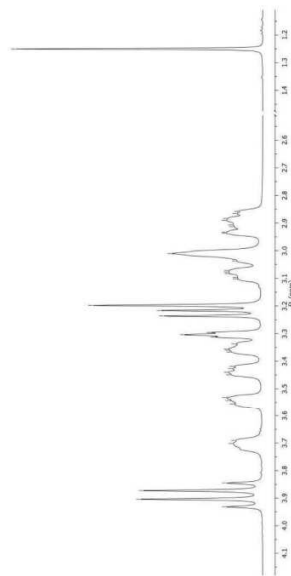


Figure S5: ¹H NMR spectrum of H₄do.3aNP in D₂O, pD = 5.81, 25 °C.

Figure S6

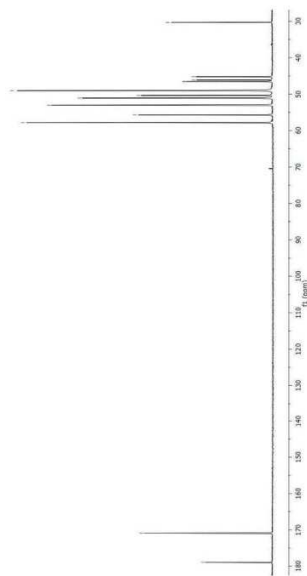


Figure S6: ¹³C{¹H} NMR spectrum of H₄do.3aNP in D₂O, pD = 5.81, 25 °C.

³¹P and ¹H NMR spectra of Hd3o3aNP

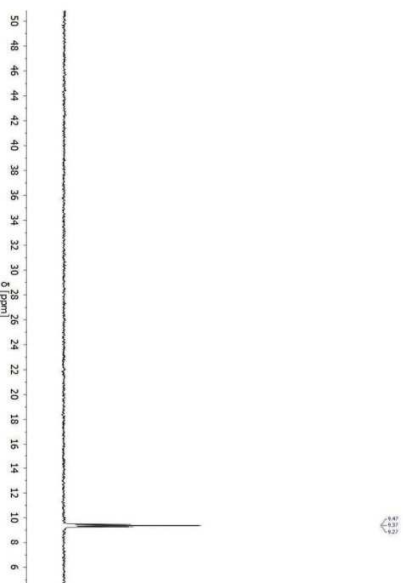


Figure S7: ³¹P NMR spectrum of Hd3o3aNP in D₂O, pD = 5.81, 25 °C.

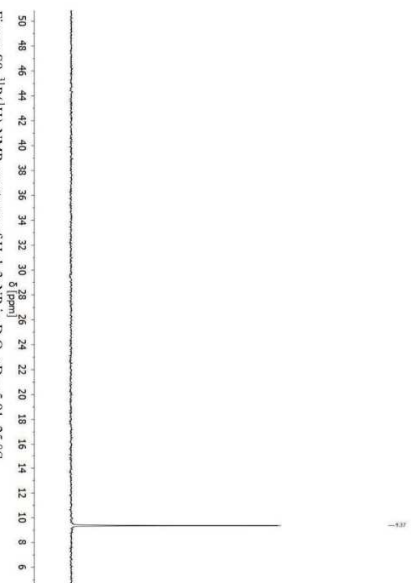
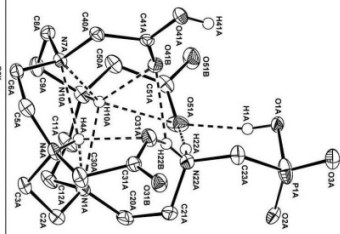


Figure S8: ¹H NMR spectrum of Hd3o3aNP in D₂O, pD = 5.81, 25 °C.

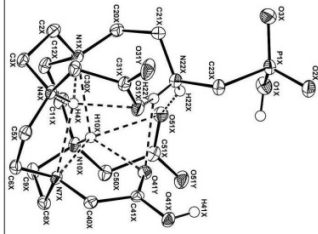
Selected hydrogen bonds found in the crystal structure of Hd3o3aNP·4.75H₂O

Table S1: Selected hydrogen bonds found in the crystal structure of Hd3o3aNP·4.75H₂O.

D-H	d(D-H)	d(H...A)	<DHA	d(D...A)	A
molecule A					
N4A-H4A	0.930	2.068	117	2.627(2)	O31A
N4A-H4A	0.930	2.580	111	3.034(2)	N1A
N4A-H4A	0.930	2.376	113	2.867(2)	N7A
N10A-H10A	0.930	2.184	136	2.924(2)	O41B
N10A-H10A	0.930	2.614	92	2.809(2)	O51A
N10A-H10A	0.930	2.524	109	2.964(2)	N1A
N22A-H22A	0.920	2.558	110	3.005(2)	N7A
N22A-H22A	0.920	1.808	175	2.726(2)	O51A
N22A-H22B	0.920	2.021	138	2.772(2)	O31A
N22A-H22B	0.920	2.234	119	2.780(2)	O41B
O1A-H1A	0.873	1.971	167	2.829(6)	O51A
O41A-H41A	0.840	1.719	165	2.539(2)	O31Y



molecule X					
N4X-H4X	0.930	2.042	117	2.605(2)	O31X
N4X-H4X	0.930	2.584	111	3.043(2)	N1X
N4X-H4X	0.930	2.390	112	2.876(2)	N7X
N10X-H10X	0.930	2.220	134	2.941(2)	O41Y
N10X-H10X	0.930	2.561	92	2.752(2)	O51X
N10X-H10X	0.930	2.490	111	2.956(2)	N1X
N10X-H10X	0.930	2.547	110	2.998(2)	N7X
N22X-H22X	0.920	2.578	112	3.040(2)	O1X
N22X-H22X	0.920	1.865	154	2.722(2)	O51X
N22X-H22Y	0.920	2.157	129	2.829(2)	O31X
N22X-H22Y	0.920	2.212	125	2.843(2)	O41Y
O1X-H1X	0.893	1.812	171	2.698(2)	O5W
O41X-H41X	0.840	1.765	165	2.586(2)	O31B



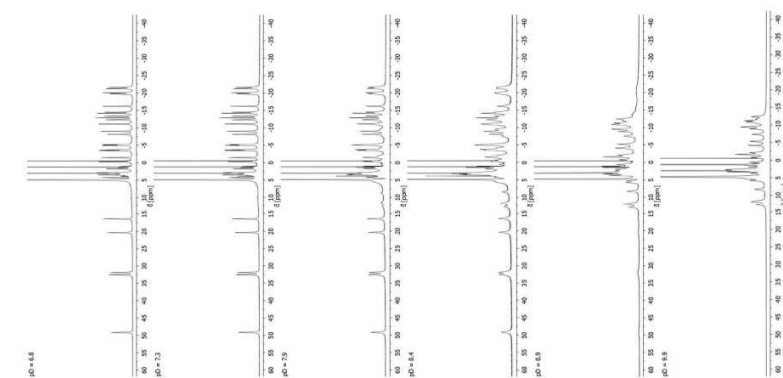


Figure S10: ¹H NMR spectra of SA-[Eu(H₄o₃aNP)]/TSA-[Eu(dota)]²⁻ (~80 mM solution in D₂O, ~250 mM NaCl, I₀ = 7.05 T, 25 °C) at different pH values (referenced to δ (BuOH) = 1.25 ppm).

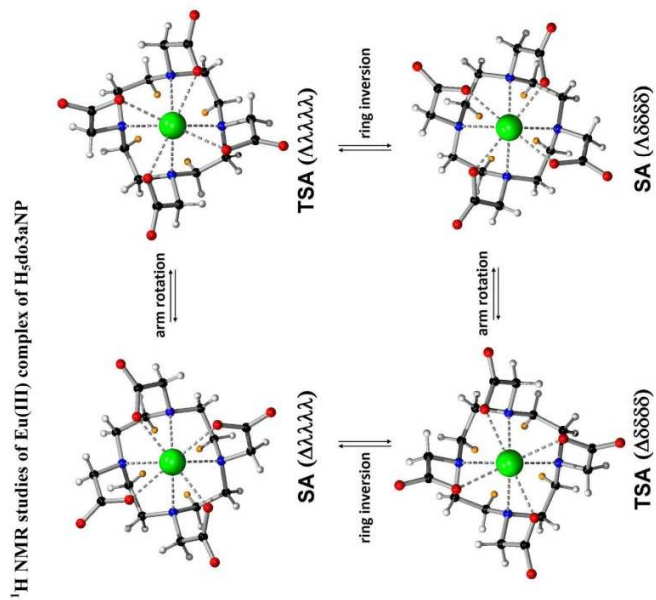


Figure S9: Schematic structure of SA/TSA-[Ln(dota)]⁻ complex species highlighting the “axial” protons (orange).

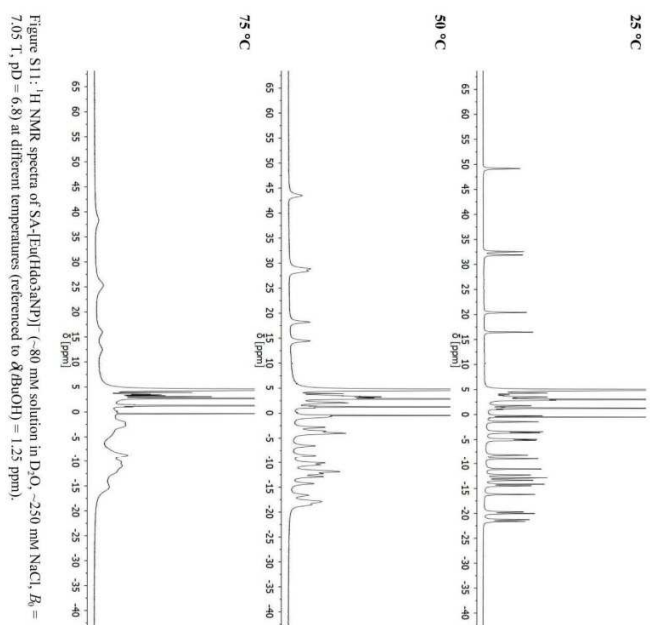


Figure S11: ^1H NMR spectra of $\text{SA-}[\text{Eu}(\text{dob3aNP})]$ (~ 80 mM solution in D_2O , ~ 250 mM NaCl , $B_0 = 7.05$ T, $\text{pD} = 6.8$) at different temperatures (referenced to $\delta(\text{H}_2\text{O}) = 1.25$ ppm).

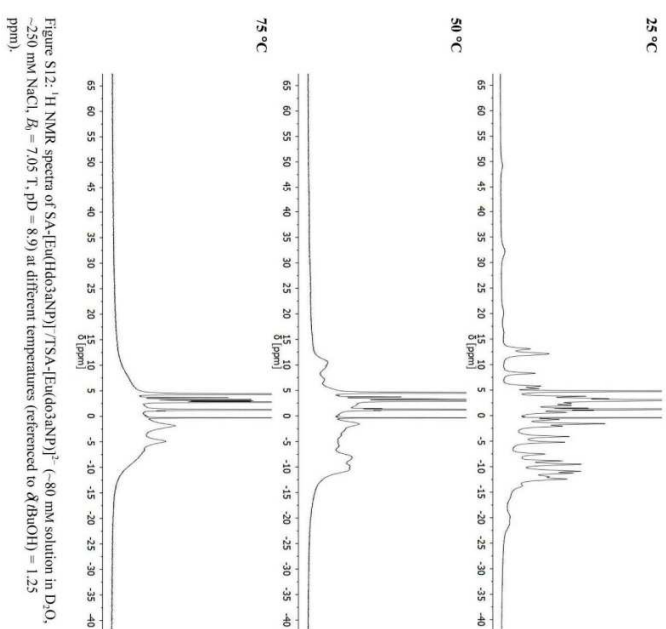


Figure S12: ^1H NMR spectra of $\text{SA-}[\text{Eu}(\text{dob3aNP})]/[\text{SA-}[\text{Eu}(\text{dob3aNP})]^{2-}$ (~ 80 mM solution in D_2O , ~ 250 mM NaCl , $B_0 = 7.05$ T, $\text{pD} = 8.9$) at different temperatures (referenced to $\delta(\text{H}_2\text{O}) = 1.25$ ppm).

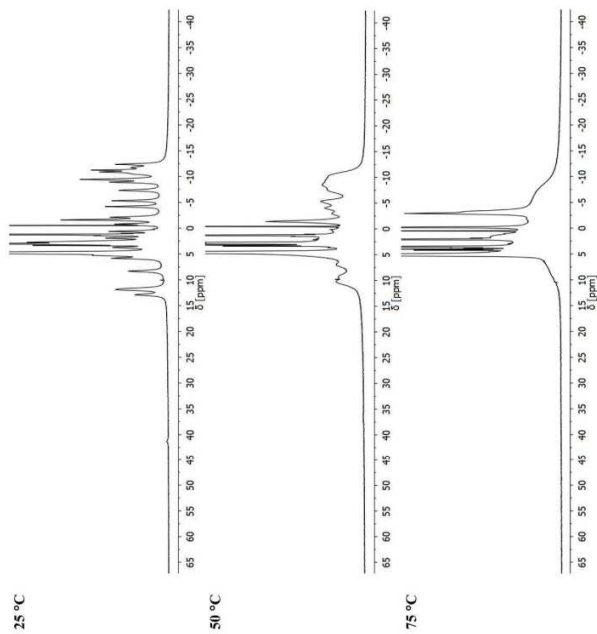


Figure S14: ^1H NMR spectra of TSA-[Eu(d 3 aNP)] $^{2-}$ (~80 mM solution in D $_2$ O, ~250 mM NaCl, $R_f = 7.05$ T, pD = 9.9) at different temperatures (referenced to δ (BuOH) = 1.25 ppm).

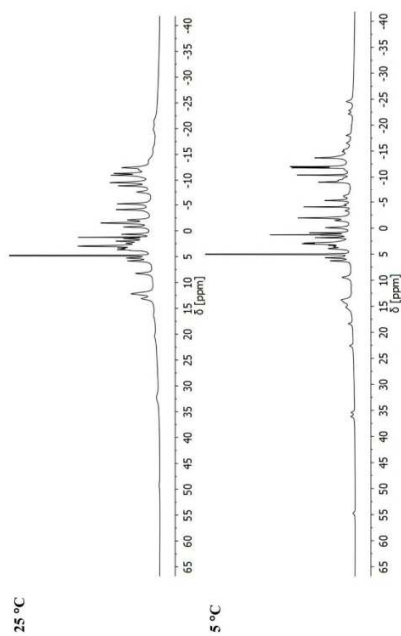


Figure S13: ^1H NMR spectra of SA-[Eu(Hd 3 aNP)]/TSA-[Eu(d 3 aNP)] $^{2-}$ (~80 mM solution in D $_2$ O, ~250 mM NaCl, $R_f = 14.1$ T, pD = 9.05) at 25 and 5 °C (referenced to δ (BuOH) = 1.25 ppm).

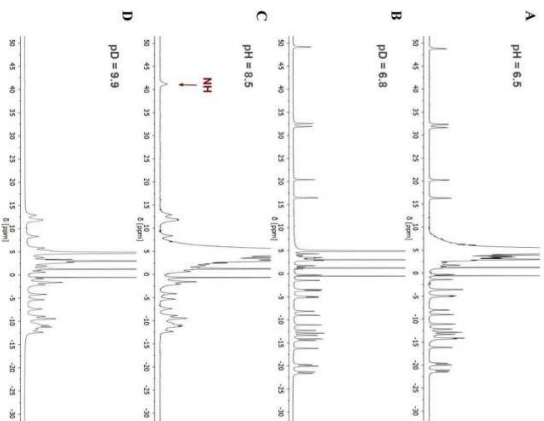


Figure S15: ^1H NMR spectra of $\text{SA}-[\text{Eu}(\text{Hdod3ANP})_2/\text{TSA}-[\text{Eu}(\text{dod3ANP})_2]^-$ complex species (~ 80 mM solution in A, C: H_2O ; B, D: D_2O ; ~ 250 mM NaCl , $B_0 = 7.05$ T, 25°C) at different pH/pD values (referenced to $\delta(\text{BuOH}) = 1.25$ ppm).

13

^{31}P NMR studies of $\text{Eu}(\text{III})$ complex of $\text{H}_2\text{dod3ANP}$

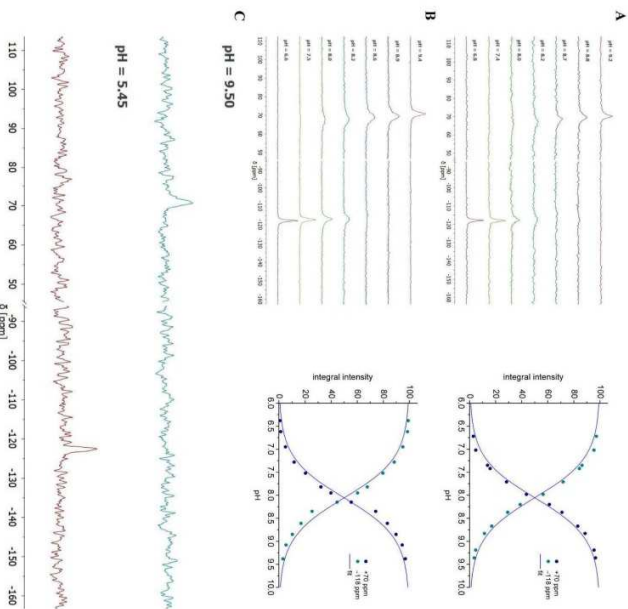


Figure S16: The pH dependence of $^{31}\text{P}\{^1\text{H}\}$ NMR spectra of $\text{SA}-[\text{Eu}(\text{Hdod3ANP})_2/\text{TSA}-[\text{Eu}(\text{dod3ANP})_2]^-$ species. A: 10 mM solution. B: 50 mM solution. C: 2 mM solution. Conditions: H_2O , ~ 150 mM NaCl , $B_0 = 7.05$ T, 25°C . For A and B, right charts show the pH dependence of an integral intensity of the corresponding ^{31}P NMR signals.

14

Table S2: Calculated protonation constants $\log K(\text{HLM})$ characterizing SA-[Eu(Hd_3aNP)]/TSA-[Eu($\text{d}_3\text{aNP})]^-$ equilibrium (25 °C). Fits of the experimental data are shown in Figure S16, Figure S17 and Figure S18.

background electrolyte	electrolyte concentration (mM)	complex concentration (mM)	$\log K(\text{HLM})$ data
NaCl	60	20	8.16(3) Figure S17-A
NaCl	120	39	8.08(2) Figure S17-B
NaCl	154	10	8.05(2) Figure S16-A
NaCl	250	50	8.06(3) Figure S16-B
NaCl	250	79	7.93(3) Figure S17-C
NaCl	1060	19	7.39(2) Figure S17-D
NaCl	1260	85	7.40(5) Figure S17-E
(NM_2Cl)	1270	90	8.53(3) Figure S17-F
NaCl + CaCl_2	190 + 65	65	7.48(3) Figure S18-A
NaCl + MgCl_2	190 + 65	65	7.58(3) Figure S18-B

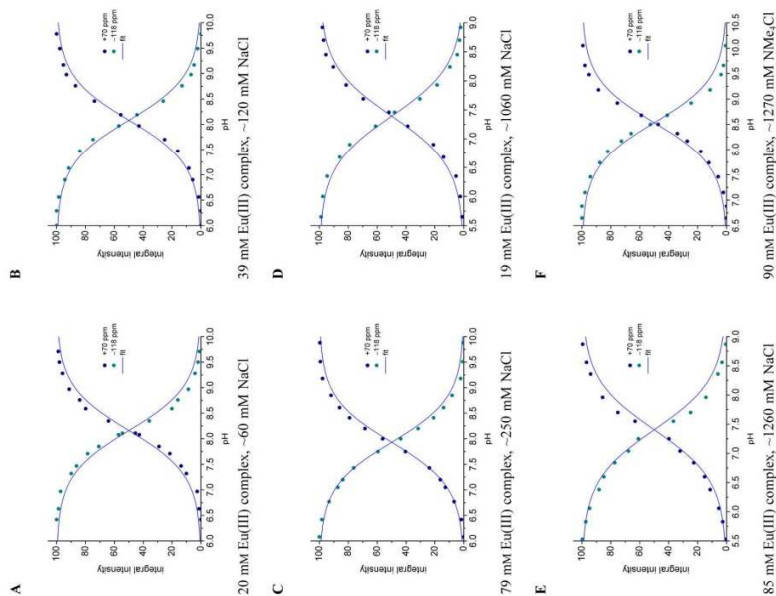


Figure S17: The pH dependence of an integral intensity of the ^1p NMR signals of SA-[Eu(Hd_3aNP)]/TSA-[Eu(d_3aNP)] $^-$ species at various concentrations and ionic strengths. $R_0 = 7.05$ T, 25 °C.

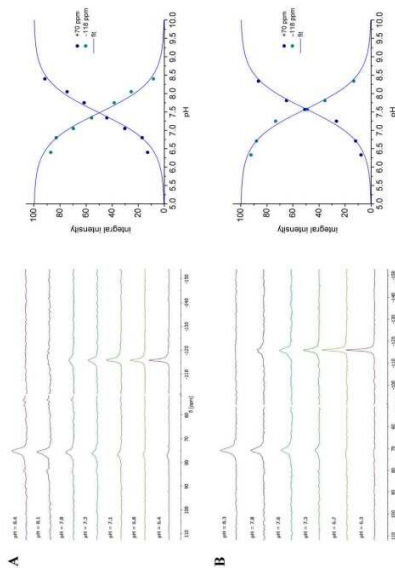


Figure S18: Left: the pH dependence of ^1p ^1H NMR spectra of SA-[Eu(Hd_3aNP)]/TSA-[Eu(d_3aNP)] $^-$ species, and right: the pH dependence of an integral intensity of the corresponding ^1p NMR signals. Conditions: 65 mM solution, H_2O , ~190 mM NaCl, $R_0 = 7.05$ T, 25 °C; **A**: ~65 mM CaCl_2 , **B**: ~65 mM MgCl_2 .

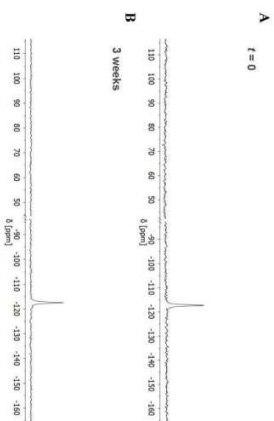


Figure S19: ^{31}P (^1H) NMR spectra of $\text{SA}-[\text{Eu}(\text{H}_4\text{O}_3\text{aNP})]^{2-}$ (80 mM solution in D_2O ; 250 mM NaCl , $D_5 = 7.05 \text{ T}$, 25 $^\circ\text{C}$) at $\text{pD} = 5.9$ measured A: immediately after the pD of the solution was changed from 8 to 5.9, and B: after heating at 60 $^\circ\text{C}$ for 3 weeks. In both cases, the xylenol orange test was negative.

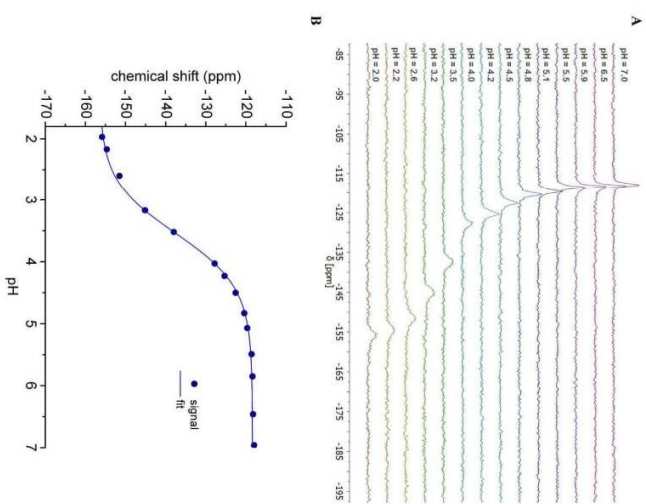
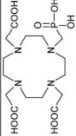
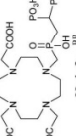
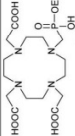

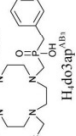
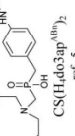


Figure S20: A: ^{31}P NMR signals for the $\text{SA}-[\text{Eu}(\text{H}_4\text{O}_3\text{aNP})]/\text{SA}-[\text{Eu}(\text{H}_4\text{O}_3\text{aNP})]$ equilibrium in acidic region and B: the related titration data showing the best fit affording $\log K = 3.55(1)$ (38 mM complex concentration; 150 mM NaCl , no ionic strength control).

Overview of ^{31}P NMR shifts of the ligands having methylenelephosphonate or methylenephosphinate pendant moieties and their Eu(III)/La(III) complexes

Table S3: ^{31}P NMR shifts (given in ppm) of the ligands and their La(III) and Eu(III) complexes and differences between chemical shifts of the Eu(III) complex and free ligand and/or La(III) complex (Lanthanide-Induced Shift, LIS).

Ligand formula	$\delta_{\text{L/La(L)}}$	$\delta_{\text{[Eu(L)] TSA}}$	$\Delta\delta_{\text{ATSA}}$	$\delta_{\text{[Eu(L)] SA}}$	$\Delta\delta_{\text{ASA}}$
	L: 20	35	15	46-49	26-29
	L: 42 La: 48	82	40 LIS: 34	95	53 LIS: 47
	L: 15	33, 35	18, 20	45, 49	30, 34
	L: 33	49	16	55	22
	L: 33	80, 92	47, 59	87	54
	L: 33	75-82, 90	42-49, 55	82-89, 94	49-56, 61

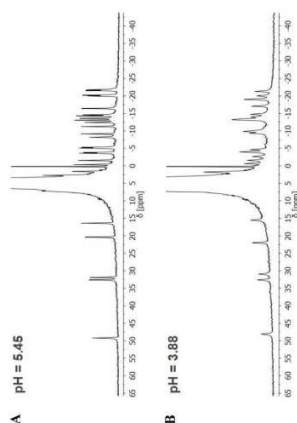
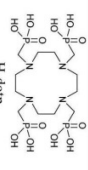
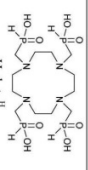
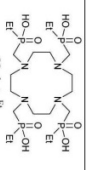
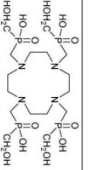
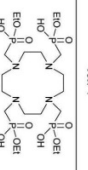
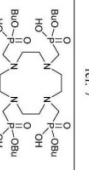
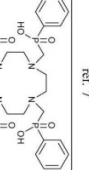
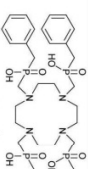
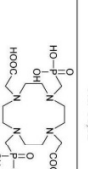
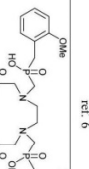
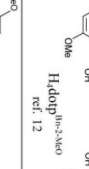
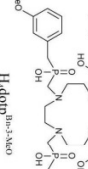
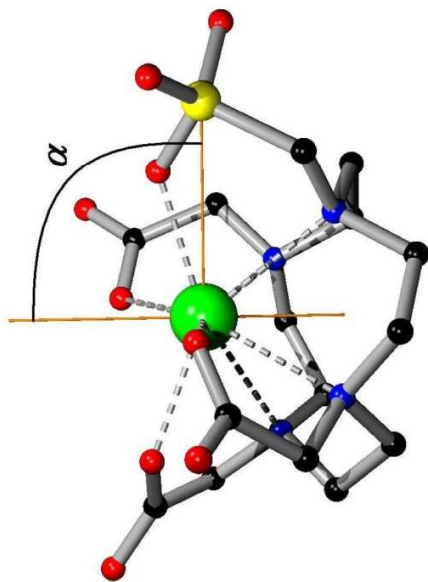
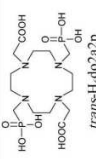


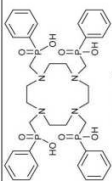
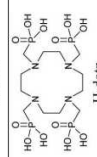
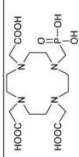
Figure S21: ^1H NMR spectra of the Eu(III) complex of $\text{H}_4\text{d03ap}$ (~ 50 mM solution in H_2O , ~ 150 mM NaCl , $T_f = 7.05$ T, 25°C) at A: pH = 5.45, B: pH = 3.88 (referenced to $\delta(\text{BuOH}) = 1.25$ ppm).

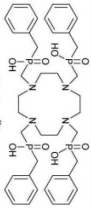
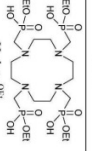
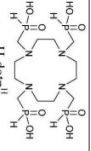
	—	—	LIS: 29	—	—
Hddtp ref. 6					
	L: 23	55-95	32-72	—	—
Hddtp ^{II} ref. 7					
	L: 47	101, 96, 99	LIS: 54, 49, 52	—	—
Hddtp ^{III} ref. 7, 8					
	L: 38	83, 80, 86, 105	45, 42, 48, 67	—	—
Hddtp ^{III} ref. 7					
	L: 19	35-63	16-44	—	—
Hddtp ^{III} ref. 7					
	—	40-55	—	—	—
Hddtp ^{III} ref. 7					
	L: 29	67	38	—	—
Hddtp ^{III} ref. 9, 10					
	L: 38, 39	86	LIS: 47, 48	—	—
Hddtp ^{III} ref. 11, 12					
	L: 6 L: 15	44	38 LIS: 29	—	—
trans-Hddtp ^{III} ref. 6					
	L: 37	90	53	—	—
Hddtp ^{III} ref. 12					
	L: 32 L: 38, 39	87	55 LIS: 48, 49	—	—
Hddtp ^{III} ref. 12					
	L: 22, 36	85	63, 49	—	—
Hddtp ^{III} ref. 12					

Overview of complex geometries found in the solid state

Figure S22. Graphical definition of angle between Ln-P vector and arbitrary magnetic axis (= pseudo- C_4 axis).Table S4. Angles between Ln-P vector and pseudo- C_4 axis observed in crystal structures of Ln(III) complexes with DOTfA-like ligands.

Ligand formula	Ln	α (°)	Coord. no.
	Ce	79.2, 81.3	9
<i>trans</i> -H ₄ d ₀ 2a ₂ p ref. 6			
<i>trans</i> -H ₄ d ₀ 2a ₂ p ref. 6	Dy	73.6	8
<i>trans</i> -H ₄ d ₀ 2a ₂ p ref. 6	Er	73.2	8
<i>trans</i> -H ₄ d ₀ 2a ₂ p ref. 6	Eu	74.6	8
<i>trans</i> -H ₄ d ₀ 2a ₂ p ref. 6	Nd	78.7, 80.4	9

<i>trans</i> -H ₄ d ₀ 2a ₂ p ref. 6	Sm	74.6	8
<i>trans</i> -H ₄ d ₀ 2a ₂ p ref. 6	Sm	78.7, 79.2 78.6, 79.3	9
<i>trans</i> -H ₄ d ₀ 2a ₂ p ref. 6	Tb	73.8	8
<i>trans</i> -H ₄ d ₀ 2a ₂ p ref. 6	Yb	72.8	8
			
<i>H₄d₀p</i> ^{ph} ref. 13	La	81.6, 81.9, 84.5, 88.9 82.0, 83.3, 84.1, 86.1	9
<i>H₄d₀p</i> ^{ph} ref. 13	Ce	81.4, 82.3, 83.5, 87.8 81.8, 83.5, 84.0, 85.6	9
			
<i>H₄d₀p</i> ref. 14	Gd	78.0	8
			
<i>H₄d₀3ap</i> ref. 1	Nd	84.7 85.6	9
<i>H₄d₀3ap</i> ref. 15	Dy	80.8	8
<i>H₄d₀3ap</i> ref. 15	Er	77.4	8
<i>H₄d₀3ap</i> ref. 15	Lu	79.4	8
<i>H₄d₀3ap</i> ref. 15	Lu	77.3	8
<i>H₄d₀3ap</i> ref. 15	Tb	81.7	9

	Eu	76.5, 77.5, 77.8, 79.0	8
H4dopIII ref. 12	La	81.6, 82.2, 82.3, 82.7	9
H4dopIII ref. 12	Yb	75.4, 75.9, 76.6, 76.8	8
H4dopIII ref. 12	Dy	75.1, 75.9, 76.3, 78.0	8
H4dopIII ref. 16	Dy	76.6, 76.8, 77.8, 78.8	8
	Gd	76.6, 77.6, 77.9, 78.4	8
H4dopIII ref. 7	Gd	76.7, 76.9, 77.1, 79.4	8
	Gd	76.5, 77.1	8
H4dopII ref. 7			

Assignment of hydrogen atom signals in ¹H NMR spectra of Eu(III)-H₅d₃aNP complexes

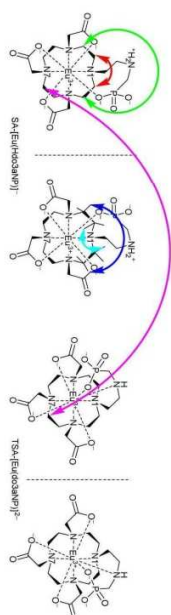


Figure S23: Enantiomeric pairs of SA-[Eu(H₅d₃aNP)] and TSA-[Eu(d₃aNP)]⁻ complexes showing EXSY interactions between hydrogen atoms.

¹H-¹H COSY spectra distinguished groups of four protons belonging to ethylene groups (typically, each proton has cross-peaks with two of remaining three protons of given ethylene) and pairs belonging to methylene groups of acetate and N-C-P fragment.

¹H-¹H EXSY spectra distinguished pairs of hydrogen atoms of the same isomer (SA or TSA, respectively) related through C₂-symmetry (plane defined by aminophosphonate and "odd" acetate pendants), N1, N7 and Eu atoms.

¹H-¹H EXSY spectra distinguished between "odd" and "double" methylene groups of acetate pendant arms.

Selectively ¹H-presaturated ¹³C NMR spectra assigned hydrogen atoms bound to given carbon atom (geminal hydrogen atoms).

Few very weak ¹H-¹H COSY cross-peaks of "odd" and "double" methylene protons of SA isomer to some macrocyclic hydrogen atoms were assigned as interactions to closest macrocycle hydrogen atom, fixing position of macrocycle ethylene bridge.

With assumption that most shifted signals of the SA isomer (signals 1A, 2A, 3A and 4A) are the "axial" ones, remaining hydrogen signals were assigned.

From ¹H-¹H EXSY spectra showing weak cross peaks between SA and TSA isomers, assignment of TSA skeleton was done, showing that "axial" protons are not the most shifted ones, but they are 4B, 6B, 7B and 8B (the second option with 1B, 21B, 26B and 28B as "axial" protons did not give a sense as induced chemical shift of other signals was random with no spatial rules).

Hydrogen atoms belonging to ethylene of aminophosphonate pendant groups were randomly assigned on the basis of sign and magnitude of induced shift to give a "optical" sense in Figure 5.

Table S5: Table of cross-peaks in 2D ^1H - ^1H COSY NMR spectra of SA-[Eu(Hdo3aNP)] $^-$ at pD = 6.78 (left) and TSA-[Eu(d3a3aNP)] $^-$ at pD = 9.05 or 9.30 (right), ~80 mM solution in D_2O , ~250 mM NaCl, $T_{\text{R}} = 14.1$ T, 5 or 25 $^\circ\text{C}$. Less intensive cross-peaks are in brackets.

Signal of the SA-isomer	COSY cross-peak with:	Signal of the proton of TSA-isomer	COSY cross-peak with:
1A	5A, 9A	1B	21B
2A	10A, 7A, (6A)	2B	19B
3A	12A, 19A, (20A, 22A)	3B	-
4A	18A, 28A, (22A)	4B	17B
5A	1A, 8A, (9A)	5B	14B
6A	7A, (2A, 10A)	6B	18B
7A	6A, 2A	7B	25B
8A	9A, 5A	8B	22B
9A	8A, 1A	9B	13B
10A	2A, 6A, 7A, (24A)	10B	-
11A	16A, (17A)	11B	-
12A	3A, 20A, 19A, (28A)	12B	-
13A	15A	13B	9B
14A	17A, (16A)	14B	5B
15A	13A	15B	-
16A	11A, (14A)	16B	-
17A	14A, (11A)	17B	4B
18A	4A, 22A, 28A, (26A)	18B	6B
19A	20A, 3A, 12A	19B	2B
20A	19A, 3A, 12A	20B	26B
21A	25A, (27A)	21B	-
22A	28A, 18A, 4A, (3A)	22B	8B
23A	26A	23B	-
24A	27A, (25A)	24B	-
25A	21A, (24A)	25B	7B
26A	23A	26B	20B
27A	24A, (21A)	27B	-
28A	22A, 4A, (12A)	28B	-

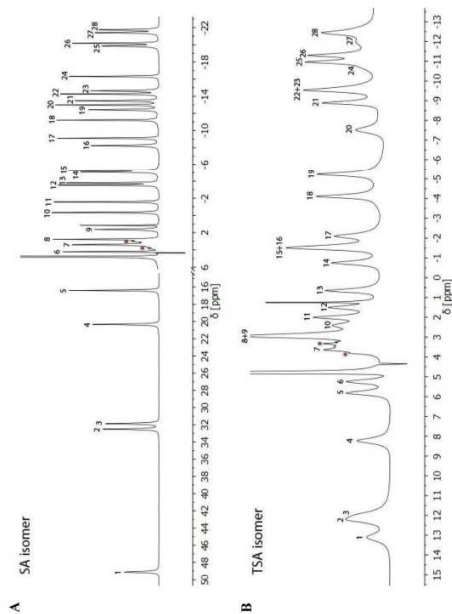


Figure S24: ^1H NMR spectra with numbering of the signals of **A**: SA-[Eu(Hdo3aNP)] $^-$ at pD = 6.78 and **B**: TSA-[Eu(d3a3aNP)] $^-$ at pD = 9.05 (~80 mM solution in D_2O , ~250 mM NaCl, $T_{\text{R}} = 14.1$ T, 25 $^\circ\text{C}$; referenced to $\delta(\text{BuOH}) = 1.25$ ppm). ^1H NMR resonances of the free ligand are labelled with *.

Table S6: Table of cross-peaks in 2D ^1H - ^1H EXSY NMR spectra of SA-[Eu(d3ANP)] $^2-$ at pD = 6.78 (left) or 8.66 and TSA-[Eu(d3ANP)] $^2-$ at pD = 9.05 or 8.66 (right), -80 mM solution in D_2O , -250 mM NaCl, $I_{\text{H}} = 14.1$ T, 5 or 25 $^\circ\text{C}$.

Signal of the proton of SA-isomer	EXSY with:	Signal of the proton of TSA-isomer	EXSY with:
1A	6A (6R, 28B)	1B	25B (28A, 12A)
2A	8A (8B, 19B)	2B	22B (10A, 9A)
3A	22A (7B, 21B)	3B	10B (16A, 11A)
4A	20A (4B, 26B)	4B	26B (20A, 4A)
5A	7A (18B, 24B)	5B	14B (13A, 15A)
6A	1A (6B, 28B)	6B	28B (1A, 6A)
7A	5A (18B, 24B)	7B	21B (22A, 3A)
8A	2A (8B, 19B)	8B	19B (2A, 8A)
9A	10A (2B, 22B)	9B	13B (26A, 23A)
10A	9A (2B, 22B)	10B	3B (11A, 16A)
11A	16A (3B, 10B)	11B	23B (21A, 27A)
12A	28A (1B, 25B)	12B	27B (25A, 24A)
13A	15A (5B, 14B)	13B	9B (26A, 23A)
14A	17A (15B, 16B)	14B	5B (13A, 15A)
15A	13A (5B, 14B)	15B	16B (14A, 17A)
16A	11A (3B, 10B)	16B	15B (14A, 17A)
17A	14A (15B, 16B)	17B	20B (18A, 19A)
18A	19A (17B, 20B)	18B	24B (7A, 5A)
19A	18A (17B, 20B)	19B	8B (2A, 8A)
20A	4A (4B, 26B)	20B	17B (18A, 19A)
21A	27A (11B, 23B)	21B	7B (22A, 3A)
22A	3A (7B, 21B)	22B	2B (10A, 9A)
23A	26A (9B, 13B)	23B	11B (27A, 21A)
24A	25A (12B, 27B)	24B	18B (5A, 7A)
25A	24A (12B, 27B)	25B	1B (28A, 12A)
26A	23A (9B, 13B)	26B	4B (20A, 4A)
27A	21A (11B, 23B)	27B	12B (24A, 25A)
28A	12A (1B, 25B)	28B	6B (1A, 6A)

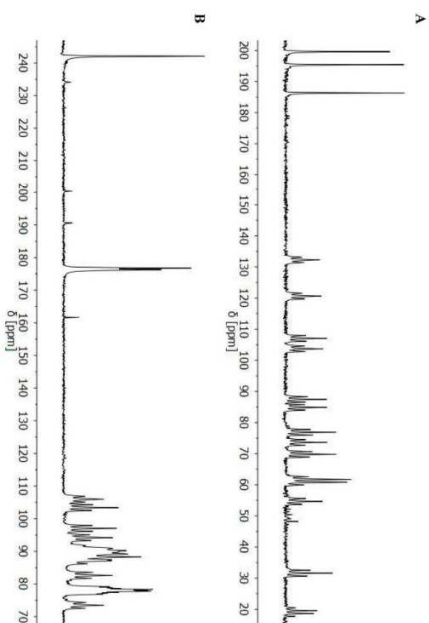


Figure S25: ^{13}C NMR spectra of A: SA-[Eu(d3ANP)] $^2-$ at pD = 6.78 and 25 $^\circ\text{C}$ and B: TSA-[Eu(d3ANP)] $^2-$ at pD = 9.70 and 5 $^\circ\text{C}$ without H decoupling.

Table S7: The couples of geminal proton signals in the NMR spectra of SA-[Eu(Hdo3aNP)]⁻ at pD = 6.78 and 25 °C (left) and TSA-[Eu(do3aNP)]⁻ at pD = 9.70 and 5 °C (right); ~80 mM solution in D₂O, ~250 mM NaCl, B₀ = 14.1 T. Assignment comes from selective ¹H decoupled ¹³C NMR spectra.

Signal of the proton of SA-isomer	Signal of the geminal proton	Signal of the proton of TSA-isomer	Signal of the geminal proton
1A	5A	1B	21B
2A	10A	2B	19B
3A	12A	3B	10B
4A	18A	4B	17B
5A	1A	5B	14B
6A	7A	6B	18B
7A	6A	7B	25B
8A	9A	8B	22B
9A	8A	9B	13B
10A	2A	10B	3B
11A	16A	11B	27B
12A	3A	12B	23B
13A	15A	13B	9B
14A	17A	14B	5B
15A	13A	15B	16B
16A	11A	16B	15B
17A	14A	17B	4B
18A	4A	18B	6B
19A	20A	19B	2B
20A	19A	20B	26B
21A	25A	21B	1B
22A	28A	22B	8B
23A	26A	23B	12B
24A	27A	24B	28B
25A	21A	25B	7B
26A	23A	26B	20B
27A	24A	27B	11B
28A	22A	28B	24B

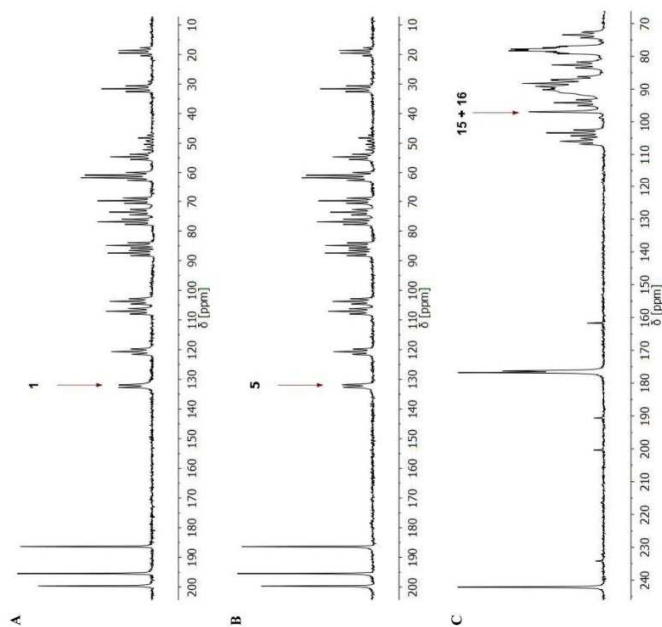


Figure S26: Examples of ¹³C NMR spectra of **A**, **B**, SA-[Eu(Hdo3aNP)]⁻ at pD = 6.78 and 25 °C and **C**: TSA-[Eu(do3aNP)]⁻ at pD = 9.70 and 5 °C with ¹H decoupling at the ¹H frequency of **A**; **A**, **B**: SA, **C**: 15B + 16B.

Potentiometric, ^1H and ^{31}P NMR studies – protonation and stability constants of $\text{H}_6\text{d}_3\text{a}_3\text{NP}$ and its $\text{Eu}(\text{III})$ complex

Table S8: Overall protonation constants ($\log\beta_n$)^(a) and derived consecutive protonation constants ($\log(K_{i,1})$)^(b) of $\text{H}_6\text{d}_3\text{a}_3\text{NP}$. Potentiometric conditions: 0.1 M (NMe₄)Cl, 25 °C. Conditions of ^{31}P NMR and ^1H NMR titration: HCl/(NMe₄)OH and HCl/KOH, respectively, no ionic strength control, 25 °C.

<i>n</i>	$\log\beta_n$ (potent.)	$\log(K_{i,1})$ (potent.)	$\log\beta_n$ (^{31}P NMR)	$\log(K_{i,1})$ (^{31}P NMR)	$\delta^{\text{P}}(^1\text{P})$ ppm	$\delta^{\text{H}}(^1\text{H})$ NCH ₃ P ppm	$\delta^{\text{H}}(^1\text{H})$ acetate ppm	$\delta^{\text{H}}(^1\text{H})$ trans ppm	$\delta^{\text{H}}(^1\text{H})$ acetates ppm
0	–	–	–	–	16.86(4)	2.55(4)	3.11(9)	3.15(9)	–
1	12.561(6)	12.56	12.52(17)	12.52	16.32(8)	2.61(2)	3.39(2)	3.36(2)	–
2	22.935(6)	10.37	23.11(3)	10.59	10.43(18)	2.86(2)	3.47(2)	3.47(3)	–
3	32.164(7)	9.23	32.48(8)	9.37	8.16(2)	2.98(1)	3.21(1)	3.85(1)	–
4	38.336(8)	6.17	38.44(8)	5.96	9.30(2)	–	–	–	–
5	42.522(8)	4.19	40.49(32) ^(c)	–	9.19(2)	–	–	–	–
6	44.426(9)	1.90	–	2.05 ^(d)	–	–	–	–	–

^(a) $\beta_n = [\text{H}_n\text{L}]/([\text{H}]^n[\text{L}])$; ^(b) $K_{i,1} = [\text{H}_i\text{L}]/([\text{H}]_i[\text{H}_{i-1}\text{L}])$; Changes of species are omitted for clarity reasons. ^(c) In fact, this step corresponds to a sixth protonation (corresponding $\log K = 40.49 - 38.44 = 2.05$), although it was formally calculated as the fifth one. It is due to the fact that the fifth protonation occurs far away from the phosphonate group (on the pendant acetate group located *trans* to the aminophosphonate moiety) and thus, it does not influence the ^{31}P NMR chemical shift.

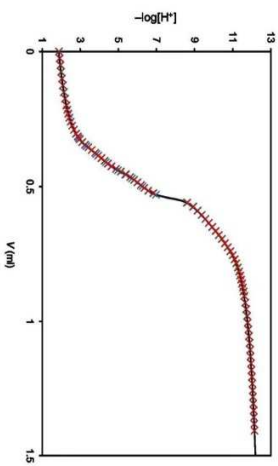


Figure S27: Titration data of the acid-base titration of the free ligand $\text{H}_6\text{d}_3\text{a}_3\text{NP}$ showing the best fit calculated using the protonation constants from Table S8.

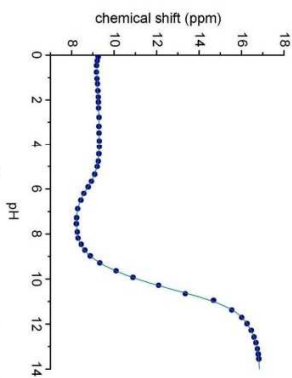


Figure S28: Titration data of the ^{31}P NMR titration of the free ligand $\text{H}_6\text{d}_3\text{a}_3\text{NP}$ showing the best fit calculated using the protonation constants and chemical shifts from Table S8.

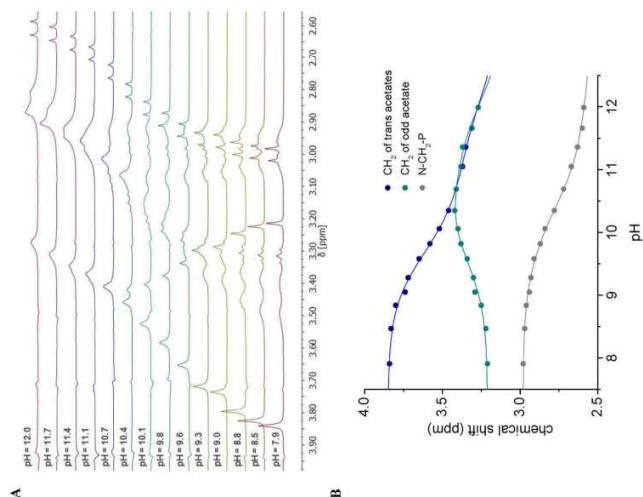


Figure S29: **A:** ^1H NMR signals of ^1H NMR titration of the free ligand $\text{H}_4\text{do3aNP}$ and **B:** titration data of the ^1H NMR titration of the showing the best fit.

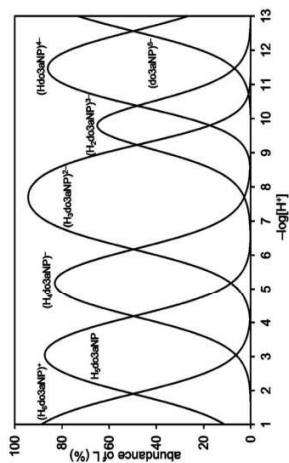


Figure S30: Distribution diagram of variously protonated species of the free ligand $\text{H}_4\text{do3aNP}$ ($c_1 = 0.004 \text{ M}$, $0.1 \text{ M (NMe}_3\text{)Cl}$, 25°C).

Table S9: Overall stability constants ($\log\beta_{ij}$)^[a] of $\text{Eu}(\text{H}_i\text{do3aNP})_j$ complexes and derived consecutive protonation constants ($\log\alpha(\text{H}_i, \text{L}, \text{M})$)^[b] ($0.1 \text{ M (NMe}_3\text{)Cl}$, 25°C).

i	j	Eu	$\log\beta_{ij}$	$\log\alpha(\text{H}_i, \text{L}, \text{M})$
0	1	1	23.49(3)	—
1	1	1	31.49(3)	8.00
2	1	1	35.23(5)	3.75
3	1	1	39.59(4)	4.35
4	1	1	42.90(3)	3.31

^[a] $\beta_{ij} = [\text{H}_i\text{L}_j\text{Eu}]/([\text{H}]^i[\text{L}]^j[\text{Eu}])$; ^[b] $\alpha(\text{H}_i, \text{L}, \text{M}) = [\text{H}_i\text{L}_j\text{M}]/([\text{H}]^i[\text{L}_j\text{M}])$. Charges of species are omitted for clarity reasons.

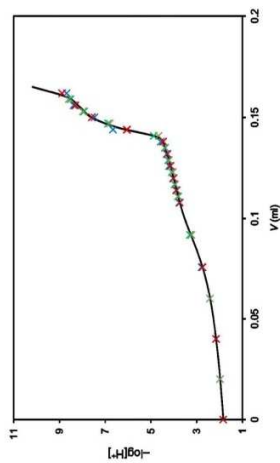


Figure S31: Titration data of the out-of-cell titration of $\text{Eu}(\text{III})\text{-H}_4\text{do3aNP}$ systems showing the best fits calculated using the stability constants from Table S9 ($c_{\text{Eu}} = c_1 = 0.004 \text{ M}$, $0.1 \text{ M (NMe}_3\text{)Cl}$, 25°C , equilibration time = 4 weeks).

Table S10: Overall protonation constants ($\log\beta_{HL}^{HL}$) of pre-formed $[\text{Eu}(\text{d}3\text{NP})]^{2-}$ complex and derived consecutive protonation constants ($\log K(\text{H},\text{L},\text{M})^{HL}$) (0.1 M NMe_4Cl , 25 °C).

h	$\log\beta_{HL}^{HL}$	$\log K(\text{H},\text{L},\text{M})^{HL}$
1	8.29(2)	8.29
2	12.36(3)	4.07
3	14.11(3)	1.75

$^{HL}\beta_{HL} = [\text{H}_h\text{L}_h\text{M}]/[\text{H}^h][\text{L}_h\text{M}]$, $^{HL}K(\text{H},\text{L}) = [\text{H}_h\text{L}_h\text{M}]/[\text{H}^h][\text{L}_h\text{M}]$. Changes of species are omitted for clarity reasons.

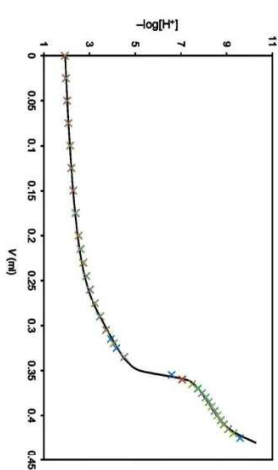


Figure S32: Titration data of the acid-base titration of the pre-formed $[\text{Eu}(\text{d}3\text{NP})]^{2-}$ complex with the best fits calculated using the protonation constants from Table S10 ($G_{HL} = 0.003 \text{ M}$, 0.1 M NMe_4Cl , 25 °C).

- ¹ Rudovský, J.; Cigler, P.; Hermann, P.; Vojtěšek, P.; Lukeš, I.; Peters, J. A.; Vander Elst, L.; Muller, R. N. Lanthanide (III) complexes of a mono (methylphosphonate) analogue of H₄do₃: The influence of protonation of the phosphonate moiety on the TSAP/SAP isomer ratio and the water exchange rate. *Chem. - Eur. J.* **2005**, *11*, 2373–2384.
- ² Vidha, T.; Kubiček, V.; Kocik, J.; Hermann, P.; Vander Elst, L.; Muller, R. N.; Lukeš, I.; Peters, J. A. Gd(III) complex of a monophosphate-bis(phosphonate) DOTA analogue with a high relaxivity: Lanthanide(III) complexes for imaging and radiotherapy of calcified tissues. *Dalton Trans.* **2009**, 3204–3214.
- ³ Lebtušková, P.; Hermann, P.; Helm, L.; Toth, E.; Kocik, J.; Binnemans, K.; Rudovský, J.; Lukeš, I.; Mersbach, A. E. Gadolinium(III) Complexes of Mono- and Dicyclyl Esters of Monophosphonic Acid Analogue of DOTA as Potential MRI Contrast Agents: Solution Structures and Relaxometric Studies. *Dalton Trans.* **2007**, 493–501.
- ⁴ Rudovský, J.; Kocik, J.; Hermann, P.; Lukeš, I.; Mahuro, V.; Aime, S. Synthesis of a Bifunctional Monophosphonic Acid DOTA Analogue Ligand and Its Lanthanide(III) Complexes. A

37

Gadolinium(III) Complex Endowed with an Optimal Water Exchange Rate for MRI Applications. *Org. Biomol. Chem.* **2005**, *3*, 112–117.

⁵ Rudovský, J.; Botta, M.; Hermann, P.; Koridze, A.; Aime, S. Relaxometric and solution NMR structural studies on ditopic lanthanide(III) complexes of a phosphinate analogue of DOTA with a fast rate of water exchange. *Dalton Trans.* **2006**, 2323–2333.

⁶ Campello, M. P. C.; Lacerda, S.; Santos, I. C.; Pereira, G. A.; Geraldes, C. F. G. C.; Kocik, J.; Hermann, P.; Vanek, J.; Lubal, P.; Kubiček, V.; Toth, E.; Santos, I. Lanthanide(III) complexes of 4,10-bis(phosphonomethyl)-1,4,7,10-tetraazacyclododecane-1,7-diacetic acid (trans-H₄d₆2a₂) in solution and in the solid state: structural studies along the series. *Chem. - Eur. J.* **2010**, *16*, 8446–8465.

⁷ Kolková, Z.; Pereira, G. A.; Djanashvili, K.; Kocik, J.; Rudovský, J.; Hermann, P.; Vander Elst, L.; Muller, R. N.; Geraldes, C. F. G. C.; Lukeš, I.; Peters, J. A. Lanthanide(III) Complexes of Phosphonic Acid Analogues of H₄DOTA as Model Compounds for the Evaluation of the Second-Sphere Hydration. *Eur. J. Inorg. Chem.* **2009**, 119–136.

⁸ Pereira, G. A.; Ball, L.; Sherry, A. D.; Peters, J. A.; Geraldes, C. F. G. C. NMR Characterization of Lanthanide(3+) Complexes of Tetraazatetrakisphosphinato and Tetraazatetrakisphosphonato Ligands. *Helv. Chim. Acta* **2009**, *92*, 2532–2551.

⁹ Rohovec, J.; Lukeš, I.; Hermann, P. Lanthanide complexes of a cyclen derivative with phenylphosphinic pendant arms for possible ¹H and ³¹P MRI temperature sensitive probes. *New J. Chem.* **1999**, *23*, 1129–1132.

¹⁰ Rohovec, J.; Křiváta, M.; Vojtěšek, P.; Hermann, P.; Lukeš, I. Synthesis, Crystal Structures, and Solution Properties of N-Methylbenzylphosphinic Acid Derivatives of Cyclen and Cyclam. *Eur. J. Inorg. Chem.* **2000**, 195–203.

¹¹ Aime, S.; Batsanov, A. S.; Botta, M.; Howard, J. A. K.; Parker, D.; Senanayake, K.; Williams, J. A. G. Solution and Solid-state Characterization of Highly Rigid, Eight-Coordinate Lanthanide(III) Complexes of a Macrocyclic Tetra-benzylphosphinate. *Inorg. Chem.* **1994**, *33*, 4696–4706.

¹² Aime, S.; Batsanov, A. S.; Botta, M.; Dickens, R. S.; Faulkner, S.; Foster, C. E.; Harrison, A.; Howard, J. A. K.; Moloney, J. M.; Norman, T. J.; Parker, D.; Royle, L.; Williams, J. A. G. Nuclear magnetic resonance, luminescence and structural studies of lanthanide complexes with cyclen-like macrocyclic ligands bearing benzylphosphinate groups. *J. Chem. Soc., Dalton Trans.* **1997**, 3623–3636.

38

- ¹³ Rohovec, J.; Vojtišek, P.; Hermann, P.; Mosinger, J.; Žák, Z.; Lukeš, I. Synthesis, crystal structures and NMR and luminescence spectra of lanthanide complexes of 1,4,7,10-tetraazacyclododecane with *N*-methylene(phenyl)phosphinic acid pendant arms. *J. Chem. Soc., Dalton Trans.* **1999**, 3585–3592.
- ¹⁴ Aveilla, F.; Peters, J. A.; Geraldes, C. F. G. C. X-ray Crystal Structure of a Sodium Salt of [Gd(DOTP)]⁻: Implications for Its Second-Sphere Relaxivity and the ²³Na NMR Hyperfine Shift Effects of [Tm(DOTP)]⁻. *Eur. J. Inorg. Chem.* **2003**, 4179–4186.
- ¹⁵ Vojtišek, P.; Cigler, P.; Kotek, J.; Rudovský, J.; Hermann, P.; Lukeš, I. Crystal Structures of Lanthanide(III) Complexes with Cyclen Derivative Bearing Three Acetate and One Methylphosphonate Pendants. *Inorg. Chem.* **2005**, *44*, 5591–5599.
- ¹⁶ Luck, R. L.; Maupin, C. L.; Parker, D.; Riehl, J. P.; Williams, J. A. G. Circularly polarized luminescence and structural studies of a dysprosium(III) complex with an octadentate macrocyclic ligand bearing benzylophosphinate groups. *Inorg. Chim. Acta.* **2001**, *377*, 331–337.